

ANDROGEN-DEPENDENT EXCITABILITY OF MOUSE VENTRAL HIPPOCAMPAL
AFFERENTS TO NUCLEUS ACCUMBENS UNDERLIES SEX-SPECIFIC
SUSCEPTIBILITY TO STRESS

By

Elizabeth Spencer Williams

A DISSERTATION

Submitted to
Michigan State University
in partial fulfillment of the requirements
for the degree of

Pharmacology & Toxicology – Doctor of Philosophy

2019

ABSTRACT

ANDROGEN-DEPENDENT EXCITABILITY OF MOUSE VENTRAL HIPPOCAMPAL AFFERENTS TO NUCLEUS ACCUMBENS UNDERLIES SEX-SPECIFIC SUSCEPTIBILITY TO STRESS

By

Elizabeth Spencer Williams

Women experience major depressive disorder (MDD) nearly twice as often as men, but the neurophysiology of this sex difference in prevalence is not fully understood. In preclinical animal models of depression utilizing male mice, activity of glutamatergic afferents from ventral hippocampus (vHPC) to nucleus accumbens (NAc) regulates mood-related behavioral responses to stress, but the circuit-level mechanisms underlying stress responses in female mice are not as clear. Female mice, however, uniquely exhibit susceptibility to anhedonia, a common symptom of depression, following subchronic variable stress (SCVS). Using whole-cell patch clamp electrophysiology, we identify a lower excitability of male vHPC-NAc projections compared to those in female mice. We demonstrate that the lower excitability in male projections is adult testosterone-dependent, and that this accompanies resilience to anhedonia in males following stress: orchidectomy induces increased vHPC-NAc excitability and susceptibility to SCVS in male mice, and exogenous testosterone levels vHPC-NAc excitability and mitigates anhedonia susceptibility in ovariectomized female mice. We further demonstrate a causal link between vHPC-NAc excitability and SCVS susceptibility using designer receptors exclusively activated by designer drugs (DREADDs), with circuit activity inversely correlated to anhedonia resilience in both sexes. We also find that anhedonia following SCVS requires an extended increase in vHPC-NAc activity, as activation of vHPC-NAc

only during behavioral assessment does not result in decreased sucrose preference in male mice. Using translating ribosome affinity purification (TRAP), we interrogate male and female vHPC-NAc circuit-specific gene expression and uncover differential expression of genes in multiple pathways that may regulate differing circuit excitability between the sexes, and ultimately may explain sex differences in SCVS susceptibility. Lastly, we investigate the role of Δ FosB, a transcription factor known to reduce HPC excitability, in vHPC-NAc neurons in male and female mice, and demonstrate that this molecule is a key influencer of chronic social defeat stress (CSDS) responses in male mice. This study highlights hormone-dependent differences in vHPC-NAc circuit excitability in adult mice, which are directly causative of resilience to SCVS-induced anhedonia, and identifies sex differences in vHPC-NAc gene transcription that may mediate sex-specific responses to stress and depression pathogenesis.

To my family, for their unwavering love and support.

ACKNOWLEDGEMENTS

I am very grateful to have worked with many outstanding scientists and collaborators during my graduate research. All past and present members of the Robison and Mazei-Robison laboratories have been phenomenal colleagues and friends, and have provided the support and knowledge necessary to complete the current dissertation. The Pharmacology & Toxicology and Physiology Departments have provided an ideal work environment, and I would like to recognize the work of the staff of both departments in their support of students and research.

I have been very fortunate to have worked with a brilliant group of scientists in the Robison laboratory. All students and postdoctoral fellows have been valuable influences on my scientific career, and have also been good friends. Ken Moon, our Laboratory Manager, helped to provide the tools and reagents necessary for the experiments presented in this document, as well as outstanding technical support for many of the techniques used in this thesis. I would like to specifically recognize Dr. Andrew Eagle, whose guidance and research were essential to much of the data presented in Chapter IV. Andrew is a thoughtful and careful scientist, and has become a great model for my own research goals. A fellow graduate student, Claire Manning, has also been an invaluable colleague and friend, and without her this dissertation would not have made for the story that it is. Claire's behavioral work has paralleled my own physiology work beautifully, and truly makes the electrophysiology presented in Chapters III and IV shine. I cannot thank her enough for being such a wonderful friend and collaborator, and her

elegant work presented in Chapters III and IV has been critical in establishing the importance of our studies.

I would also like to thank my thesis committee: Dr. Anne Dorrance, Dr. Greg Fink, Dr. Jim Galligan, and Dr. Bill Jackson. Their input and guidance throughout my research and their patience and availability for meetings was much appreciated. Dr. Cindy Arvidson and Mrs. Jonelle Golding of the MSU-CHM MD/PhD program have also been critical to my success in this long and arduous process, and I thank them sincerely for their guidance and support. I would also like to thank my mentor, Dr. A.J. Robison. His guidance and insight have been essential to my education and growth as a scientist. Moreover, he has been patient and understanding throughout my medical and graduate studies, and has always put my personal well-being and growth as a student first. His mentorship will undoubtedly shape the rest of my career, and his work on my behalf is forever appreciated. Dr. Michelle Mazei-Robison's guidance throughout my research is also very much appreciated, and she is a great inspiration to me as a woman in research.

Lastly, I would like to recognize the continuing love and support of my family. My parents, Anna Kalkman, Scott Kalkman, Danny Williams, and Robert Ingram, and my brother Daniel have given me the inspiration and support necessary to complete the current work and pursue my goals in research and medicine. I cannot thank them enough for putting up with me during my completion of two doctorate degrees, as well as for their humor and kindness in keeping my spirits up during challenging times. My husband, Tom, is the best friend and partner I could ask for in life and has been with me every step of the way in graduate and medical school. His love and support have been key in the

completion of this dissertation, and I thank him for pushing me to be the best researcher and physician I can be.

TABLE OF CONTENTS

LIST OF FIGURES	ix
I. INTRODUCTION	1
General Introduction to the Brain and Disease	1
Major Depressive Disorder (MDD) and Preclinical Animal Models of Depression	3
<i>Epidemiology and Disease Burden</i>	4
<i>MDD differences in men and women</i>	5
<i>Preclinical Animal Models of Depression</i>	7
<i>Subchronic Variable Stress (SCVS)</i>	12
<i>Sex differences in stress responses</i>	15
The Hippocampus	19
<i>Distinctive Dorsal and Ventral HPC Functions</i>	21
<i>Neurotransmitters of the HPC – Implications in Mood disorders</i>	23
<i>HPC Sex Differences in Stress and Depression</i>	31
The Nucleus Accumbens	33
<i>NAc Cell Types – Direct and Indirect Pathways</i>	33
<i>NAc function in stress models of depression</i>	34
<i>Sex differences in NAc</i>	38
HPC to NAc connectivity	39
Ion Channels of the Hippocampus	44
<i>Leak Channels</i>	44
<i>Potassium Channels</i>	45
<i>Sodium channels</i>	47
<i>Calcium channels</i>	49
<i>HCN Channels</i>	51
Hormone Signaling in the Brain – Effects on Stress and Depression	52
II. MATERIALS AND METHODS.....	60
Animals.....	60
Gonadectomies	61
Intracranial Injections & Viral Vectors.....	61
Subchronic Variable Stress	63
Chronic social defeat stress (CSDS).....	63
DREADD activation	63
CRISPR Guide RNA design and testing	64
Behavior	65
Electrophysiology	66
Immunohistochemistry	68
Translating Ribosome Affinity Purification (TRAP) and cDNA library preparation	69
Statistical Analysis.....	70

III. ANDROGEN-DEPENDENT EXCITABILITY OF MOUSE VENTRAL HIPPOCAMPAL AFFERENTS TO NUCLEUS ACCUMBENS UNDERLIES SEX-SPECIFIC SUSCEPTIBILITY TO STRESS	72
Introduction.....	72
Results	74
<i>Female mice are selectively susceptible to anhedonia following SCVS</i>	74
<i>Female mice have increased vHPC-NAc neuronal excitability</i>	77
<i>Sex differences in baseline excitability are unique to the vHPC-NAc circuit</i>	85
<i>SCVS does not affect basal vHPC-NAc excitability in female mice</i>	89
<i>Orchidectomy induces male susceptibility to SCVS-induced anhedonia</i>	89
<i>Orchidectomy reduces excitability of vHPC-NAc neurons</i>	92
<i>Orchidectomy reduces excitability of vHPC-BLA neurons</i>	100
<i>Androgen receptor antagonism increases male vHPC-NAc excitability</i>	106
<i>Exogenous testosterone in female mice ameliorates susceptibility to SCVS</i>	109
<i>Exogenous testosterone mitigates hyperexcitability in female vHPC-NAc neurons</i>	114
<i>vHPC-NAc excitability directly mediates SCVS-induced susceptibility to anhedonia</i>	122
<i>Sex-specific transcriptome interrogation of vHPC-NAc neurons</i>	131
Discussion	134
 IV. VENTRAL HIPPOCAMPUS TO NUCLEUS ACCUMBENS Δ FOSB UNDERLIES RESILIENCE TO SOCIAL STRESS AND REGULATES CIRCUIT-SPECIFIC EXCITABILITY	142
Introduction.....	142
Results	143
<i>Chronic social defeat stress and fluoxetine induce ΔFosB in ventral hippocampus</i>	143
<i>vHPC-NAc ΔFosB is necessary for resilience to social stress</i>	145
<i>ΔFosB regulates vHPC-NAc projection excitability</i>	152
Discussion	162
 V. SUMMARY, DISCUSSION AND FUTURE DIRECTIONS	168
Summary	168
Discussion and Future Directions.....	173
<i>Resilience as an active process</i>	173
<i>Gene expression changes in stress</i>	176
<i>Intrinsic excitability and plasticity</i>	179
Final Summary	183
 REFERENCES	184

LIST OF FIGURES

Figure 1 Chronic social defeat stress and social interaction test.....	10
Figure 2 Subchronic variable stress (SCVS) and associated behavioral assays.....	14
Figure 3 Hypothalamic-pituitary-adrenal (HPA) axis and hippocampal negative feedback regulation.....	16
Figure 4 Information pathways of the hippocampus.....	20
Figure 5 Depression and reward circuitry.....	24
Figure 6 Classical and nuanced direct and indirect pathways of NAc signaling.....	35
Figure 7 Selective female susceptibility to SCVS in the measure of sucrose preference.....	75
Figure 8 Additional behavioral assays of male vs. female SCVS.....	76
Figure 9 Retrograde HSV-heF1 α -Cre injection at NAc predominantly labels vHPC CA1 pyramidal cells.....	78
Figure 10 Female vHPC-NAc projections are more excitable than male vHPC-NAc projections.....	79
Figure 11 Membrane properties of male vs. female vHPC-NAc projections.....	80
Figure 12 Spontaneous activity measures of male vs female vHPC-NAc projections.....	82
Figure 13 Spike frequency adaptation is elevated in male vHPC-NAc projections compared to female vHPC-NAc projections.....	83
Figure 14 AMPA to NMDA ratio of male and female vHPC-NAc projections.....	84
Figure 15 Male and female vHPC-BLA projections do not differ in excitability.....	86
Figure 16 Membrane properties of male vs. female vHPC-BLA projections.....	87
Figure 17 Spontaneous activity measures of male vs female vHPC-BLA projections.....	88
Figure 18 Female control and post-SCVS vHPC-NAc projections do not differ in excitability.....	90

Figure 19 Membrane properties of control and post-SCVS female vHPC-NAc neurons	91
Figure 20 Orchidectomy of male mice induces susceptibility to SCVS as measured by sucrose preference, but only with extended time following surgery.	93
Figure 21 Additional behavioral assays of sham vs. orchidectomy SCVS.	94
Figure 22 Orchidectomy in male mice increases vHPC-NAc excitability.	95
Figure 23 Membrane properties of sham vs. orchidectomy male vHPC-NAc projections.	96
Figure 24 Spontaneous activity measures of orchidectomy vs sham male vHPC-NAc neurons.	97
Figure 25 Spike frequency adaptation is impaired in male vHPC-NAc projections following orchidectomy.	98
Figure 26 Sham and OVX female vHPC-NAc projections do not differ in excitability. .	99
Figure 27 Membrane properties of sham vs. ovariectomy female vHPC-NAc projections.	101
Figure 28 Spontaneous activity measures of ovariectomy vs sham female vHPC-NAc neurons.	102
Figure 29 Spike frequency adaptation did not differ between female sham and OVX vHPC-NAc neurons.	103
Figure 30 Orchidectomy increases the excitability of vHPC-BLA neurons in male mice.	104
Figure 31 Membrane properties for orchidectomy and sham vHPC-BLA neurons. ...	105
Figure 32 Female ovariectomy and sham vHPC-BLA neurons did not differ in excitability.	107
Figure 33 Membrane properties for female ovariectomy and sham vHPC-NAc neurons.	108
Figure 34 Ventral HPC to NAc projections express androgen receptors (ARs).	110
Figure 35 Acute application of the AR antagonist cause flutamide causes an increase in vHPC-NAc neuronal excitability in male mice.	111

Figure 36 Membrane properties of male vehicle- and flutamide-treated vHPC-NAc projections.	112
Figure 37 Spontaneous activity measures of male vHPC-NAc projections treated with vehicle or flutamide.	113
Figure 38 Female susceptibility to SCVS-induced anhedonia is ameliorated by adult testosterone.	115
Figure 39 Additional behavioral assays of female OVX + Blank and OVX + T SCVS.	116
Figure 40 Female OVX vHPC-NAc excitability is decreased with chronic testosterone.	118
Figure 41 Membrane properties of female OVX + Blank and OVX + T vHPC-NAc projections.	119
Figure 42 Spontaneous activity measures of female OVX + Blank and OVX + T vHPC-NAc projections.	120
Figure 43 Spike frequency adaptation is enhanced by chronic testosterone in OVX female vHPC-NAc projections.	121
Figure 44 Viral DREADD proof-of concept electrophysiology.	123
Figure 45 Long-term reduction of vHPC-NAc activity causes susceptibility to SCVS-induced anhedonia in male mice.	125
Figure 46 Additional behavioral assays of G _q -coupled (male) DREADD-expressing vHPC-NAc mice.	126
Figure 47 Exposure to CNO without the presence of DREADD expression in vHPC-NAc neurons in male mice does not cause SCVS-induced anhedonia.	127
Figure 48 Inhibition of vHPC-NAc activity directly mediates resilience to SCVS-induced anhedonia.	129
Figure 49 Additional behavioral assays of G _i -coupled (female) DREADD-expressing vHPC-NAc mice.	130
Figure 50 Translating ribosome affinity purification (TRAP) allows interrogation of circuit-specific vHPC-NAc transcriptome.	132
Figure 51 TRAP strategy is efficient in pulldown of neuronal mRNA.	133

Figure 52 Plot of transcript reads vs fold change in females vs males verifies efficacy of sex-specific vHPC-NAc TRAP and highlights most analysis-ready genes.	135
Figure 53 Ingenuity pathway analysis reveals many differentially regulated pathways in female vs male vHPC-NAc transcriptomes.	136
Figure 54 Chronic social defeat stress and fluoxetine induce Δ FosB in ventral hippocampus.	144
Figure 55 Δ FosB is induced in vHPC-NAc projections by CSDS.	146
Figure 56 vHPC Δ FosB is necessary for resilience to social stress.	148
Figure 57 vHPC-NAc Δ FosB is necessary for resilience to social stress.	150
Figure 58 vHPC-BLA FosB KO is anxiolytic.	151
Figure 59 Δ FosB regulates vHPC neuronal excitability.	153
Figure 60 Δ FosB expression in vHPC-NAc neurons is reduced in FosB circuit-specific KO mice.	154
Figure 61 Δ FosB regulates the cellular excitability of vHPC-NAc neurons in male mice.	156
Figure 62 Membrane properties of male WT vs FosB KO vHPC-NAc projections.	157
Figure 63 Spike frequency adaptation is decreased in male FosB KO vHPC-NAc projections.	158
Figure 64 Δ FosB regulates the cellular excitability of vHPC-NAc neurons in female mice.	159
Figure 65 Membrane properties of female WT vs FosB KO vHPC-NAc projections. ..	160
Figure 66 Spike frequency adaptation is decreased in female FosB KO vHPC-NAc projections.	161
Figure 67 FosB KO does not affect the cellular excitability of vHPC-BLA neurons in male mice.	164
Figure 68 Membrane properties of male WT vs FosB KO vHPC-BLA projections.	165
Figure 69 FosB KO does not affect the cellular excitability of vHPC-BLA neurons in female mice.	166

Figure 70 | Membrane properties of female WT vs FosB KO vHPC-BLA projections.. 167

I. INTRODUCTION

General Introduction to the Brain and Disease

The nervous system allows animals to perceive information from their surroundings and integrate this information to learn, think, feel, and act. The functional unit of the nervous system is the neuron¹, which individually and as a part of large network conveys information via the transmission of chemical and electrical signals. Neurons are extraordinarily diverse within the mammalian brain, with thousands of different classes of neurons intersecting functionally and structurally to drive behavior and cognition. Neuronal communication is accomplished through highly specialized areas of synaptic contact that function electrically via the flow of current or chemically via the release of neurotransmitters. The ultimate signaling mechanism of neurons and neuronal networks is the action potential: the generation of an electrical signal via the sufficient depolarization of the cell membrane following the movement of ions through selectively opened ion channels. Neurons have many forms of functional plasticity, including the ability to change the strength and number of synapses (synaptic plasticity) and to alter the conditions required for an action potential (intrinsic plasticity). Plasticity of individual neurons as well as that of circuits and other higher-level organizations is the foremost mechanism by which the brain grows and changes to accomplish complex tasks such as learning and memory; however, aberrancies in plasticity potentially contribute to disorders of the brain such as depression.

Neurons and supporting cells are organized within the brain into many functionally distinct structures and circuits. One such structure, the hippocampus, is a highly-

organized region classically understood to mediate learning and memory. The hippocampus is stress-sensitive and plastic, and is thus a substrate in the development of mood disorders, including major depression. Specifically, the connectivity of the hippocampus to other stress- and reward-related regions, particularly the nucleus accumbens, is directly causal of depressive-like behaviors in preclinical animal stress models². Additionally, the hippocampus has been characterized in depressed patients as being decreased in volume³, and fMRI studies have revealed less hippocampal activation in depressed patients when challenged with a recollection memory task⁴.

Psychiatric disorders continue to rise in prominence each year as a significant social and financial burden, with depression recently highlighted by the World Health Organization as the number one cause of disability globally⁵. Surprisingly, women have roughly twice the lifetime risk of men for experiencing depression⁶, but the reasons for this remain unknown. Many genetic and environmental factors, such as inherited traits, early life adversity, and societal inequities, intersect at the level of the individual to produce depressive disorders. One of the most important of these factors is neurophysiology, which itself is influenced by countless external and internal forces, such as hormone status, stress exposure, age, and many others. The neurophysiology of depression is difficult to study in humans, as direct study of the structure and function of neurons and circuits requires invasive or terminal procedures. Accordingly, the field has relied on animal models of depression, which utilize stress and behavioral assays to assess depressive-like symptoms, most prominently in rodents. While previous work in animals has been instrumental in defining some basic physiological mechanisms of depression, the bulk of mood disorder research has been done in males and as such has

only just begun to explore the etiology of sex differences in depression incidence. As our current body of knowledge regarding sex differences in depression is lacking, more preclinical studies must investigate neurophysiology, hormonal signaling, and other factors that intersect to produce these differences.

This introduction will outline the fundamental body of knowledge and relevant background studies that provide the foundation for this work. First, a review of current knowledge regarding major depression and preclinical stress models will provide significance and relevance to the experiments performed in this dissertation. Next, a summary of the anatomy and physiology of the major brain regions studied, the hippocampus and nucleus accumbens, will provide context for the focus of experiments on the connection between these two regions. Mechanisms of action potential generation with respect to intrinsic excitability and ion channel function in the hippocampus will then be outlined, followed by an introduction to the importance of neuronal steroid hormone signaling in the brain with respect to sex differences in stress and depression.

Major Depressive Disorder (MDD) and Preclinical Animal Models of Depression

Major depressive disorder (MDD), as currently characterized by the Diagnostic and Statistical Manual of Mental Disorders, 5th Edition (DSM-V), is a syndrome comprising a constellation of symptoms over at least a two-week period, with symptoms occurring for the majority of days and representing a departure from previous functional status⁷. One of the primary symptoms that must be present to warrant an MDD diagnosis is depressed mood and decreased interest or pleasure in most activities (anhedonia). Three or more of the following symptoms must also be present: fluctuations in weight and/or appetite,

sleep disruption (insomnia or hypersomnia), psychomotor disturbances, fatigue, feelings of worthlessness or guilt, difficulty in concentration, indecisiveness, and thoughts of death or suicidal ideation. The constellation of symptoms present in an individual must be disruptive to daily life, and may impair socialization or occupational functioning. Importantly, to be considered a diagnosis of MDD, the symptoms cannot be better explained by the effects of another condition (e.g. hypothyroidism) or substance (e.g. drugs of abuse). Major depressive symptoms can also be further complicated by the presence of a specifier; depression specifiers include anxiety, peripartum onset, or change in season.

Epidemiology and Disease Burden

Twelve-month prevalence of MDD in adults, according to the World Mental Health survey administered to nearly 90,000 persons across the globe, is estimated this decade at approximately 6%⁸. This survey also estimates that between one in five and one in six adults will experience MDD in their lifetime. Prevalence rates are similar in most countries regardless of economic status, with about 5.5% affected in countries classified as high-income and 5.9% in low-income countries. The difference between these country classifications is most apparent in availability and access to treatment, with about 50% of affected individuals in high-income countries receiving MDD treatment, compared to 10% or less of those in low-income countries⁹.

In terms of disability-adjusted life years (i.e., number of years of life lost due to poor health), it is estimated that MDD is the second highest contributor to disease burden globally¹⁰. The economic burden of MDD is striking: over \$200 billion in the United States

alone¹¹, with 38% of these costs attributed to MDD itself. Most of the cost, however, is due to conditions commonly comorbid with MDD such as heart disease, diabetes mellitus, cancer, obesity, and others. Meta-analysis of longitudinal studies of depression comorbidities has shown that the relative risk of developing these and other conditions is increased in MDD patients¹², a phenomenon attributed to the somatic effects of depression ranging from unhealthy lifestyle to complex physiological changes such as upregulation of stress-related immune and endocrine functions¹³.

MDD differences in men and women

One of the most striking statistics of MDD is that women are twice as likely to develop the disorder as men¹⁴. This sex difference does not seem to be due to frequency or length of major depressive episodes nor likelihood of recurrence in women, but due to a true difference in incidence¹⁵. Interestingly, when considering sex differences in MDD before puberty, boys are more likely to meet diagnostic criteria than girls¹⁶. The orientation of the difference in MDD prevalence begins to reverse at puberty, with female prevalence increasing to adulthood levels with each year of age post-puberty¹⁷. Symptom profiles also differ between men and women suffering depression: women are more likely to report “atypical” symptoms of increased appetite and sleep, and to experience more fatigue and pain¹⁸.

Psychiatry has offered many explanations for the elevated risk and prevalence of depression in women. Some have posited that the sex difference may be artificial due to women being more likely to seek treatment, or to depression in men being more difficult to recognize due to diagnostic criteria being biased towards female-specific depression

symptoms. However, epidemiological studies of the recall of mental health disorders over the lifetime revealed no gender bias in the recall of depression¹⁹. Studies of sex-specific depression symptoms have also shown that the various internalizing (e.g. social withdrawal, somatic disturbances) and externalizing (e.g. substance abuse, attention problems) symptoms of depression do not differ significantly between men and women²⁰. As such, the sex difference in depression prevalence is likely not an artefact of diagnostic bias; rather, the field must look to other physiological and environmental factors to explain this phenomenon.

Sex differences in depression rates may arise in part due to specific biological and environmental risk factors experienced by men and women²¹. Twin studies suggest that MDD carries approximately 37% heritability²², and genome-wide association studies (GWAS) have uncovered a wide variety of potential heritable genetic loci that can contribute to depression pathogenesis²³. Hormonal influences can also affect individual susceptibility to MDD, with evidence supporting hormone fluctuation as one factor that increases MDD risk in women²⁴ (discussed further below). Differential activation of the HPA axis in men and women has also been implicated in the pathogenesis of MDD, as women experience hypoactivation of HPA hormone stress responses that, evolutionarily, may protect a fetus from the effects of maternal stress²⁵. This hypoactivation, however, may deprive women of the possible protective effects of cortisol on depression-related changes to emotional brain circuitry²⁶. Many environmental factors, especially during development, can also affect gender disparities in MDD development. For example, gender-based violence, such as domestic violence, rape, and sex trafficking, is more commonly experienced by women²⁷. Early life adversity rates are generally equal in girls

and boys, but girls are more likely to be victims of child sexual abuse, which can contribute to myriad perturbations of neurological development²⁸. Gender discrimination in the workplace, for example the wage gap between men and women, can also contribute to sex differences in MDD rates²⁹. While not an exhaustive list, these biological and environmental risk factors, along with many others, begin to outline the complexity and heterogeneity of mood disorder etiology. Recognition of these factors, taken together with the neurophysiological bases for depression in this and other basic science studies, inform our understanding of individual variations in MDD experience.

Preclinical Animal Models of Depression

As mentioned above, it is difficult to study the basis of mood disorders in humans due to the invasive nature of many procedures that investigate the physiology of the brain. Therefore, we must rely on animal models, which are most effective when they exhibit high validity³⁰. To study a complex human disease like MDD, the model's behavioral phenotype must resemble the clinical symptom(s) (face validity). These symptoms must also be responsive to clinically effective treatments (e.g. antidepressants) and non-responsive to clinically ineffective treatments (predictive validity). The model phenotype must also have similar physiological bases (construct validity) and triggers (etiological validity) to the human disorder. As MDD symptoms vary from case to case, and often symptoms may be opposite in some individuals (e.g. insomnia vs. hypersomnia), establishing reliable animal models has been challenging. As depression also occurs episodically, it is difficult to create a model by manipulating genetics as this causes congenital abnormalities of behavior that do not fully resemble the human condition. Many

traditional genetic models based on theories of depression pathophysiology exist, such as the corticotropin-releasing hormone receptor knockout model³¹. These are problematic, however, as they often focus on only one potentially involved molecule, when many molecular pathways are known to be involved in depression pathogenesis. Neuronal activity-based optogenetic techniques have also been used to model depression, and are advantageous as they are able to consider circuit-level mechanisms of psychiatric disease³². Optogenetic techniques have demonstrated face and construct validities, but are relatively expensive and difficult to achieve. As such, depression research has largely focused on stress models, many of which have achieved high levels of face, construct, etiological, and in many cases, predictive validity.

Stress, along with other environmental factors, can be very influential on the highly plastic circuitry of the brain. A stressful circumstance can activate many systems and circuits in the brain that attempt to maintain the animal's homeostasis, such as the hypothalamic-pituitary-adrenal (HPA) system. Stress responses in the brain target many limbic brain regions, including the hippocampus and nucleus accumbens, as well as many others such as the prefrontal cortex and amygdala. Changes in activity or connectivity in the brain in response to an initial stressful scenario can alter many functional processes (e.g. learning, memory), resulting in an adaptation that better prepares the animal for future stressful events³³. However, when stress is chronic or traumatic, these changes can also coalesce to cause maladaptation to stress with accompanying susceptibility to depression or anxiety, as well as other somatic disorders such as heart disease. Vulnerability to stress and subsequent maladaptation vary from individual to individual, with some individuals maintaining physiological and psychological function even in the

face of stress, while others may suffer any number of pathologies in response to the same stress. Those that do not experience maladaptive stress response are considered resilient, and those that develop depression or other conditions in response to stress are susceptible. Gene expression profiling of resilient and susceptible rodents has revealed that resilience may be an active mechanism (i.e., not simply due to the “absence” of susceptibility): more genes are uniquely regulated in resilient individuals compared to non-stressed controls than are in susceptible individuals³⁴. Two major stress paradigms modeling human depression, chronic social defeat stress (CSDS) and subchronic variable stress (SCVS), are discussed below.

Many life events, such as divorce, moving to a new city, or suffering an illness represent significant stressors and as such can precipitate the onset or recurrence of depression³⁵. Many life stressors in humans involve social factors (e.g. job loss leading to loss of income) that can lead to loss of social rank or loss of control over one’s life circumstances. To mimic these social stressors in humans, rodent models of depression have utilized social defeat to study environmental perturbations that a mouse or rat might face. These perturbations may cause loss of control of the social situation, and in susceptible rodents, lead to the development of depression-like behaviors.

CSDS (Figure 1, left) utilizes a resident-intruder paradigm, in which a male mouse (intruder) is placed into the home cage of another male mouse (resident), usually of a different strain (e.g. a small brown C57BL/6 mouse is placed into the home cage of a larger, white-coated CD-1 mouse). The intruder (experimental) mouse is quickly attacked by the resident (aggressor); bouts of aggressive attack on the experimental mouse are allowed to continue for up to 10 minutes of physical stress. The experimental mouse is

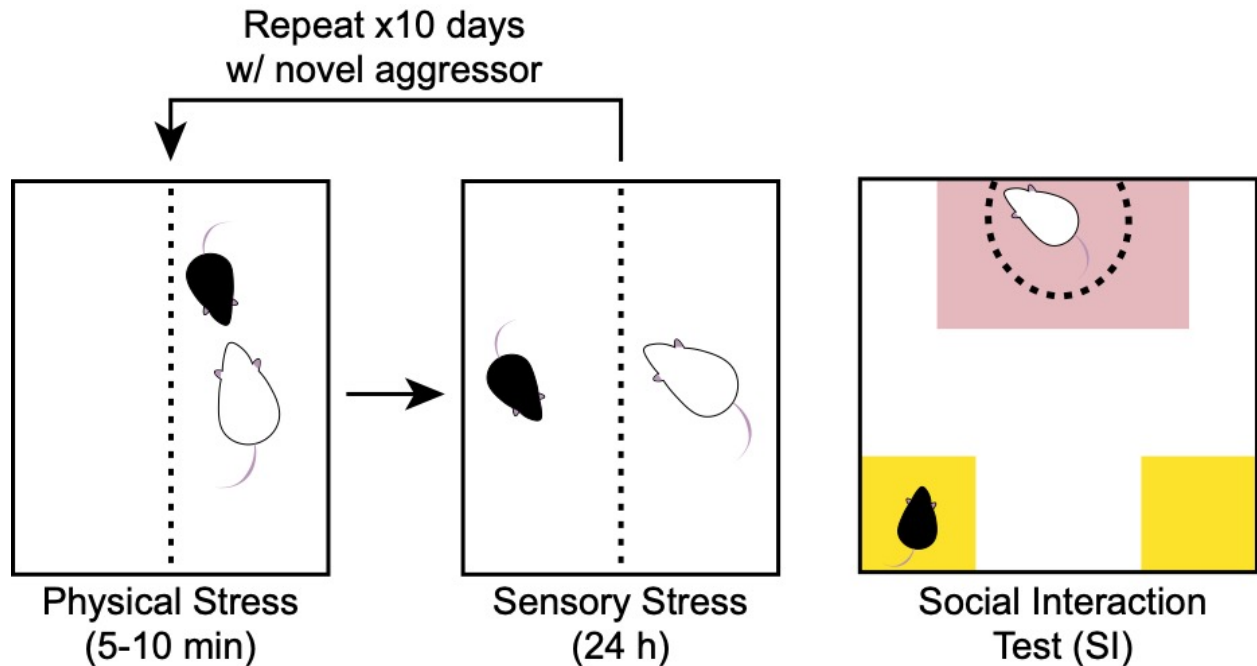


Figure 1 | Chronic social defeat stress and social interaction test.

Resident aggressor mice (e.g. CD-1) are singly housed in cages for several days prior to testing to establish territory. The experimental intruder mouse (e.g. C57BL/6) is placed into the home cage of the aggressor and the two mice interact for 5-10 minutes (Physical Stress, left). Typically, the experimental mouse is quickly attacked by the aggressor mouse, and these attacks continue throughout the duration of the physical stress period. The experimental mouse is then moved to the other side of a perforated divider where it is safe from further attack, but can still see, hear, and smell the aggressor (Sensory Stress, middle). The experimental mouse is housed here for 24 hours. The cycle then repeats for 10 or more days with the experimental mouse exposed to a novel aggressor mouse each day. Social interaction (SI) testing (right) is used following the chronic stress to evaluate social withdrawal as a measure of stress susceptibility. Susceptible mice exhibit social withdrawal and spend less time in the interaction zone (red) with the social target, and more time in the corners (yellow), withdrawn and isolated.

then moved to the other side of a perforated divider to be protected from further attack (Figure 1, middle). The divider, however, allows for the experimental mouse to see, smell, and hear the aggressor mouse; this separated co-habitation lasts 24 hours as a form of sensory stress. This combination of physical and sensory stress repeats for 10 or more days, with the experimental mouse exposed to a novel aggressor each day³⁶. Evaluation of susceptibility to CSDS is typically achieved through the social interaction (SI) test (Figure 1, right), in which the experimental mouse is placed into an arena containing a novel aggressor mouse (social target) in a caged enclosure. The experimental mouse is free to roam the arena and interact with the social target. Social withdrawal behavior is quantified by calculation of a social interaction ratio: the time spent in the interaction zone (red) near the social target over the time spent away from the social target in the rest of the arena and in the corners (yellow). The time spent in the corners by the experimental mouse is also indicative of social withdrawal, as susceptible mice are more likely to “hide” in the corners, the most isolated portions of the arena and furthest away from the social target. In contrast, resilient mice are eager to interact with the social target, as this interaction is rewarding.

In addition to exhibiting social withdrawal, susceptible mice also show many other depression-like behaviors³⁴. Compared to non-stressed controls, susceptible mice show a significant decrease in body weight. They also demonstrate a reduction in sucrose preference, which is a measure of anhedonia (loss of interest in activities one previously found rewarding)³⁷. Additionally, only susceptible mice demonstrate conditioned place preference (CPP) for low-dose cocaine, which is indicative of sensitization to drug reward. While only susceptible mice demonstrate these changes in reward-related behavior, both

resilient and susceptible groups experience anxiety, as measured by elevated corticosterone responses to forced swim test (FST) as well as decreased open arm time in the elevated plus maze (EPM).

The predictive validity of CSDS has been verified by experiments utilizing standard human antidepressant treatments^{38,39}. Treatment of defeated (susceptible) animals with one of the two pharmacologically distinct antidepressants imipramine and fluoxetine reduced the social withdrawal behavior caused by CSDS. Importantly, chronic administration of the antidepressant was required, as an acute injection with the drug did not reverse the withdrawal behavior³⁸. Interestingly, this study also demonstrated that the reversal of social withdrawal is specific to antidepressant drugs, as chlordiazepoxide (used to treat anxiety, but not depression) did not alleviate the stress-induced withdrawal behavior. The relationship between CSDS and the vHPC-NAc circuit is discussed in an upcoming section of this introduction entitled “vHPC-NAc Connectivity.”

Subchronic Variable Stress (SCVS)

One of the major limitations of CSDS is that, in the resident-intruder paradigm, it relies on the intrasexual aggression between two conspecific males. As a male mouse will not attack a female intruder due primarily to her status as a potential mate, and intrasexual aggression does not typically occur in females of commonly used laboratory mouse species, it is difficult to include the study of female subjects in traditional social defeat experiments. As such, depression research has suffered a lack of the study of depression in females until recently⁴⁰. One solution to this issue is to use a stress model that does not rely upon aggression between individuals. One such paradigm is subchronic

variable stress (SCVS), in which only female subjects are subsequently susceptible to depression-like behaviors. SCVS comprises six days of alternating stressors: foot shock, tail suspension, and restraint (Figure 2, top). Following stress, mice are then assessed for depression-like changes in behavior using a variety of assays: sucrose preference in two-bottle choice task, SI, EPM, novelty-suppressed feeding (NSF) test, and splash test (Figure 2, bottom). In one of the first studies to utilize SCVS as an assessment of sex differences in stress outcomes, Hodes et al discovered that only female mice are susceptible to this subchronic battery of stressors⁴¹. Specifically, female mice spent less time grooming in the splash test following SCVS than male mice or unstressed female mice, indicating a reduced motivation for self-care. Female mice also displayed increased latency to eat in a novel environment, indicating an increase in anxiety induced by the stress of a novel environment. Sucrose preference, a key measure of anhedonia (loss of motivation to consume a rewarding sucrose solution), was also reduced exclusively in stressed female mice. This study also highlighted an increased corticosterone in stressed female mice only, indicating dysregulation of the HPA axis. Female mice did not differ from male mice or unstressed control females in EPM measures, indicating no change in exploratory behavior induced by anxiety. SCVS represents a useful stress model of depression that is distinct in that only females exhibit depression-like behaviors following its stress battery. This sex difference and its etiology are further discussed throughout this introduction.

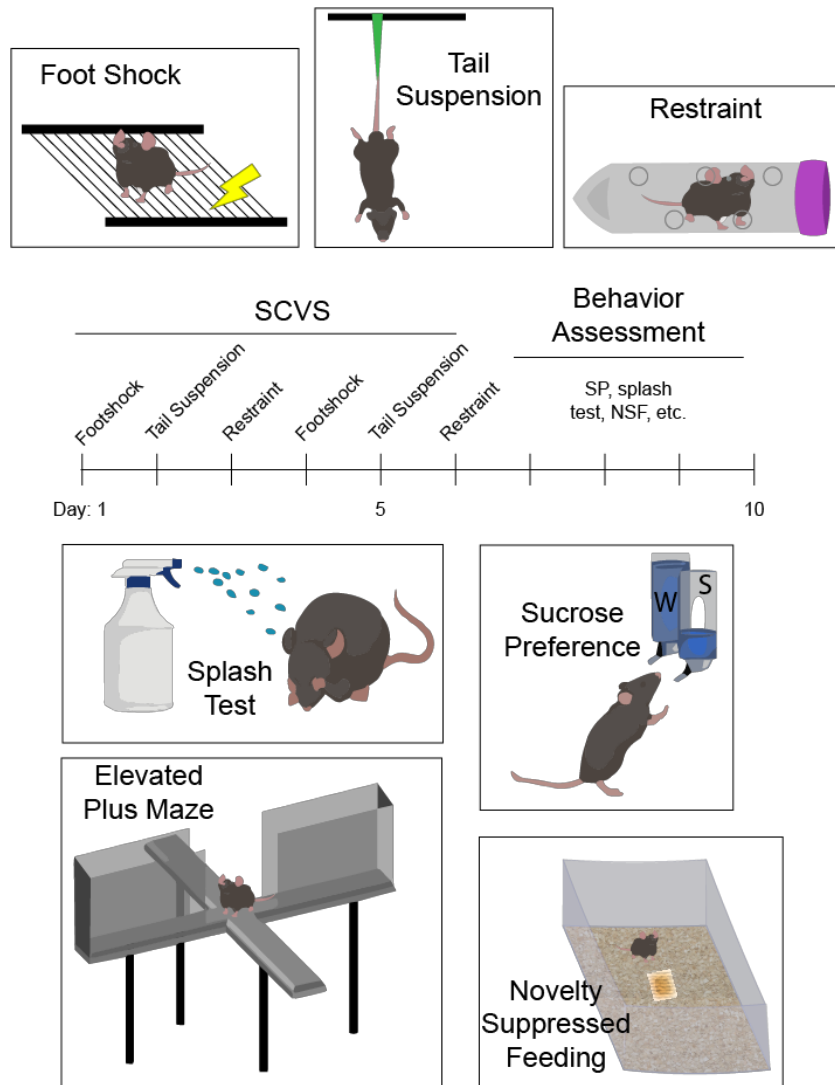


Figure 2 | Subchronic variable stress (SCVS) and associated behavioral assays.

SCVS comprises a 6-day battery of repeated stressors (top): foot shock, tail suspension, and restraint stress. Each stress session typically lasts 1 hour per day. Following the stress period, a variety of behavioral assays are used to assess stress susceptibility (bottom): splash test, sucrose preference, elevated plus maze (EPM), novelty suppressed feeding (NSF), and social interaction (SI, not pictured). Splash test measures grooming behavior, with susceptible animals showing reduced grooming time when sprayed with a sticky solution. Sucrose preference indicates anhedonic response with two-bottle choice task, with susceptible animals showing no preference for sucrose drinking solution. EPM measures anxiety response, with “anxious” animals spending less time in open arms and more time in closed arms of the apparatus. Novelty suppressed feeding represents a more subtle measure of anxiety, with “anxious” animals exhibiting increased latency to eat (following overnight food deprivation) in a novel environment.

Sex differences in stress responses

It is clear from the female-specific susceptibility in the SCVS paradigm that sex differences in stress response exist. These differences may account for the disproportionate number of women diagnosed with depression compared to men. Studies of stress responses in animal models of depression have revealed myriad sex differences, including differences in cellular and hormonal responses, brain circuits, synaptic and intrinsic plasticity, cognition, and emotional processing.

The HPA axis has long been recognized as a central component of stress responses in humans, and in particular, of the pathophysiology of anxiety and depression. Corticotropin-releasing factor (CRF) is the hormonal initiator of the HPA response. Neurons in the paraventricular nucleus of the hypothalamus (PVN) release CRF in response to stress, which reaches the pituitary and stimulates the release of adrenocorticotrophic hormone (ACTH) into the systemic circulation, stimulating glucocorticoid release from the adrenal glands (Figure 3); the PVN is known to receive negative feedback regulation from the HPC and other limbic structures⁴². CRF also acts at the level of individual neurons via CRF receptors⁴³, and is released from the emotion-regulating limbic regions such as the bed nucleus of the stria terminalis (BNST) and central nucleus of the amygdala (CeA)⁴⁴ and can act throughout the brain as a neuromodulator. Indeed, CRF is elevated in cerebrospinal fluid of depressed humans⁴⁵ and antidepressant pharmacotherapies are known to decrease these levels^{46,47}. CRF₁ receptor expression is also disturbed in many areas of the brain in depressed patients, including an increase in PVN⁴⁸ and possible compensatory decreases in cortical regions⁴⁹. Generally, HPA axis hormones (e.g. corticosterone) are known to be elevated

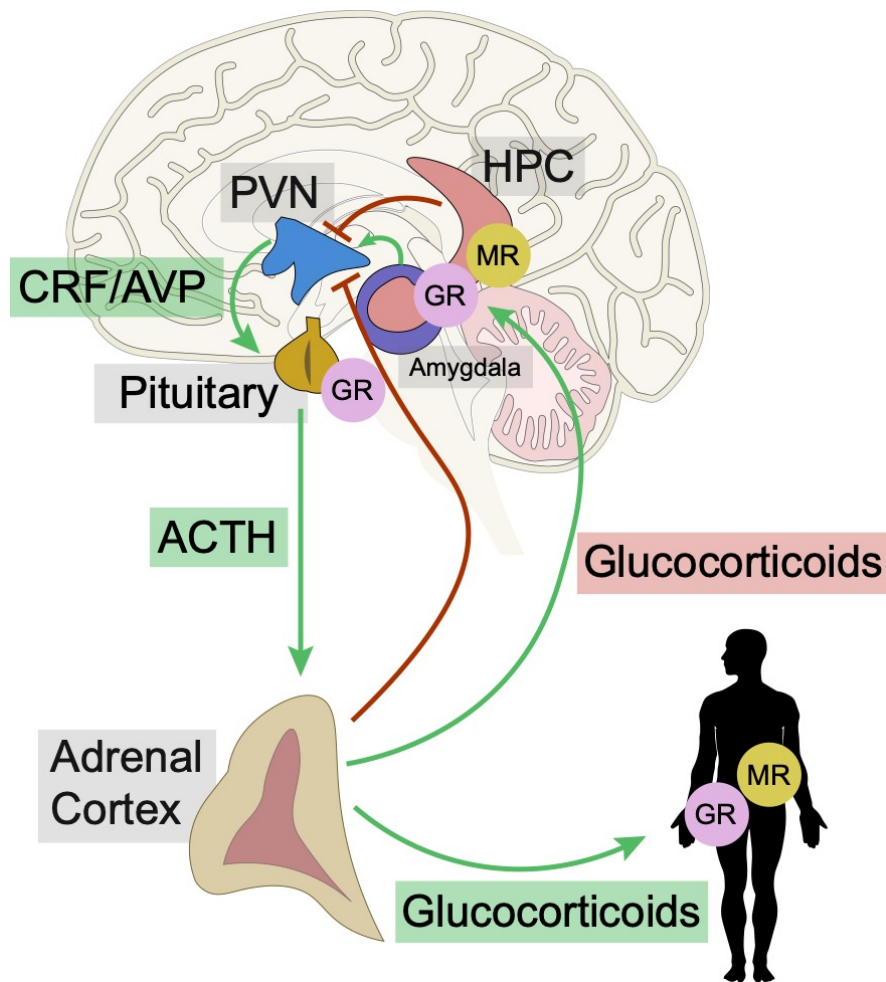


Figure 3 | Hypothalamic-pituitary-adrenal (HPA) axis and hippocampal negative feedback regulation.

The hypothalamic-pituitary-adrenal (HPA) axis is activated by stress and integrates stress responses. Anxiety responses via activation of the amygdala can exacerbate the stress response through its projections to the paraventricular nucleus of the hypothalamus (PVN). The hippocampus (HPC) is important for the evaluation of stress and is a site of glucocorticoid receptor (GR)-mediated negative feedback to the PVN. Release of the neuropeptides corticotrophin-releasing hormone (CRH) and arginine vasopressin (AVP) from the hypothalamus promotes the release of adrenocorticotrophin (ACTH) from the pituitary. ACTH then stimulates the release of glucocorticoids from the adrenal cortices. These hormones circulate to the body and brain and bind to intracellular steroid hormone receptors.

in female rodents compared to males at baseline⁵⁰. Female rodents, when stressed, release more ACTH and corticosterone than males and elevated levels also persist longer^{51,52}. These sex differences in rodents appear to reflect increased activation of the HPA system by CRF in females. PVN expression of CRF appears to be elevated in females at baseline, particularly when estrogen levels are high (i.e. proestrus stage). Furthermore, early life and footshock stresses increase CRF in female rodents only^{53,54}. Sex differences in epigenetic regulation of CRF have also recently been demonstrated, with elevated methylation of *Crf* gene globally in the brain of female rats, but only in BNST and CeA in male rats⁵⁵. Particularly interesting to the current dissertation study is the differential expression of CRF₁ receptors in the CA1 region of the hippocampus. Female rats, especially with elevated estrogen levels, have an elevated CRF₁ receptor expression on pyramidal cells of the CA1 region⁵⁶; however, males have higher CRF₁ receptor expression on inhibitory interneurons in the DG. The same study demonstrated that CRF₁ receptor expression does increase in CA1 pyramidal cells in male and female rodents following chronic immobilization stress (CIS), but male levels do not even reach the female baseline expression level. The higher CRF₁ expression level on CA1 pyramidal cells in the hippocampus represents one mechanism by which females may be more sensitive to stress. Collectively, these studies indicate that increased CRF signaling in females can differentially influence the HPA axis and central neuromodulation, contributing to observed sex differences in stress outcomes⁵⁷.

In addition to the vHPC-NAc circuit discussed below and investigated in the current work, a variety of other circuits are implicated in mediating sex differences in stress responses. The connection between the medial prefrontal cortex (mPFC) and amygdala

is of particular interest, as the amygdala regulates responses to negative and traumatic stimuli⁵⁸ and the mPFC regulates a wide range of functions including cognition and determination of affect⁵⁹. Together, these brain regions play a significant role in generating behavioral responses to emotionally relevant contexts⁶⁰. Indeed, mood disorders including MDD have been correlated with overactivity in the amygdala⁶¹, as well as decreased mPFC activity⁶². Regarding stress models of depression, chronic restraint stress in rodents causes restructuring and reorganization of dendrites in pyramidal cells of mPFC, which is posited to decrease the region's ability to suppress HPA activation⁶³. Chronic stress has also been found to cause hyperexcitability⁶⁴ and increased dendritic arborization⁶⁵ in rat basolateral amygdala (BLA) neurons. As such, the mPFC-amygdala circuit is of interest in the exploration of sex differences in stress response. Shansky et al demonstrated sensitivity of BLA-projecting mPFC neurons to stress in estrogen-treated, ovariectomized female rats, with only this group experiencing an increase in dendritic arborization in these cells⁶⁶.

Preclinical animal studies of depression have also highlighted sex differences in locus coeruleus (LC) norepinephrine (NE) circuitry⁶⁷. Dendritic architecture of LC neurons in female rats has been shown to be more complex than in males, with LC dendrites receiving significantly more synaptic input⁶⁸. Moreover, tonic and phasic firing patterns are linked to changes in arousal, and, while not significantly different at baseline, male and female changes in LC neuron firing were found to differ following swim stress in rats⁶⁹. Specifically, female rat LC NE neurons were found to have a greater increase in firing than those of male rats, indicating heightened sensitivity to stress. Taken together, these findings identify the LC NE circuitry as a key substrate in the mediation of sex differences

in arousal, which may contribute to differences in male and female stress response and development of psychiatric disorders such as MDD. However, the remainder of this introduction will focus on the HPC, NAc, and their connectivity in the context of stress with special attention to sex differences.

The Hippocampus

The hippocampus is a medial temporal region of the brain long-known to be necessary for memory^{70,71} and spatial reasoning⁷². The hippocampus, named due to its resemblance to a seahorse, is a long, C-shaped, bilateral brain region that is typically described along a dorsal-ventral (septotemporal) axis in rodents (corresponding to posterior-anterior axis in humans). In rodents, the hippocampus spans the distance between the neocortex and diencephalon and curves ventrally adjacent to the temporal lobe. The hippocampal formation is made up of four regions: the dentate gyrus (DG), the hippocampus proper (CA1, CA2, and CA3), the subicular complex, and the entorhinal cortex (Figure 4). The primary inputs to the hippocampus extend from the entorhinal cortex to the DG via the perforant pathway (blue)⁷³. The body of the hippocampus, or the hippocampus proper, shares efferent and afferent connections with many cortical and subcortical regions (green)⁷⁴. The hippocampus proper is made up of the *cornu ammonis* (CA) regions, with the CA3 receiving input from DG granule cells via mossy fiber tracts. CA3 pyramidal cell axons (Schaffer collaterals) then project to the CA1 region, which then projects to the entorhinal cortex and the subiculum, as well as many other brain regions, including the nucleus accumbens (NAc) and basolateral amygdala (BLA) via the fornix. The CA2 region is small and lies between CA3 and CA1, and receives some input from

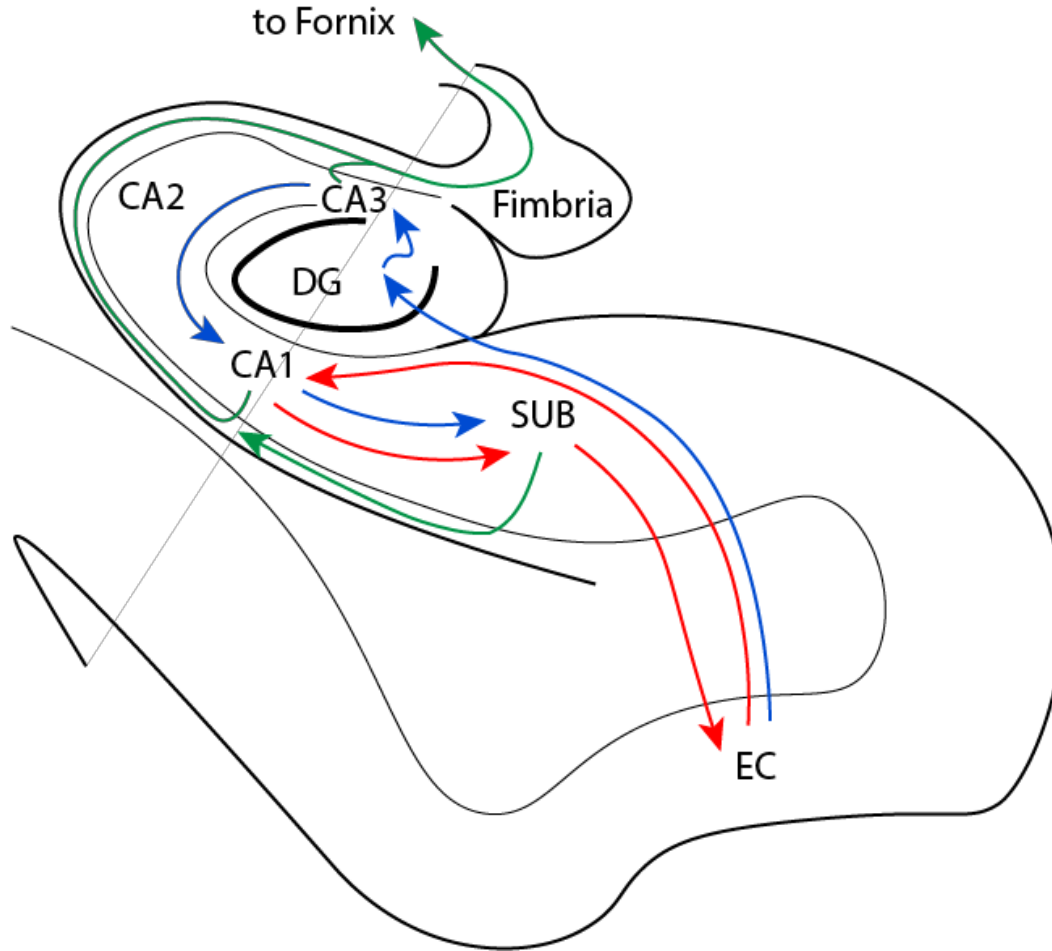


Figure 4 | Information pathways of the hippocampus.

The red arrows represent the direct internal hippocampal pathway of information flow from the entorhinal cortex (EC) Layer III to CA1 to the subiculum (SUB). The green arrows represent the primary output projections of the hippocampus: SUB sends fibers back to EC or to the fimbria via the alveus (white matter outer layer of hippocampus). The main output region of the hippocampus is the CA1, which send fibers through alveus. The alveus fibers merge to form the fimbria, which eventually becomes the fornix through which the hippocampus sends projections to outside regions such as the nucleus accumbens (NAc). The blue arrows represent the canonical trisynaptic loop: the EC sends fibers to the dentate gyrus (DG) via the perforant pathway (synapse 1), the DG then projects to CA3 via the mossy fiber tracts (synapse 2), and the CA3 then sends fibers to the CA1 via Schaffer collaterals (synapse 3). The subiculum is also included in this circuit as it receives input from CA1.

the entorhinal cortex perforant pathway. The entorhinal cortex → DG → CA3 → CA1 series of synaptic transmission is known as the trisynaptic loop, first described by Santiago Ramon y Cajal⁷⁵ in his seminal Golgi staining neuroanatomy work. Other internal hippocampal pathways of information flow have also been observed, for example EC → CA1 → SUB → EC (red).

Distinctive Dorsal and Ventral HPC Functions

As mentioned above, the hippocampus is classically recognized as a key memory center, as exemplified by the case of H.M., who experienced severe amnesia after bilateral medial temporal lobectomy (including removal of both hippocampi) in a radical attempt to cure his intractable epilepsy⁷⁰. The hippocampus was later identified as critical for the processing of spatial memory in navigation tasks, as “place cells” within the hippocampus fire at specific locations within an experimental arena⁷⁶. Furthermore, rats with bilateral hippocampal lesions are incapable of navigation relying only upon spatial cues in the Morris water maze⁷². Functional imaging studies in humans also confirmed the importance of the hippocampus in visual and verbal information coding and memory^{77,78}.

Intrahippocampal connectivity remains largely conserved along the dorsal-ventral (septotemporal) plane⁷⁹, but connections to (afferent) and from (efferent) the hippocampal formation differ, suggesting the dorsal and ventral hippocampus (dHPC and vHPC, respectively) have distinct functions. Another key difference between these two subdivisions of the hippocampus is their intrinsic excitability: vHPC CA1 neurons are hyperexcitable compared to their dHPC counterparts⁸⁰. This is likely due to differential ion

channel expression and unbalanced excitatory and inhibitory inputs⁸¹, further discussed later in this introduction.

As the connections within the entorhinal cortex, the major informational relay that sends projections to the hippocampus proper, are topographically organized, dHPC receives information from sensory cortical regions (visual, auditory, somatosensory) that is distinct from vHPC input. Lesions of dHPC, but not vHPC, result in impaired maze learning⁸² proportional to the severity of the lesion⁸³. These and other related studies demonstrate the unique necessity of the dHPC for spatial learning, further supported by the majority of “place cells” being located in dHPC⁸⁴. The vHPC has more extensive efferent connections with major forebrain structures than dHPC, including the hypothalamus and the amygdala^{74,85}, and as discussed extensively in this work, the NAc. Due to its associations with these and other regions, the vHPC distinguishes itself from the dHPC in its involvement in mediating stress responses, emotion, and anxiety- and depression-related behaviors. While the vHPC does have some role in spatial learning and memory in unison with dHPC function⁸⁶, the vHPC is uniquely suited to influence emotional processing, physiological and behavioral stress responses, and motivation. Strict lesions of the vHPC reduce fear and anxiety behaviors^{87,88} and increase conditioned place preference for food⁸⁸. Ventral HPC function regarding the mediation of stress outcomes and depression is discussed in more detail throughout this introduction.

Anterograde and retrograde tracing studies have demonstrated extremely diverse targets of CA1 projections⁸⁹, with, as alluded to above, projection areas differing based on location of cell bodies along the CA1 septotemporal axis. The temporal (ventral) CA1 has unique projections compared to the septal (dorsal) and splenial (middle) CA1

divisions, with outputs to the subiculum/parasubicular area, entorhinal cortex, anterior olfactory nucleus, and olfactory bulb. Many subcortical regions also receive projections from the ventral CA1, including the amygdala, hypothalamus, lateral septal nucleus, and NAc. Interestingly, the anterograde labeling studies in question did not highlight the labeling of any commissural axons, indicating that the ventral CA1 region likely sends its projections to the ipsilateral hemisphere. Van Groen and Wyss⁸⁹ describe a great number of projection axons traveling to the septum via the fornix, where they split into three groups to project to the lateral septal nucleus and the nearby NAc, a number of cortical regions, and the hypothalamus.

Neurotransmitters of the HPC – Implications in Mood disorders

A wide range of neurotransmitters (NTs) and their receptors can be found in the hippocampus, with the most prominent being glutamate, γ -amino butyric acid (GABA), norepinephrine (NE), serotonin (5-HT), and acetylcholine (ACh). Synaptic transmission in the hippocampus happens in the classically understood sense: upon sufficient influx of calcium generated by the propagation of an AP down the axon, NTs are released from the presynaptic terminal and diffuse through the synaptic cleft to reach receptors on the postsynaptic membrane. In addition to postsynaptic receptors, presynaptic autoreceptors for many NTs (e.g. ACh, GABA, and 5-HT) can also serve to regulate the activity of NTs via feedback modulation⁹⁰. A diagram of the diverse circuitry implicated in depression, including inputs to and from the HPC and reward circuitry, can be found in Figure 5.

The main excitatory neurotransmitter in the brain is the amino acid glutamate, and the majority of the brain functions as a “glutamatergic excitatory machine”⁹¹, as evidenced

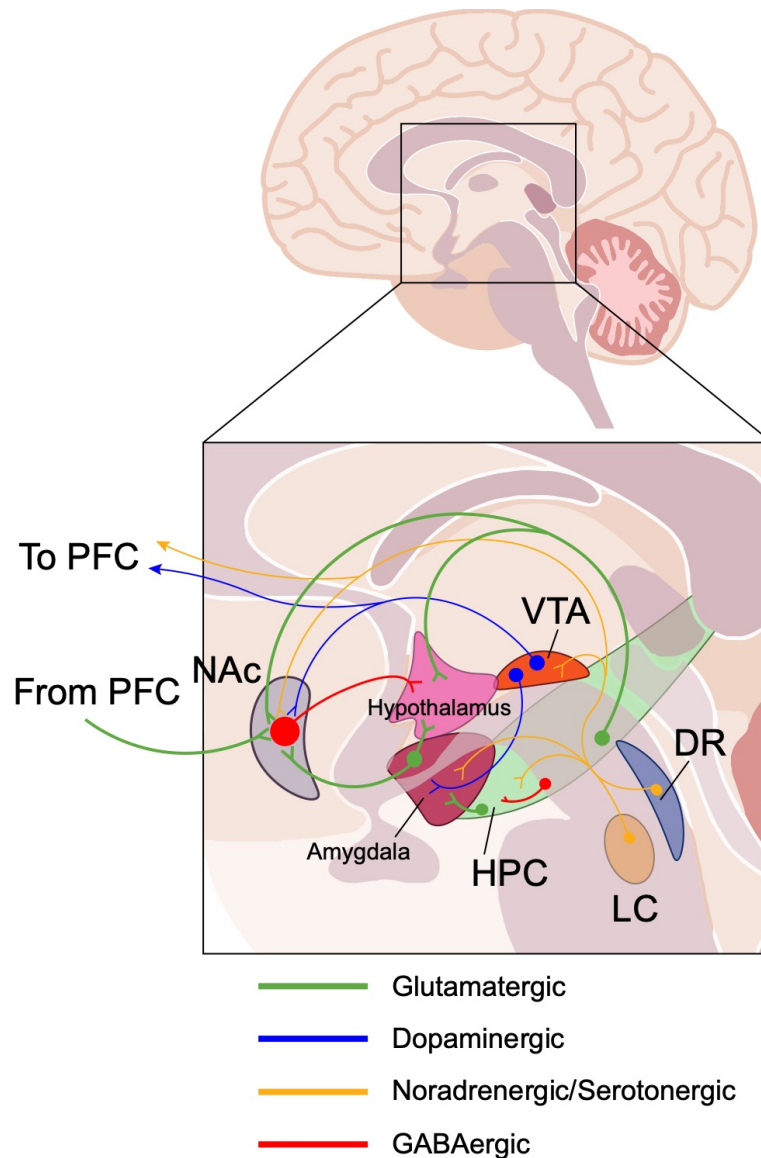


Figure 5 | Depression and reward circuitry.

A simplified summary of neural circuits that have been implicated in the pathophysiology of depression. The glutamatergic projections of the hippocampus (HPC) and prefrontal cortex (PFC) are prominently featured, and many subcortical regions that mediate reward, fear, and motivation are also involved: nucleus accumbens (NAc), amygdala, and hypothalamus. This diagram also shows the innervation of many regions by monoaminergic projections from the ventral tegmental area (VTA) (dopaminergic input to NAc, amygdala, PFC) and other structures: noradrenergic projections from the locus coeruleus (LC) and serotonergic projections from the dorsal raphe (DR). The NAc also sends GABAergic projections to the hypothalamus, and GABAergic interneurons are found within the HPC. This diagram, while not exhaustive, highlights some of the major circuits involved in depression and referenced throughout this dissertation.

by the fact that up to 85% of synapses in the neocortex are excitatory⁹². Receptors for glutamate can be either ionotropic or metabotropic, with the ionotropic receptors mediating fast excitatory neurotransmission while the metabotropic receptors permitting more prolonged stimuli⁹³. The ionotropic glutamate receptors (iGluRs) are classified by their responses to synthetic agonists N-methyl-D-aspartate (NMDA) or α -amino-3-hydroxy-5-methyl-4-isoxazole propionate (AMPA), or the naturally occurring kainate; all three iGluRs are found throughout the hippocampus. AMPA receptors are formed by different combinations of four different subunits (GluA1, 2, 3, and 4), and can be further diversified by alternative splicing (in all subunits) and editing of introns in their primary transcripts (specific to GluA2). AMPA receptors are primarily permeable to monovalent cations (i.e. Na^+ and K^+) and Ca^{2+} , but become impermeable to Ca^{2+} if they contain the edited form of the GluA2 subunit (containing an arginine in place of a glutamine at the Q/R editing site). The arginine in the edited form of the GluA2 subunit presents a positively-charged side chain in the channel and hence blocks the passage of the larger, divalent Ca^{2+} . Furthermore, all AMPA receptor subunits can undergo alternative splicing to form “flip” or “flop” isoforms. Flip isoform-containing receptors allow more inward current to pass than those that contain only flop isoform subunits. Kainate receptors are tetramers formed by combinations of subunits GluA5, 6, 7 and KA1, and 2. GluA5 and 6, much like the GluA2 subunit of AMPA receptors, are subject to editing, and the GluA5, 6 and 7 subunits can undergo alternative splicing to alter their conductances. As the sequences of these subunits are similar to AMPA receptor subunits, kainate receptors are permeable to cations. Editing of GluR5 or 6 accordingly changes the Ca^{2+} permeability of a given kainate receptor.

NMDA receptors represent heteromeric complexes formed by combinations of GluN1, GluN2B, GluN2A-D, and GluN3A and B subunits that bind glycine and glutamate. NMDA receptors are blocked by Mg^{2+} at voltages near the resting membrane potential of the neuron, and, when the Mg^{2+} block is released by AMPA-mediated depolarization, they are highly permeable to monovalent cations and Ca^{2+} . Glycine binding at the GluN1 subunit potentiates the NMDA response by increasing frequency of its channel opening; glycine binding is required for full activation of the NMDA receptor by glutamate binding at the GluN2A-D subunits.

When synaptic glutamate diffuses to the postsynaptic membrane of a neuron at rest, it binds to AMPA and NMDA receptors. Inward current through AMPA receptors, the major driver of excitatory postsynaptic current (EPSC), causes an evoked postsynaptic excitatory potential (EPSP). Depolarizing currents, if strong enough, allow the release of the Mg^{2+} blockade of NMDA channels and further membrane depolarization. The further membrane depolarization allows for unblocking of additional NMDA receptors. Ca^{2+} entry through unblocked NMDA channels increases intracellular Ca^{2+} concentrations, leading to an increase in the function of Ca^{2+} -dependent processes.

One such process is long-term potentiation (LTP), which represents a persistent increase in synaptic strength⁹⁴. First described by Bliss and Lomo in the rabbit hippocampus⁹⁵, LTP is a process that occurs frequently at the excitatory glutamatergic synapses of dendritic spines of postsynaptic CA1 pyramidal cells and, in part, mediates the plasticity required for learning and memory. In brief, CA1 LTP strengthens synapses by increasing the depolarization at the postsynaptic cell caused by a given presynaptic release of glutamate (i.e., the postsynaptic cell can reach the threshold for AP generation

with a lesser stimulus; verified by the increase in response to glutamate receptor agonists following LTP⁹⁶). This is accomplished by increased postsynaptic Ca²⁺ influx via NMDA channels, which activates adenylyl cyclase (AC). AC acts to produce cyclic AMP (cAMP), which in turn activates protein kinase A (PKA). PKA phosphorylates a variety of postsynaptic mediators, including Ca²⁺/calmodulin-dependent kinase II (CaMKII). CaMKII drives LTP by facilitating AMPA receptor trafficking to the postsynaptic membrane and subsequent exocytosis⁹⁷, as well as phosphorylating AMPAR GluA1 subunits, increasing AMPAR conductance⁹⁸. It is important to note that LTP at other synapses (e.g., not CA3-CA1) may involve many different or additional mechanisms, including presynaptic components⁹⁹. CA1 LTP and its importance in mediating stress responses in preclinical models of MDD is further discussed in later sections of this introduction.

Chronic stress, used in preclinical animal models to mimic human depression pathologies, has been associated with atrophy of HPC pyramidal neuron apical dendrites, the main site of excitatory glutamatergic synapses, as well as reductions in number and size of dendritic spines^{100,101}. Chronic stress impairs LTP¹⁰² at synapses from Schaffer collateral projections from CA3 to CA1 and reduce GluA1 transcripts in CA1 pyramidal neurons¹⁰³. Schmidt et al further investigated the behavioral phenotypes following chronic social stress, and found that susceptible mice displayed a decreased GluA1/GluA2 AMPA subunit ratio in CA1 compared to resilient mice; susceptibility was predictable based on performance in a short-term memory, a CA1 AMPAR-mediated task. CA1 synapses from EC are also affected by stress: chronic unpredictable stress (CUS) has been shown to significantly reduce AMPAR-mediated excitation at these synapses, an effect that resulted in sucrose preference reduction¹⁰⁴. This study further demonstrated that the

change in excitation at EC-CA1 synapses as well as the sucrose preference reduction were reversed by chronic fluoxetine treatment. Additionally, Chourbaji et al showed that GluA1 knockout mice exhibit a depression-like phenotype as indicated by increased learned helplessness¹⁰⁵. These studies suggest that glutamatergic transmission at the level of CA1 pyramidal neurons is directly influenced by chronic stress, and that changes in excitatory signaling at these neurons can influence depression-like behaviors in mouse models of depression. Excitatory output from the HPC in the form of glutamatergic afferents to areas such as the NAc also have great influence over stress responses and the development of depression-like behaviors; this output is further discussed below with focus on vHPC connectivity to NAc.

In addition to the ionotropic glutamate receptors discussed above, glutamate neurotransmission can also act through metabotropic receptors (mGluRs). There are eight members of this family of receptors (mGluR1-8), and belong to the G-protein coupled receptor (GPCR) class. Like other GPCRs, mGluRs comprise seven transmembrane segments and initiate intracellular signaling through their coupled G-proteins. These receptors are further grouped based on their G-protein mediators: mGluR1 and 5 are coupled to stimulatory G_q proteins, and the other family members are coupled to inhibitory $G_{i/o}$ proteins. The G_q -coupled mGluRs are, in the hippocampus, mainly found at postsynaptic membranes, and the $G_{i/o}$ are largely found presynaptically¹⁰⁶.

Metabotropic GluRs can modulate neuronal excitability by modulating ion channels. For example, hippocampal mGluR5 can inhibit afterhyperpolarization current mediated by K^+ channels, resulting in reduced K^+ efflux and impaired spike frequency

adaptation¹⁰⁷. These receptors can also modulate synaptic transmission: $G_{i/o}$ -coupled mGluRs in the CA1 region can mediate Ca^{2+} influx, particularly when paired with a backpropagating AP¹⁰⁸. Although the role of mGluRs in mediating mood disorders is not fully understood, there is evidence that their expression may be related to depression pathogenesis. For example, Wieronska et al demonstrated changes in mGluR5 expression in rat hippocampus following chronic mild stress in rats, with levels increased in CA1 and decreased in CA3¹⁰⁹. Metabotropic GluRs can also modulate the release of glutamate via negative feedback mechanisms at the presynaptic membrane, and it is hypothesized that changes in this feedback and subsequent perturbations in synaptic availability of glutamate may be involved in mood disorder pathogenesis. Indeed, mGluR antagonists exhibit antidepressant effects in the forced swim and tail suspension despair models of depression in mice¹¹⁰. Accordingly, mGluRs represent interesting potential mediators of cellular excitability and glutamatergic synaptic transmission in the context of mood disorders and stress models of depression.

While glutamate represents the main excitatory neurotransmitter in the brain, the “excitatory machine” formed by glutamatergic transmission must be regulated to allow for normal neurologic function. Much of this regulation is accomplished by inhibitory GABAergic neurotransmission, which comprises the majority of synaptic connections that are not excitatory. In the CNS, two classes of GABA receptors can be found: $GABA_A$ and $GABA_B$. $GABA_A$ receptors are ligand-gated ion channels: receptor activation results in the opening of a chloride-selective pore¹¹¹. Increased chloride (Cl^-) conductance causes a decrease in membrane potential towards the chloride reversal potential ($\cong -75$ mV), inhibiting depolarization and the generation of APs. $GABA_B$ receptors are metabotropic

GPCRs that are coupled to K^+ channels. Stimulation of $GABA_B$ receptors results in the opening of additional K^+ channels, driving the membrane potential closer to that of the equilibrium potential of K^+ ($\cong -84mV$) and, much like the increased Cl^- conductance caused by $GABA_A$ activation, inhibits depolarization and AP generation. Both $GABA_A$ and $GABA_B$ receptors are found in the HPC, and deficiency of GABAergic neurotransmission has been hypothesized as a mechanism of depression pathogenesis¹¹². In the hippocampus, mice lacking specific functional $GABA_A$ receptor subunits are deficient in object location memory tasks¹¹³ as well as more sensitive to trace fear conditioning¹¹⁴. $GABA_A$ receptor-mediated currents are also decreased in DG granule cells following stress, an effect reversed by treatment with the antidepressant escitalopram¹¹⁵. As excitatory-inhibitory imbalance in HPC has been implicated in mediating stress outcomes in rodents¹¹⁶, dysfunction of GABA circuitry must be considered when investigating the etiology of mood disorders and depression-like behaviors in preclinical models.

Glutamatergic and GABAergic neurotransmission as summarized above are also accompanied and modulated by other types of neurotransmission. Nicotinic acetylcholine (ACh) receptor subunit mRNA, for example, is found in all neuronal types of the CA1 region, though currents mediated by these ligand-gated ion channels are detectable in interneurons in the strata radiatum and oriens, but not in pyramidal cells¹¹⁷. Both muscarinic and nicotinic (mACh and nACh) presynaptic receptors may mediate the release of glutamate^{118,119}, leading to the enhancement of synaptic transmission. The CA1 is also innervated by serotonergic (from dorsal raphe¹²⁰), noradrenergic (from locus coeruleus¹²⁰), and dopaminergic (from midbrain¹²¹) projections, all of which can affect the excitability of CA1 pyramidal cells as well as their synaptic plasticity. Through β -

adrenergic, D1, and 5-HT₄ receptors, respectively, these monoamines are known to increase pyramidal cell excitability through cAMP-mediated mechanisms¹²²⁻¹²⁴. Serotonergic signaling via the 5-HT₂ receptors at pyramidal neurons, however, decrease cellular excitability¹²². Inhibitory neurons in the CA1 are activated by α -adrenergic¹²⁵ and 5-HT₃¹²⁶ signaling, which may have downstream effects on the excitability of their connected pyramidal neurons. NE also facilitates LTP induction¹²⁷, and dopamine D1/D5 receptors induce a slow, long-lasting potentiation of field EPSPs associated with LTP¹²⁸, both in CA1. While not an exhaustive account of the complex neurotransmission of the HPC, the above discussion highlights the many NT systems that can affect excitatory transmission within and from this critical brain region.

HPC Sex Differences in Stress and Depression

Many systems in the brain converge to affect the complex function of cognition and emotional processing, both of which are impaired in MDD and other mood disorders. The HPC has been recognized as a central substrate in the pathophysiology of a wide range of mood disorders, including MDD¹²⁹⁻¹³¹, bipolar disorder¹³², and post-traumatic stress disorder (PTSD)¹³³. Many of these studies have identified varying degrees of hippocampal atrophy in patients with MDD¹³⁴, with an inverse correlation between depression duration and hippocampus volume¹³⁵. This atrophy is likely due to decreased neurogenesis in the DG¹³⁶, as well as shrinking and retraction of dendrites and possible loss of glial support¹³⁷, and these stress-induced processes are often prevented by antidepressant treatment¹³⁸. HPC abnormalities in MDD also extend to sex differences. For instance, women that do not respond to the antidepressant fluoxetine have smaller

hippocampal volumes than those women that do respond to fluoxetine treatment³. Critically, this difference in hippocampus size with respect to antidepressant response was not observed in men.

The differences in hippocampus in women that may contribute to increased susceptibility to depression are also mirrored by sex differences in preclinical models. Woolley et al demonstrated a fluctuation of dendritic spine density in the CA1 region corresponding to changes in estrogen levels throughout the rodent estrous cycle: spine density was found to decrease in late proestrus to estrus, then return to early proestrus levels over a period of days¹³⁹. This difference was exclusive to CA1, as spine densities in CA3 and DG did not vacillate over the estrous cycle. Further studies determined that the effects of estradiol on the spine density in CA1 were dependent upon glutamate neurotransmission via NMDA receptors (NMDARs), as density did not fluctuate when rats were treated with competitive NMDAR antagonists¹⁴⁰. Changes in CA1 spine density were further investigated by Shors et al, who found that male rat CA1 spine density increased following just one bout of tail shock stress, while female rat CA1 spine density decreased following the same stressor¹⁴¹. This group later showed that the opposite effects of stress on CA1 spine density were, like the estradiol-dependent changes, also NMDAR-dependent: NMDAR antagonism prevented both the increase in spine density in female rats and the decrease in spine density in male rats following stress¹⁴². The effects of steroid hormones (i.e. estradiol and testosterone and derivatives) on stress outcomes and MDD with focus on the HPC in human and preclinical rodent models are further discussed in later sections of this introduction.

The Nucleus Accumbens

The nucleus accumbens (NAc), along with the olfactory tubercle, are parts of the basal forebrain that form the ventral striatum, a portion of the basal ganglia. It contains two substructures: the core and shell. The NAc shell functions in the processing of reward (i.e. “liking” of a pleasurable stimulus)¹⁴³, as well as mediating the cognitive process of motivational salience (i.e. “wanting” of a reward or associated cues that motivates an animal to attain a goal)¹⁴⁴. The NAc core acts to process reward-related motor function¹⁴⁵. As such, the NAc is widely recognized as a key mediator of reward-related behaviors, and has also gained attention over recent decades for its involvement in the pathophysiology of depression^{146,147}. In stress models of depression, molecular and synaptic adaptations to physical or psychological stress are dysregulated in NAc, ultimately leading to pathological behaviors¹⁴⁸.

NAc Cell Types – Direct and Indirect Pathways

Both NAc core and shell substructures primarily contain GABAergic medium spiny neurons (MSNs – 95% of all NAc neurons), which primarily express either D1-type or D2-type dopamine receptors (D1-MSNs and D2-MSNs, respectively), with a subset of MSNs containing both¹⁴⁹. The remaining population of cells comprise interneurons, either cholinergic or GABAergic¹⁵⁰. Classically, D1-MSNs are thought to inhibit the dopaminergic ventral mesencephalon (i.e. the ventral tegmental area, VTA and substantia nigra, SN) via the “direct pathway,” resulting in disinhibition of the thalamus and the overall effect of enhancing motivated behavior. D2-MSNs, on the other hand, act through the “indirect pathway” via the ventral pallidum which usually inhibits the ventral

mesencephalon, resulting in an overall inhibition of the thalamus and in turn, inhibition of motivated behavior (Figure 6). This classical understanding of NAc MSN signaling is supported by the promotion of drug-seeking behavior by D1-MSN activation and converse inhibition of seeking by D2-MSNs¹⁵¹. However, optogenetic studies have recently demonstrated that the direct and indirect NAc pathways are not as well-differentiated by dopamine receptor MSN types in NAc as they are in dorsal striatum¹⁵². This work shows that many D1-MSNs are involved in the indirect pathway via innervation of ventral pallidum neurons that project to the ventral mesencephalon, and that many D2-MSNs project to ventral pallidum neurons that innervate the thalamus as part of the direct pathway. As such, signaling of the NAc is more nuanced than previously thought, and further study of the dynamics of this system may reveal more specialized mental health treatments.

NAc function in stress models of depression

The NAc is a key substrate in the expression of depression-related behaviors in mouse models, as well as in mediating resilience to stress. Berton et al demonstrated an increase in c-Fos (a marker of neuronal activation) in the NAc and VTA of mice following exposure to a social target, an effect that was exaggerated in defeated subjects³⁸. This group also highlighted an increase in brain-derived neurotrophic factor (BDNF) expression in the NAc following CSDS; BDNF is known to increase dopamine release in this region through TrkB receptor activation on terminals of dopaminergic projections¹⁵³. The functional knockout of BDNF in the VTA, including in those projections to the NAc, induced the antidepressant effect of mitigating social withdrawal behavior following

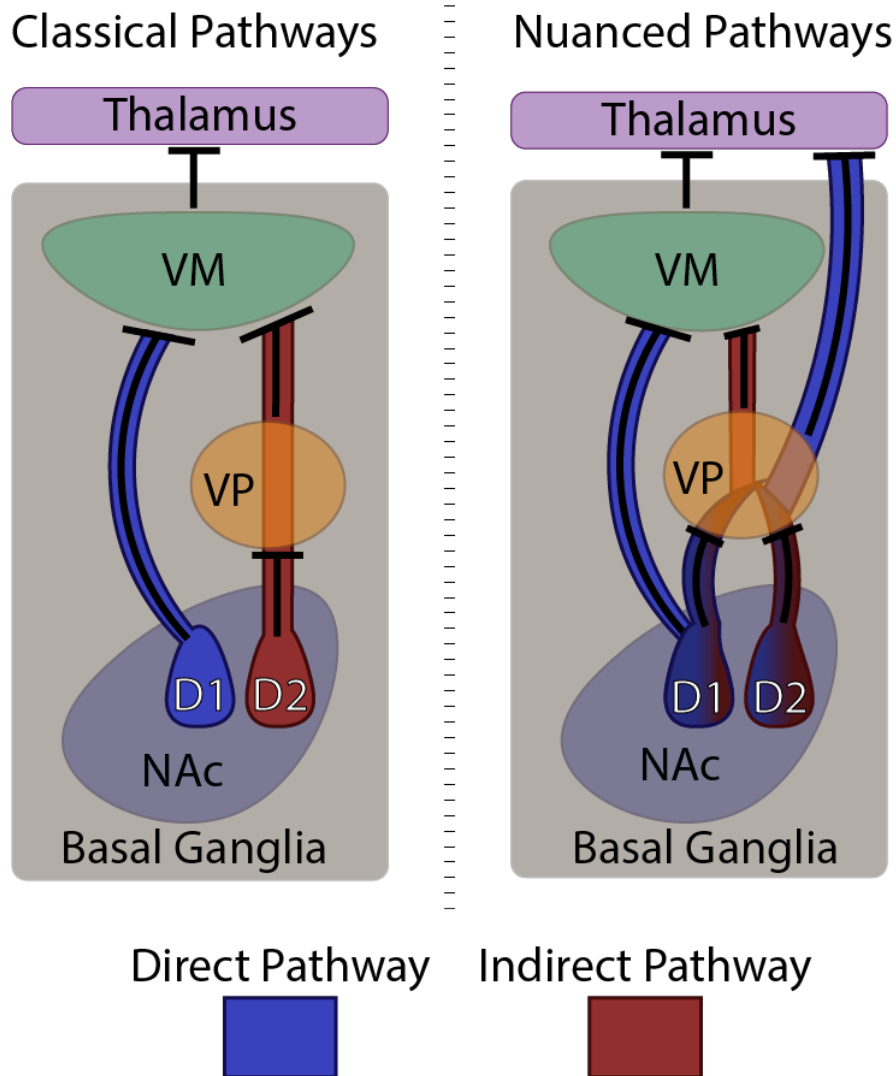


Figure 6 | Classical and nuanced direct and indirect pathways of NAc signaling.

The classical distinction of “direct” and “indirect” pathways of motivated behavior drive being mediated by D1-MSNs and D2-MSNs, respectively, is shown on the left. The classic direct pathway (blue) was understood to involve direct inhibition of the dopaminergic areas of the mesencephalon (VTA and SN, collectively VM) by GABAergic D1-MSNs, resulting in disinhibition of the thalamus. The classic indirect pathway (red) was thought to involve the inhibition of the VP, which in turn inhibits the VM, resulting in inhibition of the thalamus. However, recent optogenetic studies have demonstrated mixed populations of D1-MSNs and D2-MSNs participating in the direct and indirect innervation pathways that result in the initiation and fine-tuning of motivated behavior. NAc: nucleus accumbens; VTA: ventral tegmental area; SN: substantia nigra; VM: ventral mesencephalon; VP: ventral pallidum.

CSDS. In experiments investigating epigenetic changes in the NAc following stress, Wilkinson et al demonstrated widespread and persistent changes in methylation of histones, as well as differences in the binding of cAMP response element binding protein (CREB)¹⁵⁴. Interestingly, these changes were largely reversed by treatment with the antidepressant imipramine, and the changes observed in animals resilient to CSDS mirrored those induced by the antidepressant treatment. To this end, Covington et al showed that increases in repressive histone methylation in NAc of mice following CSDS are paralleled by decreases in histone deacetylase 2 (HDAC2) levels, and that inhibition of HDAC function produces antidepressant effects in social interaction, sucrose preference, and forced swim tests in defeated mice¹⁵⁵.

Much of the focus of the role of the NAc in mediating resilience to stress has been on the transcription factor, Δ FosB. This transcription factor is a member of the Fos family, and is a truncated splice variant of the full-length FosB protein. Fos family proteins form heterodimers with Jun family proteins to form activator protein-1 (AP-1) complexes, which bind to corresponding consensus sequences in the promoters of a variety of genes to affect their transcription¹⁵⁶. Fos family proteins are induced in a number of brain regions following acute stress¹⁵⁷, but this induction is transient due to the instability of Fos proteins. Chronic stress, however, causes a unique induction of Δ FosB, particularly in the NAc^{157,158}. Δ FosB's induction by chronic stimuli is unique as it is more stable than its other Fos family relatives: while other Fos family members are mostly degraded within 8 hours of translation, Δ FosB has a half-life *in vivo* of 8 days¹⁵⁹. This is due to the truncation of degron domains present in the full-length form of FosB, as well as phosphorylation at its N-terminus¹⁶⁰. This stability affords Δ FosB the ability to accumulate with repeated

exposures to stress, and this accumulation is observed in both D1- and D2-MSNs but not interneurons nor structural support cells of the NAc¹⁶¹. This study by Lobo et al also observed the striking phenomenon of differential cell subtype-specific induction of Δ FosB in animals susceptible or resilient to CSDS: susceptible mice exhibited a modest induction in D2-MSNs, while resilient mice exhibited a higher degree of induction in D1-MSNs. Indeed, mice overexpressing Δ FosB in D1-MSNs via inducible transgenic mouse line or with non-cell type-specific virally-induced overexpression in NAc are resilient to CSDS^{158,162}. Conversely, mice expressing Δ JunD in the NAc - a dominant negative form of Δ FosB's AP-1 complex binding partner JunD - demonstrate heightened susceptibility to even subchronic exposure to social defeat stress¹⁵⁸. Additionally, while Δ FosB is induced in the NAc in response to fluoxetine, this treatment's antidepressant effects are blocked by viral overexpression of Δ JunD. An important gene target of Δ FosB is the aforementioned AMPA receptor subunit GluA2: Δ FosB overexpression in the NAc is accompanied by a specific induction of GluA2¹⁶³. Mice with viral-mediated overexpression of GluA2 in the NAc demonstrate resilience to CSDS¹⁵⁸, a particularly interesting effect due to the Ca^{2+} -impermeable nature of AMPARs containing this subunit. Reduced glutamatergic response in NAc due to the increased induction of GluA2 represents an important mechanism of resilience. Glutamatergic inputs to the NAc, including those originating in vHPC, are discussed further below with regard to stress outcomes and depression.

Sex differences in NAc

There is mounting evidence regarding sex differences in the NAc in the context of motivated behavior and the dysfunction thereof. For example, female rats are more susceptible to addiction (a NAc-dependent process) than male rats, as they are faster to acquire drug-self administration and are more likely to relapse¹⁶⁴. Female rats are also quicker at acquiring CPP for cocaine, and this CPP was achieved at half the dose or less required for male rats¹⁶⁵. These differences may be attributable to differences in development of the male and female brain conferred by the actions of ovarian hormones¹⁶⁶. Gonadal steroid hormones can also influence the density and activity of dopamine (DA) terminals in the NAc, as many DA neurons in the ventral tegmental area (VTA) contain estrogen and androgen receptors and are also regulated by glia and other afferents that may be affected by hormone signaling¹⁶⁷. Structural sex differences are also apparent in the NAc. For example, Forlano and Woolley discovered that distal dendritic spine density in NAc MSNs is higher in female rats¹⁶⁸, indicating that excitatory synaptic connections in the NAc likely differ between the sexes, which may in part explain sex differences observed in drug addiction and depression. Indeed, Wissman et al demonstrated sex-dependent variability in the morphology and distribution of dendritic spine synapses in NAc¹⁶⁹.

Brancato et al have also recently demonstrated sex-specific effects on glutamatergic synapses in the NAc¹⁷⁰, which are implicated in the development of mood disorders^{171,172}. This group investigated pre- and postsynaptic plasticity of glutamatergic synapses in the NAc shell in male and female mice by evaluating the expression of VGLUT transporters, which essentially represent vesicles in glutamatergic nerve

terminals. They found an interaction between stress and sex in the expression of VGLUT1 in the NAc shell, with a significant decrease of VGLUT1 labeling only in female mice exposed to SCVS, but no post-stress sex differences in PSD95, a postsynaptic marker, nor sex differences in MSN spine density or morphology. Overall, this study suggests sex differences in presynaptic glutamate neurotransmission in the NAc shell, which supports aberrations of excitatory signaling in this brain region as potential mediator of disparities in MDD prevalence in men and women. Excitatory neurotransmission to NAc originating in the vHPC is discussed in the following section, with focus on this circuit's contribution to stress outcomes and depression.

HPC to NAc connectivity

As mentioned above, the NAc is a key mediator of motivated behaviors, and is thought to influence the seeking of reward by integrating both dopaminergic and glutamatergic inputs. The dopaminergic input to the NAc via the mesolimbic pathway mediates reinforcement of incentive salience (i.e. “wanting”) of a reward^{173,174}, while the glutamatergic input to NAc and midbrain dopamine neurons encodes information regarding reward-related environmental stimuli¹⁷⁵. The excitatory input into the NAc specifically is thought to mediate the integration of context and cues with goal-directed behavioral output¹⁷⁶. Dopaminergic and glutamatergic signaling in the NAc are thought to coincide to affect synaptic plasticity, and this plasticity allows for processing of environmental information to prioritize the salience of some cues over others (i.e. in the case of drug reward processing)^{177,178}. Dysfunction of the NAc's capacity to properly integrate these inputs, then, leads to perturbations in reward processing that can result in

a change in motivated behavior. Accordingly, an increase in the NAc's drive of motivated behavior may lead to addiction, and a weakening of this drive may lead to anhedonic behaviors such as those found in MDD and other mood disorders.

In a functional magnetic resonance imaging (fMRI) study, Kahn and Shohamy demonstrated low-frequency changes in signal that correlate to resting-state functional connectivity between the vHPC, NAc, and VTA in humans¹⁷⁹. In rodents, Britt et al elegantly profiled three different glutamatergic projections to the NAc: those from BLA, PFC, and vHPC¹⁸⁰. This group demonstrated that projections from the vHPC are concentrated mainly at the medial NAc shell, and that projections from the BLA and PFC are mixed between the shell and the core in their destinations. Furthermore, their retrograde labeling studies indicated that the majority of all cells projecting to the medial shell are located in the vHPC, with fewer also coming from the BLA and PFC. Next, they characterized pathway-specific NAc strength of synapses originating at each of these areas using optogenetic stimulation, and demonstrated that the amplitude of optically evoked EPSCs are largest after stimulation of vHPC input to the NAc shell. Ventral HPC to NAc synapses were also shown to be unique in their NMDAR-mediated passage of inward current, possibly due to NMDARs of these synapses being less sensitive to blockade by Mg^{2+} , a known phenomenon at thalamocortical synapses¹⁸¹. The authors suggested that this may be the primary mechanism of the exaggerated vHPC-NAc EPSC, and posit that this could also be the mechanism by which this pathway is able to uniquely induce a stable depolarized state in NAc MSNs, increasing their likelihood of activity¹⁸². This phenomenon was first described by O'Donnell and Grace, who showed that this depolarized state induced by vHPC input into the NAc was necessary for the induction of

spike firing by inputs from the PFC (i.e., vHPC inputs are capable of “gating” the response of the NAc to other excitatory inputs). Britt et al in the same study also found that cocaine selectively potentiates synaptic responses at vHPC-NAc inputs at the medial NAc shell, as measured by an increase in AMPA to NMDA ratio. This was accompanied by attenuation of cocaine-induced locomotion with vHPC-NAc optical inhibition and an increase with optical stimulation. This study highlights the importance of vHPC-NAc input in integration of dopaminergic reward signaling, as well as the unique properties of vHPC-NAc synapses at the medial NAc shell.

Bagot et al in 2015 made crucial contributions to our understanding of the function of vHPC-NAc projections with respect to stress outcomes². In male mice, this group demonstrated opposite regulation of vHPC-NAc and mPFC-NAc activity by CSDS by first examining immediate early gene (IEG) expression in vHPC and mPFC. Expression of the IEGs *Arc* and *Egr1* was reduced in vHPC of resilient mice, but the expression of *Arc* was reduced in mPFC of susceptible mice. Next, optically induced activation of glutamatergic projections from vHPC and mPFC to NAc was accomplished using glutamatergic neuron-specific expression of channelrhodopsin (ChR2) in either region and illuminating projection nerve terminals in NAc. Paired pulse ratio (PPR) of EPSCs was assessed to examine the vesicle release probabilities suggestive of alterations in presynaptic glutamate release, and PPR was elevated in vHPC-NAc in resilient mice but decreased in mPFC-NAc in resilient mice. These findings suggest that glutamate release from vHPC-NAc projections is reduced in resilient mice, but oppositely, glutamate release from mPFC-NAc projections is increased in resilient mice. Next, the group used optically-induced LTD at vHPC-NAc synapses to investigate whether weakening the connectivity

between these two regions would affect stress outcomes. Following CSDS, LTD was induced shortly before assessing SI ratio, and the weakening of vHPC-NAc connectivity with this strategy resulted in an increase in social interaction to levels observed in resilient mice. LTD induced at mPFC-NAc inputs did not affect social interaction. Acute optical stimulation of vHPC-NAc projections, however, reduced SI ratio following CSDS and increased immobility in the FST, thus promoting susceptibility to stress. The opposite was found in acute stimulation of mPFC-NAc projections, which increased SI ratio following CSDS in a pro-resilient fashion. This seminal study, while only examining male mice, highlights the importance of glutamatergic inputs to the NAc in regulating susceptibility to stress, and demonstrates that increasing vHPC-NAc activity is pro-depressive in male mice.

In another recent study of the vHPC-NAc connection, LeGates et al demonstrated that these synapses display activity-dependent plasticity, and that their strength directly regulates reward behavior¹⁸³. This elegant study characterized the nature of vHPC-NAc synapses, and showed similar LTP induction at D1-MSNs and D2-MSNs by electrical and light-induced optogenetic stimulation of vHPC projections, and that the plasticity was accomplished through postsynaptic mechanisms (i.e., there was no change in paired-pulse ratio following high-frequency stimulation to induce LTP). The induction of LTP was blocked by AP5 (a selective NMDAR antagonist), BAPTA (a Ca²⁺ chelator), KN62 (a CaMKII inhibitor), and Rp-cAMPs (a blocker of PKA activation by cAMP), indicating that the induction of LTP at vHPC-NAc synapses is NMDAR-, Ca²⁺-, CaMKII- and PKA-dependent, much like the classical LTP induced at CA3-CA1 synapses in the HPC discussed above¹⁸⁴. Furthermore, LTP induction was not blocked by D1R nor D2R

antagonists, suggesting that plasticity at vHPC-NAc synapses occurs in a dopamine-independent fashion. With respect to motivated behavior, high frequency, but not low frequency, optical stimulation of vHPC-NAc synapses was sufficient to induce CPP of the stimulation-paired chamber. In contrast, interruption of vHPC-NAc plasticity using optical inhibition was sufficient to abolish CPP of a chamber containing the natural reward of a social target. Pertinent to the current work was this group's investigation of vHPC-NAc plasticity with respect to stress: chronic multimodal stress (CMS) was sufficient to weaken synapses at D1R-MSNs but not D2R-MSNs. This weakening of synapses by stress was accompanied by a deficit in LTP induction at D1R-MSN synapses, as well as an abolishment of the CPP induced by optical high-frequency stimulation mentioned above. The link between stress-induced alterations at vHPC-NAc synapses and MDD was further strengthened by the mitigation of these alterations by the antidepressant fluoxetine. Chronic, but not acute, fluoxetine was sufficient to restore pre-stress sucrose preference levels, as well as the optically-induced CPP of the light stimulation-paired chamber. Furthermore, chronic fluoxetine rescued the decrease in synaptic strength as measured by AMPA to NMDA ratio caused by chronic stress in D1R-MSNs, and accordingly was sufficient to ameliorate the accompanying deficit in LTP induction. This study is critical in our understanding of the effects of chronic stress on vHPC-NAc synapses and the plasticity thereof, and suggests the key role of the connection between these two regions in mediating reward- and stress-related behaviors.

Ion Channels of the Hippocampus

As alluded to above, changes in excitability and activity of vHPC-NAc neurons, driven by changes in current passage by ion channels, is implicated in stress responses and depression pathogenesis. Current in all excitable cells, including neurons, exists in the form of ions that pass across the cell membrane with the aid of ion channels. Ion channels are specialized proteins that, according to their genetic coding and post-translational modification, can comprise specialized structures to drive specific ion permeabilities and cellular excitability states. The heterogeneity of ion channels conferred through subunit diversity allows different neuronal subtypes, for example those in different hippocampal regions, to have specific membrane properties and excitabilities that are malleable through changes in gene transcription, translation, and modification. Pharmacology studies paired with the study of single ion channel types in cell culture have allowed for the identification of distinct currents generated by specific ion channels; many of the major ion channel types found in the hippocampus and the currents they facilitate are discussed below, followed by an overview of intrinsic excitability and the plasticity thereof.

Leak Channels

At rest, neuronal cell membranes are more permeable to potassium (K^+) than other ions, which causes the cell's resting membrane potential (RMP) to lie near potassium's equilibrium potential. Resting membrane potential is established by the Goldman-Hodgkin-Katz relationship, which takes into account charges, concentrations, and membrane permeability of all relevant ions, including potassium¹⁸⁵. The basis for this high

permeability to potassium is the presence of leak channels, which are constitutively open, potassium-selective channels of the *KCNK* gene family¹⁸⁶. KCNK family channels comprise two α subunits that, across the family, differ in their biophysical and pharmacological properties. The α subunits each contain four transmembrane segments having two pore loops. Accordingly, density of K^+ leak channels and differential expression of subunits can dramatically affect neuronal intrinsic excitability via modulation of RMP. For example, TASK-3 subunit expression is higher in the excitable CA1 pyramidal neurons than in the less excitable stratum oriens interneurons¹⁸⁷. In CA1 neurons and many others, the density of K^+ leak channels directly regulates the RMP and membrane resistance.

Potassium Channels

Potassium channels comprise three major classes: tandem pore domain, calcium-activated, and voltage-gated. All are tetramers that form a pore-loop structure that allows for potassium-selective permeability. The tandem pore domain potassium channels, or “leak” channels, were discussed above. Calcium-activated potassium channels in neurons, such as the pyramidal cells of the hippocampus, are activated by calcium entry through voltage-gated calcium channels. These channels are involved in the regulation of neuronal excitability, particularly through the mechanisms of interspike interval maintenance and spike frequency adaptation¹⁸⁸. Two types of calcium-activated potassium channels in the HPC are large-conductance (BK channels) or small-conductance (SK) channels. Activation of BK channels underlies repolarization in HPC pyramidal cells, as well as formation of fast afterhyperpolarization (AHP)¹⁸⁹. SK channel

activation causes formation of the slow AHP following AP bursts¹⁹⁰, which limits the frequency of repeated APs (spike frequency adaptation). Adaptation of this kind is a mechanism by which a neuron is protected from the effects of repetitive activity and contributes to normal neuronal function and neurotransmission.

Voltage-gated potassium channels comprise four α subunits, a pore, and a voltage sensing domain. Subunit variation and combination give rise to a wide range of channels differing in voltage dependence, pharmacology, and kinetic and gating properties. *KCNA*, *B*, *C*, and *D* genes code for the canonical voltage-gated potassium channels K_v1 , 2, 3, and 4. Localization of different voltage-gated potassium channels in different neuronal compartments, e.g. axons, soma, and dendrites, confers distinct membrane electrical properties to each part of the neuron¹⁹¹.

The transiently active (A-type) channels are a subset of voltage-gated potassium channels that regulate the passage of transient outward current subject to rapid inactivation. In hippocampal CA1 pyramidal neurons, A-type channels are predominantly found in dendrites and are responsible for preventing AP initiation and backpropagation of APs, as well as the reduction of the magnitude of synaptic events¹⁹² and synaptic integration. This influence of A-type channels on synaptic integration and long-term potentiation is characterized by the inactivation of the channel. When an EPSP is present in a CA1 neuron, the dendritic membrane is depolarized and A-type channels are inactivated. If these channels are unable to diminish the generation of a dendritic spike, the summation of the EPSP and the dendritic spike will result in an increased calcium influx, which can affect many downstream processes such as long-term potentiation¹⁹¹. A-type channels are also present in presynaptic neurons, where they may act to filter low-

frequency signals (by which they are only transiently inactivated). Higher-frequency signals result in longer lasting A-type channel inactivation, resulting in AP prolongation accompanied by increased calcium influx and neurotransmitter release¹⁹³. In the context of stress-related conditions such as depression, there is also evidence that corticotropin-releasing hormone (CRH, released in response to stress) increases CA1 pyramidal cell excitability via the modulation of A-type and delayed rectifier potassium channels¹⁹⁴, the channels primarily responsible for the repolarization of the neuronal membrane following an AP.

Sodium channels

Throughout the body, sodium (Na^+) channels exist as a single α subunit containing four repeat homologous domains that often associate with other proteins (sometimes referred to as β subunits). These domains comprise six transmembrane segments (S1-S6) and a pore-forming region. In voltage-gated Na^+ channels (the predominant class in neurons responsible for the rising phase of APs), the S4 segment of the channel acts as the voltage sensor by way of positively-charged amino acids every third position in the primary structure of the channel¹⁹⁵. When a neuronal membrane is depolarized (e.g. by excitatory input activity), Na^+ channels activate quickly by the movement of the S4 segment to the extracellular side of the neuron, which opens the channel's pore. The S5 and S6 segments form the narrow portion of the channel, allowing for its selectivity for Na^+ . Na^+ channels can exist in resting (closed), active (open), or inactive states. The transition between states are referred to as activation, inactivation, and recovery. Activation represents the transition between resting (closed) and active (open) states,

inactivation between open and inactivated states, and recovery between inactivated and resting states. Inactivation is accomplished by the segment of the channel linking the third and fourth domains, and essentially plugs the pore following prolonged activation (i.e. when enough Na⁺ has entered the neuron to increase the membrane potential at which the “plug” moves to the inactivating conformation). This ceases the rise of the membrane potential, and the channel remains inactivated for a period of time known as the refractory period. The decrease in voltage (the falling phase of the AP) repolarizes the membrane, and sodium channels are “deinactivated” back to the resting (closed, but not inactivated) state and are able to participate in the generation of another AP.

The role of the sodium channel in generating APs makes obvious its connection to cellular excitability, but there is scarce research available regarding sodium channel changes in the context of mood disorders. One interesting association between sodium channels and mood disorder pathogenesis is the observation that lamotrigine, an anticonvulsant drug that blocks sodium channels and subsequently blocks glutamate release¹⁹⁶, is effective in the treatment of bipolar disorder¹⁹⁷. This effectiveness is thought to in part be due to the prevention of epileptiform burst activity in the hippocampus. Other anticonvulsants, such as carbamazepine and valproate, are also used to treat bipolar disorder, but primarily affect the manic stage, and have been associated with exacerbation of the depressive stage. Lamotrigine, on the other hand, is more effective at treating the depressive stages of bipolar disorder, and, while not mitigating manic symptoms, has been shown to delay the onset of manic episodes¹⁹⁸. The overall effectiveness of lamotrigine in treating bipolar disorder, however, is contested, with some studies demonstrating that the drug has little clinical efficacy¹⁹⁹. Further research into the

role of sodium channels in the pathogenesis of mood disorders, particularly with respect to their effects on cellular excitability in reward-related circuits such as vHPC-NAc, is needed to determine how these channels may be targeted for novel antidepressant treatments.

Calcium channels

The maintenance of intracellular calcium (Ca^{2+}) is important for normal neuronal function. Neurons possess various mechanisms to maintain low cytoplasmic Ca^{2+} concentrations, including Ca^{2+} -sequestration in organelles and the employment of Ca^{2+} buffering molecules. The equilibrium potential of Ca^{2+} is very high (≈ 140 mV), and as such, Ca^{2+} is the source of depolarizing current. Ca^{2+} is also involved in a variety of other cellular processes, including activation of Ca^{2+} -activated K^+ channels, initiation of second messenger signaling (e.g. in LTP, discussed above), apoptosis, and stimulating the release of neurotransmitters. The release of neurotransmitters at the synapse is triggered when an AP reaches a nerve terminal, causing the elevation of intracellular Ca^{2+} via the opening of voltage-gated Ca^{2+} channels. These channels are formed as a complex of α_1 , $\alpha_2\delta$, β_{1-4} and γ subunits. The ion conducting pore is formed by the α_1 subunit, and the other subunits of the complex participate in the other functions of the channel such as gating²⁰⁰. Ca^{2+} stimulates the release of neurotransmitters by facilitating the interaction of synaptotagmins, phospholipids, and SNARE proteins, which mechanically influence the fusion of neurotransmitter vesicles with the presynaptic membrane²⁰¹. Three families of voltage-gated Ca^{2+} channels have been described (Ca_v1 , 2, and 3), with the α subunits of each being coded by various *CACN* genes²⁰². Ca_v1 and Ca_v2 families comprise the high-

voltage activated (HVA) channels, with the Ca_v1 family inactivating slowly (500 ms) and the Ca_v2 family inactivating quickly (50 ms) at positive membrane potentials. The current produced by the Ca_v1 channels is the L-type Ca^{2+} current, which is blocked by dihydropyridines. Ca_v2 channels are more diverse based on alternative splicing, and are blocked by a variety of toxins specific to their subfamilies. Ca_v2 channels produce the P-type, Q-type, N-type, and R-type currents. Ca_v3 channels, unlike other voltage-gated Ca^{2+} channels, activate at hyperpolarized potentials and produce the T-type current.

Disrupted intracellular calcium homeostasis has been implicated in a variety of psychiatric disorders, including bipolar disorder and MDD. For instance, GWAS studies have uncovered an association of a variation of the 1C α -subunit of the L-type voltage-gated calcium channel encoded by the gene *CACNA1C* with bipolar disorder and unipolar depression (i.e., MDD)²⁰³. Isoform-specific knockout studies have suggested that $Ca_v1.2$ may contribute to spatial memory formation, and that $Ca_v1.3$ contributes to consolidation of fear memory, and both may be involved in the expression of drug sensitization in rodent models²⁰⁴.

Further support for the contribution of intracellular calcium homeostasis in mood disorder pathogenesis is provided by the actions of the NMDAR antagonist ketamine. NMDARs (described above) are antagonized by ketamine to prevent excessive Ca^{2+} influx, and modulate the firing rate of glutamatergic neurons²⁰⁵. In rodent models of depression, ketamine has potent antidepressant actions²⁰⁶, with ventral hippocampal activity being implicated as a key mediator of the drug's antidepressant efficacy²⁰⁷. In addition, ketamine induces Δ FosB in vHPC CA3 neurons, and this is critical for some aspects of its antidepressant function²⁰⁷. Voltage-gated calcium channel blockers also

display antidepressant effects. For example, the dihydropyridine agent nifedipine, which blocks the aforementioned L-type calcium current, reduces immobility time in the forced swim test and the tail suspension test in mice²⁰⁸. However, the nondihydropyridine calcium channel blockers diltiazem and verapamil increase immobility time in the forced swim test and block the effects of tricyclic and atypical antidepressants²⁰⁹. These studies together may muddy the interpretation of calcium's role in depression and related behaviors in rodents, but calcium homeostasis and calcium-mediated currents are clearly implicated in mood disorder pathogenesis.

HCN Channels

Hyperpolarization-activated cyclic nucleotide-gated (HCN) channels are nonselective voltage-gated cation channels found in excitable cells throughout the body, particularly in the heart and brain. They consist of four subunits of six membrane-spanning domains each (S1-6), with S4 acting as the voltage sensor, S5 and 6 creating the pore region, and the C-terminus acting as the cyclic nucleotide binding domain. Cyclic nucleotides (cAMP, cGMP, and cCMP) bind to the C-terminus to lower the threshold potential of the channel. In the brain, HCN channels influence neuronal response to synaptic input, and are expressed on dendrites in the HPC²¹⁰. HCN channels mediate the I_h non-selective cation current, are activated in states of neuronal hyperpolarization, and are critical regulators of neuronal excitability²¹¹. Trafficking of HCN channels to dendrites in the CA1 is thought to correspond to neuronal activity, with increased cell surface expression of HCN channels and subsequent increases in I_h current in response to increased glutamatergic input. This phenomenon could represent a fast response of

neuronal intrinsic plasticity in response to a change in the activity of inputs. This consideration is especially interesting due to the HCN channel's unique open state at hyperpolarized potentials less than -40 mV, and the observation that these channels do not inactivate, so they are often active when the cell is at rest²¹². These properties allow HCN channels to stabilize neuronal excitability by reacting to excitatory and inhibitory inputs.

HCN channels have gained recent attention as possible mediators of depressive behavior²¹³. In a transgenic mouse lines with various knockouts (*HCN1*, *HCN2*, and auxiliary subunit *TRIP8b*) that cause attenuation of the I_h current in HPC pyramidal cells, mice displayed resilience to a wide range of tests measuring behavioral despair²¹⁴. As HCN channels are expressed in CA1 pyramidal cell dendrites with increasing density with distance from the soma, they are thought to act to integrate inputs and modulate the cell's response by attenuating Ca^{2+} signaling^{215,216}. In this sense, they function to regulate intrinsic excitability independent of synaptic mechanisms and provide a homeostatic feedback mechanism that prevents CA1 hyperexcitability²¹⁷. This regulation by HCN channels of CA1 excitability may play a part in modulating vHPC-NAc circuit activity, thereby affecting stress outcomes and development of depressive behaviors.

Hormone Signaling in the Brain – Effects on Stress and Depression

Hormones are chemical messengers that are secreted by endocrine glands and travel to a distant effector sites via the bloodstream to enact regulation of physiological processes. The primary hormones of the ovary, estrogen and progesterone, are synthesized and secreted to affect many actions throughout the body, including in the

brain. Release of these hormones by the ovary is regulated by the hypothalamus and pituitary via various feedback loops of the HPA axis. Neurons of the hypothalamus secrete gonadotropin-releasing hormone (GnRH), which signals the pituitary to secrete follicle-stimulating hormone (FSH). FSH signals the maturation of the ovarian follicle, which releases estrogens (e.g. estradiol) and inhibin, which feed back to the hypothalamus and pituitary to inhibit further FSH secretion. Estrogens also positively feed back to the hypothalamus, resulting in pulses of GnRH secretion, stimulating luteinizing hormone (LH) secretion from the pituitary. This LH release stimulates ovulation, and the resultant ruptured follicle (corpus luteum) secretes progesterone. Progesterone then feeds back to the hypothalamus and pituitary to inhibit the secretion of GnRH, FSH, and LH. The corpus luteum matures, progesterone secretion decreases, and this negative feedback diminishes to allow for the initiation of a new reproductive cycle²¹⁸.

Estrogen signaling in the brain is primarily accomplished via intracellular estrogen receptors (ERs), which, when bound to estrogen, can translocate to the cell nucleus and bind to hormone response elements in target genes to affect their transcription; these events typically occur over hours²¹⁹. Intracellular ERs are most densely expressed in the BNST, ventromedial nucleus of the hypothalamus, amygdala, various midbrain structures, and the pituitary²²⁰, and more sparsely expressed in the HPC and cortex²²¹. Progesterone receptors (PRs) are generally expressed in the same pattern as ERs²²². *In situ* hybridization and immunocytochemical studies suggest that most cells in the HPC that express intracellular ERs are interneurons^{223,224}.

Progesterone, estrogen, and their derivatives can also have non-genomic effects on neuronal physiology, including on cellular excitability²²⁵. Progesterone metabolites

have been demonstrated to allosterically bind GABA_A receptors in the HPC, causing potentiated chloride conductance and dampened excitability²²⁶. Estrogens (primarily estradiol) can also act rapidly in a non-genomic fashion to affect excitability of CA1 pyramidal cells. For example, Wong and Moss demonstrated prolonged EPSPs in CA1 pyramidal cells of ovariectomized female rats that were “primed” with estrogen injections for two days prior to acute slice preparation and recording²²⁷. This group also demonstrated that EPSCs were potentiated via the actions of second messenger cascades (e.g. cAMP signaling)^{228,229}. These non-genomic effects make ovarian-derived hormones, especially estradiol, interesting potential mediators of sex differences in stress outcomes, particularly in the context of circuit-level excitability.

Estrogens also modulate synaptic plasticity in the hippocampus. Warren et al demonstrated that LTP is enhanced during proestrus in rats²³⁰, and Cordoba Montoya and Carrer showed that LTP induction in CA1 is facilitated by estradiol treatment in ovariectomized rats²³¹. Furthermore, Joels and Karst showed that the priming of ovariectomized rats with a combined treatment of estrogen and progesterone enhances voltage-gated calcium channel conductances in CA1 pyramidal neurons²³². These studies complement well the finding by Gould et al that estradiol has a potent effect on CA1 dendritic spine density²³³, and, taken together, highlight important effects of estrogens on CA1 excitatory neurotransmission. Whether through transcriptional or non-genomic effects, ovarian hormones clearly play a role in regulating HPC physiology through modulation of excitability and synaptic transmission.

As discussed previously, animal models of stress have revealed changes in the structure and function of the HPC²³⁴. Male and female rodents react differently to stress

in HPC-dependent learning tasks such as Morris water maze, with the most robust differences being identified when females are in proestrus²³⁵. Furthermore, studies of ovariectomized rats have shown that stress enhances performance in the radial arm maze (another HPC-dependent measurement of spatial memory and learning) in animals with estrogen replacement, but not in those without²³⁶. Stress effects on CA1 dendritic spine density (discussed previously) also appear to be estrogen-dependent: a single stressor can induce an increase in spine density in male rats but a decrease in female rats in proestrus¹⁴¹, when spine density is usually the highest for females¹³⁹. Estrogen and stress can interact to cause sex differences in other regions as well. For example, the amygdala-dependent process of extinction of a conditioned fear response is impaired in estrogen-treated female rats²³⁷. There is also evidence that estrogen can enhance stress effects in the mPFC, as proestrus or estrogen-replaced ovariectomized female rats demonstrated more deficiencies in mPFC-dependent working memory tasks²³⁸. Overall, estrogens have a clear effect on stress outcomes and brain function, and are likely key mediators of sex differences in depression.

Testosterone has also been implicated in mediating stress outcomes and depression development. In humans, hypogonadism leading to lower testosterone levels in men is associated with a higher prevalence of MDD^{239,240}, and treatment with testosterone has been shown to alleviate depression symptoms in hypogonadal²⁴⁰ and eugonadal men^{241,242}. There is also evidence that low-dose testosterone treatment can improve depression scores and augment the effectiveness of traditional depression pharmacotherapies in treatment-resistant women²⁴³.

Testosterone is metabolized to a variety of different effectors. For example, 5 α -reductase converts testosterone into dihydrotestosterone (DHT), which is a more potent agonist at ARs and has a longer half-life than testosterone. DHT can then be converted by aldo-keto reductases to 3 α -diol or 3 β -diol. The former of these metabolites has a low affinity for AR but acts in the brain as an agonist at the GABA_A receptor²⁴⁴, and the latter acts primarily through ER β in the brain to affect gene transcription²⁴⁵. Like estrogens, androgens can also act through genomic and non-genomic mechanisms. Androgens also diffuse across the cellular membrane to interact with intracellular receptors and diffuse into the nucleus to affect gene transcription via androgen receptor binding to DNA at hormone response elements²⁴⁶. Androgens and estrogens, as alluded to above, can also cause more rapid, non-genomic effects through activation of cell membrane-bound receptors²⁴⁷. The rapid effects of androgens in the brain include modulation of neuronal excitability and plasticity. There is evidence that androgens acutely decrease neuronal excitability²⁴⁸, but some studies indicate increased excitability with acute application of testosterone by measure of field potentials²⁴⁹. These studies, however, assess general excitability in various brain regions, including the HPC CA1, and do not address specific subpopulations of neurons (e.g. those in the vHPC-NAc circuit). The current work will help to clarify hormonal effects on the physiology of the vHPC-NAc circuit, and the observed effects of testosterone on the HPC are discussed further below.

Testosterone has potent effects on anxiety- and depression-related behaviors in animal models. Orchidectomy of adult male rodents, for example, causes an increase in anxiety behaviors in marble burying, EPM and open field tests²⁵⁰⁻²⁵², as well as behavioral despair in the forced swim test following chronic mild unpredictable stress (CMS), which

was accompanied by a decrease in hippocampal cell proliferation and neurogenesis²⁵³. Testosterone relieves these anxiety behaviors in intact adult male rodents²⁵⁴ as well as in the orchidectomized adult males of studies cited above. Testosterone enhances hippocampal neurogenesis induced by the antidepressant imipramine²⁵⁵. Particularly relevant to the current work, testosterone prevents anhedonia in aged adult male rats exposed to CMS if administered weeks before stress exposure²⁵⁶. Interestingly, this mitigation of anhedonia as measured by sucrose preference was not observed if testosterone was administered following stress exposure, suggesting the necessity of testosterone's actions before and during stress in male resilience. Further investigation of testosterone's actions with respect to behavior following stress revealed that the prevention of anhedonia and behavioral despair by testosterone was likely mediated by aromatization to estradiol, as gonadectomized rats treated with DHT (insensitive to aromatase) still exhibited these depressive behaviors, but those treated with estradiol did not²⁵⁷. However, other studies did implicate androgen metabolites in the mediation of stress resilience, as treatment with DHT or 3 α -diol in intact adult male rodents did indeed decrease behavioral despair in the forced swim test²⁵⁸.

The effects of testosterone treatment in female rodents with respect to stress outcomes is even less clear. Testosterone, DHT, or 3 α -diol treatment in intact female mice reduces anxiety behaviors in open field and EPM tests²⁵⁹ and depression behavior in the forced swim test²⁵⁸. In contrast, however, other groups have observed no amelioration of anxiety (EPM) or depression (sucrose preference, NSF) behaviors following administration of testosterone in ovariectomized female rats²⁵⁵. The difference between these observations may lie in the ovariectomy, as the studies demonstrating

benefits of testosterone treatment in female animals did not include gonad removal. This could suggest that higher doses of testosterone are needed to induce anxiolytic or antidepressant effects in females, as maintaining the ovaries would accomplish this.

As alluded to above, the protective effects of androgens against stress-induced changes in behavior may in part be mediated through the HPC. Indeed, the volume of the hippocampal formation, its neuronal soma sizes, and extent of dendritic branching increase with androgen treatment in the perinatal period^{260,261}. The protective effects of neonatal androgens are associated with HPC neurogenesis and spine density, as male pups treated with the AR antagonist flutamide demonstrated depressive behaviors in forced swim and sucrose preference tests that correlated with decreased microtubule associated protein-2 (MAP-2) labeling in the CA1 and DG and decreased spine density in CA1²⁶². Additionally, testosterone in orchidectomized adult male rodents may offer protection against oxidative damage and consequent changes in morphology²⁶³, and its metabolites in intact female adults appears to reduce HPC cell death induced by adrenalectomy²⁶⁴. Testosterone and DHT also reverse orchidectomy-induced reduction of spine synapse density in males (independently of ER-mediated effects), while offering partial protection to females with contribution of the aromatization to estrogens²⁶⁵. These morphological changes in response to steroid hormones may relate to HPC neuronal excitability. Teyler et al observed field potential differences in HPC slices from rat brains in response to treatment with testosterone and estradiol: male rat slices showed increased excitability in response to estradiol but not testosterone, and female rat slices showed increased excitability in response to testosterone in diestrus but decreased excitability in proestrus²⁶⁶. Thus, there is a pressing need to uncover additional effects of

steroid hormone manipulation on HPC physiology and effects on stress outcomes. The work described in this thesis addresses this need by providing novel cellular and molecular circuit-based mechanisms for sex differences in vulnerability to depression.

II. MATERIALS AND METHODS

Animals

All experiments were approved by the Institutional Animal Care and Use Committee (IACUC) at Michigan State University and performed in accordance with AAALAC and NIH guidelines. All behavioral experiments were performed on group housed C57BL6/J 8-12 week old male and female mice purchased from Jackson Labs at 8 weeks of age, or transgenic mice bred in our colony (Cre-inducible Rosa^{eGFP-L10a}). All electrophysiology experiments were performed on 9-13 week old male and female Rosa^{eGFP-L10a} transgenic mice. The *floxed FosB* mouse strain (FosB^{fl/fl})²⁶⁷ was a gift from the laboratory of Dr. Eric Nestler at the Icahn School of Medicine at Mount Sinai, and the Rosa26^{eGFP-L10a} strain²⁶⁸ was a gift from the laboratory of Dr. Gina Leininger at Michigan State University. Unless otherwise stated, all mice were group housed in a 12:12 h light/dark cycle with *ad libitum* food and water.

Rosa^{eGFP-L10a} genotyping primers:

Mutant forward: 5' – TCTACAAATGTGGTAGATCCAGGC – 3'

Wild type forward: 5' – GAGGGGAGTGTTGCAATACC – 3'

Common reverse: 5' – CAGATGACTACCTATCCTCCC – 3'

FosB^{fl/fl} genotyping primers:

FB loxPu sequence: 5' – GCTGAAGGAGATGGGTAACAG – 3'

LIPz sequence: 5' – AAGCCTGGTGTGATGGTGA – 3'

LNEo1 sequence: 5' – AGAGCGAGGGGAAGCGTCTACCTA – 3'

Gonadectomies

Eight-week old male and female mice were anesthetized with a mixture of ketamine and xylazine 0.9/0.1 mg/kg and either testes or ovaries were removed according to previously published protocols²⁶⁹. In electrophysiology experiments, gonadectomy occurred one week following intracranial injection surgery. In hormone replacement studies, either empty 1.5 cm Silastic pellets or filled with 0.6 cm of testosterone (Sigma-Aldrich; 1001774366) were placed subcutaneously between the scapulae at the time of ovariectomy. Mice then either recovered for 10 days (electrophysiology) or 28 days (behavior).

Intracranial Injections & Viral Vectors

Male and female mice were anesthetized with a mixture of ketamine and xylazine 0.9/0.1 mg/kg and injected with 0.5uL/hemisphere of virus with Hamilton syringes. Herpes simplex retrograde Cre viral vector (HSV-heF1 α -Cre) was purchased from Massachusetts General Hospital Viral Core, and adeno-associated viral vectors encoding DREADDs were purchased from Addgene (Watertown, Massachusetts, USA). For Δ JunD experiments, viral vectors (AAV2-CMV-GFP or AAV2-CMV- Δ JunD-GFP) were bilaterally infused at two dHPC sites (10° angle; Bregma -2.2 AP, \pm 2.0 ML, -2.1 and -1.9; 0.3 μ L per DV site) or two vHPC sites (5° angle; Bregma -3.6 AP, \pm 3.2 ML, -4.8 & -3.0 DV; 0.3 μ L per DV site). Two coordinates were used to ensure viral transduction throughout each structure. Experimental procedures began at least 4 weeks after surgery. For vHPC-NAc induction of L10-GFP expression and vHPC-NAc *FosB* KO (where applicable), the retrograde Cre viral vector (HSV-hEF1 α -Cre; 0.5 μ L each hemisphere) was injected

bilaterally into NAc (Angle: 10° AP:+1.6, ML:±1.5, DV:-4.4) or BLA (Angle: 0° AP:-1.3, ML:+3.4, DV:-4.5) of Rosa^{eGFP-L10a} mice. For electrophysiology of ΔFosB-expressing vHPC neurons, viral vectors (HSV-IE4/5-ΔFosB-CMV-GFP; or HSV-CMV-GFP as control; 0.5 μL each hemisphere) were bilaterally injected into vHPC (Angle: 3° AP:-3.4, ±3.2, DV:-4.8) and experimental procedures commenced 2-4 d following surgery.

For DREADD experiments, either rAAV2-hSyn-DIO-hM3D-mCherry (44361-AAV2 lot v30428; 0.5 μL) or rAAV2-hSyn-DIO-hM4D-mCherry (44362-AAV2 lot v30430; 0.5 μL) was injected bilaterally into vHPC (Angle: 3° AP:-3.4, ML:±3.2, DV:-4.8) and HSV-hEF1α-Cre (0.5 μL) was injected bilaterally into NAc (Angle: 10° AP:+1.6, ML:±1.5, DV:-4.4). Electrophysiology and immunohistochemistry experimental procedures in Rosa^{eGFP-L10a} mice began at least three weeks following HSV-hEF1α-Cre injection. In DREADD SCVS experiments, stress procedures began at least three weeks following intracranial injection of rAAV2-hSyn-DIO-hM3D-mCherry (male mice) or rAAV2-hSyn-DIO-hM4D-mCherry (female mice) and HSV-hEF1α-Cre.

For dual virus CRISPR/Cas9 *FosB* gene silencing experiments, Cas9-expressing retrograde vector (HSV-hE1α-LS1L-myc-Cas9; 0.5 uL) was infused into NAc (+1.6 AP, ±1.5 ML, -4.4 DV relative to bregma, 10° angle) or BLA (-1.6 AP, ±3.4 ML, -4.5 DV relative to bregma, 0° angle). After 3 wks, control viral vector (HSV-IE4/5-TB-eYFP-CMV-IRES-Cre) or *FosB* gRNA (HSV-IE4/5-TB-*FosB* gRNA-CMV-eYFP-IRES-CRE) were infused into the ventral CA1 region of vHPC (vCA1; -3.4 AP, ±3.2 ML, -4.8 DV relative to bregma, 3° angle; 0.5 uL). Experimental procedures commenced at least 2 weeks following vHPC surgeries.

Subchronic Variable Stress

SCVS was performed according to previously published protocols^{41,170}. Briefly, group-housed mice were exposed to a stressor every day for six days under white light conditions. Stressors were administered daily in the following order on consecutive days: group foot shock of 10 mice with 100 random foot shocks over an hour at 0.45mA (Shock Box H13-15, Coulbourn Instruments, Holliston, MA), one hour tail suspension, and one hour restraint stress; sequence repeated once for six days total stress. Restraint tubes were manufactured in-house by drilling air holes in 50mL falcon tubes.

Chronic social defeat stress (CSDS)

CSDS was performed as previously described^{38,270-272}. In brief, mice were placed into the home cage of an aggressive retired breeder CD1 mouse containing a perforated plexiglass divider placed between the walls of the cage. The experimental mice were allowed to physically interact with the CD1 for 10 min. Following the aggressive encounter, the mice were placed into the other side of the divider from the CD1 aggressor mouse allowing sensory, but not physical, contact for 24 hours. This protocol was repeated daily for 10 d with a new aggressor every day. Behavioral testing began the day following the final day of stress.

DREADD activation

Clozapine N-oxide (CNO; Fischer Scientific NC1044836) was diluted in vehicle solution: 5%DMSO and 95% 0.9% saline. CNO or vehicle was administered i.p.

throughout DREADD SCVS experiments at 0.3mg/kg daily an hour prior to the stressor or behavior.

CRISPR Guide RNA design and testing

Guide RNAs (gRNAs) targeting exon 2 of the *FosB* gene were designed using e-CRISP software (www.e-CRISP.org). The top four sequences were:

gRNA1: TACACCGGGAGCCGGAGTCG

gRNA2: TTACGATCTAAACTTACCT

gRNA3: TCAACATCCGCTAAGGAAGA

gRNA4: CCGTCTTCCTTAGCGGATGT

This gRNA was most effective and was selected for all *in vivo* work described in the current manuscript; also referred to as AJR4 as it was the fourth gRNA produced for our lab). Each gRNA was tested by transfection in a mammalian expression plasmid also containing Cas9. Briefly, Neuro2a cells (N2a, American Type Culture Collection) were cultured in EMEM (ATCC) supplemented with 10% heat-inactivated fetal bovine serum (ATCC) in a 5% CO₂ humidified atmosphere at 37° C. Cells were plated into 12-well plates, and 24 h later (when cells were ~30% confluent) cells were transiently transfected using Effectene (Qiagen) with a total of 200 ng DNA per well. Cells were transfected with empty vector, Cas9 alone, or Cas9 with a gRNA to be tested. Cells were then serum starved for 24 h, then re-fed for 4 h to induce *FosB* gene expression. Cells were pelleted, samples were run on gradient polyacrylamide gels and transferred to PVDF membranes, and Western blot was performed using rabbit anti-FosB antibody (2251; 1:500; Cell

Signaling) and HRP conjugated anti-rabbit secondary at (PI-1000; 1:40,000; Vector). Signal was detected on film and quantified using ImageJ software.

Behavior

All behavioral tests were performed under red light conditions after one hour habituation, except sucrose preference. Splash test: Splash test was performed according to previously published protocols^{41,170}. Mice were sprayed twice on their backs with a 10% sucrose solution and placed in an empty cage and videotaped for 5 minutes. The time spent autogrooming was hand-scored by blind video observers. After splash tests, animals were singly housed for the remainder of behavioral tests. Novelty suppressed feeding: After an overnight fast, mice were placed into a corner of a bare novel arena measuring 38 x 38cm with a single pellet of chow at the center of the arena, and videotaped up to 10 minutes. The videos were then scored by blind observer for the latency to feed. Feeding was defined as using forepaws during mastication. Sucrose Preference: Mice were given two bottles in the home cage from which they could drink freely. During the first day, the two bottles contained water and allowed habituation to the bottles. On the following day, one bottle was replaced with a 1% sucrose solution. Mice were then allowed to drink from the bottles over two days, and consumption of each bottle (weight and volume) was recorded daily. The bottles were switched daily to ameliorate side bias. Elevated Plus Maze: EPM was performed as previously described²⁷³. In brief, mice were placed with heads in the center of the maze parallel to the open arms and allowed to roam for 5 minutes while video recorded. The amount of time spent in the open arms and distance travelled were quantified by Anymaze software (CleverSys). Animals

that fell or jumped from the arena were excluded from analyses. Social Interaction: SI was performed as previously described²⁷². Briefly, mice were placed into the corner of a 38 x 38cm arena with a mesh cage at one end. After 3 minutes of habituation to the arena, a novel conspecific mouse (CD1 strain) was placed into the mesh cage, and the experimental mouse was again allowed to move around the arena for 3 minutes. Time spent within a 5cm radius of the conspecific mouse and in the opposing corners was measured for both sessions. SI ratio was calculated as a ratio of the time spent in the interaction radius while the conspecific mouse is present to the time spent in the same location with empty mesh cage.

Electrophysiology

Ex vivo acute brain slices were prepared from 9-13 week old male or female L10-GFP transgenic mice. Animals were anesthetized with isoflurane and transcardially perfused with ice-cold sucrose artificial cerebrospinal fluid (sucrose aCSF, in mM: 234 sucrose, 11 D-glucose, 26 NaHCO₃, 2.5 KCl, 1.25 NaH₂PO₄, 10 MgSO₄, 0.5 CaCl₂). Animals were decapitated and brains rapidly removed and placed in oxygenated (95% O₂, 5% CO₂) slurried sucrose aCSF for 15 seconds. Brains were blocked and transferred to a vibratome slicing chamber (Leica; Germany) containing aCSF (in mM: 126 mM NaCl, 2.5 KCl, 1.25 NaH₂PO₄, 2 MgCl, 2 CaCl₂, 26 NaHCO₃, 10 glucose). Coronal slices (250 μm) were obtained and transferred to an incubation chamber containing oxygenated aCSF. Slices were incubated at 34C for 30 minutes and then at room temperature for a minimum of 30 min before recording. Whole-cell patch clamp recordings were made with slices held in a submersion chamber perfused at 2 mL/min with oxygenated aCSF held

at $30(\pm 2)$ C using a single inline heater (Warner Instruments; Hamden, CT). Borosilicate glass electrodes with a tip resistance of 3-6 M Ω were filled with internal solution (in mM: 115 potassium gluconate, 20 KCl, 1.5 MgCl, 10 phosphocreatine-Tris, 2 Mg-ATP, 0.5 Na₃-GTP; pH 7.2-7.4; 280-290 mOsm). L10-GFP+ cells representing vHPC-NAc or vHPC-BLA projections were visualized in the ventral CA1 region of the hippocampus with an upright epifluorescent microscope (BX51WI Olympus; Japan). Pyramidal cells were distinguished from other cell types by their morphology and location in the cell body layer of the CA1 region. Recordings were made from projection cells using a Multiclamp 700B amplifier and Digidata 1440A digitizer (Molecular Devices; San Jose, CA). Membrane properties and cell excitability data were sampled (10 kHz), filtered (10 kHz), and stored on a PC for analysis. Membrane capacitance, membrane resistance, and access resistance were automatically calculated by pClamp 10 software (Molecular Devices; San Jose, CA). Any cell with a resting membrane potential more positive than -60mV or access resistance >25 M Ω were omitted from analyses. Resting membrane potential was measured automatically by the Multiclamp 700B Commander while injecting no current ($I=0$); this value was recorded immediately after breaking into a cell. Rheobase measurements were taken by administering 250ms, +5pA steps starting from 0pA with 250ms between current injections. The first current level issued to elicit a spike was recorded as rheobase for each cell. Action potential (AP, or spike) numbers were measured using a +25pA increasing current step protocol. The number of spikes at each step from 0 to 300 pA was manually counted. Input resistance was determined as the slope of the line best fit to the I-V plot generated by the input-output current clamp protocol, with the minimum current step being that which generated a voltage of

approximately -120 mV. Sag ratio was determined using peak and steady-state potentials obtained at the first current step that reached lower than -120 mV and was calculated as steady-state/peak. Spontaneous event frequency and amplitude were determined using MiniAnalysis software (Synaptosoft, Inc.) by manual selection of events from the first 60-120 seconds of gap free voltage clamp recording from each cell.

For DREADD validation, projection cells were identified as described above and recordings were obtained in regular aCSF. After initial baseline recordings were collected, aCSF + Clozapine-N-Oxide (CNO, 1 μ M) was washed onto the slice. Approximately 8 minutes were allowed for the solution to reach the bath from the reservoir and for the DREADDs to bind CNO before excitability was measured again. For flutamide studies, vehicle vHPC-NAc recordings were collected with the slice washed in aCSF + vehicle (DMSO, 0.001%). The slices were incubated as described above, now with the addition of 0.001% DMSO in the aCSF. Treatment recordings were collected from slices incubated and bathed in aCSF plus flutamide (100 nM) and picrotoxin (100 μ M) in DMSO. Picrotoxin was included due to the ability of flutamide to affect GABAergic transmission²⁷⁴.

Immunohistochemistry

Animals were deeply anesthetized with chloral hydrate and transcardially perfused with cold phosphate buffered saline for 9 minutes followed by 9 minutes of 10% formalin at a rate of 3 mL/min. Brains were fixed overnight in 10% formalin and subsequently switched to 30% sucrose. Brains were sliced to 35 μ m sections on a frozen SM2010R microtome (Leica; Wetzlar, Germany) and stained using an antigen retrieval step (for AR staining only), 0.05% sodium borohydride (Sigma-Aldrich; 452882-25g lot:SHBK0324) in

PBS, and the following primary antibodies: Mouse anti-FosB (ab11959; 1:1000; Abcam), Goat anti-GFP (Abcam; ab5450 1:1000) and Rabbit anti-AR (Abcam; ab52615 1:1000); and secondary antibodies: Alexa-Fluor 488 anti-goat IgG (Jackson; 705-545-147 1:200) and Cy3 or Cy5 anti-rabbit IgG (Jackson; 711-165-152 1:200). Fluorescent images were visualized on an Olympus FluoView 1000 filter-based laser scanning confocal microscope.

Translating Ribosome Affinity Purification (TRAP) and cDNA library preparation

Three weeks following injection of retrograde HSV-Cre into NAc, Cre-dependent L10-GFP-expressing mice (*Rosa26^{eGFP/L10a}*) were sacrificed and brains were immediately dissected into 1 mm coronal sections. Transduced tissue from ventral hippocampi (vHPC) of male and female mice was collected using 14-gauge biopsy punches guided by a fluorescent dissecting microscope (Leica) and stored at -80° C until processing ($n = 4$ /biological replicate, 3-4 mice pooled per replicate). Polyribosome-associated RNA was affinity purified as previously described²⁷⁵. Briefly, tissue was homogenized in ice-cold tissue-lysis buffer (20 mM HEPES [pH 7.4], 150 mM KCl, 10 mM MgCl₂, 0.5 mM dithiothreitol, 100 µg/ml cycloheximide, protease inhibitors, and recombinant RNase inhibitors) using a motor-driven Teflon glass homogenizer. Homogenates were centrifuged for 10 minutes at 2000 g (4° C), supernatant was supplemented with 1% NP-40 (AG Scientific, #P1505) and 30 mM DHPC (Avanti Polar Lipids, #850306P), and centrifuged again for 10 minutes at 20000 g (4°C). Supernatant was collected and incubated with Streptavidin MyOne T1 Dynabeads (Invitrogen, #65601) that were coated with anti-GFP antibodies (Memorial Sloan-Kettering Monoclonal Antibody Facility; clone

names: Htz-GFP-19F7 and Htz-GFP-19C8, 50 ug per antibody per sample) using recombinant biotinylated Protein L (Thermo Fisher Scientific, # 29997) for 16-18 hours on a rotator (4° C) in low salt buffer (20 mM HEPES [pH 7.4], 350 mM KCl, 1% NP-40, 0.5 mM dithiothreitol, 100 µg/ml cycloheximide). Beads were isolated and washed with high salt buffer (20 mM HEPES [pH 7.4], 350 mM KCl, 1% NP-40, 0.5 mM dithiothreitol, 100 µg/ml cycloheximide) and RNA was purified using the RNeasy Micro Kit (Qiagen, #74004). To increase yield, each RNA sample was initially passed through the Qiagen MinElute™ column 3 times. Following purification, RNA was quantified using a Qubit fluorometer (Invitrogen) and RNA quality was analyzed using a 4200 Agilent TapeStation (Agilent Technologies). cDNA libraries from 5 ng total RNA were prepared using the SMARTer® Stranded Total RNA-Seq Kit (Takara Bio USA, #635005), according to manufacturer's instructions. cDNA libraries were pooled following Qubit measurement and TapeStation analysis, with a final concentration ~5-10 nM. Sequencing was performed at the Icahn School of Medicine at Mount Sinai Genomics Core Facility (icahn.mssm.edu/research/genomics/core-facility).

Statistical Analysis

Statistical analysis was performed with PRISM software 7.0 (Graphpad). Alpha criterion was set to 0.05 for all experiments. Behavior 2-way ANOVAs were followed by Sidak post hoc comparisons between groups. Spike number in electrophysiology experiments was analyzed by mixed 2-way ANOVAs with current as the within factor followed by Holm-Sidak corrected post hoc comparisons between groups. For all other electrophysiological measures: rheobase, spike amplitude, spike half-width, sEPSC

amplitude, sEPSC frequency, and other cellular properties data were analyzed by independent samples t-tests between groups. All error bars throughout this work represent the mean \pm SEM.

III. ANDROGEN-DEPENDENT EXCITABILITY OF MOUSE VENTRAL HIPPOCAMPAL AFFERENTS TO NUCLEUS ACCUMBENS UNDERLIES SEX-SPECIFIC SUSCEPTIBILITY TO STRESS

The experiments in the following chapter are the subject of a manuscript currently in revision at Nature Neuroscience. Claire E. Manning performed the stress, behavior, and microscopy. Elizabeth S. Williams performed the electrophysiology experiments and performed stress and behavior protocols with the coauthor.

Introduction

Psychiatric disorders of affect, such as major depression disproportionately affect women^{6,276}, but studies investigating depression-related behaviors in animal models that include both female and male subjects are unfortunately lacking. There are sex differences in brain regions that regulate anhedonia following some stress paradigms in rodent models of depression, including subchronic variable stress (SCVS)¹⁷⁰, chronic mild stress²⁷⁷ and *Peromyscus californicus* social defeat stress²⁷⁸. However, the physiological mechanisms underlying sex differences in stress responses and depression-related behaviors remain unclear. As previously introduced, numerous studies have demonstrated the importance of the nucleus accumbens (NAc) in regulating depression-like behaviors after stress^{34,158,279,280}, and glutamatergic inputs to NAc from areas such as prefrontal cortex and ventral hippocampus (vHPC) are critical in regulation of these stress responses^{281,282}. Critically, the vHPC is essential for social and affective memories²⁸³⁻²⁸⁵, and, as discussed in the previous chapter, excitatory vHPC afferents to the NAc directly regulate male behavioral responses to chronic social defeat stress²,

making this circuit a potential candidate mediating sex differences in mood-related disorders.

Unfortunately, most circuit-specific animal model studies investigating depression-related behaviors have not included female subjects. This gap in research exists despite sex differences in several depression-related brain regions, including the hippocampus. For example, hippocampal spine morphology differs between male and female rats prior to stress, and can exhibit sex-specific responses to stressful events¹⁴¹, and male and female rats differ in hippocampal LTP and hippocampus-dependent contextual learning²⁸⁶. Direct sex differences in responses to stress are also well-documented, and one key model in mice is subchronic variable stress (SCVS), after which only female mice exhibit anhedonic responses^{41,170}. To this end, gonadal steroid hormone receptors have been identified in the NAc as modulators of female susceptibility to SCVS²⁸⁷. However, whether vHPC-NAc activity in male and female mice is regulated by gonadal hormones has not been tested. In this chapter, we demonstrated testosterone-dependent differences in adult male and female vHPC-NAc excitability as well as corresponding changes in susceptibility to SCVS. Importantly, we established a causal link between vHPC-NAc physiology and SCVS-induced anhedonia using a circuit-specific viral DREADD system to artificially manipulate vHPC-NAc excitability. We showed that stress-induced anhedonia is dependent upon long-term adaptation of vHPC-NAc projections, as activation of this circuit prior to behavioral assessment, and not simply during behavior, was necessary for induction of anhedonia. We also investigated circuit-specific transcriptional genomic differences between male and female vHPC-NAc neurons using translating ribosome affinity purification (TRAP), which identified many sex differences in

gene transcription that will inform future study of male and female circuit-level physiology. This chapter introduces a novel, circuit-specific physiological difference between male and female mice that drives corresponding sex differences in depression-related stress outcomes that may enhance future understanding of depression susceptibility and potential treatments in men and women.

Results

Female mice are selectively susceptible to anhedonia following SCVS

We observed that female mice are selectively vulnerable to SCVS-induced anhedonia, in agreement with prior studies utilizing this protocol^{41,170,288}. Following the 6-day SCVS battery of stressors (foot shock, tail suspension, and restraint; Figure 2 and Figure 7, top), female mice showed a significant reduction in free-choice preference for sucrose solution over water alone (Fig 7, bottom). As previously discussed, reduction of sucrose preference is an indicator of anhedonia^{34,289,290}, thus SCVS models this aspect of female-specific depression vulnerability. We also used a variety of other assays to evaluate anxiety, reduced self-care, and social withdrawal behaviors in the same male and female mice (Figure 8a-e), but we did not observe the robust, sex-specific vulnerability to stress in any measure other than sucrose preference. Therefore, we focused on sucrose preference and anhedonia for the remainder of the current chapter, though we report all other behaviors measured throughout.

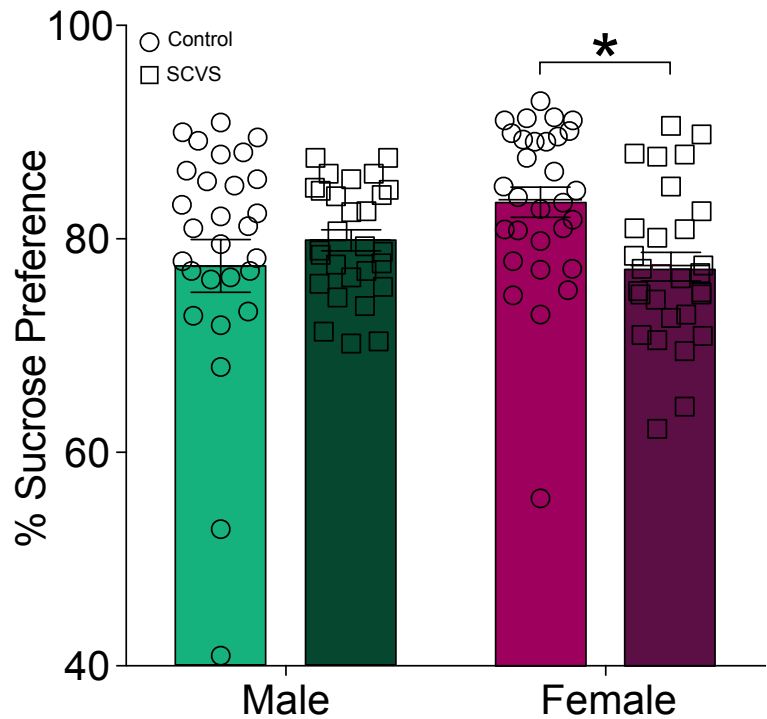
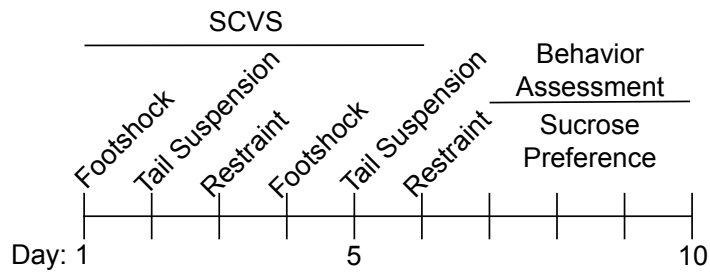


Figure 7 | Selective female susceptibility to SCVS in the measure of sucrose preference.

Experimental time course of stress and behavior assessment, including sucrose preference (top). Only female mice displayed reduced sucrose preference following SCVS as measured by two bottle choice task (bottom). Two-way ANOVA: Group: Male vs Female $F(1,112) = 1.109$, $p = 0.2946$; Trial: Control vs Stress $F(1,112) = 1.212$, $p = 0.2734$; Group X Trial $F(1,112) = 6.518$, $p = 0.0120$. Sidak's multiple comparisons: Male Control vs Stress Mean Diff = -2.406, 95% CI = -7.763 to 2.951; Female Control vs Stress Mean Diff = 6.054, 95% *CI = 0.7882 to 11.32; $n = 30/\text{group}$.

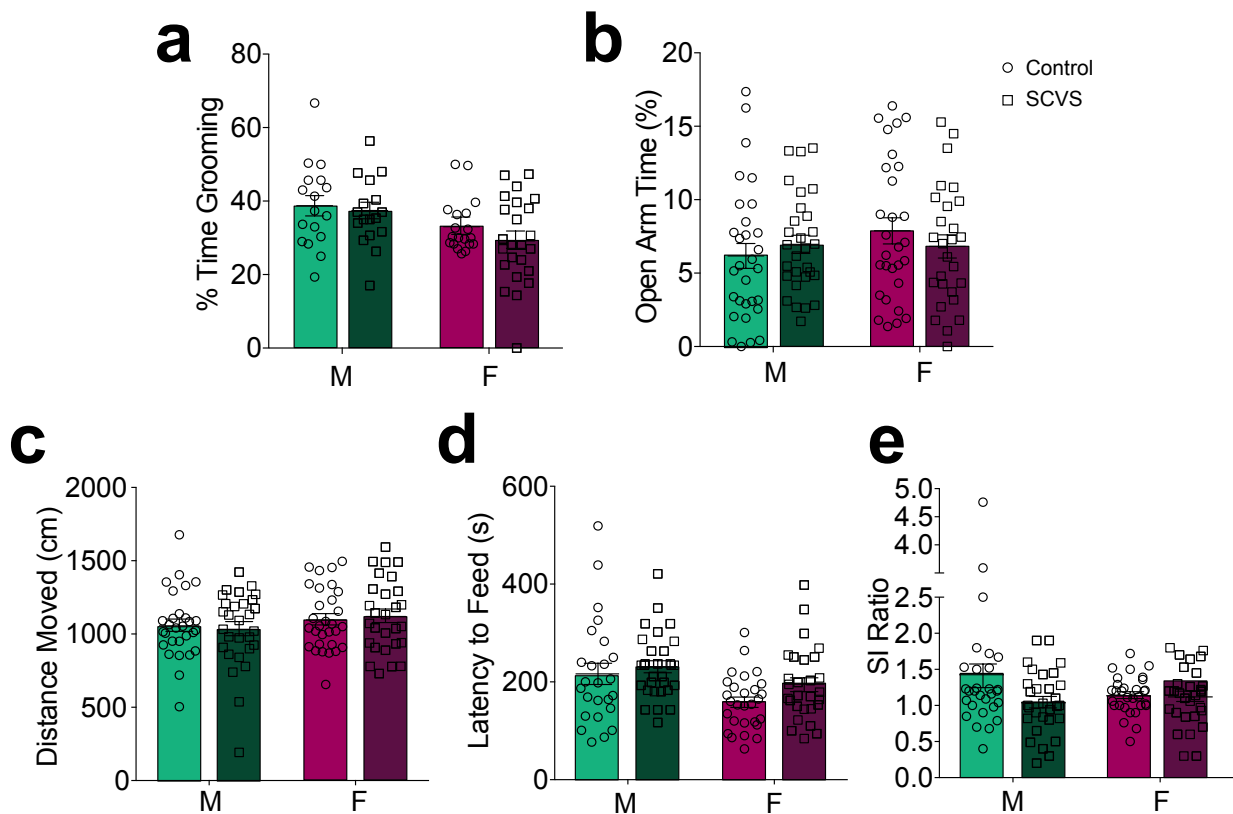


Figure 8 | Additional behavioral assays of male vs. female SCVS.

All behavioral assays other than sucrose preference did not reflect sex differences in SCVS as there was no interaction of stress and sex in any of the following measures: **(a)** Percent time grooming in splash test. Two-way ANOVA: Group: Male vs Female $F(1,73) = 6.223$, $p = 0.0149$; Trial: Control vs Stress $F(1,73) = 1.481$, $p = 0.2276$; Group X Trial $F(1,73) = 0.1272$, $p = 0.07223$ (no interaction). **(b)** Percent open arm time in EPM. Two-way ANOVA: Group: Male vs Female $F(1,111) = 0.9638$, $p = 0.3284$; Trial: Control vs Stress $F(1,111) = 0.0319$, $p = 0.8585$; Group X Trial $F(1,111) = 1.358$, $p = 0.2465$ (no interaction). **(c)** Distance moved (cm) in EPM. Two-way ANOVA: Group: Male vs Female $F(1,112) = 2.112$, $p = 0.1489$; Trial: Control vs Stress $F(1,112) = 4.352e-6$, $p = 0.9983$; Group X Trial $F(1,112) = 0.2906$, $p = 0.5909$ (no interaction). **(d)** Latency to feed (s) in novelty suppressed feeding test. Two-way ANOVA: Group: Male vs Female $F(1,107) = 10.23$, $p = 0.0018$; Trial: Control vs Stress $F(1,107) = 2.92$, $p = 0.0904$; Group X Trial $F(1,107) = 0.5162$, $p = 0.4741$ (no interaction). **(e)** SI Ratio in social interaction test. Two-way ANOVA: Group: Male vs Female $F(1,115) = 0.8692$, $p = 0.3531$; Trial: Control vs Stress $F(1,115) = 3.712$, $p = 0.0565$; Group X Trial $F(1,115) = 3.093$, $p = 0.0813$ (no interaction).

Female mice have increased vHPC-NAc neuronal excitability

The sex difference in susceptibility to SCVS suggests an underlying difference in physiology between male and female mice. Glutamatergic vHPC-NAc projections have been linked to stress susceptibility and reward in several elegant studies^{2,282}. To explore the vHPC-NAc circuit and its role in mediating anhedonic responses in mice following stress, we utilized whole cell patch clamp electrophysiology and the circuit-specific retrograde HSV-Cre labeling strategy²⁹¹ used in the previous chapter to record from vHPC-NAc cells in both male and female mice. As described above, transgenic mice expressing the Cre-inducible L10-GFP²⁷⁵ were injected in NAc with a retrograde herpes simplex virus (HSV) expressing Cre recombinase (Figure 9, left), leading to GFP expression in all neurons projecting to or within NAc. After 21 days to allow full retrograde expression, brain slices containing vHPC were prepared for whole-cell recordings from GFP-positive vHPC neurons projecting to NAc. In hippocampus, only pyramidal neurons of the ventral CA1/subiculum region were found to project to NAc using this method (Figure 9, right). We found female vHPC-NAc neurons to be more excitable than those of male mice, as indicated by an elevated number of action potentials elicited by increasing depolarizing current injections (Figure 10 top, example traces for each group below). No differences in resting membrane potential (V_M , Figure 11a) or membrane resistance (R_M , Figure 11b) were observed between male and female vHPC-NAc neurons. Despite the apparent heightened excitability of female vHPC-NAc neurons, input resistance (R_{in}) was significantly lower in these neurons compared to male vHPC-NAc neurons (Figure 11c). Membrane capacitance was significantly higher in female vHPC-NAc neurons (Figure 11d), again despite the female neurons' exaggerated response to injected current

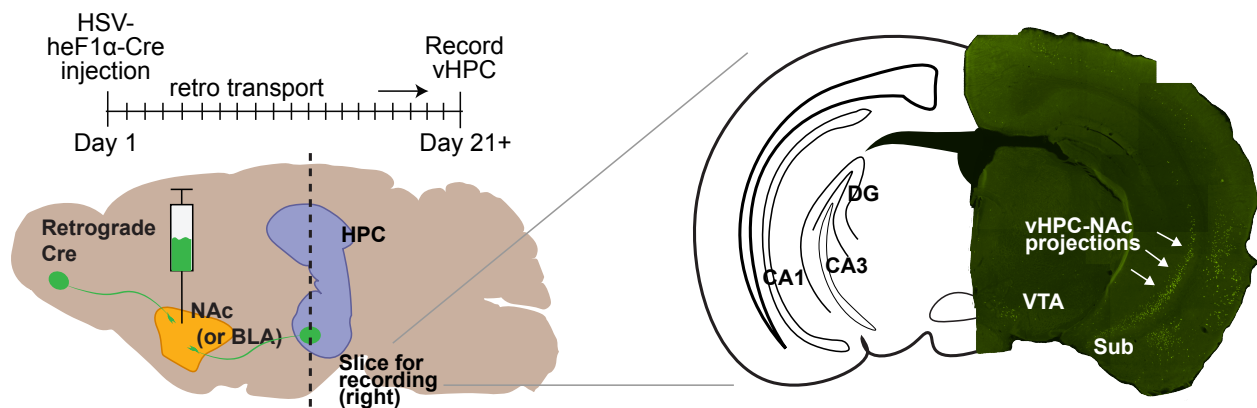


Figure 9 | Retrograde HSV-heF1 α -Cre injection at NAc predominantly labels vHPC CA1 pyramidal cells.

Schematic depicting retrograde Cre viral vector strategy and electrophysiology time course (left) and L10-GFP vHPC stained with anti-GFP demonstrating vHPC-NAc projections (right). Hippocampal projections to NAc arise from the ventral CA1 region and subiculum. Other areas appearing with projections to NAc as labeled by GFP staining include BLA and VTA.

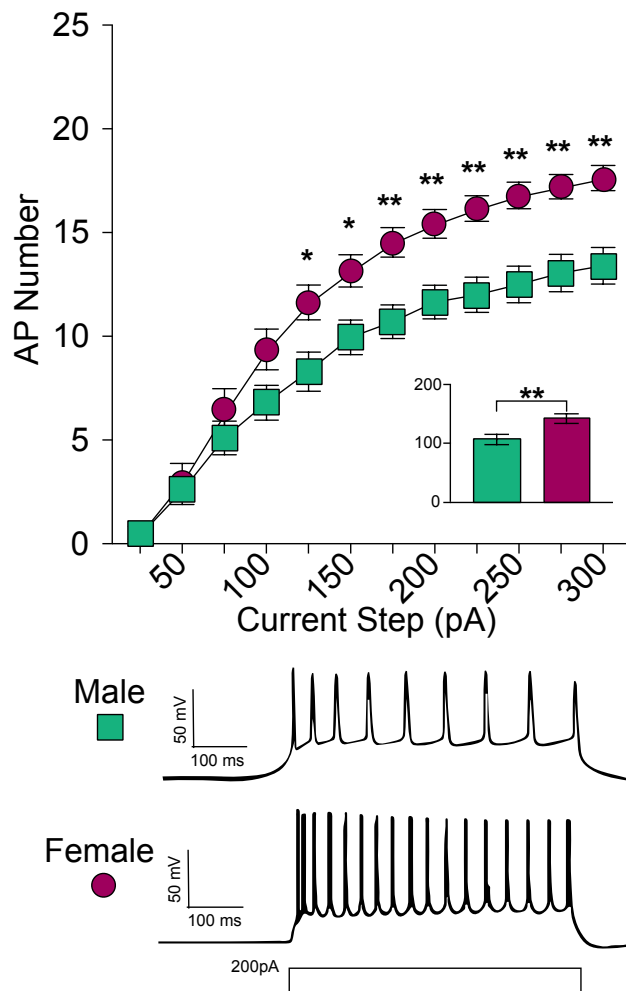


Figure 10 | Female vHPC-NAC projections are more excitable than male vHPC-NAC projections.

Action potential (AP) number across sequential depolarizing current steps (25-300 pA) for male (n = 20 cells from n = 6 animals) and female (n = 19 cells from n = 5 animals) vHPC-NAC projections. Females showed significantly higher AP number at all steps ≥ 125 pA (top). Two-way repeated measures ANOVA, Holm-Sidak multiple comparisons: Male vs Female [25 pA $t(444) = 0.1142$, $p = 0.9091$], [50 pA $t(444) = 0.4545$, $p = 0.8773$], [75 pA $t(444) = 1.147$, $p = 0.5816$], [100 pA $t(444) = 2.322$, $p = 0.0801$], [125 pA $t(444) = 3.012$, $*p = 0.0163$], [150 pA $t(444) = 2.901$, $*p = 0.0194$], [175 pA $t(444) = 3.46$, $**p = 0.0047$], [200 pA $t(444) = 3.41$, $**p = 0.0050$], [225 pA $t(444) = 3.76$, $**p = 0.0019$], [250 pA $t(444) = 3.879$, $**p = 0.0015$], [275 pA $t(444) = 3.762$, $**p = 0.0019$], [300 pA $t(444) = 3.826$, $**p = 0.0016$]. Inset: sum of AP number across all current steps. Two-tailed t-test $t(37)=2.96$, $**p = 0.0053$. Representative traces for male and female vHPC-NAC groups, 200 pA step (bottom).

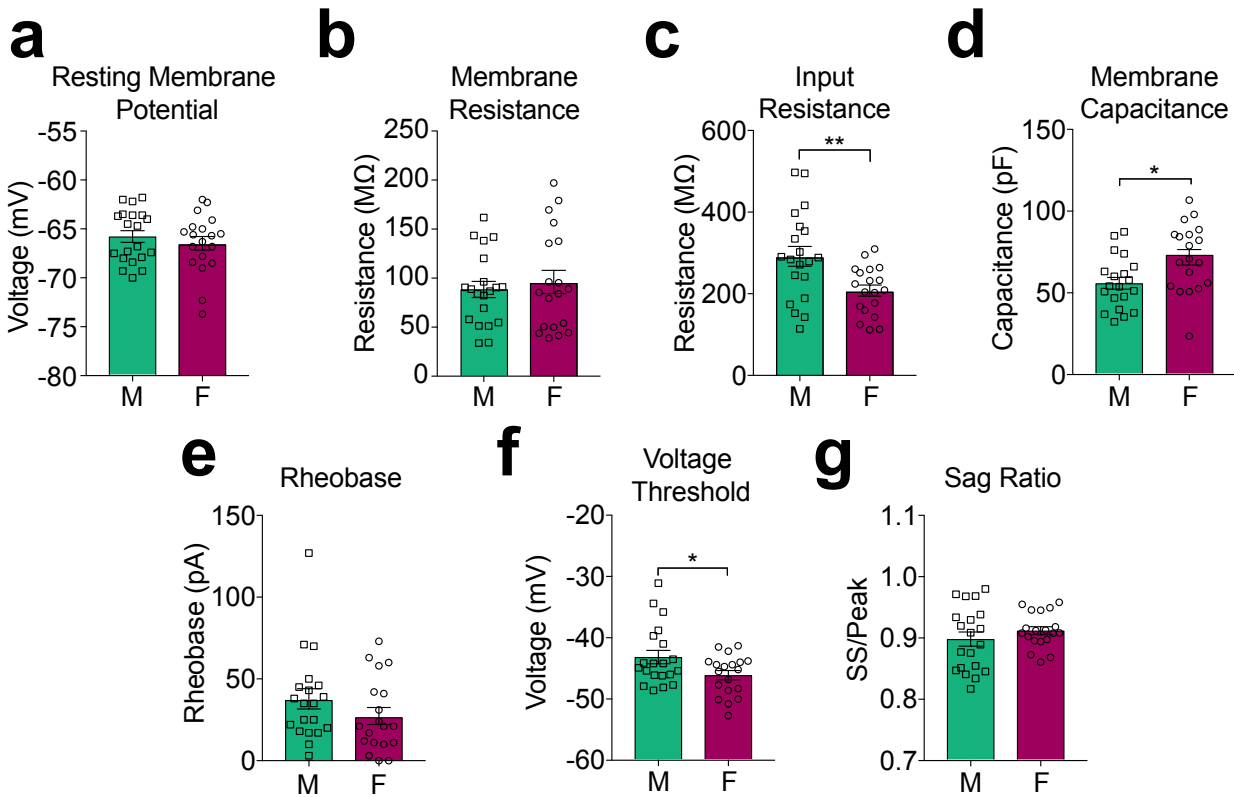


Figure 11 | Membrane properties of male vs. female vHPC-NAC projections.

(a) Resting membrane potential (mV) [two-tailed t-test $t(37) = 0.7643$, $p = 0.4495$] and **(b)** membrane resistance (MΩ) [two-tailed t-test: $t(37) = 0.5434$, $p = 0.5901$] did not differ between male and female vHPC-NAC projections. **(c)** Input resistance (MΩ) was significantly lower in female vHPC-NAC cells. Two-tailed Mann-Whitney U-test: $U = 96$, sum of ranks $M = 494$, $F = 286$, $**p = 0.0075$. **(d)** Membrane capacitance (pF) was significantly higher in female vHPC-NAC cells. Two-tailed t-test: $t(37) = 2.687$, $*p = 0.0107$. **(e)** Rheobase (pA) did not differ between male and female vHPC-NAC cells. Two-tailed t-test: $t(37) = 1.293$, $p = 0.2042$. **(f)** Action potential voltage threshold (mV) was lower in female vHPC-NAC cells. Two-tailed t-test: $t(37) = 2.202$, $*p = 0.0340$. **(g)** I_H as measured by sag ratio did not differ between male and female vHPC-NAC cells. Two-tailed Mann-Whitney U-test: $U = 163$, sum of ranks $M = 373$, $F = 407$, $p = 0.4609$.

compared to male neurons. Rheobase was not significantly different between male and female vHPC-NAc neurons (Figure 11e). Action potential threshold voltage was significantly lower in female neurons (Figure 11f), also indicating a heightened excitability in vHPC-NAc projections in female mice. There was no difference in sag ratio between male and female vHPC-NAc neurons (Figure 11g), indicating no difference in after-hyperpolarization current (I_h) in this circuit between sexes. Frequency of spontaneous excitatory postsynaptic currents (sEPSCs) did not differ between male and female vHPC-NAc neurons (Figure 12a), but sEPSC amplitude was significantly decreased in female mice (Figure 12b), suggesting that increased excitability in these neurons could be a homeostatic response to decreased excitatory input over time via modulation of postsynaptic effectors in females. Female vHPC-NAc neurons also demonstrate a dramatically lowered spike frequency adaptation compared to male neurons of the same circuit, as indicated by less increase in the interspike interval over the course of a depolarizing current injection step (Figure 13a), but no difference was observed between male and female neurons in the measure of latency to first spike in the same current step (Figure 13b). There was also no difference between male and female vHPC-NAc AMPA:NMDA ratio (Figure 14), indicating that there is no difference in the strength of synapses at the level of the vHPC in this circuit. Taken together, these results indicate robust sex differences in the neurophysiology of vHPC-NAc neurons, which may explain sex differences in stress responses to SCVS and disparities in depression prevalence between men and women.

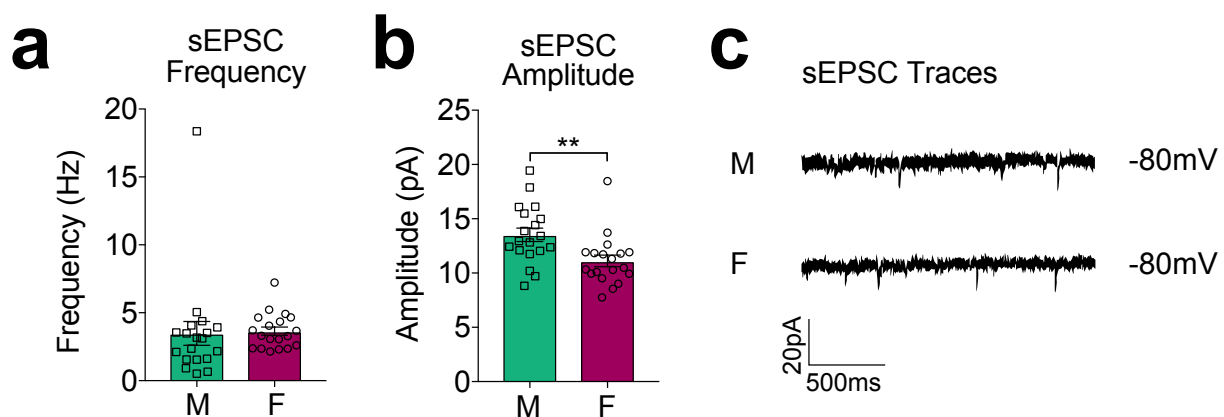


Figure 12 | Spontaneous activity measures of male vs female vHPC-NAc projections.

(a) sEPSC frequency did not differ between male and female vHPC-NAc cells [two-tailed Mann-Whitney U-test: $U = 125$, sum of ranks $M = 315$, $F = 426$, $p = 0.1089$], but sEPSC amplitude (b) was lower in female cells. Two-tailed t-test: $t(37) = 2.938$, $**p = 0.0057$. (c) Example sEPSC traces for male (M) and female (F) vHPC-NAc cell gap-free recordings at -80 mV holding potential.

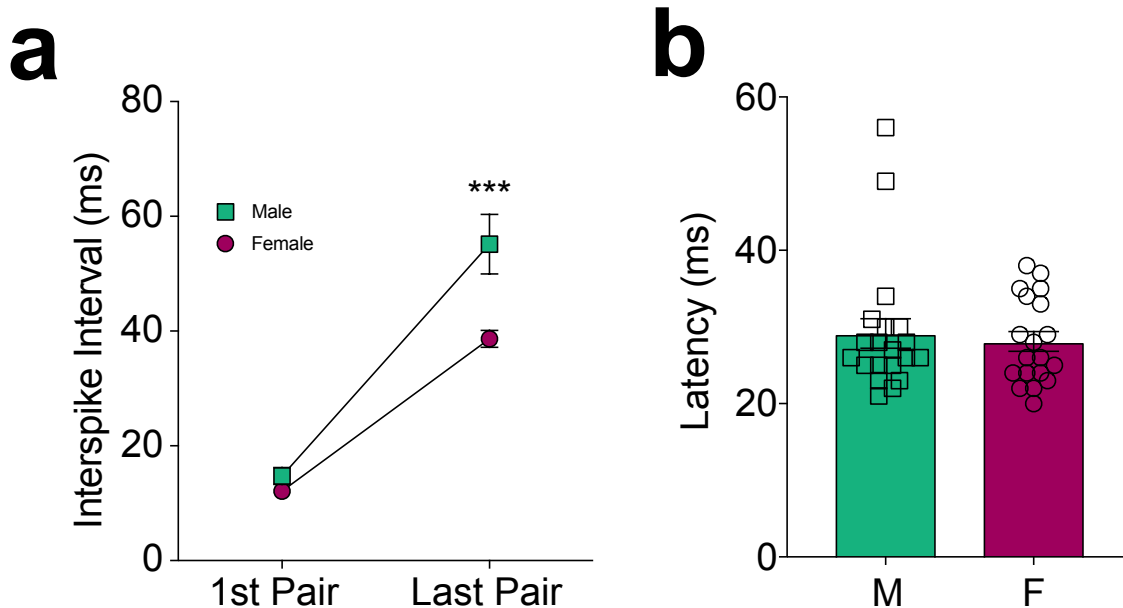


Figure 13 | Spike frequency adaptation is elevated in male vHPC-NAC projections compared to female vHPC-NAC projections.

Interspike interval increases over the course of 500 ms current injection as measured by the time (ms) between the 1st pair of spikes and last pair of spikes. **(a)** Males had more spike frequency adaptation as measured by the interspike interval increase; interspike interval of the last pair of spikes was significantly longer in male vHPC-NAC projections than in female projections. One-way ANOVA: $F(3,74) = 50.87$, $p < 0.0001$. Sidak's multiple comparisons: Male Last Pair vs Female Last Pair mean difference 16.52, 95% ***CI = 6.094 to 26.94, Adj. $p = 0.0005$. **(b)** Latency to 1st spike (ms) from beginning of current injection did not differ between male and female vHPC-NAC projection neurons. Two-tailed t-test: $t(37) = 0.4442$, $p = 0.6595$. Interspike intervals and latency to 1st spike were evaluated at the rheobase current for each cell.

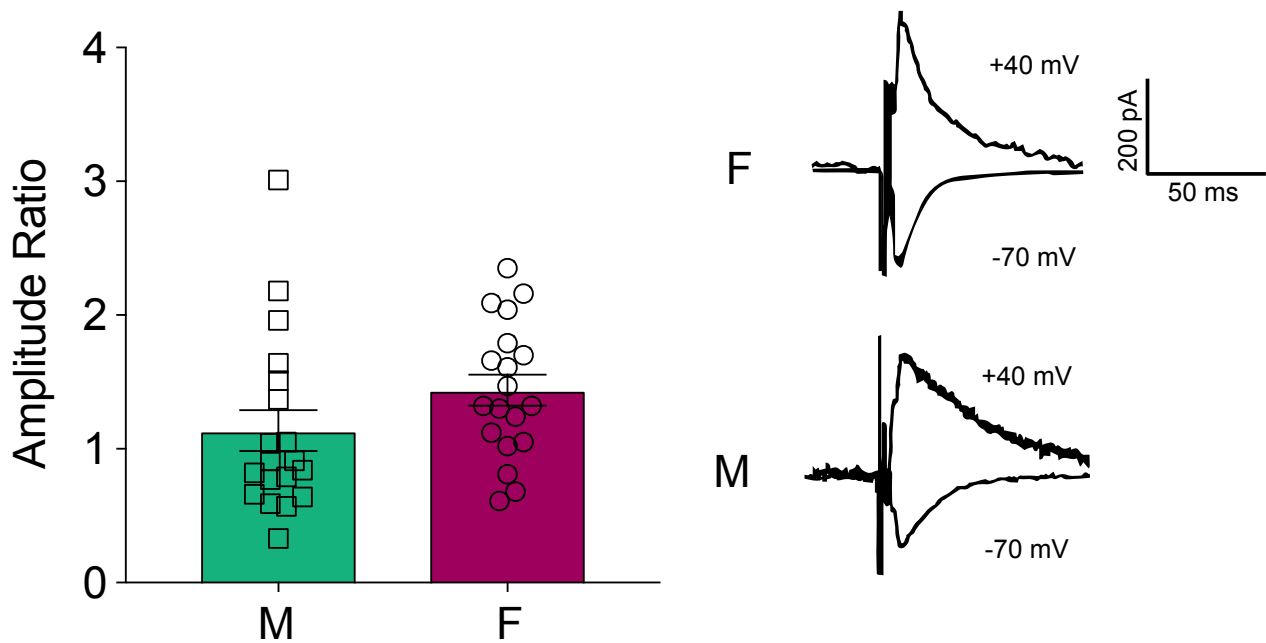


Figure 14 | AMPA to NMDA ratio of male and female vHPC-NAc projections.

Evoked AMPA and NMDA response amplitudes were used to calculate AMPA:NMDA as an indicator of synaptic strength. AMPA-mediated current amplitudes were evaluated at -70 mV holding potential, and NMDA-mediated current amplitudes were evaluated at +40 mV holding potential (amplitudes measured 50 ms following stimulation). AMPA:NMDA did not differ between male and female vHPC-NAc projections (left). Two-tailed t-test: $t(37) = 1.576$, $p = 0.1238$. Example traces of AMPA and NMDA evoked responses (right).

Sex differences in baseline excitability are unique to the vHPC-NAc circuit

To investigate whether the observed excitability differences were specific to the vHPC-NAc circuit, we injected retrograde HSV-Cre into basolateral amygdala (BLA) of a separate cohort of male and female mice. Whole-cell recordings obtained from vHPC-BLA projections revealed no significant difference in excitability of female vHPC-NAc neurons compared to male (Figure 15 top, example traces for each group below). There were also no differences between male and female vHPC-BLA neuron membrane properties in any measure (V_M , R_M , R_{in} , C_M , and rheobase; Figure 16a-e). No difference was observed between sexes in AP voltage threshold (Figure 16f), supporting similar male and female excitability in this circuit. Sag ratio was observed to be lower in female vHPC-BLA neurons (Figure 16g), indicating a possible sex difference in after-hyperpolarization current in this circuit. Spontaneous EPSCs did not differ in frequency or amplitude between male and female vHPC-BLA projections (Figure 17a-c). These findings, contrasted with the above vHPC-NAc circuit observations, demonstrate the specificity of the vHPC-NAc difference in excitability between male and female mice.

Overall, our electrophysiology experiments demonstrate that female vHPC-NAc, but not vHPC-BLA, neurons have increased excitability compared to males, suggesting a circuit-specific physiological difference that could underlie the sex differences in susceptibility to the anhedonia following stress. Next, we investigated the effects of adult hormone manipulation on susceptibility to SCVS and corresponding changes in vHPC-NAc projection physiology.

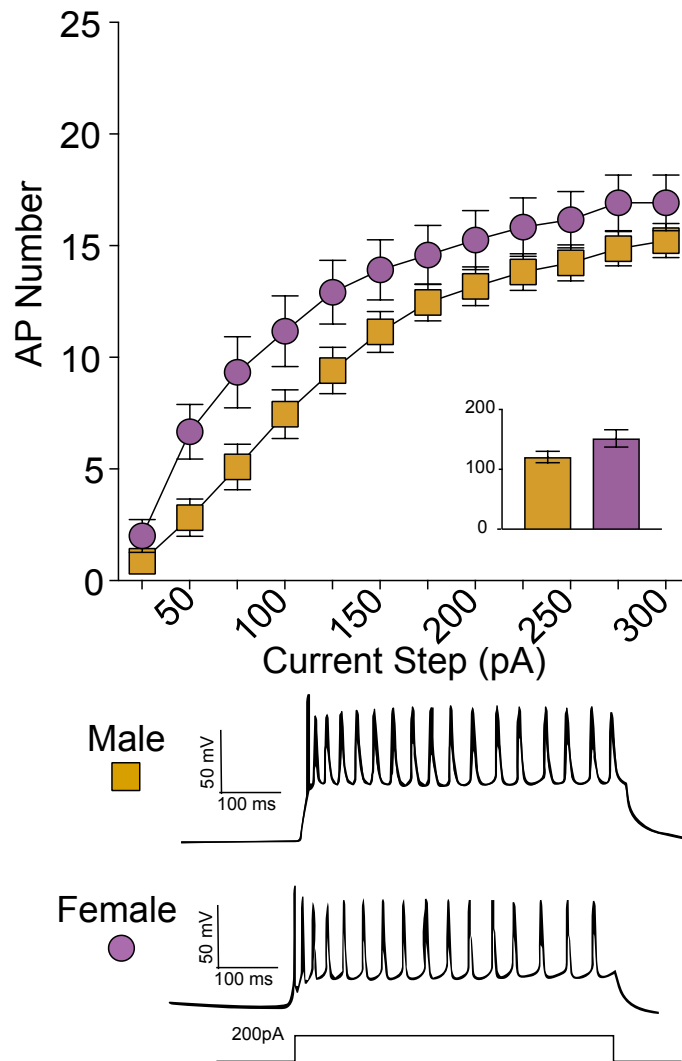


Figure 15 | Male and female vHPC-BLA projections do not differ in excitability.

AP number across sequential depolarizing steps for male (n = 22 cells from n = 7 animals) and female (n = 12 cells from n = 4 animals) vHPC-BLA projections. Male and female AP number did not differ at any current step (top). Two-way repeated measures ANOVA, Holm-Sidak multiple comparisons: [25 pA t(384) = 0.745, p = 0.9993], [50 pA t(384) = 2.523, p = 0.1352], [75 pA t(384) = 2.781, p = 0.0661], [100 pA t(384) = 2.434, p = 0.1699], [125 pA t(384) = 2.3, p = 0.2343], [150 pA t(384) = 1.823, p = 0.5765], [175 pA t(384) = 1.396, p = 0.8828], [200 pA t(384) = 1.356, p = 0.9019], [225 pA t(384) = 1.321, p = 0.9169], [250 pA t(384) = 1.272, p = 0.9356], [275 pA t(384) = 1.346, p = 0.9063], [300 pA t(384) = 1.108, p = 0.9766]. Inset: sum of AP number across all current steps. Two-tailed t-test: t(32) = 1.861, p = 0.0720. Representative traces for male and female vHPC-BLA groups, 200 pA step (bottom).

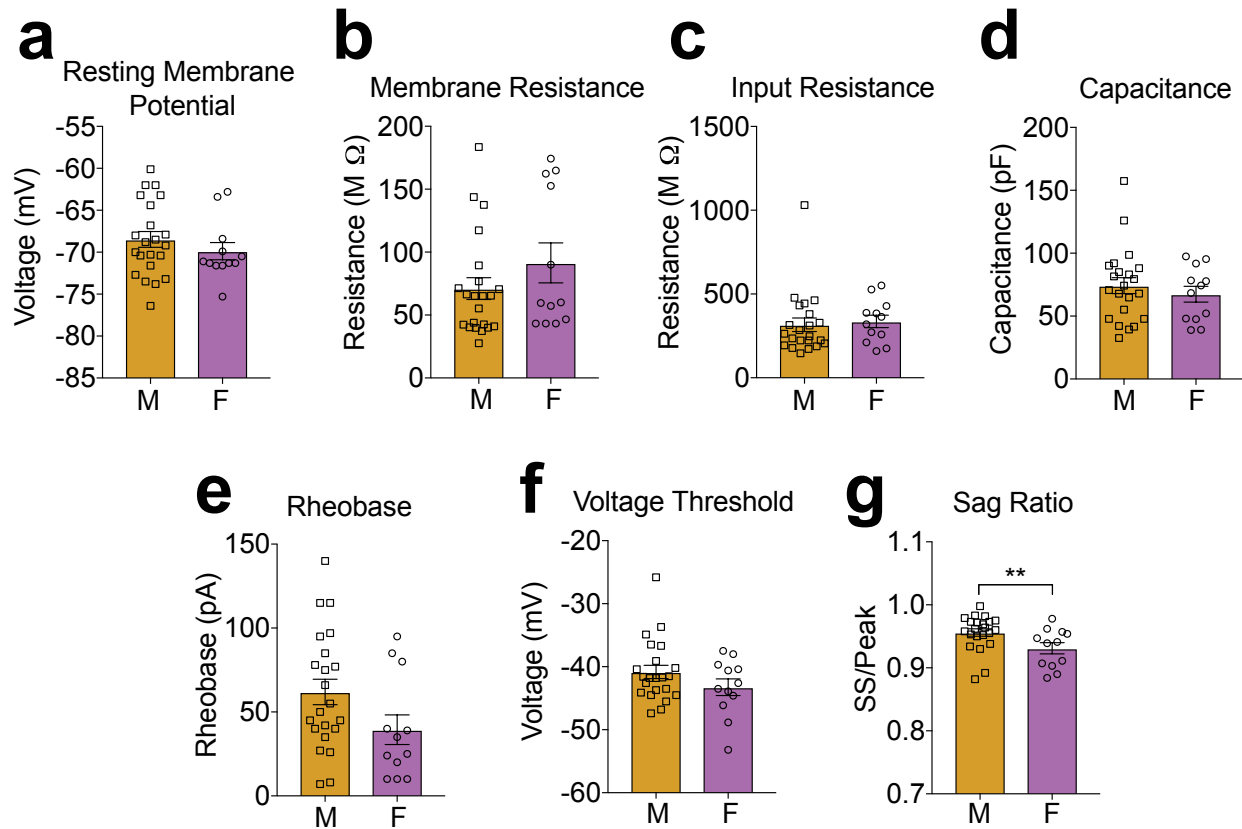


Figure 16 | Membrane properties of male vs. female vHPC-BLA projections.

vHPC-BLA projection cells did not differ between male and female groups in any of the following measures: **(a)** resting membrane potential (mV). Two-tailed t-test: $t(32) = 0.9449$, $p = 0.3518$; **(b)** membrane resistance ($M\Omega$). Two-tailed t-test: $t(32) = 1.24$, $p = 0.2238$; **(c)** input resistance ($M\Omega$). Two-tailed t-test: $t(32) = 0.3264$, $p = 0.7463$; **(d)** capacitance (pF). Two-tailed t-test: $t(32) = 0.7014$, $p = 0.4881$; **(e)** rheobase (pA). Two-tailed t-test: $t(32) = 1.852$, $p = 0.0733$; and **(f)** voltage threshold (mV). Two-tailed t-test: $t(32) = 1.399$, $p = 0.1713$. **(g)** I_H as measured by sag ratio was lower in female vHPC-BLA cells. Two-tailed t-test: $t(32) = 2.41$, $**p = 0.0219$.

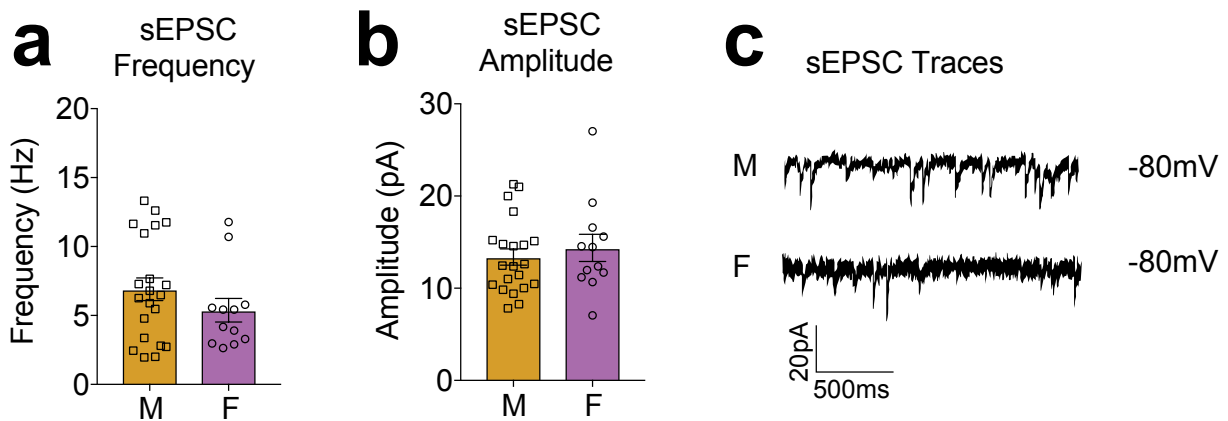


Figure 17 | Spontaneous activity measures of male vs female vHPC-BLA projections.

Spontaneous ESPC frequency [two-tailed t-test: $t(32) = 1.205$, $p = 0.2373$] **(a)** nor amplitude [two-tailed t-test: $t(32) = 0.6158$, $p = 0.5425$] **(b)** did not differ between male and female vHPC-BLA cells. **(c)** Example sEPSC traces for male (top) and female (bottom) vHPC-BLA gap-free cell recordings at -80 mV holding potential.

SCVS does not affect basal vHPC-NAc excitability in female mice

To investigate whether SCVS affects the excitability of vHPC-NAc neurons in female mice, we injected 7-week-old female C57/Bl6 mice with retrograde Cre virus at the NAc (as previously described). Following two weeks for recovery, mice were then subjected to the same SCVS protocol used above and immediately sacrificed within two days of completion of stress for whole-cell patch clamp recordings. We found no difference in the excitability of vHPC-NAc projections in these mice, as indicated by no change in spike number at any current injection step (Figure 18) nor an increase in the total number of spikes across all steps (Figure 18, inset). SCVS also did not cause a change in any membrane property measured (V_M , R_M , R_{in} , C_M , and rheobase; Figure 19a-e). These data indicate that SCVS does not cause a change in the physiology of female vHPC-NAc neurons when recordings were taken immediately following stress.

Orchidectomy induces male susceptibility to SCVS-induced anhedonia

To investigate the role of adult sex hormones in susceptibility to SCVS, male mice were orchidectomized (ORCH), allowed to recover for 10 or 28 days, and exposed to SCVS (Figure 20a-b). Ten days of recovery resulted in main effects of ORCH and stress without interaction between the two (Figure 20a), suggesting that SCVS this close to the stressful surgery (sham or ORCH) was sufficient to render male mice susceptible to SCVS-induced anhedonia. In contrast, twenty-eight days following ORCH, male mice displayed reduced sucrose preference following SCVS, while those undergoing sham surgeries remained resilient to decrease in sucrose preference

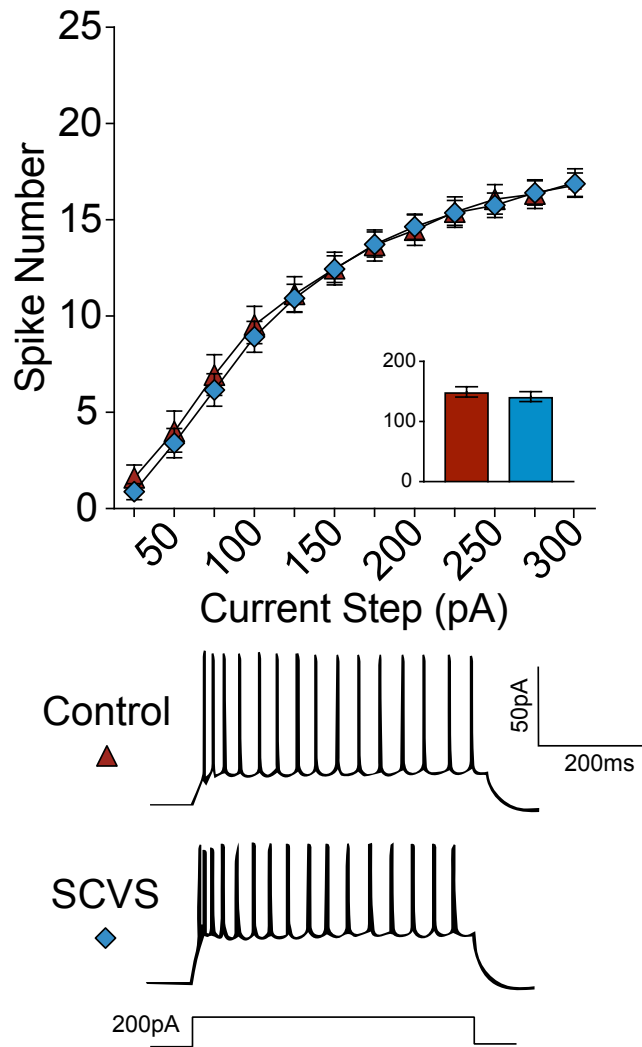


Figure 18 | Female control and post-SCVS vHPC-Nac projections do not differ in excitability.

Action potential (AP) number across sequential depolarizing current steps (25-300 pA) for female control (n = 15 cells from n = 4 animals) and female SCVS (n = 27 cells from n = 7 animals) vHPC-Nac projections. Groups did not differ in number of spikes at any step (top). Two-way repeated measures ANOVA, Holm-Sidak multiple comparisons: Male vs Female [25 pA $t(456) = 0.6533$, $p = 0.9998$], [50 pA $t(456) = 0.5444$, $p > 0.9999$], [75 pA $t(456) = 0.7017$, $p = 0.9996$], [100 pA $t(456) = 0.5565$, $p > 0.9999$], [125 pA $t(456) = 0.1936$, $p > 0.9999$], [150 pA $t(456) = 0.0242$, $p > 0.9999$], [175 pA $t(456) = 0.04839$, $p > 0.9999$], [200 pA $t(456) = 0.1573$, $p > 0.9999$], [225 pA $t(456) = 0.03629$, $p > 0.9999$], [250 pA $t(456) = 0.2783$, $p > 0.9999$], [275 pA $t(456) = 0.06049$, $p > 0.9999$], [300 pA $t(456) = 0.121$, $p > 0.9999$]. Inset: sum of AP number across all current steps. Two-tailed t-test $t(29) = 0.607$, $p = 0.5486$. Representative traces for control and SCVS female vHPC-Nac groups, 200 pA step (bottom).

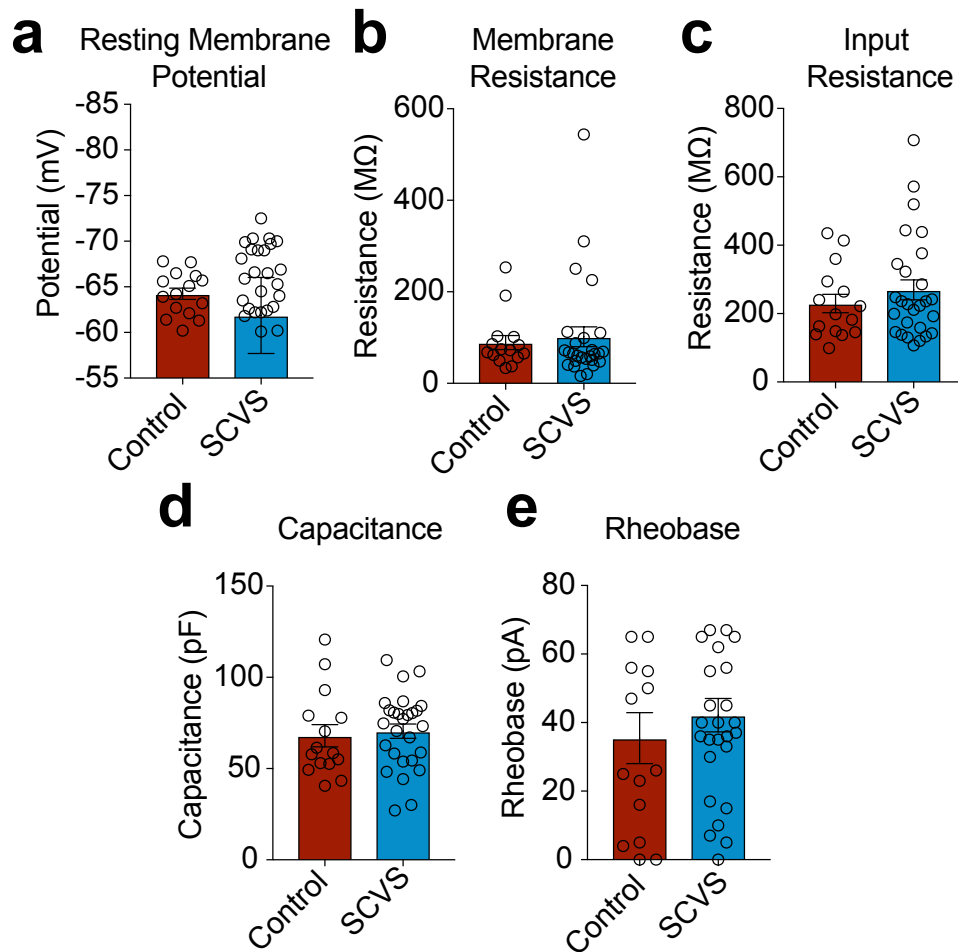


Figure 19 | Membrane properties of control and post-SCVS female vHPC-NAc neurons.

Control and SCVS female vHPC-NAc neurons did not differ in any of the following measures: **(a)** resting membrane potential (mV; two-tailed Mann-Whitney U-test: $U = 151$, sum of ranks control = 374, SCVS = 529, $p = 0.1806$); **(b)** membrane resistance (MΩ; Mann-Whitney U-test: $U = 177$, sum of ranks control = 348, SCVS = 555, $p = 0.5161$); **(c)** input resistance (MΩ; $t(40) = 0.903$, $p = 0.3719$); **(d)** membrane capacitance (pF; $t(40) = 0.3628$, $p = 0.7187$); and **(e)** rheobase (pA; $t(40) = 0.7795$, $p = 0.4402$).

(Figure 20b), with an interaction between the two variables. There were no differences between sham and ORCH groups in any other behavioral measure at either time point (Figure 21a-d). These data thus suggest that long-term reduction in androgen signaling is sufficient for SCVS-induced anhedonia in male mice.

Orchidectomy reduces excitability of vHPC-NAc neurons

To determine whether the sex difference we observed in vHPC-NAc excitability is also dependent on adult sex hormones, we compared vHPC-NAc excitability in ORCH vs. sham male and OVX vs. sham female mice at 10 days post-gonadectomy. Retrograde Cre was injected into NAc, 10 days following intracranial injection gonads were removed, and 10 days following gonadectomy, vHPC-NAc activity was recorded (Figure 22a). ORCH significantly increased the excitability of male vHPC-NAc neurons compared to that of sham controls (Figure 22b top, example traces for each group below). ORCH had no effect on V_M , R_M , R_{in} , or C_M (Figure 23a-d), but did increase rheobase (Figure 23e), with no change in AP voltage threshold (Figure 23f). There was no observed difference between sham and ORCH animals in sag ratio (Figure 23g), and ORCH did not affect sEPSC frequency or amplitude (Fig 24a-c). Orchidectomy did cause a decrease in spike frequency adaptation, as indicated by a smaller interspike interval duration over the course of a depolarizing current injection (Figure 25a). This was accompanied by an increase in the latency to first spike in the same current step (Figure 25b).

In contrast, ovariectomy (OVX) was performed using the same experimental timeline as the above ORCH experiment. OVX had no effect on the excitability of female vHPC-NAc neurons compared to those neurons in sham-operated mice (Figure 26 top,

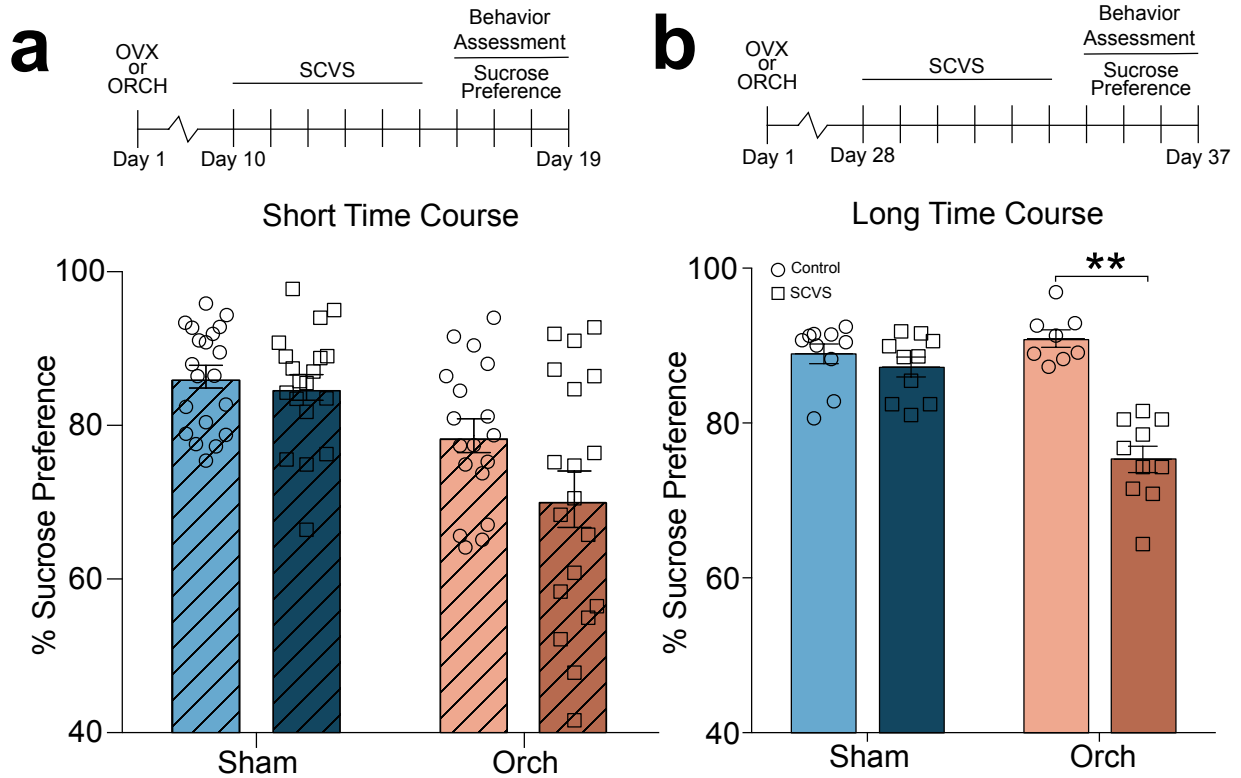


Figure 20 | Orchidectomy of male mice induces susceptibility to SCVS as measured by sucrose preference, but only with extended time following surgery.

(a, top) Schematic depicting experimental time course of surgery, stress, and measurement of sucrose preference for short time course orchidectomy experiment. **(a, bottom)** Short time course sham vs orchidectomized male mice showed no interaction between surgery and stress. Two-way ANOVA: Group: Sham vs ORCH $F(1,73) = 21.78$, $p < 0.0001$; Trial: Control vs Stress $F(1,73) = 0.0462$; Group X Trial $F(1,73) = 2.116$, $p = 0.1500$ (no interaction); $n = 20$ control sham, 18 control ORCH, 20 SCVS sham, 18 SCVS ORCH. **(b, top)** Schematic depicting experimental time course of surgery, stress, and measurement of sucrose preference for long time course orchidectomy experiment. **(b, bottom)** Orchidectomized male mice showed significant reduction in sucrose preference compared to non-stress controls, while sham male sucrose preference was unaffected by SCVS. Two-way ANOVA: Group: Sham vs ORCH $F(1,34) = 24.76$, $p < 0.0001$; Trial: Control vs Stress $F(1,34) = 12.74$, $p = 0.0011$; Group X Trial $F(1,34) = 38.33$, $p < 0.0001$. Sidak's multiple comparisons: Orch Control vs Stress Mean Difference = 15.59, 95% **CI = 10.84 to 20.35; $n = 10$ control sham, 8 control ORCH, 10 SCVS sham, 9 SCVS ORCH.

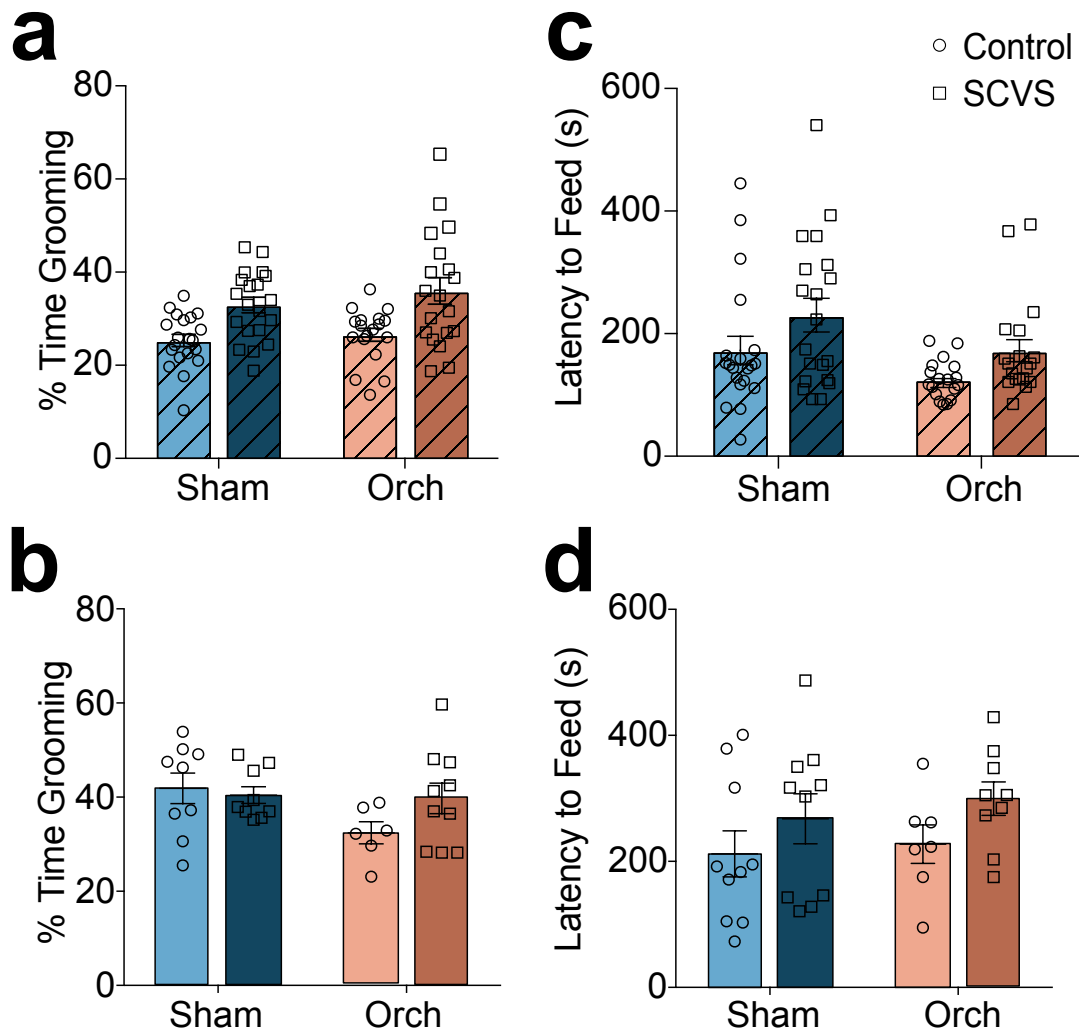


Figure 21 | Additional behavioral assays of sham vs. orchidectomy SCVS.

All behavioral assays other than sucrose preference did not reflect an interaction of hormone status and stress in any of the following measures: Percent time grooming in splash test in the 10-day [two-way ANOVA: Group: Sham vs ORCH $F(1,73) = 1.244$, $p = 0.2684$; Trial: Control vs Stress $F(1,73) = 20.28$, $p < 0.0001$; Group X Trial $F(1,73) = 0.2295$, $p = 0.6333$ (no interaction)] **(a)** and 28-day [two-way ANOVA: Group: Sham vs ORCH $F(1,30) = 0.0934$, $p = 0.1460$; Trial: Control vs Stress $F(1,30) = 1.007$, $p = 0.3237$] **(b)** time courses; and latency to feed (s) in novelty suppressed feeding test in the 10-day [two-way ANOVA: Group: Sham vs ORCH $F(1,73) = 6.339$, $p = 0.0140$; Trial: Control vs Stress $F(1,73) = 6.258$, $p = 0.0146$; Group X Trial $F(1,73) = 0.06081$ (no interaction)] **(c)** and 28-day (two-way ANOVA: Group: Sham vs ORCH $F(1,32) = 0.45$, $p = 0.5072$; Trial: Control vs Stress $F(1,32) = 3.28$, $p = 0.0795$; Group X Trial $F(1,32) = 0.0534$, $p = 0.8187$ (no interaction)] **(d)** time courses.

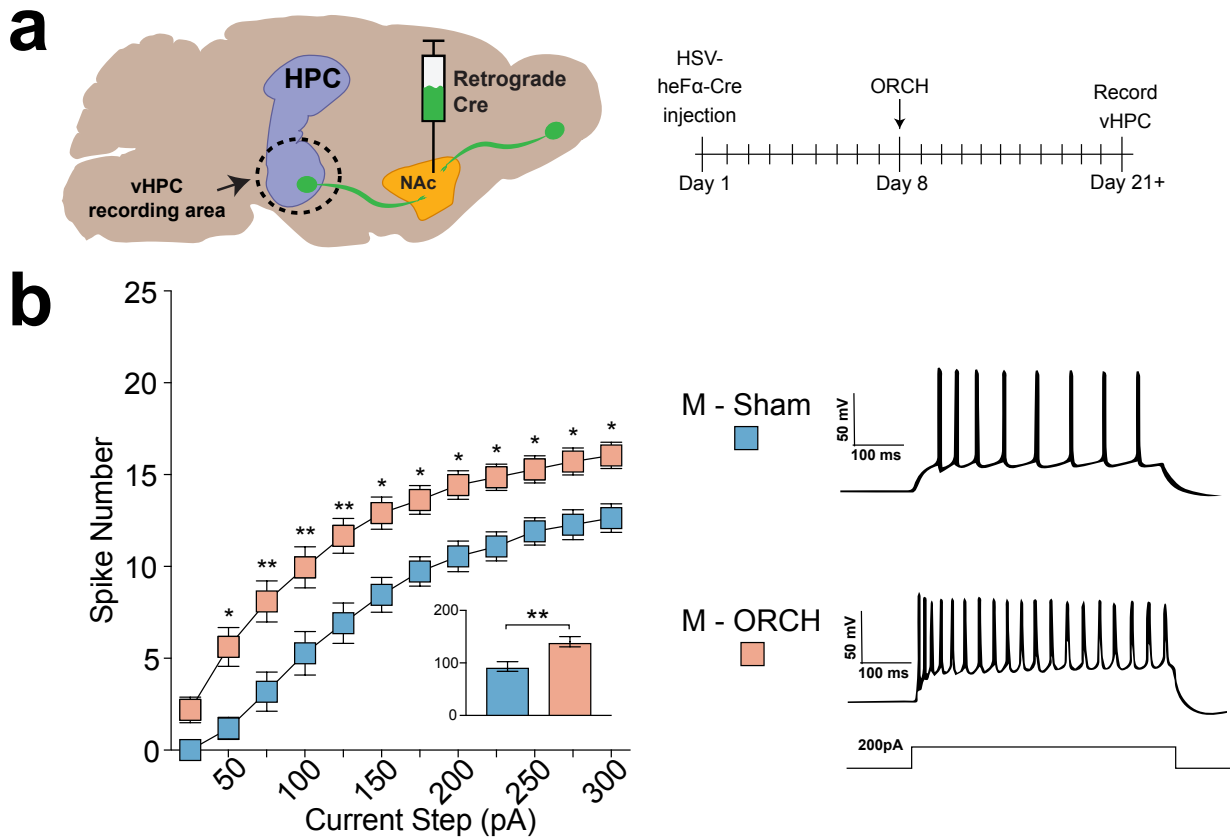


Figure 22 | Orchidectomy in male mice increases vHPC-NAc excitability.

(a) Schematic depicting retrograde Cre viral strategy for labeling vHPC-NAc projections (left) and experimental time course for surgery and recording (right). **(b, left)** Action potential number across sequential depolarizing current steps (25-300 pA) for sham male ($n = 11$ cells from $n = 3$ animals) and orchidectomized male ($n = 31$ cells from $n = 6$ animals) vHPC-NAc projections. Orchidectomized male projections showed significantly higher AP number at all steps > 25 pA. Two-way repeated measures ANOVA, Holm-Sidak multiple comparisons: [25 pA $t(360) = 1.614$, $p = 0.1073$], [50 pA $t(360) = 3.27$, $*p = 0.0102$], [75 pA $t(360) = 3.621$, $**p = 0.0040$], [100 pA $t(360) = 3.449$, $**p = 0.0063$], [125 pA $t(360) = 3.506$, $**p = 0.0056$], [150 pA $t(360) = 3.28$, $*p = 0.0102$], [175 pA $t(360) = 2.868$, $*p = 0.0302$], [200 pA $t(360) = 2.862$, $*p = 0.0302$], [225 pA $t(360) = 2.776$, $*p = 0.0302$], [250 pA $t(360) = 2.489$, $*p = 0.0457$], [275 pA $t(360) = 2.536$, $p = 0.0457$], [300 pA $t(360) = 2.514$, $*p = 0.0457$]. Inset: sum of AP number across all current steps. Two-tailed t-test: $t(30) = 3.131$, $**p = 0.0039$. **(b, right)** Representative traces for sham and ORCH vHPC-NAc projections, 200 pA step.

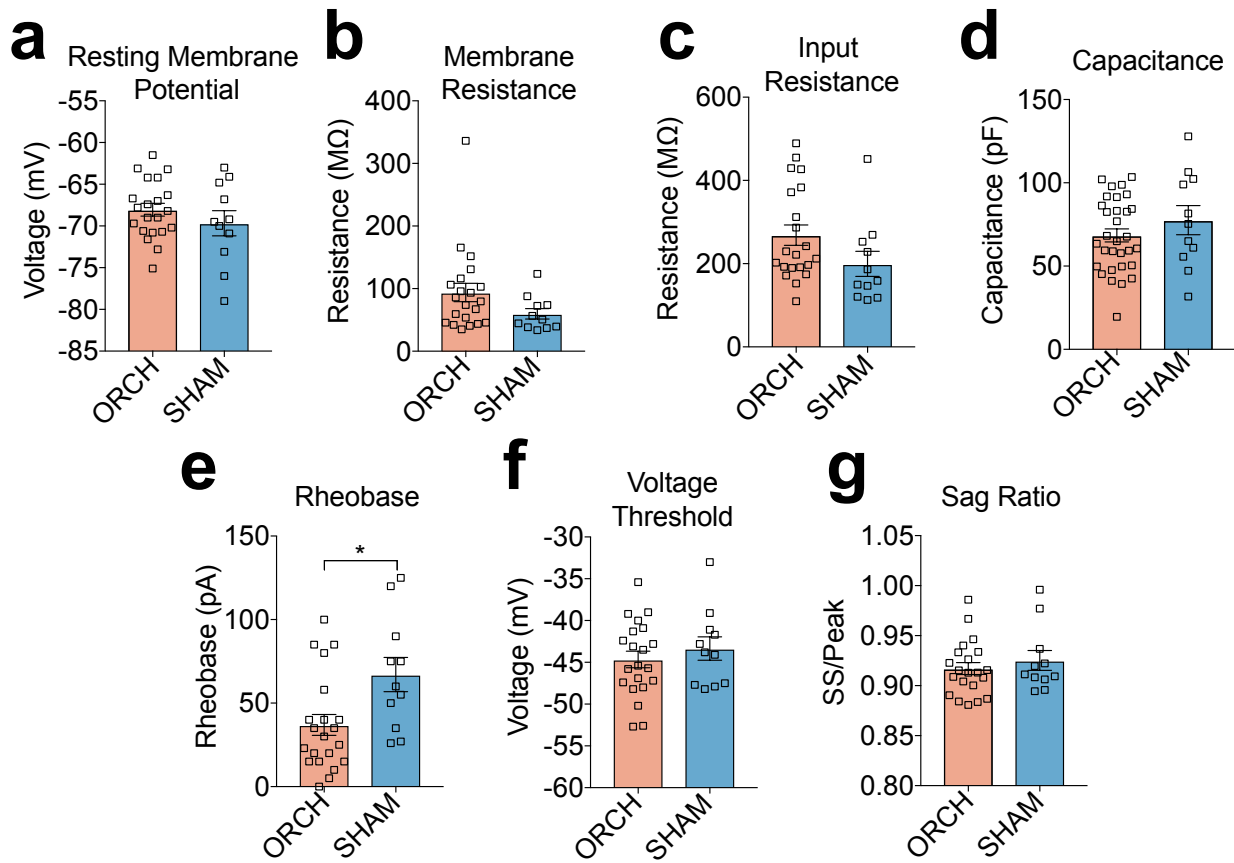


Figure 23 | Membrane properties of sham vs. orchidectomy male vHPC-NAC projections.

vHPC-NAC projection cells did not differ between male sham and orchidectomy groups in any of the following measures: **(a)** resting membrane potential (mV). Two-tailed t-test: $t(30) = 1.077$, $p = 0.2902$; **(b)** membrane resistance (MΩ). Two-tailed Mann-Whitney U-test: $U = 67.5$, sum of ranks ORCH = 394.5, Sham = 133.5, $p = 0.0573$; **(c)** input resistance (MΩ). Two-tailed t-test: $t(30) = 1.713$, $p = 0.0970$; and **(d)** membrane capacitance (pF). Two-tailed t-test: $t(30) = 1.098$, $p = 0.2786$. **(e)** Orchidectomy male vHPC-NAC projection cells showed a decreased rheobase (pA) compared to sham projections. Two-tailed t-test: $t(30) = 2.648$, $*p = 0.0128$. **(f)** Voltage threshold (mV) [two-tailed t-test: $t(30) = 0.7637$, $p = 0.4510$] and **(g)** sag ratio [two-tailed t-test: $t(30) = 0.74$, $p = 0.4651$] did not differ between sham and orchidectomy groups.

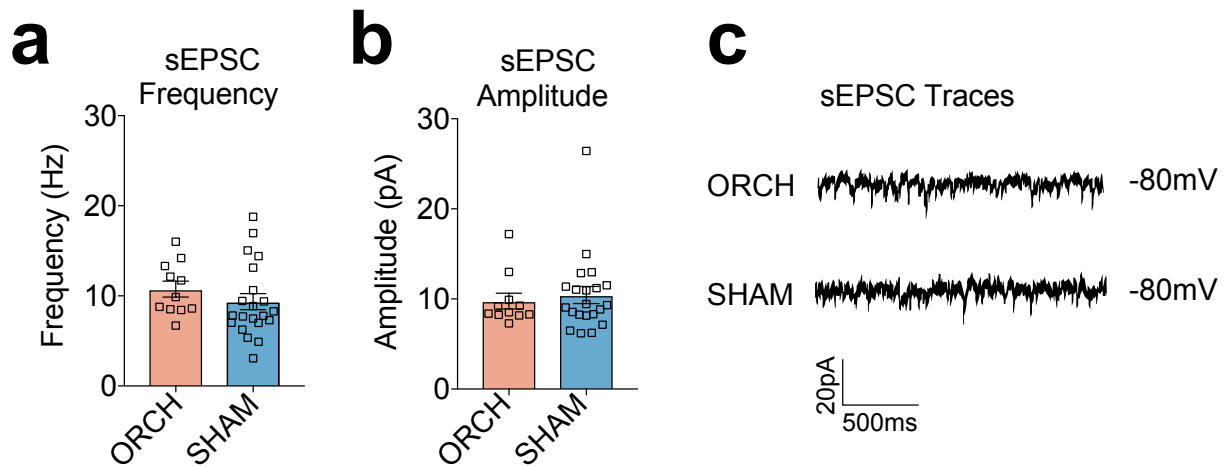


Figure 24 | Spontaneous activity measures of orchidectomy vs sham male vHPC-NAc neurons.

(a) Spontaneous EPSC frequency (Hz) [two-tailed t-test: $t(30) = 0.9992$, $p = 0.3257$] and (b) amplitude (pA) [two-tailed t-test: $t(30) = 0.4635$, $p = 0.6464$] did not differ between sham and orchidectomy groups. (c) Example sEPSC traces for ORCH (top) and sham (bottom) vHPC-NAc recordings.

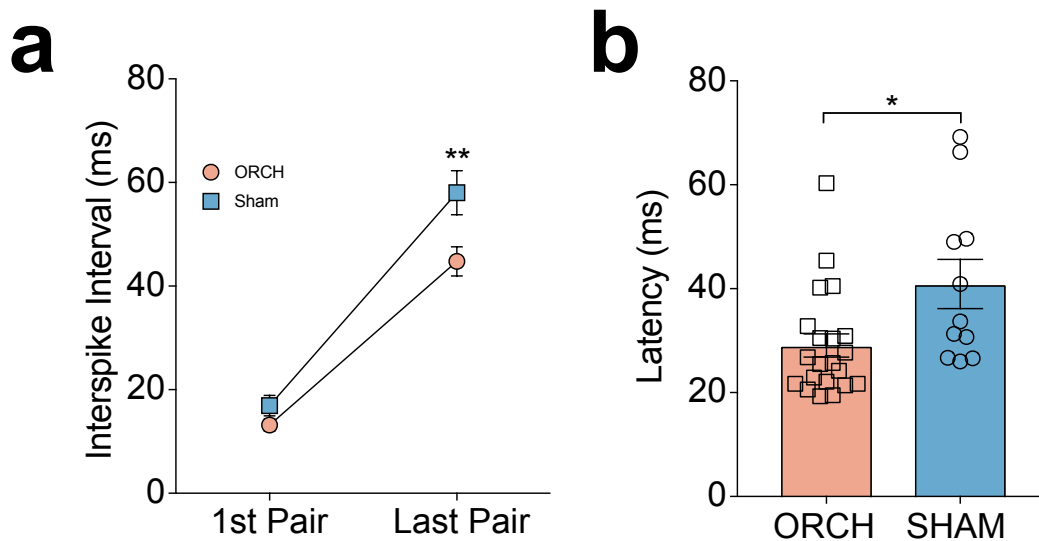


Figure 25 | Spike frequency adaptation is impaired in male vHPC-NAc projections following orchidectomy.

Interspike interval increases over the course of 500 ms current injection as measured by the time (ms) between the 1st pair of spikes and last pair of spikes in male sham and ORCH vHPC-NAc neurons. **(a)** ORCH vHPC-NAc neurons had less spike frequency adaptation as measured by the interspike interval increase over current step; interspike interval of the last pair of spikes was significantly shorter in ORCH vHPC-NAc projections than in sham projections. One-way ANOVA: $F(3, 60) = 65.91$, $p < 0.0001$. Sidak's multiple comparisons: ORCH Last Pair vs Sham Last Pair mean difference -13.25 , 95% **CI = -23.05 to -3.439 , Adj. $p = 0.0039$. **(b)** Latency to 1st spike (ms) from beginning of current injection was also decreased in ORCH vHPC-NAc neurons compared to sham. Two-tailed t-test: $t(30) = 2.587$, $*p = 0.0148$. Interspike intervals and latency to 1st spike were evaluated at the rheobase current for each cell.

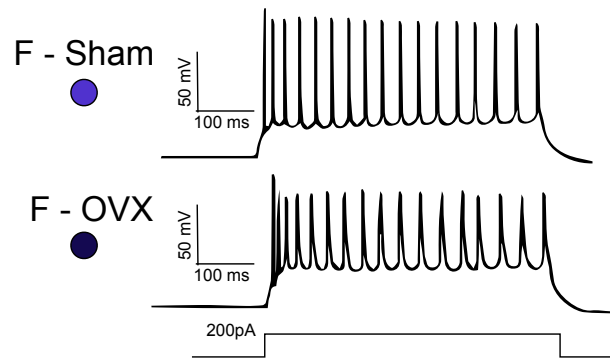
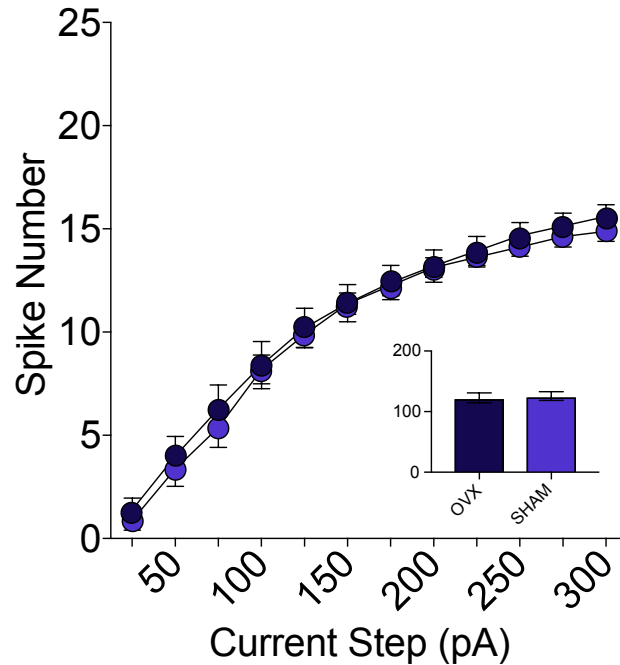


Figure 26 | Sham and OVX female vHPC-NAc projections do not differ in excitability.

Sham (n = 16 cells from n = 4 animals) and OVX (n = 15 cells from n = 4 animals) female vHPC-NAc neurons did not differ in excitability as measured by number of spikes per 25 pA current injection step from 25-300 pA (top); Two-way repeated measures ANOVA, Holm-Sidak multiple comparisons: [25 pA t(348) = 0.5113, p = 0.9997], [50 pA t(348) = 0.6087, p = 0.9996], [75 pA t(348) = 0.8684, p = 0.9971], [100 pA t(348) = 0.2069, p = 0.9998], [125 pA t(348) = 0.3165, p = 0.9998], [150 pA t(348) = 0.0244, p = 0.9998], [175 pA t(348) = 0.1461, p = 0.9998], [200 pA t(348) = 0.0730, p = 0.9998]. [225 pA t(348) = 0.3003, p = 0.9998], [250 t(348) = 0.5275, p = 0.9997], [275 pA t(348) = 0.4951, p = 0.9997], [300 pA t(348) = 0.7061, p = 0.9993]. Inset: total number of spikes summed over all current injection steps did not differ between sham and OVX groups. Two-tailed t-test: t(29) = 0.2763, p = 0.7843. Representative traces for sham and OVX vHPC-NAc projections, 200 pA step (bottom).

example traces for each group below). OVX also did not affect membrane properties (Figure 27a-f), sag ratio (Figure 27g) nor sEPSC frequency or amplitude (Figure 28a-c). There was also no change in spike frequency adaptation following OVX compared to sham-operated controls (Figure 29a), and no change in the latency to first spike at the same current step (Figure 29b). Taken together with the above ORCH experiments, these findings demonstrate the importance of testes-derived mediators (e.g. androgen hormones) in the time-dependent regulation of vHPC-NAc excitability in male mice. This points to male gonadal hormone reduction of vHPC-NAc activity as the possible mechanism for the established sex difference in SCVS-induced anhedonia, and may work to elucidate neurophysiological differences between men and women that lead to differential MDD diagnoses.

Orchidectomy reduces excitability of vHPC-BLA neurons

To determine whether vHPC-BLA excitability is also dependent on adult sex hormones, we compared ORCH vs. sham male and OVX vs. sham female mice at 10 days post-gonadectomy. Retrograde Cre was injected into BLA, 10 days following intracranial injection gonads were removed, and 10 days following gonadectomy, vHPC-BLA activity was recorded. ORCH increased the excitability of male vHPC-BLA neurons compared to that of sham controls as indicated by an increase in the total number of spikes over all current injection steps (Figure 30, inset), but did not cause significant differences in spike number at any individual current step (Figure 30). ORCH had no effect on resting membrane potential (Figure 31a), but did increase membrane resistance (Figure 31b). Input resistance did not differ between groups (Figure 31c), but

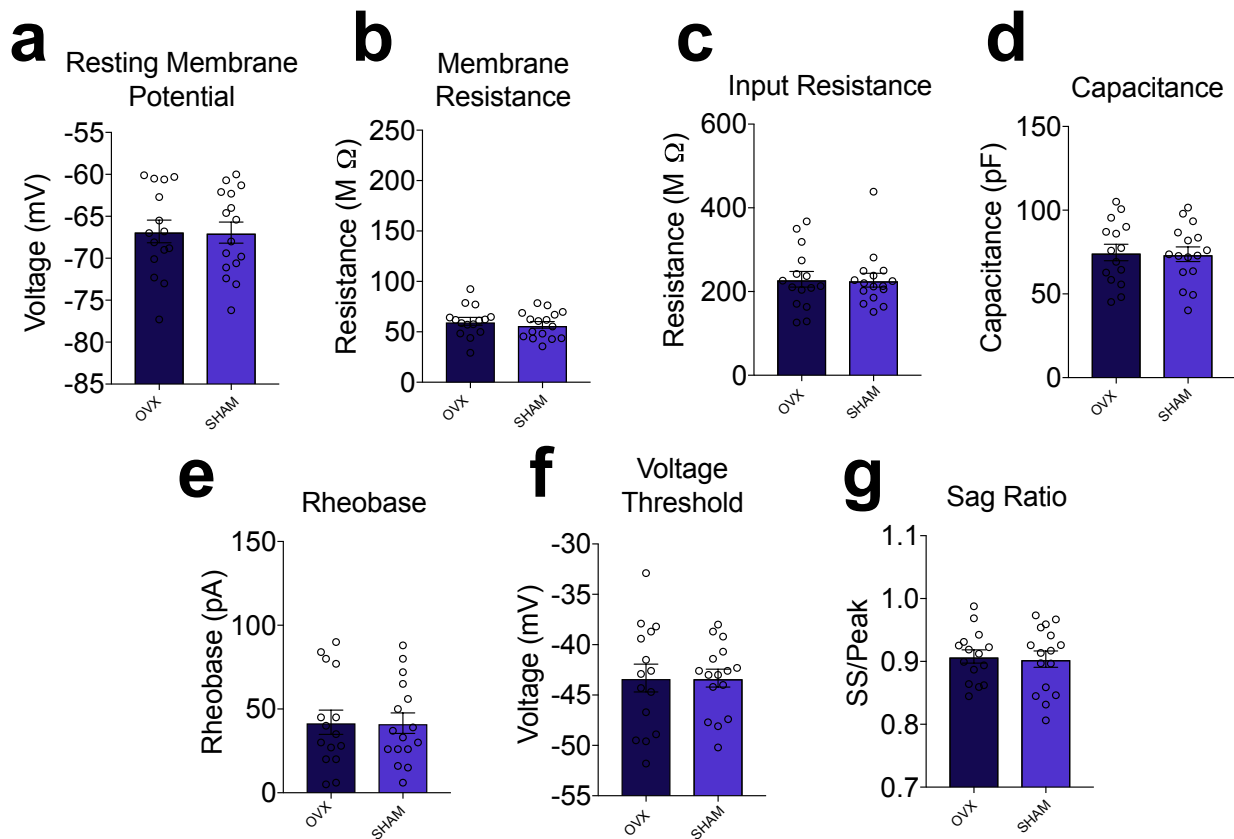


Figure 27 | Membrane properties of sham vs. ovariectomy female vHPC-NAc projections.

Sham and OVX groups did not differ over any of the following measures: **(a)** resting membrane potential (mV). Two-tailed t-test: $t(29) = 0.0709$, $p = 0.9439$; **(b)** membrane resistance ($M\Omega$). Two-tailed t-test: $t(29) = 0.708$, $p = 0.4846$; **(c)** input resistance ($M\Omega$). Two-tailed t-test: $t(29) = 0.7262$, $p = 0.4761$; **(d)** membrane capacitance (pF). Two-tailed t-test: $t(29) = 0.0903$, $p = 0.9287$; **(e)** rheobase (pA). Two-tailed t-test: $t(29) = 0.0605$, $p = 0.9522$; **(f)** voltage threshold (mV). Two-tailed t-test: $t(29) = 0.0075$, $p = 0.9941$; **(g)** sag ratio. Two-tailed t-test: $t(29) = 0.2533$, $p = 0.8018$.

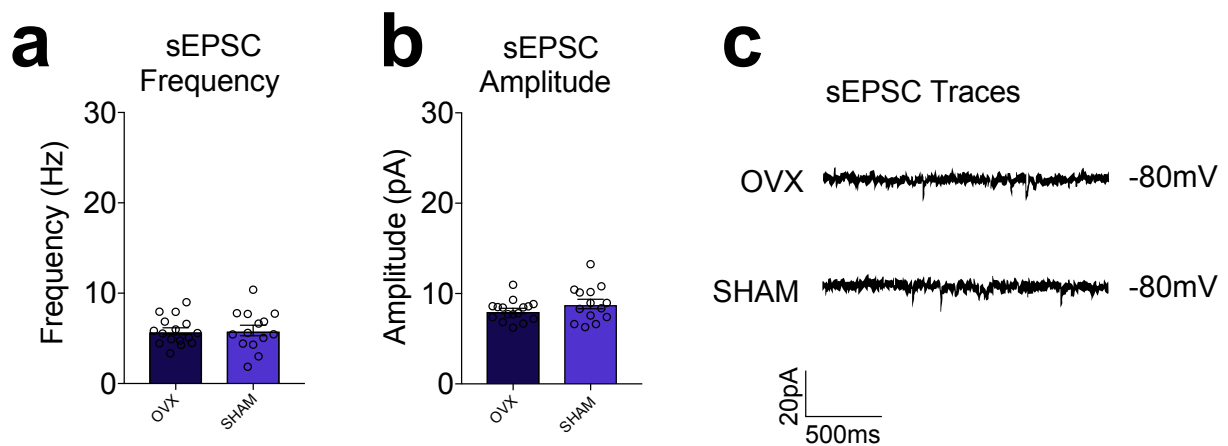


Figure 28 | Spontaneous activity measures of ovariectomy vs sham female vHPC-NAc neurons.

Female OVX and sham vHPC-NAc neurons did not differ in the measures of **(a)** sEPSC frequency (Hz) [two-tailed t-test: $t(29) = 0.1247$, $p = 0.9017$] and **(b)** sEPSC amplitude [two-tailed t-test: $t(29) = 1.326$, $p = 0.1954$]. **(c)** Example sEPSC traces for OVX (top) and sham (bottom) vHPC-NAc cell gap-free recordings at -80 mV holding potential.

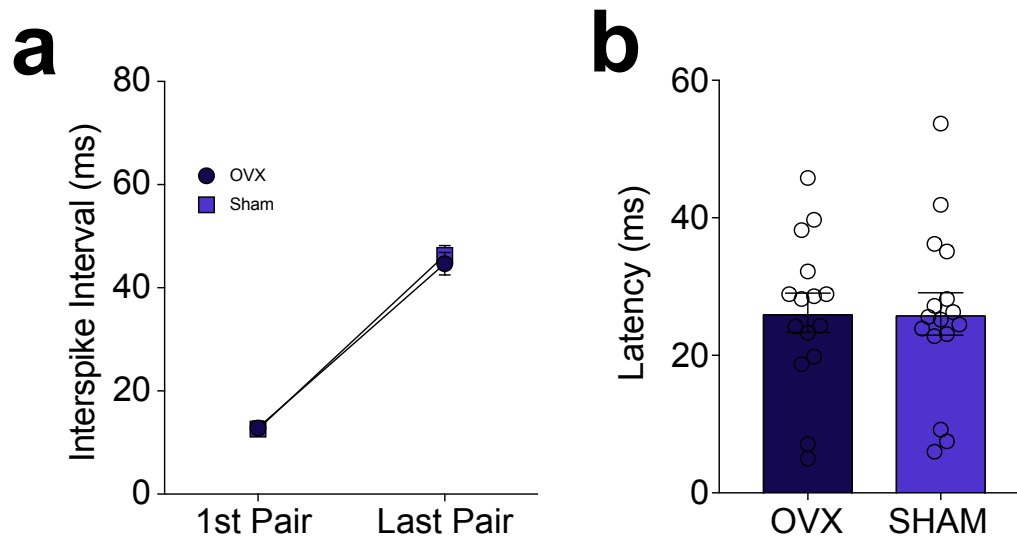


Figure 29 | Spike frequency adaptation did not differ between female sham and OVX vHPC-NAc neurons.

Interspike interval increases over the course of 500 ms current injection as measured by the time (ms) between the 1st pair of spikes and last pair of spikes in female sham and OVX vHPC-NAc neurons. **(a)** Spike frequency adaptation of vHPC-NAc neurons did not differ between sham and OVX groups. One-way ANOVA $F(3,58) = 122.6$, $p < 0.0001$. Sidak's multiple comparisons: OVX last pair vs sham last pair mean difference = -1.622 , 95% CI = -7.839 to 4.596 . **(b)** Latency to 1st spike following start of current injection did not differ between OVX and sham groups. Two-tailed t-test: $t(29) = 0.04007$, $p = 0.9683$. Interspike interval and latency to 1st spike were evaluated at rheobase current step for each cell.

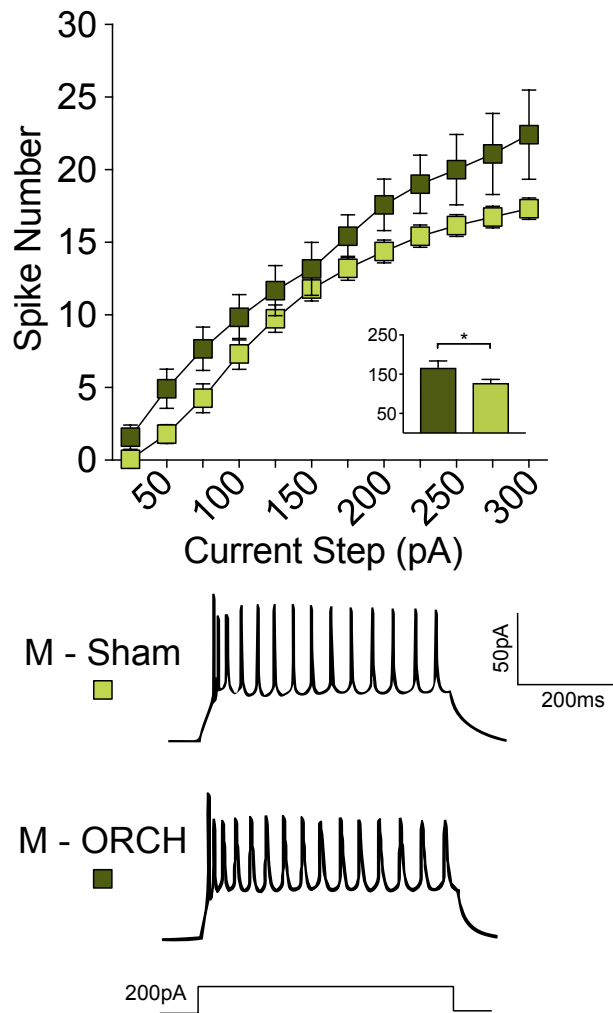


Figure 30 | Orchidectomy increases the excitability of vHPC-BLA neurons in male mice.

Action potential (AP) number across sequential depolarizing current steps (25-300 pA) for sham male (n = 19 cells from n = 4 animals) and orchidectomized male (n = 11 cells from n = 3 animals) vHPC-BLA projections. Orchidectomized male projections showed significantly higher AP number at all steps > 25 pA. Two-way repeated measures ANOVA, Holm-Sidak multiple comparisons: [25 pA t(348) = 0.8312, p = 0.9981], [50 pA t(348) = 1.698, p = 0.6791], [75 pA t(348) = 1.848, p = 0.5560], [100 pA t(348) = 1.367, p = 0.8969], [125 pA t(348) = 1.048, p = 0.9850], [150 pA t(348) = 0.7479, p = 0.9993], [175 pA t(348) = 1.198, p = 0.9577], [200 pA t(348) = 1.746, p = 0.6405], [225 pA t(348) = 1.944, p = 0.4782], [250 pA t(348) = 2.086, p = 0.3692], [275 pA t(348) = 2.36, p = 0.2038], [300 pA t(348) = 2.77, p = 0.0686]. Inset: sum of AP number across all current steps. Two-tailed t-test: t(28) = 2.298, *p = 0.0039. Representative traces below for sham and ORCH vHPC-NAc projections, 200 pA step.

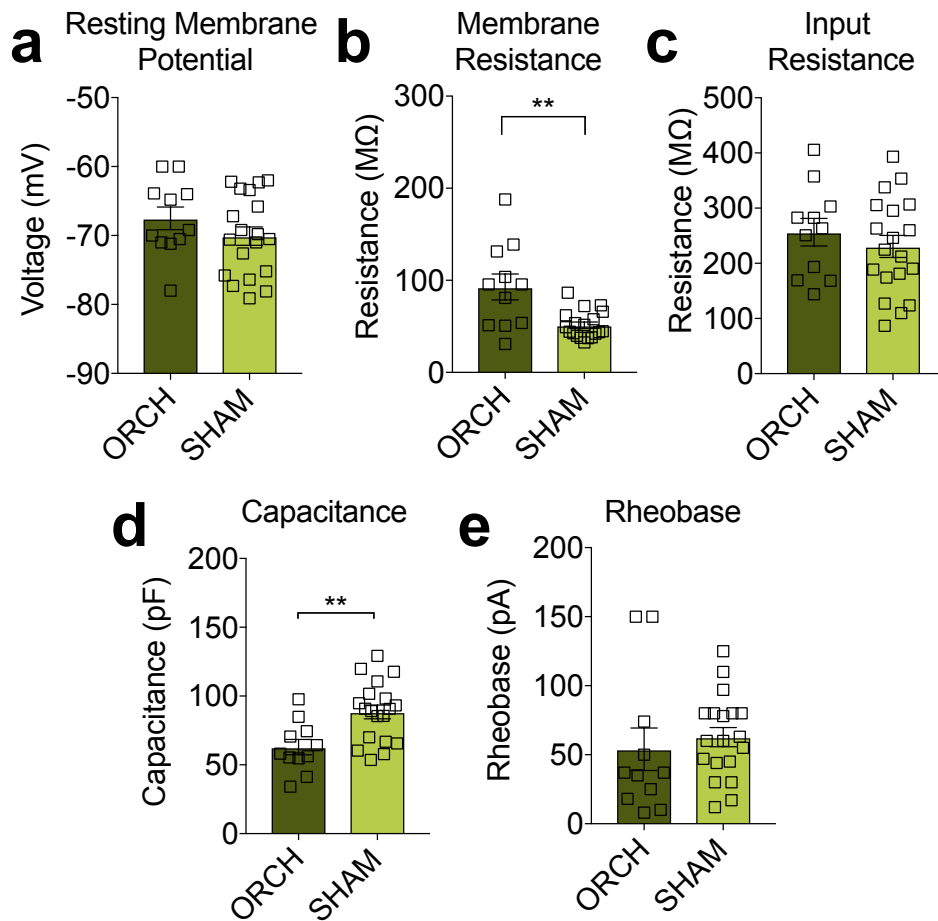


Figure 31 | Membrane properties of orchidectomy vs sham vHPC-BLA neurons.

(a) Orchidectomy (ORCH) and sham vHPC-BLA neurons did not differ in the measure of resting membrane potential (mV; two-tailed t-test: $t(28) = 1.194$, $p = 0.2425$). (b) Orchidectomy vHPC-BLA neurons had a higher membrane resistance compared to sham neurons (MΩ; two-tailed Mann-Whitney U-test: $U = 42$, sum of ranks ORCH = 233, Sham = 232, $**p = 0.0060$). (c) ORCH and Sham vHPC-BLA neurons did not differ in the measure of input resistance (MΩ; two-tailed t-test $t(28) = 0.7965$, $p = 0.4324$). (d) ORCH vHPC-BLA neurons had a lower membrane capacitance than sham neurons (pF; two-tailed t-test: $t(28) = 3.261$, $**p = 0.0029$). (e) ORCH and Sham vHPC-BLA neurons did not differ in the measure of rheobase (pA; two-tailed t-test: $t(28) = 0.5956$, $p = 0.5562$).

ORCH did decrease membrane capacitance (Figure 31d). There was no significant difference between groups in the measure of rheobase (Figure 31e).

Ovariectomy (OVX) was performed using the same experimental timeline as the above vHPC-BLA ORCH experiment. OVX had no effect on the excitability of female vHPC-BLA neurons compared to those neurons in sham-operated mice (Figure 32 top, example traces for each group below). OVX also did not affect resting membrane potential (Figure 33a) nor membrane resistance (Figure 33b), but OVX projections did have an increased input resistance compared to sham projections (Figure 33c). OVX did not cause a change in membrane capacitance (Figure 33d) nor rheobase (Figure 33e).

These gonadectomy experiments demonstrated that androgen hormones may also affect vHPC-BLA projections, indicating that the effect of decreasing the availability of these hormones may affect the physiology of the HPC globally. Although not as robust as an effect as vHPC-NAc projections, ORCH did increase the excitability of vHPC-BLA projections while OVX did not affect their physiology. These results may indicate a broader role for androgen hormones in the regulation of HPC physiology, and may inform future studies of sex differences in other hippocampal circuits.

Androgen receptor antagonism increases male vHPC-NAc excitability

We next questioned whether androgen receptors (ARs) are directly involved in the regulation of vHPC-NAc physiology. To verify that ARs are present on vHPC-NAc projection neurons, we used double-label immunofluorescence to stain for AR and GFP in vHPC of L10-GFP reporter mice injected with retrograde HSV-Cre in NAc. As

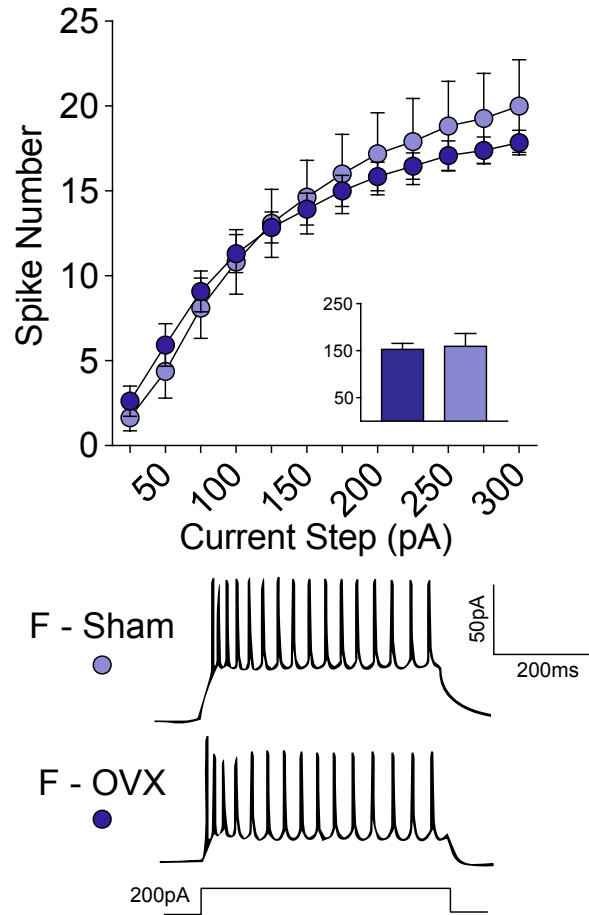


Figure 32 | Female ovariectomy and sham vHPC-BLA neurons did not differ in excitability.

Action potential (AP) number across sequential depolarizing current steps (25-300 pA) for sham male (n = 13 cells from n = 4 animals) and ovariectomy (OVX) female (n = 11 cells from n = 3 animals) vHPC-BLA projections. OVX female projections did not differ in AP number across steps. Two-way repeated measures ANOVA, Holm-Sidak multiple comparisons: [25 pA $t(264) = 0.4336$, $p > 0.9999$], [50 pA $t(264) = 0.6906$, $p = 0.9997$], [75 pA $t(264) = 0.4367$, $p > 0.9999$], [100 pA $t(246) = 0.2168$, $p > 0.9999$], [125 pA $t(246) = 0.1084$, $p > 0.9999$], [150 pA $t(246) = 0.3159$, $p > 0.9999$], [175 pA $t(246) = 0.4429$, $p > 0.9999$], [200 pA $t(246) = 0.5915$, $p > 0.9999$], [225 pA $t(246) = 0.6411$, $p = 0.9999$], [250 pA $t(246) = 0.7711$, $p = 0.9991$], [275 pA $t(246) = 0.8362$, $p = 0.9980$], [300 pA $t(246) = 0.9539$, $p = 0.9933$]. Inset: sum of AP number across all current steps. Two-tailed Mann-Whitney U -test: U = 65, sum of ranks OVX = 169, Sham = 131, $p = 0.7330$. Representative traces below for sham and OVX vHPC-NAc projections, 200 pA step.

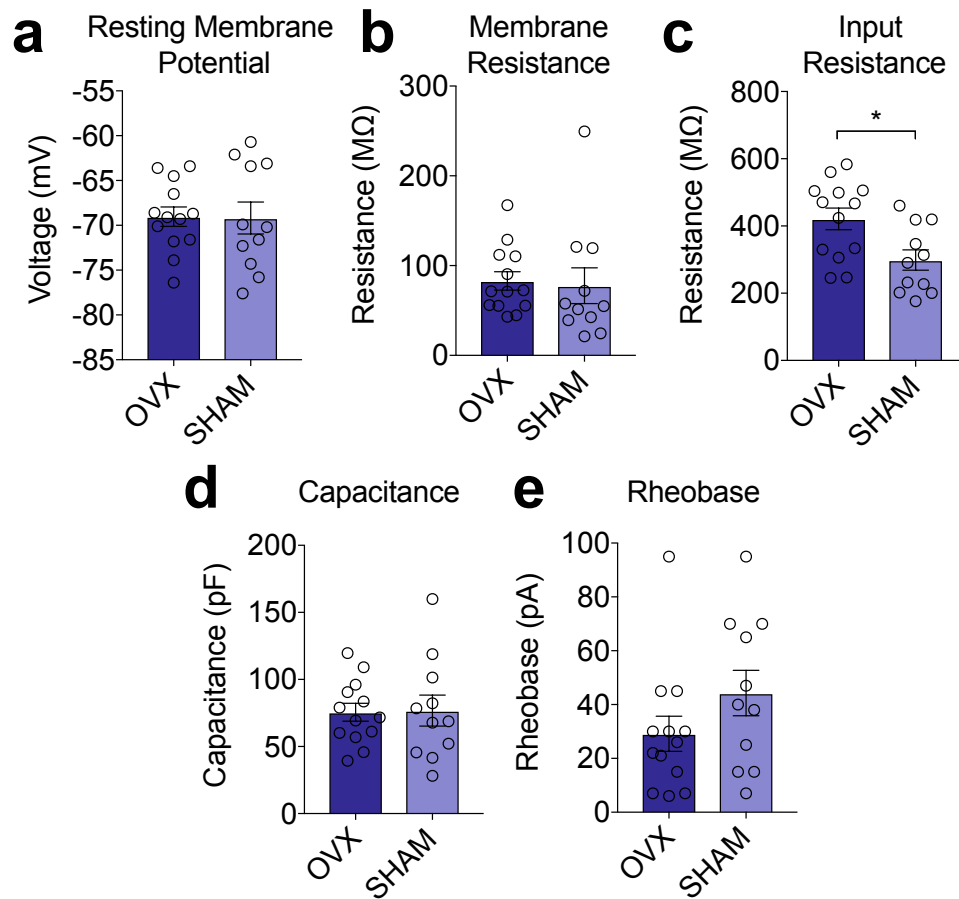


Figure 33 | Membrane properties for female ovariectomy and sham vHPC-NAc neurons.

OVX and sham vHPC-NAc neurons from female mice did not differ in the measures of **(a)** resting membrane potential (mV; two-tailed t-test: $t(22) = 0.07113$, $p = 0.9439$); or **(b)** membrane resistance (MΩ; two-tailed t-test: $t(22) = 0.2517$, $p = 0.8036$). **(c)** OVX projections compared to sham had higher input resistance (MΩ; two-tailed t-test: $t(22) = 2.738$, $*p = 0.0120$). OVX and sham projections did not differ in the measures of **(d)** membrane capacitance (pF; two-tailed t-test: $t(22) = 0.09835$, $p = 0.9225$); or **(e)** rheobase (pA; two-tailed t-test: $t(22) = 1.435$, $p = 0.1654$).

predicted, vHPC-NAc projection neurons, as well as many of the surrounding pyramidal cells in vHPC CA1, do indeed express AR (Figure 34). To test whether ARs are directly involved in the regulation of vHPC-NAc neuronal excitability, the AR antagonist flutamide was used in conjunction with slice electrophysiology to determine effects on projection physiology. Either vehicle (DMSO) or flutamide + picrotoxin-spiked aCSF solutions were used in the slice incubation chamber as well as the main bath to record from vHPC-NAc cells in L10-GFP mice injected with retrograde Cre virus at NAc. Those cells exposed to flutamide + picrotoxin aCSF were found to have increased excitability compared to those treated with vehicle aCSF, as indicated by a significantly elevated total number of spikes across all current injections (Figure 35), although no significant differences were revealed at any current injections. Vehicle- and flutamide + picrotoxin-treated male vHPC-NAc neurons did not differ in any membrane properties (Figure 36a-f), nor sag ratio (Figure 36g). There were also no observed differences in sEPSC frequency (Figure 37a) nor amplitude (Figure 37b). These data support AR activation, possibly through androgen stimulation as suggested by our orchidectomy findings, as a potential direct regulator of excitability of male vHPC-NAc neurons that could mediate resilience to anhedonia following SCVS.

Exogenous testosterone in female mice ameliorates susceptibility to SCVS

As the above studies implicate circulating androgens in the mediation of stress resilience in male mice, we next sought to determine whether exogenous testosterone could protect female mice against the anhedonic effects of SCVS. To this end, we implanted 6mm Silastic blank or testosterone pellets in adult female mice

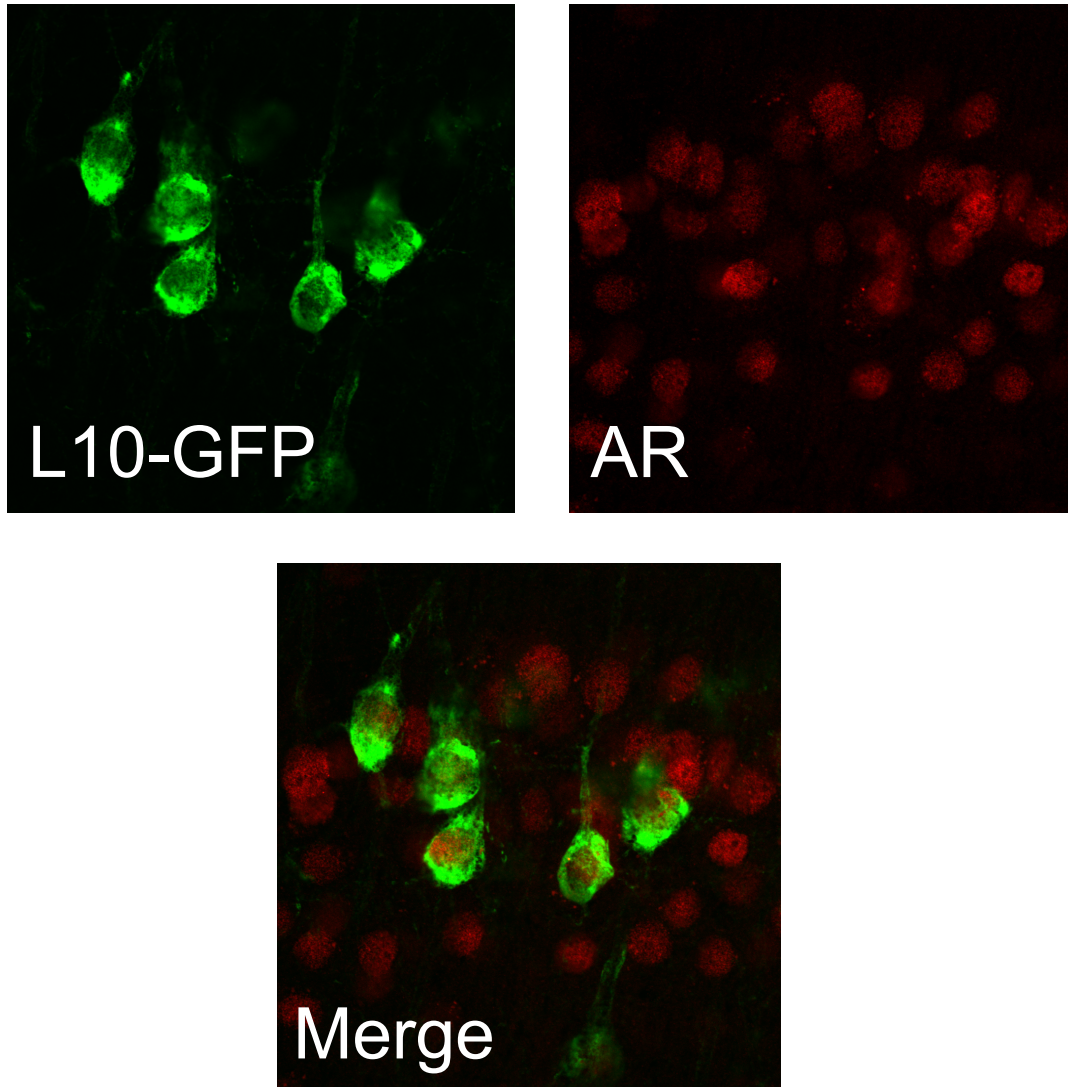


Figure 34 | Ventral HPC to NAc projections express androgen receptors (ARs).

Representative AR staining of vHPC slices from a male L10-GFP mouse; top left panel shows L10-GFP staining, top right panel shows AR staining, and the bottom panel shows a merged image demonstrating AR expression on vHPC-NAc projection cells. All images at 100x magnification. L10-GFP expression was induced in vHPC-NAc projections using same retrograde cre viral strategy described in previous figures.

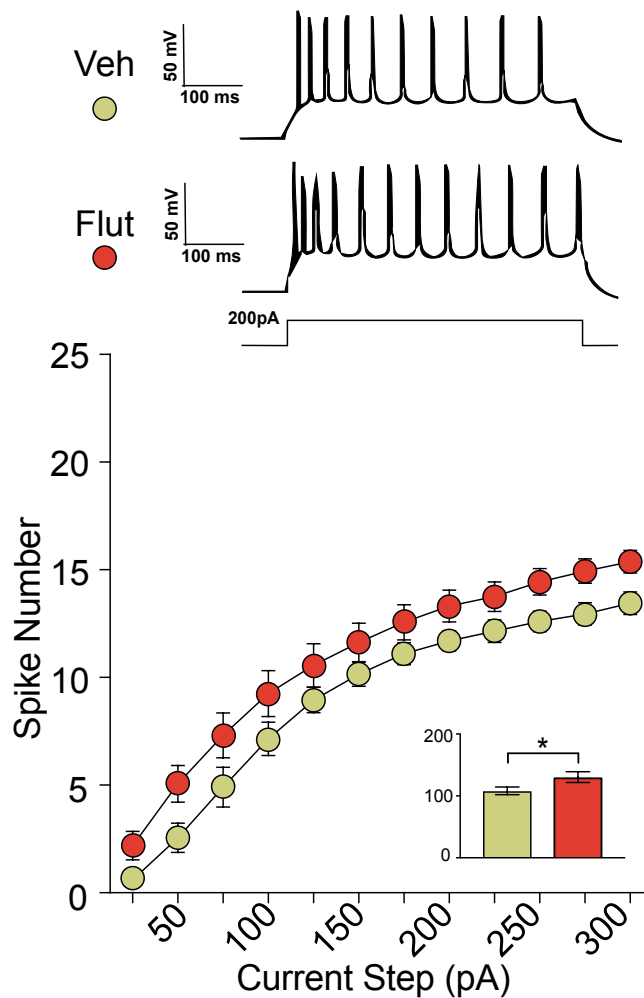


Figure 35 | Acute application of the AR antagonist flutamide causes a slight increase in vHPC-NAc neuronal excitability in male mice.

Representative traces for vehicle- and flutamide-treated vHPC-NAc neurons, 200 pA step (top). Action potential number across sequential depolarizing current steps (25-300 pA) for vehicle- (n = 20 cells from n = 7 animals) and flutamide-treated (n = 16 cells from n = 6 animals) vHPC-NAc projections. Two-way repeated measures ANOVA: [25 pA t(408) = 1.626, p = 0.4664], [50 pA t(408) = 2.573, p = 0.1182], [75 pA t(408) = 2.471, p = 0.1426], [100 pA t(408) = 2.151, p = 0.2782], [125 pA t(408) = 1.652, p = 0.4664], [150 pA t(408) = 1.511, p = 0.4664], [175 pA t(408) = 1.498, p = 0.4664], [200 pA t(408) = 1.652, p = 0.4664], [225 pA t(408) = 1.639, p = 0.4664], [250 pA t(408) = 1.882, p = 0.3542], [275 pA t(408) = 2.036, p = 0.3231], [300 pA t(408) = 1.972, 0.3328]. Total number of spikes for flutamide-treated cells vs vehicle-treated cells (inset) was increased; two-tailed t-test: t(34) = 2.119, *p = 0.0415.

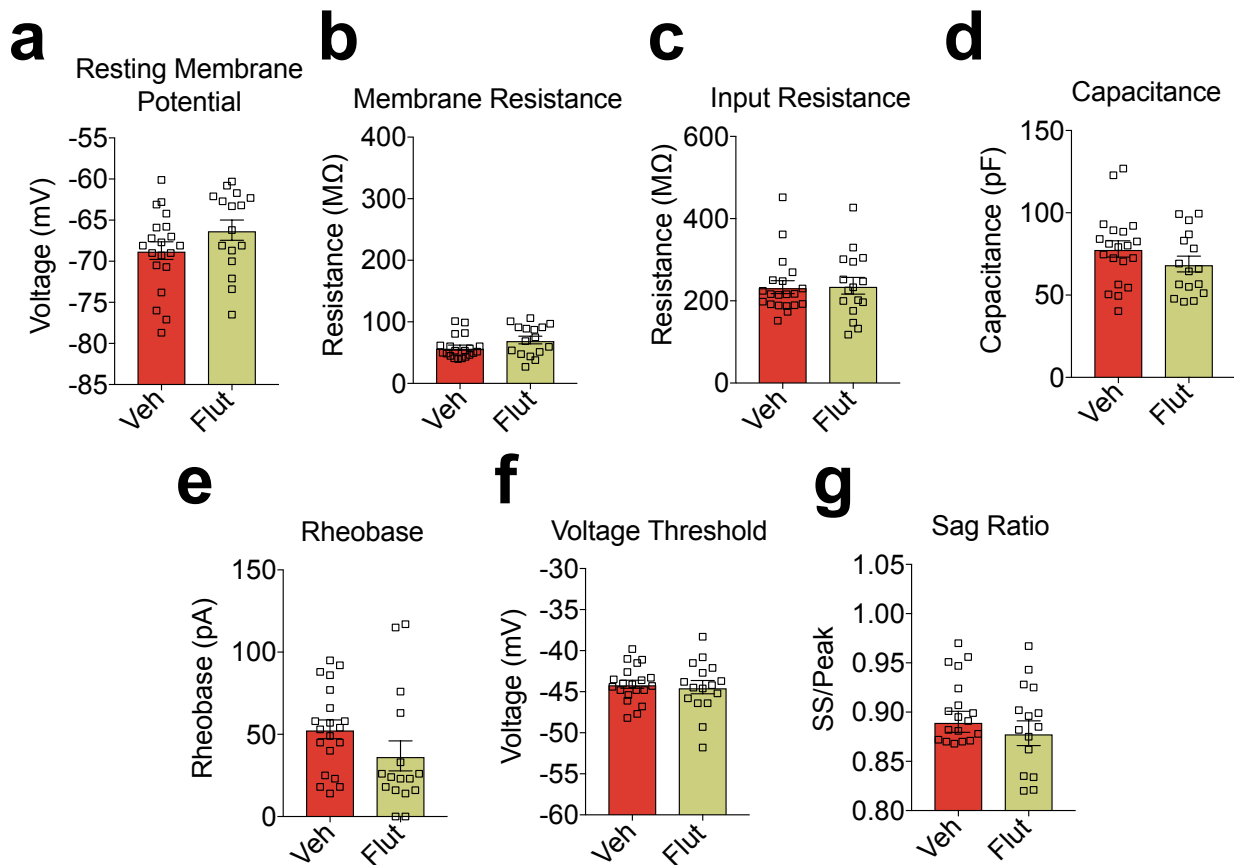


Figure 36 | Membrane properties of male vehicle- and flutamide-treated vHPC-NAc projections.

vHPC-NAc projection cells did not differ between male vehicle (DMSO) and flutamide-treated groups in any of the following measures: **(a)** resting membrane potential (mV). Two-tailed t-test: $t(34) = 1.521$, $p = 0.1375$; **(b)** membrane resistance (MΩ). Two-tailed t-test: $t(34) = 1.702$, $p = 0.0979$; **(c)** input resistance (MΩ). Two-tailed t-test: $t(34) = 0.1268$, $p = 0.8998$; **(d)** membrane capacitance (pF). Two-tailed t-test: $t(34) = 1.317$, $p = 0.1966$; **(e)** rheobase (pA). Two-tailed t-test: $t(34) = 1.562$, $p = 0.1274$; **(f)** voltage threshold (mV). Two-tailed t-test: $t(34) = 0.3899$, $p = 0.6990$; and **(g)** sag ratio. Two-tailed t-test: $t(34) = 0.705$, $p = 0.4856$.

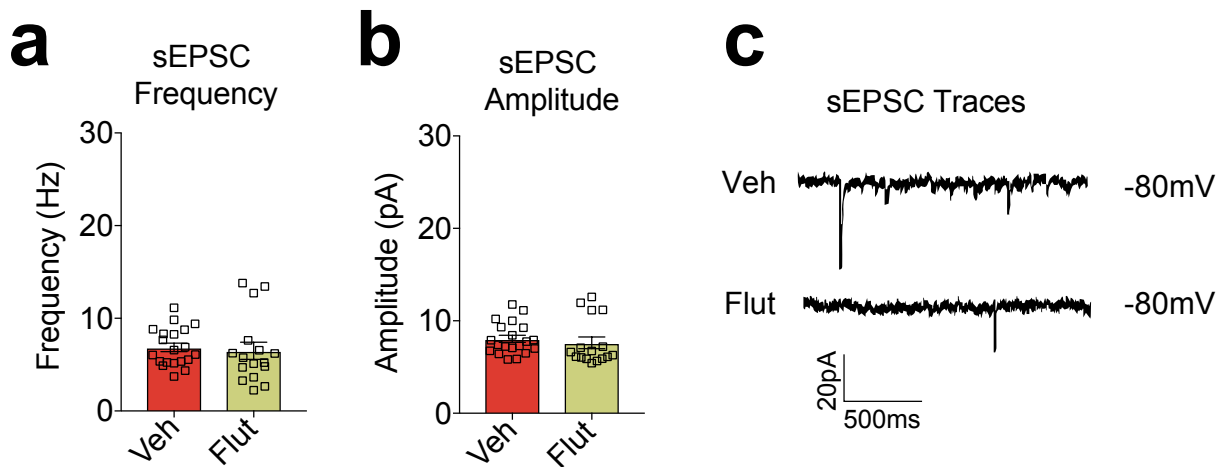


Figure 37 | Spontaneous activity measures of male vHPC-NAc projections treated with vehicle or flutamide.

(a) Spontaneous EPSC frequency (Hz) [two-tailed Mann-Whitney U-test: $U = 121$, sum of ranks Veh = 409, Flut = 257, $p = 0.2334$] and **(b)** amplitude [two-tailed t-test: $t(34) = 0.6132$, $p = 0.5438$] did not differ between Flut and Veh groups. **(c)** Example sEPSC traces for vehicle (top) and flutamide (bottom) vHPC-NAc recordings.

simultaneously with ovariectomy (OVX). Following OVX and implantation, 28 days were allowed for recovery and hormone equilibration. Mice were then subjected to the 6-day SCVS battery, and behavioral assessment began immediately following the last day of SCVS (Fig 38, top). There was a significant interaction between stress and hormone status, with female mice implanted with blank pellets having reduced sucrose preference after SCVS and those implanted with testosterone pellets showing no effect of stress on sucrose preference, indicating resilience similar to that of male mice (Figure 38, bottom). There was a main effect of stress on % time grooming in the splash test, with stress-exposed mice spending less time grooming (Figure 39a). In the EPM test, a main effect of stress was observed in the distance moved (Figure 39b), and there was an interaction between stress and sex in the % open arm time (Figure 39c) There was a main effect of testosterone on the NSF test, with testosterone-implanted mice demonstrating less latency to feed (Figure 39d). There were no main effects of stress nor testosterone nor an interaction between variables in the assessment of SI ratio (Figure 39e). These data suggest a direct protective effect of testosterone, or possibly its metabolic derivatives, against SCVS-induced anhedonia in female mice.

Exogenous testosterone mitigates hyperexcitability in female vHPC-NAc neurons

We next questioned whether exogenous testosterone could also attenuate the hyperexcitability of female vHPC-NAc neurons. To this end, we injected L10-GFP female mice with retrograde HSV-Cre in NAc, and after one week of recovery, subjected the mice to OVX and pellet implantation in a single operation. After allowing two more weeks for recovery and hormone equilibration, we then performed whole-cell patch clamp

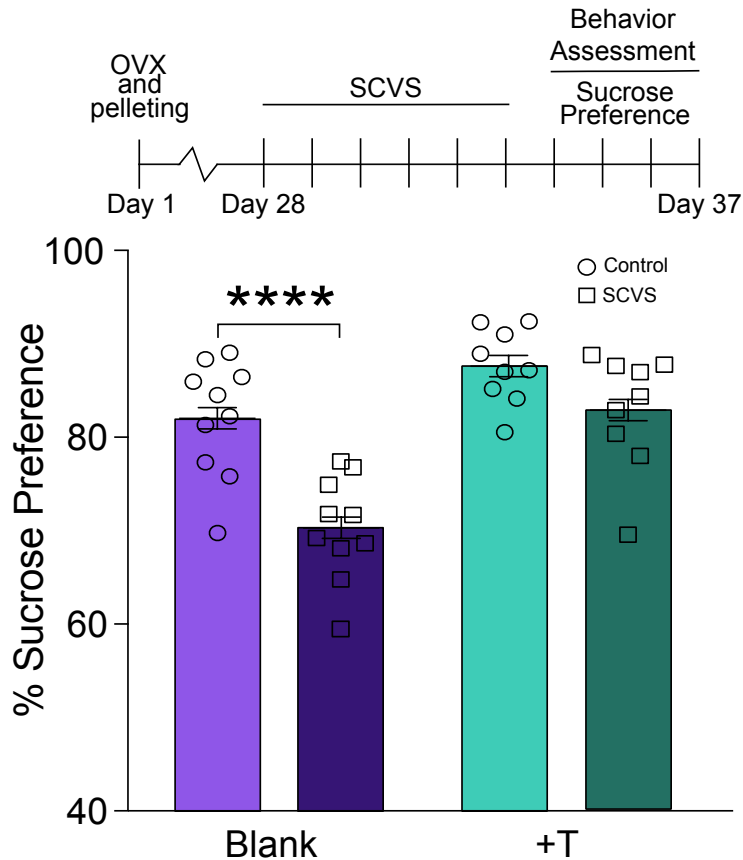


Figure 38 | Female susceptibility to SCVS-induced anhedonia is ameliorated by adult testosterone.

Schematic depicting experimental time course of pellet implantation surgery, ovariectomy, SCVS, and behavior assessment (top). OVX females with blank pellet implants maintained a reduction in sucrose preference following SCVS, while OVX female mice exposed to testosterone showed no significant reduction in sucrose preference following SCVS, indicating resilience (bottom). Two-way ANOVA: Group OVX + Blank vs OVX + T $F(1,34) = 26.00$, $p = 0.0580$; Trial: Control vs Stress $F(1,34) = 20.79$, $p < 0.0001$; Group X Trial $F(1,34) = 3.849$, $p < 0.0001$; Sidak's multiple comparisons: OVX + Blank mean difference 11.78, 95% ****CI = 5.965 to 17.6; OVX + T mean difference 4.693, 95% CI = -1.441 to 10.83.

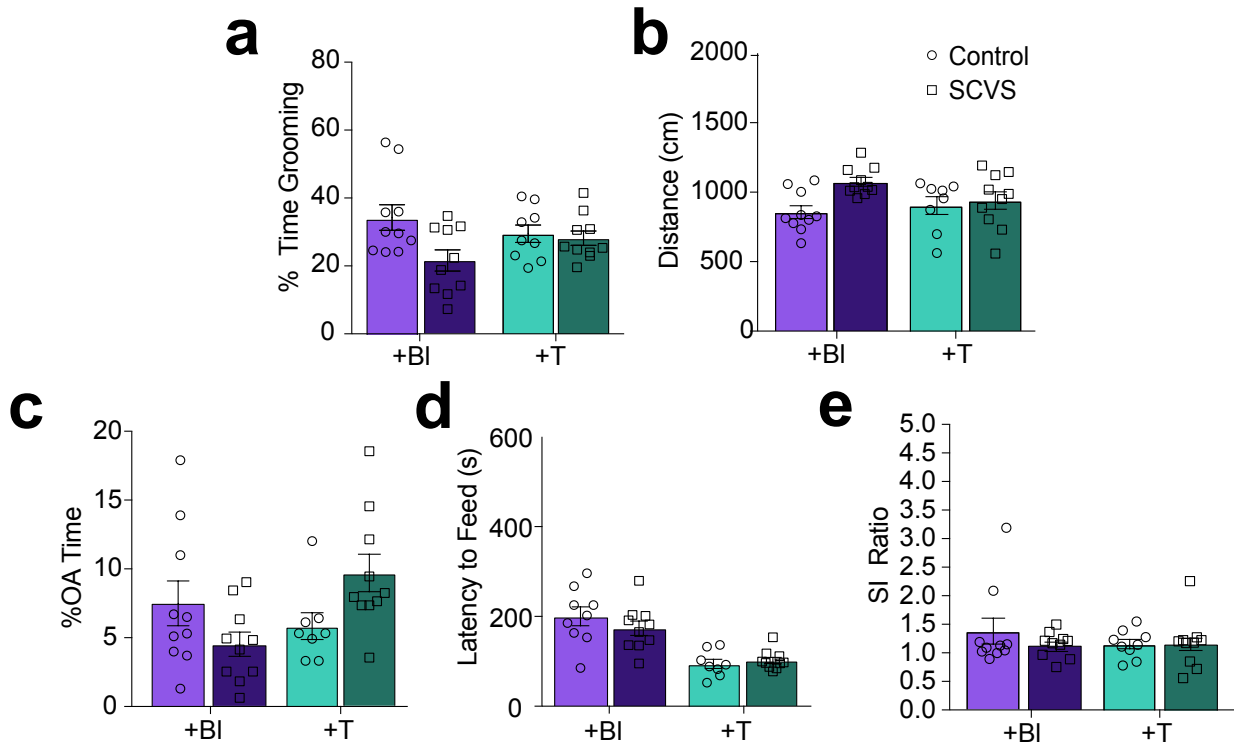


Figure 39 | Additional behavioral assays of female OVX + Blank and OVX + T SCVS.

All behavioral assays other than sucrose preference were unaffected by hormone status with SCVS in OVX + Blank and OVX + T groups, with no interaction of stress and hormone status in **(a)** Percent time grooming in splash test. Two-way ANOVA: Group OVX + BI vs OVX + T $F(1,35) = 0.0884$, $p = 0.7680$; Trial: Control vs Stress $F(1,35) = 5.449$, $p = 0.0254$; Group X Trial $F(1,35) = 3.598$, $p = 0.0661$; **(b)** Distance moved (cm) in EPM. Two-way ANOVA: Group: OVX + BI vs OVX + T $F(1,34) = 0.6634$, $p = 0.4210$; Trial: Control vs Stress $F(1,34) = 5.778$, $p = 0.0218$; Group X Trial $F(1,34) = 3.132$, $p = 0.0857$; **(c)** Percent open arm (OA) time in EPM did show a significant interaction between stress and hormone status, but no differences between stress and control in either the OVX + BI or OVX + T group with Sidak's multiple comparisons test. Two-way ANOVA: Group: OVX + BI vs OVX + T $F(1,34) = 1.78$, $p = 0.1910$; Trial: Control vs Stress $F(1,34) = 0.0865$, $p = 0.7705$; Group X Trial $F(1,34) = 7.131$, $p = 0.0114$; Sidak's multiple comparisons: OVX + BI mean difference 3.05, 95% CI = -1.07 to 7.17; OVX + T mean difference -3.805, 95% CI = -8.175 to 0.5647. There was also no interaction between hormone status and stress in the measures of **(d)** latency to feed (s) in novelty suppressed feeding test. Two-way ANOVA: Group: OVX + BI vs OVX + T $F(1,33) = 36.41$, $p < 0.0001$; Trial: Control vs Stress $F(1,33) = 0.4705$, $p = 0.4975$; Group X Trial $F(1,33) = 1.291$, $p = 0.2641$; **(e)** SI Ratio in social interaction test. Two-way ANOVA: Group: OVX + BI vs OVX + T $F(1,35) = 0.3507$, $p = 0.5575$; Trial: Control vs Stress $F(1,35) = 0.4839$, $p = 0.4913$; Group X Trial $F(1,35) = 0.681$, $p = 0.4148$.

electrophysiology on vHPC-NAc projections. We found that OVX mice implanted with testosterone pellets exhibited significantly decreased excitability in vHPC-NAc neurons compared to those with blank pellets (Figure 40 bottom, example traces for each group above). No differences were observed between testosterone- and blank-pelleted OVX mice in the measures of V_M , R_M , R_{in} , or C_M (Figure 41a-d). Mice implanted with testosterone pellets had an increased rheobase compared to those implanted with blank pellets (Figure 41e), supporting the decrease in excitability with testosterone treatment noted above. However, no difference was observed between testosterone- and blank-pelleted OVX mice in the measure of AP voltage threshold (Figure 41f), which was observed in female WT vHPC-NAc neurons compared to male WT projections. Sag ratio was no different between testosterone and blank pellet groups (Figure 41g), indicating similar afterhyperpolarization current in both groups. There were also no observed differences in sEPSC amplitude nor frequency between OVX + Blank and OVX + T groups (Figure 42a-c), suggesting no immediate pre- nor postsynaptic changes with testosterone treatment. Testosterone treatment, however, did enhance spike frequency adaptation of vHPC-NAc neurons in OVX mice, as indicated by a greater increase in interspike interval over the course of a depolarizing current step (Figure 43a). This enhancement of spike frequency adaptation was accompanied by an increase in latency to first spike in the same current step (Figure 43b). Overall, these results suggest that exogenous testosterone, or its metabolic derivatives, reduces the excitability profile of female vHPC-NAc neurons and, as noted in the SCVS experiments above, drives resilience to SCVS-induced anhedonia in female mice.

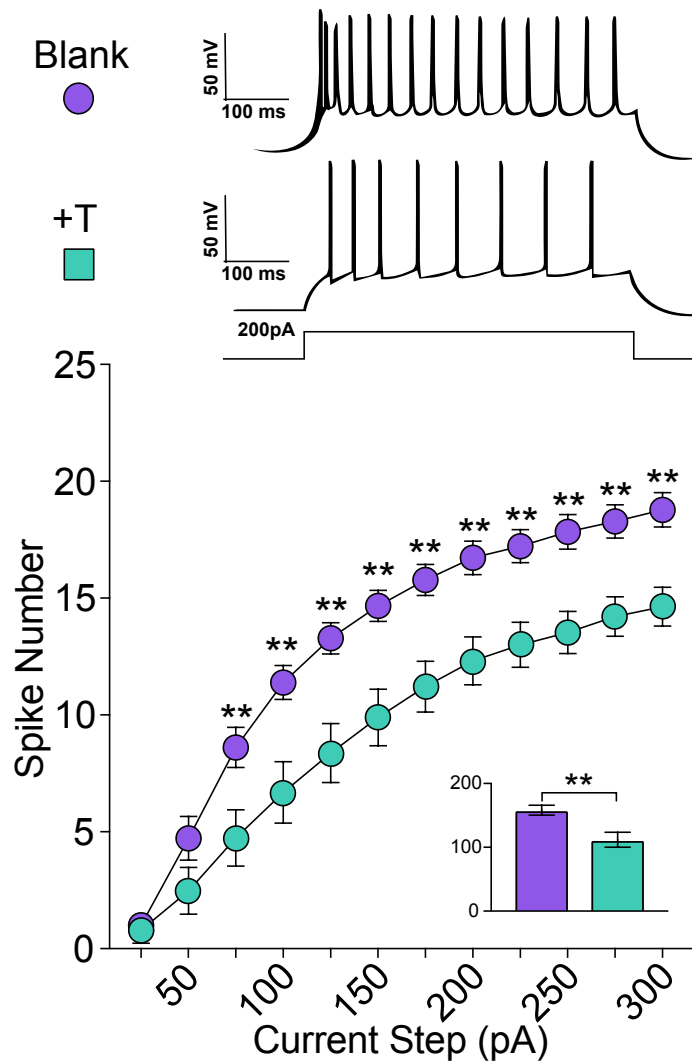


Figure 40 | Female OVX vHPC-NAc excitability is decreased with chronic testosterone.

Representative traces for OVX + BLANK and OVX + T vHPC-NAc projections, 200 pA step (top). Action potential number across sequential depolarizing current steps (25-300 pA) for OVX + BLANK (n = 11 cells from n = 3 animals) and OVX + T (n = 19 cells from n = 5 animals) vHPC-NAc projections. OVX + T projections showed significantly lower AP number at all steps > 50 pA. Two-way repeated measures ANOVA, Holm-Sidak multiple comparisons: [25 pA $t(420) = 0.165$, $p = 0.8690$], [50 pA $t(420) = 1.762$, $p = 0.1514$], [75 pA $t(420) = 3.036$, $**p = 0.0076$], [100 pA $t(420) = 3.687$, $**p = 0.0026$], [125 pA $t(420) = 3.847$, $**p = 0.0017$], [150 pA $t(420) = 3.739$, $**p = 0.0023$], [175 pA $t(420) = 3.579$, $**p = 0.0035$], [200 pA $t(420) = 3.453$, $**p = 0.0049$], [225 pA $t(420) = 3.309$, $**p = 0.0061$], [250 pA $t(420) = 3.375$, $**p = 0.0056$], [275 pA $t(420) = 3.187$, $**p = 0.0062$], [300 pA $t(420) = 3.249$, $**p = 0.0062$]. Inset: sum of AP number across all current steps. Two-tailed t-test: $t(35) = 3.254$, $**p = 0.0025$.

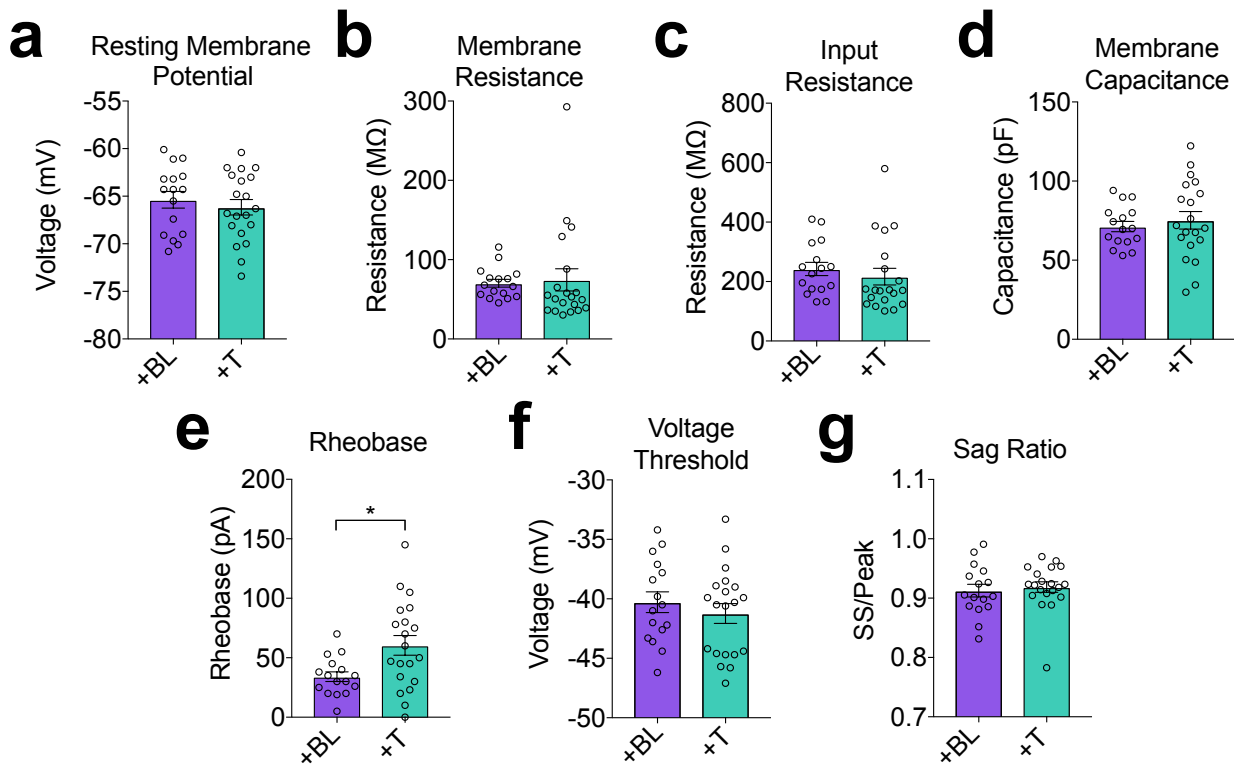


Figure 41 | Membrane properties of female OVX + Blank and OVX + T vHPC-NAC projections.

vHPC-NAC projection cells did not differ between female OVX + Blank and OVX + T groups in any of the following measures: **(a)** resting membrane potential (mV). Two-tailed t-test: $t(34) = 0.6576$, $p = 0.5152$; **(b)** membrane resistance (M Ω). Two-tailed Mann-Whitney U-test: $U = 107$, sum of ranks OVX + BI = 349, OVX + T = 317, $p = 0.0949$; **(c)** input resistance (M Ω). Two-tailed t-test: $t(34) = 0.6972$, $p = 0.4904$; and **(d)** capacitance (pF). Two-tailed t-test: $t(34) = 0.5770$, $p = 0.5672$. Female OVX + T vHPC-NAC projection cells showed an increased rheobase (pA) **(e)** compared to OVX + Blank projections. Two-tailed t-test: $t(34) = 2.643$, $*p = 0.0123$. **(f)** Voltage threshold (mV) [two-tailed t-test: $t(34) = 0.7842$, $p = 0.4384$] and **(g)** sag ratio [two-tailed t-test: $t(34) = 0.4344$, $p = 0.6668$] did not differ between OVX + Blank and OVX + T groups.

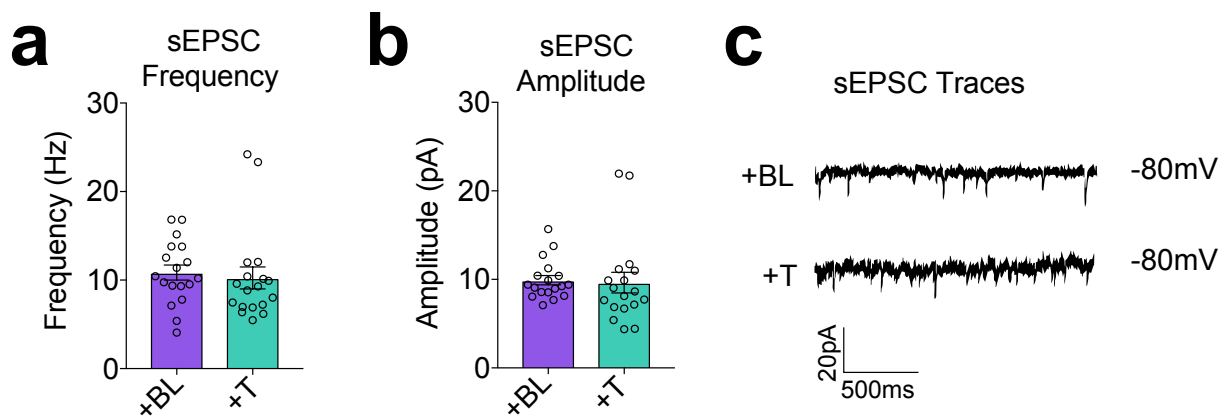


Figure 42 | Spontaneous activity measures of female OVX + Blank and OVX + T vHPC-NAc projections.

(a) Spontaneous EPSC frequency (Hz) [two-tailed t-test: $t(34) = 0.4026$, $p = 0.6898$] and (b) amplitude [two-tailed Mann-Whitney U-test: $U = 123$, sum of ranks OVX + BI = 372, OVX + T = 294, $p = 0.2231$] did not differ between OVX + Blank and OVX + T groups. (c) Example sEPSC traces for OVX + Blank (top) and OVX + T (bottom) vHPC-NAc recordings.

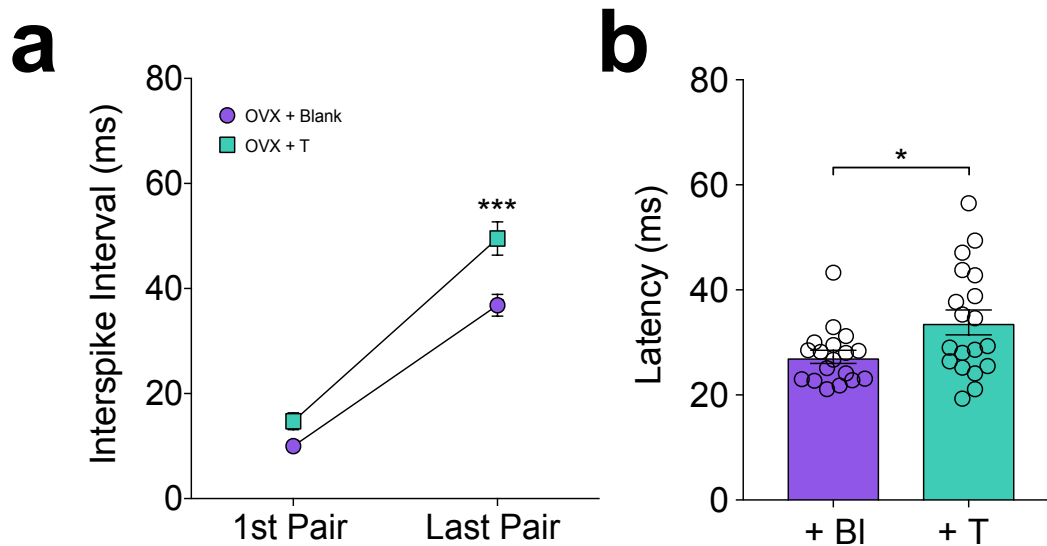


Figure 43 | Spike frequency adaptation is enhanced by chronic testosterone in OVX female vHPC-NAc projections.

Interspike interval increases over the course of 500 ms current injection as measured by the time (ms) between the 1st pair of spikes and last pair of spikes in female OVX + Blank and OVX + T vHPC-NAc neurons. **(a)** OVX + T vHPC-NAc neurons had greater spike frequency adaptation as measured by the interspike interval increase over current step; interspike interval of the last pair of spikes was significantly longer in OVX + T vHPC-NAc projections than in OVX + BI projections. One-way ANOVA $F(3,70) = 77.7$, $p < 0.0001$; Sidak's multiple comparisons: OVX + T 1st pair vs OVX + BI 1st pair mean difference = 4.714, 95% CI = -2.952 to 12.38, OVX + T last pair vs OVX + BI last pair mean difference = 12.69, 95% ***CI = 5.026 to 20.36, adjusted $p = 0.0003$. **(b)** Latency to 1st spike (ms) from beginning of current injection was also increased in OVX + T vHPC-NAc neurons compared to OVX + BI. Two-tailed Mann-Whitney U-test: $U = 105.5$, sum of ranks OVX + BI = 276.5, OVX + T = 426.5, $*p = 0.0465$.

vHPC-NAc excitability directly mediates SCVS-induced susceptibility to anhedonia

The above experiments parallel susceptibility to stress and vHPC-NAc excitability, but do not directly link the physiology of this circuit to stress outcomes. To determine whether vHPC-NAc neuronal excitability is directly causative of susceptibility to SCVS-induced anhedonia, we utilized an intersecting viral DREADD strategy. In wild-type mice, retrograde HSV-Cre was injected into NAc, and a Cre-dependent AAV- mCherry-hM4D_q (G_q-coupled DREADD in male mice) or AAV-mCherry-hM3D_i (G_i-coupled DREADD in female mice) was injected into vHPC (Figure 44a, top). Using this strategy, only vHPC-NAc neurons infected with both viruses expressed the respective DREADD and were to be affected by systemic clozapine-N-oxide (CNO) administration. We verified G_q- and G_i-coupled DREADD activation with CNO using slice electrophysiology in vHPC guided by the mCherry tag and recording before and after CNO wash-on (timeline Figure 44a, bottom). We demonstrated that mCherry⁺, G_q-coupled DREADD-expressing vHPC-NAc neurons in males had elevated excitability following CNO wash-on, indicated by an increased number of spikes at 150 pA injected current, as well as a decrease in rheobase (representative cell shown in Figure 44b). Likewise, female vHPC-NAc neurons expressing the G_i-coupled DREADD showed diminished excitability following CNO wash-on, indicated by a decrease in the number of spikes at 150 pA injected current, as well as an increase in rheobase (representative cell shown in Figure 44c). Together, these recordings verify the efficacy of DREADD activation using the designer drug CNO.

Three weeks after the second viral injection surgery male mice expressing the excitatory G_q-coupled DREADD in vHPC-NAc projections were exposed to SCVS

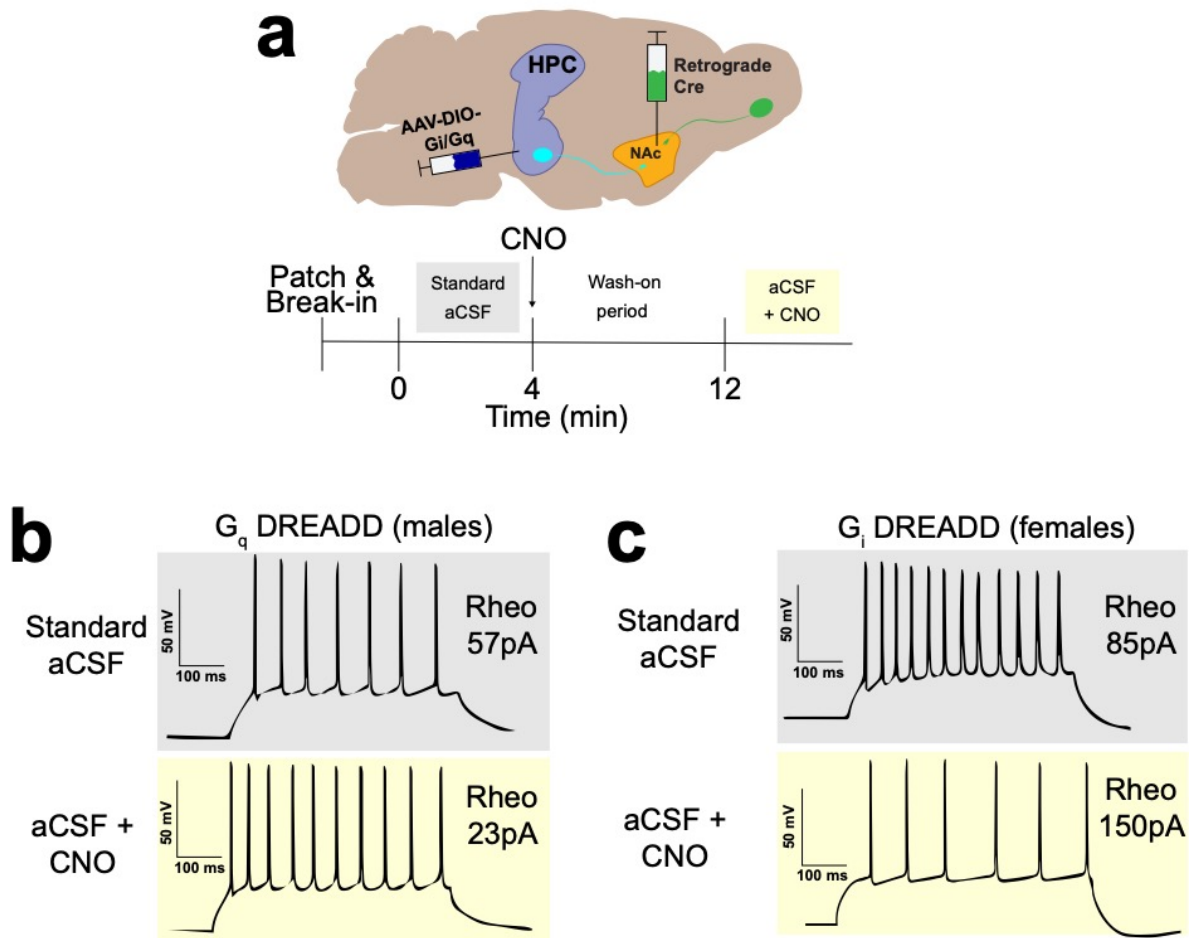


Figure 44 | Viral DREADD proof-of concept electrophysiology.

(a, top) Schematic depicting intersecting viral DREADD strategy for circuit-specific manipulation of vHPC-NAc excitability and experimental time course. AAV encoding Cre-inducible DREADD (either G_q - or G_i -coupled) was injected in vHPC, and retrograde HSV-Cre was injected in NAc, causing circuit-specific receptor expression. **(a, bottom)** Schematic depicting time course for DREADD recordings. Cells were first recorded in regular aCSF, then CNO-containing aCSF was washed on and the same cell was recorded 8-10 minutes later. **(b and c)** Whole-cell slice electrophysiology demonstrating CNO activating G_q - **(b)** and G_i -coupled **(c)** receptors. Example traces before (grey) and after (yellow) CNO application along with rheobase at time of each recording. One cell is represented each in **(b)** and **(c)**.

followed by intraperitoneal CNO or saline injection every day of behavioral testing (timeline Figure 45a, top). Interestingly, CNO failed to directly evoke changes in sucrose preference (Figure 45a, bottom), suggesting that a short-term activation of the vHPC-NAc circuit is not sufficient to induce anhedonia following stress. A second group of male mice expressing G_q-coupled DREADD in vHPC-NAc neurons was exposed to SCVS with CNO or saline administration throughout both stress and behavior assessment (Figure 45b, top). Long-term CNO treatment in male mice caused a dramatic decrease in sucrose preference even in the control-handled group, as well as a further SCVS-induced decrease in sucrose preference (Figure 45b, bottom). There was also a significant interaction between stress and CNO treatment in social interaction assessment in the short CNO administration, with SI ratio being decreased following SCVS in the CNO-treated group (Figure 46a). There was no interaction between stress and CNO treatment in EPM open arm time for the short CNO administration experiment (Figure 46b). For the long CNO administration group, SI assessment did show a main effect of stress on reduction of SI ratio, but no interaction between stress and CNO treatment variables (Figure 46c). EPM open arm time for this experiment remained unaffected by stress and CNO treatment with no interaction between the two (Figure 46d). Importantly, we also performed a control experiment with a separate cohort of male mice that did not express any DREADDs in the brain, but did receive CNO or saline IP injections during SCVS and behavior assessment (Figure 47, top). Similar to male mice with no viral modifications or drug treatments, these mice were not affected by SCVS in the measure of sucrose preference (Figure 47, bottom): there was not a main effect of stress nor CNO treatment, with no interaction between the two. These data suggest that short-term activation of the

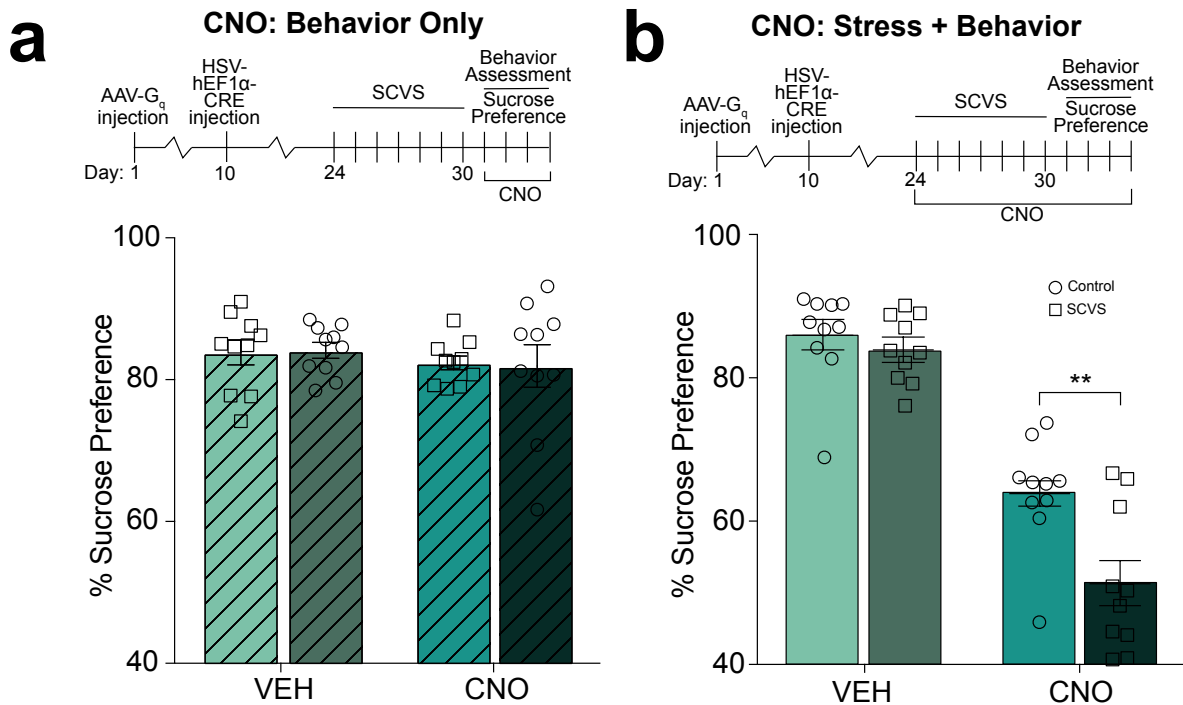


Figure 45 | Long-term reduction of vHPC-NAc activity causes susceptibility to SCVS-induced anhedonia in male mice.

(a, top) Experimental timeline of DREADD surgery, retrograde Cre surgery, SCVS, and subsequent behavioral assessment for short (behavior-only) DREADD experiment for male mice. **(a, bottom)** Male mice expressing excitatory G_q-coupled DREADD in vHPC-NAc projections and exposed to CNO only during behavior assessment did not show any change in sucrose preference following SCVS. Two-way ANOVA: Group: Saline vs CNO $F(1,36) = 0.9478$, $p = 0.3368$; Trial: Control vs Stress $F(1,36) = 0.001178$, $p = 0.9728$; Group X Trial $F(1,36) = 0.03545$, $p = 0.8517$ (no interaction); $n = 10$ control vehicle, 10 control CNO, 10 SCVS vehicle, 10 SCVS CNO. **(b, top)** Experimental timeline for long (CNO during both SCVS and behavior assessment) DREADD experiment for male mice. **(b, bottom)** Male mice expressing excitatory G_q-coupled DREADD in vHPC-NAc projections and exposed to CNO during both SCVS and behavior assessment experienced an overall reduction in sucrose preference and a further reduction in sucrose preference following SCVS. Two-way ANOVA: Group: Saline vs CNO $F(1,36) = 133.6$, $p < 0.0001$; Trial: Control vs Stress $F(1,36) = 9.481$, $p = 0.0040$; Group X Trial $F(1,36) = 5.086$, $p = 0.0303$. Sidak's multiple comparisons: VEH Control vs Stress mean difference = 1.94, 95% CI = -5.83 to 9.71; CNO Control vs Stress mean difference = 12.56, 95% **CI = 4.79 to 20.33; $n = 9$ control vehicle, 10 control CNO, 9 SCVS vehicle, 10 SCVS CNO.

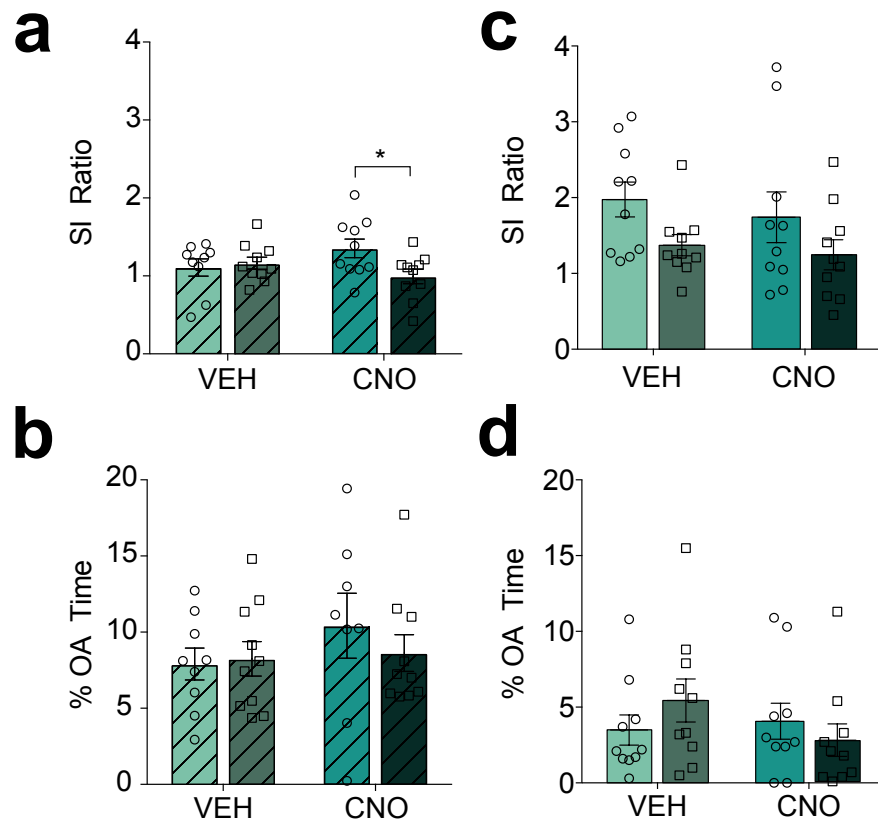


Figure 46 | Additional behavioral assays of G_q -coupled (male) DREADD-expressing vHPC-NAc mice.

For the short CNO administration G_q DREADD vHPC-NAc activation, there was also an interaction between SCVS and male vHPC-NAc activation in **(a)** SI ratio in social interaction test, with CNO injections reducing social interaction after stress [two-way ANOVA: Group: Vehicle vs CNO $F(1,35) = 0.1444$, $p = 0.7063$; Trial: Control vs Stress $F(1,35) = 0.2276$, $p = 0.1387$; Group X Trial $F(1,35) = 4.212$, $*p = 0.0477$; Sidak's multiple comparisons: Vehicle control vs stress mean difference = -0.05422 , 95% CI = -0.3922 to 0.2838 , CNO control vs stress mean difference = 0.3601 , 95% *CI = 0.03111 to 0.6891] but **(b)** percent open arm time in EPM remained unaffected [two-way ANOVA: Group: Veh vs Control $F(1,33) = 1.097$, $p = 0.3025$; Trial: Control vs Stress $F(1,33) = 0.2781$, $p = 0.6015$; Group X Trial $F(1,33) = 0.59$, $p = 0.4479$ (no interaction)]. No interaction was observed between SCVS and long CNO administration G_q DREADD vHPC-NAc activation in any of the following measures **(c)** SI ratio in social interaction test [two-way ANOVA: Group: Vehicle vs CNO $F(1,36) = 0.5818$, $p = 0.4506$; Trial: Control vs Stress $F(1,36) = 5.372$, $p = 0.0263$; Group X Trial $F(1,36) = 0.0530$, $p = 0.8192$ (no interaction)] and **(d)** percent open arm (OA) time in EPM [two-way ANOVA: Group: Vehicle vs Control $F(1,34) = 0.3007$, $p = 0.3213$; Trial: Control vs Stress $F(1,34) = 0.5462$, $p = 0.4650$; Group X Trial $F(1,34) = 0.161$, $p = 0.6908$ (no interaction)].

No DREADD, CNO: Stress + Behavior

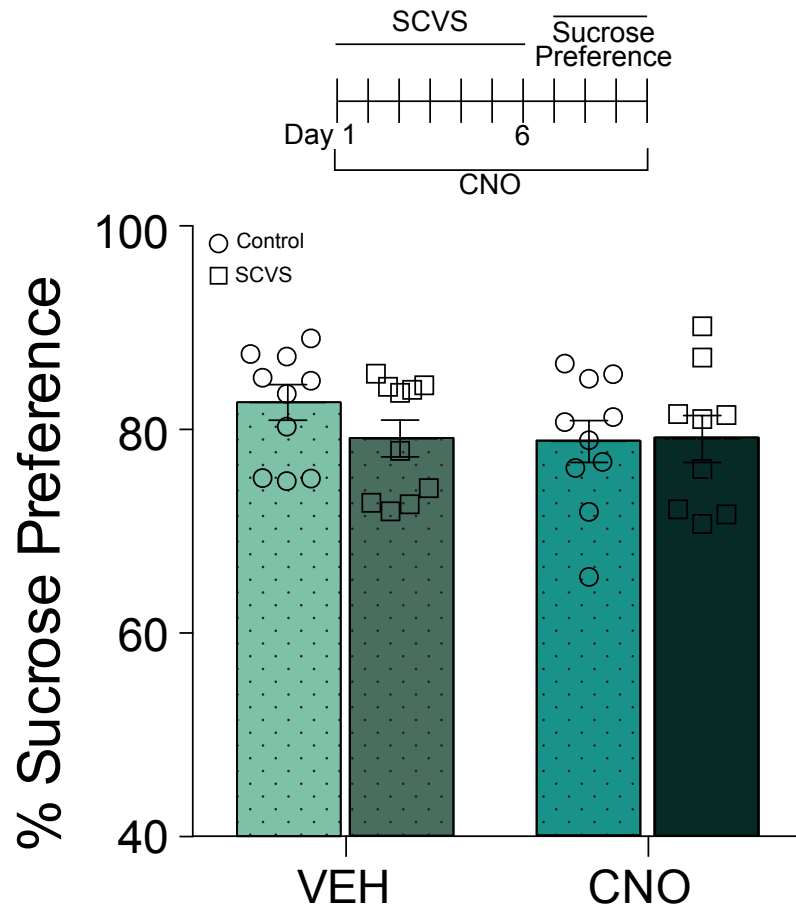


Figure 47 | Exposure to CNO without the presence of DREADD expression in vHPC-NAc neurons in male mice does not cause SCVS-induced anhedonia.

There was no interaction between stress and CNO exposure in male mice when DREADD expression was not present in male vHPC-NAc neurons [two way ANOVA: Group: Vehicle vs CNO $F(1,35) = 0.7583$, $p = 0.3898$; Trial: Control vs Stress $F(1,35) = 0.5333$, $p = 0.4701$; Group X Trial $F(1,35) = 0.7462$, $p = 0.3935$ (no interaction)].

vHPC-NAc circuit using G_q -coupled DREADDs does not cause anhedonia in stressed or non-stressed male mice. However, our findings demonstrate that a prolonged increase in the excitability of this circuit induces anhedonia even in the absence of stress, and if these changes in excitability are paired with stress, the anhedonic response in male mice is enhanced.

To complement the study of activation of the vHPC-NAc circuit in male mice in the context of stress, female mice expressing the inhibitory G_i -coupled DREADD in vHPC-NAc projections were exposed to SCVS while CNO or saline was administered intraperitoneally each day of stress and throughout behavior assessment (Figure 48, top). Saline-treated female mice showed a decrease in sucrose preference following SCVS with an interaction between stress and CNO treatment that reached $p=0.0518$, while CNO-treated female mice showed a mitigation of this susceptibility to anhedonia following stress (Figure 48, bottom). There was no significant interaction between stress and CNO treatment in the measures of SI ratio (Figure 49a) or EPM open arm time (Figure 49b), but there was a possible anxiolytic effect of CNO treatment in the EPM test, with the main effect indicating an increase in the time spent in the open arms of the maze in CNO-treated animals. Our findings in G_i -coupled DREADD-expressing female mice demonstrate that the inactivation of this circuit, in contrast to the activating experiments in male mice, can alleviate stress-induced anhedonia. Taken together with the above DREADD experiments in male mice, these data indicate that prolonged, but not acute, alterations in vHPC-NAc neuronal excitability can elicit or relieve anhedonic behavioral effect of SCVS according to whether they are activating or inactivating.

CNO: Stress + Behavior

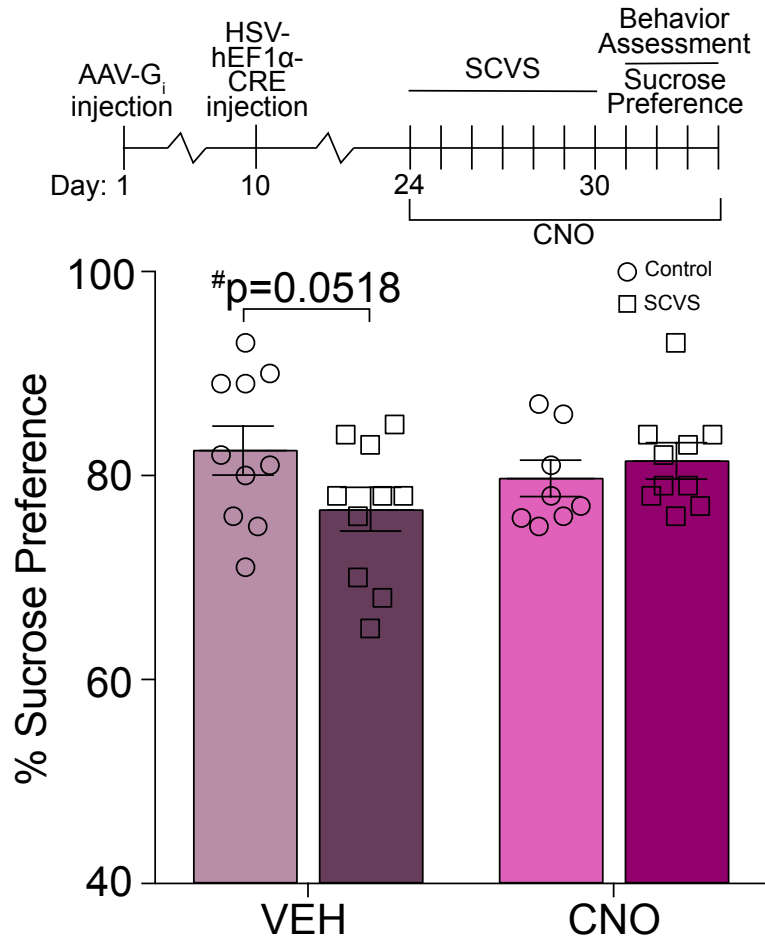


Figure 48 | Inhibition of vHPC-NAc activity directly mediates resilience to SCVS-induced anhedonia.

(Top) Experimental timeline for female mice. **(Bottom)** Female mice expressing inhibitory G_i-coupled DREADD in vHPC-NAc projections and exposed only to vehicle (saline) had decreased sucrose preference following SCVS (much like that of non-modified females), but those exposed to activating CNO showed no change in sucrose preference following SCVS, indicating resilience to SCVS-induced anhedonia. Two-way ANOVA: Group: Saline vs CNO $F(1,34) = 0.2236$, $p = 0.6393$; Trial: Control vs Stress $F(1,34) = 1.041$, $p = 0.3147$; Group X Trial $F(1,34) = 4.064$, $\#p = 0.0518$; $n = 10$ control vehicle, 8 control CNO, 10 SCVS vehicle, 10 SCVS CNO.

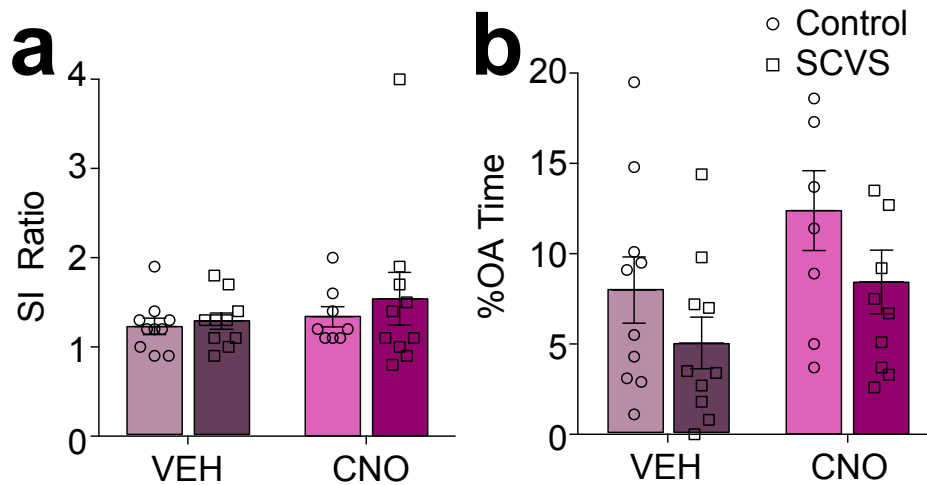


Figure 49 | Additional behavioral assays of G_i -coupled (female) DREADD-expressing vHPC-NAc mice.

Female mice expressing inhibitory G_i -coupled DREADD in vHPC-NAc projections had no interaction between CNO treatment and stress in the measures of **(a)** SI ratio [two-way ANOVA: Group: Vehicle vs CNO $F(1,36) = 0.7445$, $p = 0.3939$; Trial: Control vs Stress $F(1,36) = 0.0876$, $p = 0.7689$; Group X Trial $F(1,36) = 1.832$, $p = 0.1844$ (no interaction)]; and **(b)** percent open arm time in EPM [two-way ANOVA: Group: Vehicle vs CNO $F(1,34) = 4.658$, $p = 0.0381$; Trial: Control vs Stress $F(1,34) = 3.642$, $p = 0.0648$; Group X Trial $F(1,34) = 0.0797$, $p = 0.7794$ (no interaction)]. There was a main effect of stress on the percent OA time in EPM, with mice exposed to SCVS spending less time in the open arms.

Sex-specific transcriptome interrogation of vHPC-NAc neurons

The above findings regarding the excitability of vHPC-NAc neurons in the context of stress responses and the role of androgens in the regulation of this excitability introduces a new physiologic mechanism that works to explain why women are more likely to suffer from depression than men. However, the mechanisms by which androgens may mediate lower excitability in this circuit to cause the observed sex differences are unclear. To investigate potential mechanisms by which the excitability of male and female vHPC-NAc neurons differ and to begin to dissect how androgens affect the physiology of this circuit, we utilized translating ribosome affinity purification (TRAP; Figure 50) to interrogate circuit-specific gene expression. Using the retrograde Cre strategy described in the above experiments, vHPC-NAc neurons of male and female mice were transfected to express a GFP tag on the L10 ribosomal subunit (L10-GFP) and bilateral ventral hippocampus punches were collected and pooled (2 hippocampus punches per animal, 4 animals per pooled sample). Using this technique, actively translating mRNA from this circuit was purified and used to prepare cDNA libraries for sequencing (Figure 50). RNA sequencing (RNAseq) revealed enrichment of neuron-specific mRNA (e.g. *Vamp2*, Figure 51a) in the pulldown samples compared to input, while genes specific to glia (e.g. *Slc14a1* and *Bcas1*) were depleted (Figure 51b-c). *Vamp2* encodes synaptobrevin 2, a protein member of the complex responsible for synaptic vesicle docking and fusion to the presynaptic membrane for neurotransmitter release²⁹². *Slc14a1* is a urea transporter gene enriched in astrocytes, and *Bcas1* is a gene related to myelination in oligodendrocytes²⁹³. This enrichment of neuron-specific genes and depletion of glia-related genes indicated that our pulldown of vHPC-NAc neurons was efficient. Moreover,

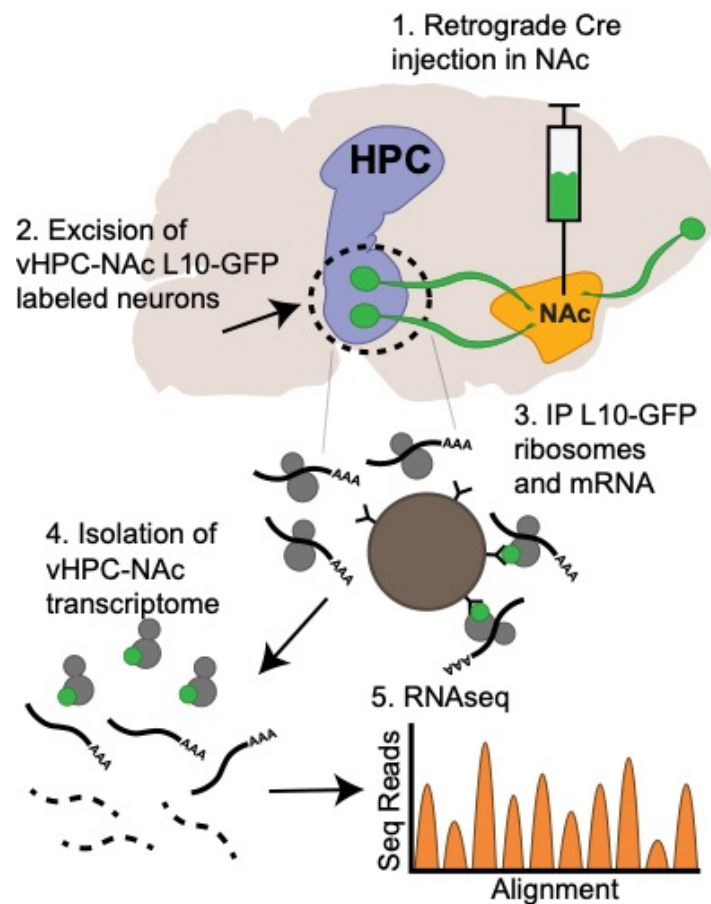


Figure 50 | Translating ribosome affinity purification (TRAP) allows interrogation of circuit-specific vHPC-NAc transcriptome.

Schematic depicting retrograde L10-GFP labeling strategy and general TRAP and sequencing steps: 1. Retrograde Cre virus (the same as used in electrophysiology experiments in this work) is injected into the NAc. Cre virus is transported via nerve terminals in the NAc to cell bodies of origin in other brain regions to induce expression of a GFP tag ribosomal subunit L10 (L10-GFP). 2. The vHPC, containing cell bodies of vHPC-NAc projection cells expressing L10-GFP, is excised for processing. 3. Tissue is processed and L10-GFP ribosomes, bound to translating messenger RNA (mRNA), are immunoprecipitated using magnetic beads bound to anti-GFP antibodies. 4. Bound mRNA is extracted from antibodies, and mRNA is prepared for sequencing. 5. RNA sequencing (RNAseq) is used to compare transcriptomes from vHPC-NAc projections in groups of interest (e.g. male vs female mice).

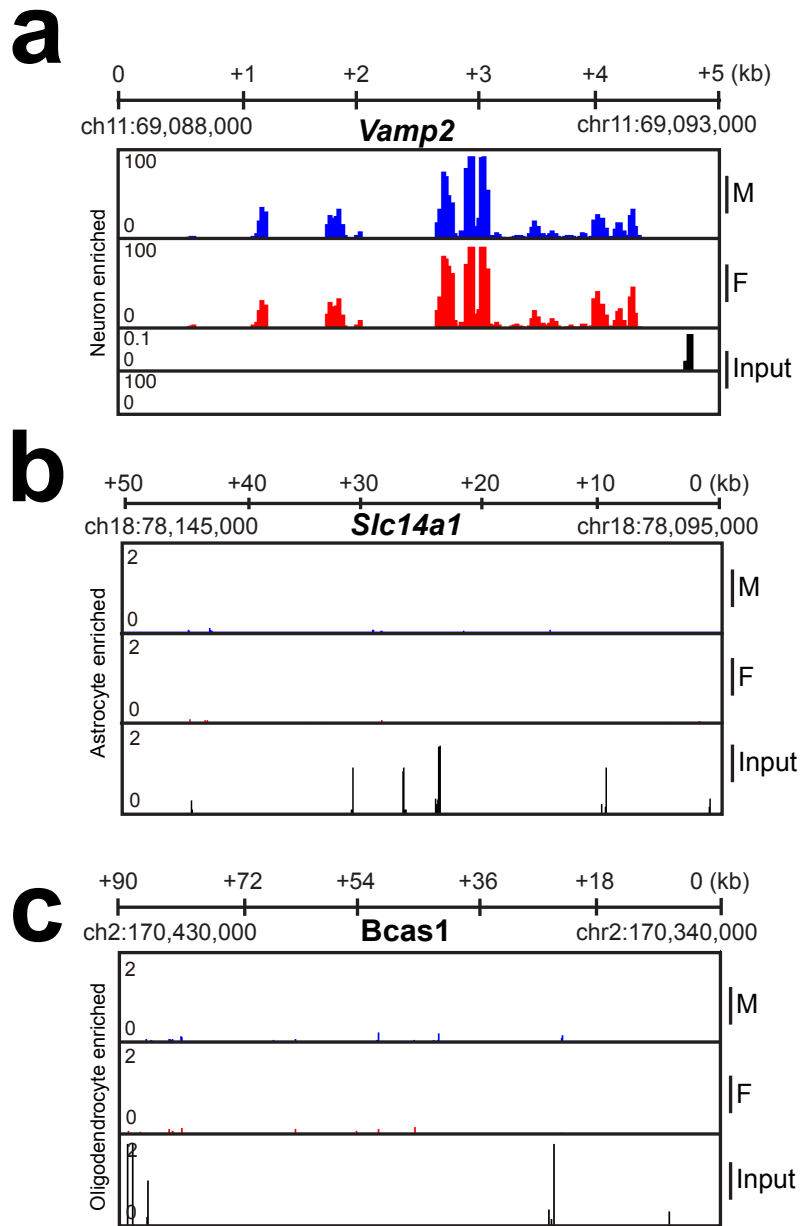


Figure 51 | TRAP strategy is efficient in pull-down of neuronal mRNA.

(a) RNA sequencing reads for neuron-specific gene vesicle-associated membrane protein 2 (*VAMP2*) in male (blue) and female (red) TRAP samples compared to input (black). Gene depletion was also verified for genes related to glia, as these genes were expected not to be enriched in the neuron-specific TRAP pull-down. (b) Astrocyte-related gene *Slc14a1* was depleted in male and female TRAP samples compared to input. (c) Oligodendrocyte-related gene *Bcas1* depleted in male and female TRAP samples compared to input. Enrichment of neuron-related genes but depletion of glia-related genes in TRAP samples verifies that the TRAP pull-downs were neuron-specific.

we observed that more transcripts were higher than were lower in abundance in male mice compared to female mice (Figure 52), suggesting the possibility of an active mechanism in this circuit driving resilience to stress-induced anhedonia. Importantly, we also observed the largest difference in transcript abundance between the sexes in Y-linked genes (many orders of magnitude more abundant in males, see inset Figure 52), indicating that our strategy for uncovering sex differences in gene expression in the vHPC-NAc circuit was valid.

Sequencing of TRAP mRNA from vHPC-NAc neurons revealed many differentially regulated genes between female and male vHPC-NAc neurons (Appendix 1), a variety of which are highlighted in Figure 53a. Many of these genes represent potential mediators of the baseline sex difference in excitability that we observed in this circuit. Moreover, Ingenuity pathway analysis (IPA, Qiagen; Hilden, Germany) applied to these TRAP RNAseq data reveals many cellular pathways that could be involved in regulating hippocampal excitability (Figure 53b). These analyses demonstrate successful enrichment of vHPC-NAc mRNA and reveal clear sex differences in the transcriptome of this circuit, and point to several potential mechanisms for the excitability differences we observed between male and female mice. These transcriptomics results uncovered myriad paths for the future study of the mechanisms of stress response in rodent models of depression, and may help to elucidate molecular mediators of the difference in MDD between men and women.

Discussion

In this chapter, we utilized behavior assessment, whole-cell slice electrophysiology, dual-viral DREADD manipulation of circuit excitability, and circuit-

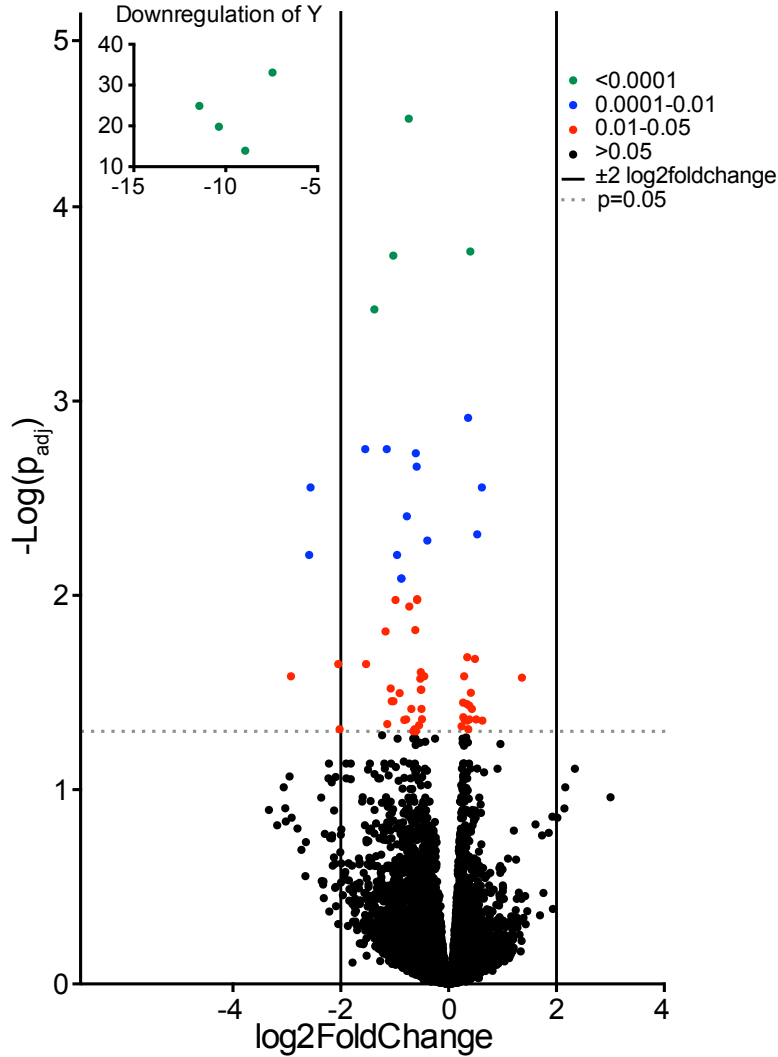


Figure 52 | Plot of transcript reads vs fold change in female and male samples verifies efficacy of sex-specific vHPC-NAc TRAP and highlights most analysis-ready genes.

Volcano plot showing distribution of transcript enrichment in female vs. male vHPC-NAc TRAP. Inset shows Y-linked genes: *Uty* [$-\log(p_{\text{adj}})=32.662$]; *Eif2s3y* [$-\log(p_{\text{adj}})=13.517$]; *Kdm5d* [$-\log(p_{\text{adj}})=19.380$]; *Ddx3y* [$-\log(p_{\text{adj}})=24.487$]. X-linked genes that were greatly significantly enriched in female mice were omitted for clarity of illustration. Genes above dashed line (indicating $p = 0.05$) are those that were significantly downregulated in females compared to males in vHPC-NAc projections, with the Y-linked genes being the extreme examples. Complete RNAseq results can be found in Appendix A, including a list of differentially expressed transcripts in female vs male vHPC-NAc neurons.

a

Gene Name	log2foldchange	p value
ADCY1	-0.395351265	6.58E-06
ADCY8	-0.640754251	0.018048473
CACNA1C	-0.277446531	0.035693124
CACNA1D	-0.308260359	0.008390456
KCNN3	-0.374359973	0.020067456
SVIL	-1.545788205	1.30E-06
NOS1	0.221996784	0.025480145
CAMK2A	0.210360400	0.009662824

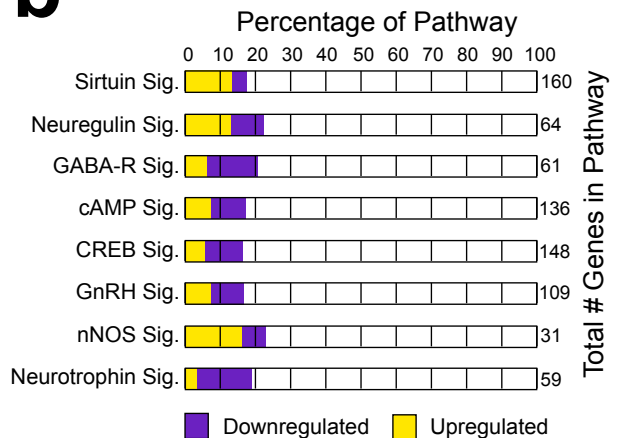
b

Figure 53 | Ingenuity pathway analysis reveals many differentially regulated pathways in female vs male vHPC-NAc transcriptomes.

(a) Table listing selected significantly differentially regulated genes. Log2foldchange listed for female vHPC-NAc neurons compared to male vHPC-NAc neurons. Selection of these genes was made based upon relevance to mood disorder pathophysiology or cellular excitability as discussed in the text. **(b)** Selected pathways affected by sex as determined by Ingenuity Pathway Analysis. Down- and upregulated gene numbers (female vs male) represented as a percentage of the total number of genes within the given pathway. Many other differentially regulated pathways were identified; this list was selected based on clear involvement in neuronal function.

specific transcriptome interrogation to uncover the potential neurophysiological mechanism for sex differences in responses to stress, with focus on stress-induced anhedonia. We found that susceptibility to anhedonia following SCVS parallels an exaggerated vHPC-NAc excitability profile in female mice. We demonstrated that androgens or androgen derivatives underlie the observed sex differences in behavior and vHPC-NAc excitability. We also demonstrated a time-dependent relationship between vHPC-NAc circuit physiology and stress susceptibility to anhedonia. Increasing the excitability of male vHPC-NAc neurons was sufficient to precipitate SCVS-induced anhedonia, but only when this excitability was increased over a prolonged period. This time dependence in behavioral changes suggests a necessary long-term adaptation to changes in circuit physiology. Complementing the male mouse studies, we demonstrated that decreasing the excitability of vHPC-NAc neurons over a prolonged period is sufficient to confer resilience to SCVS-induced anhedonia in female mice.

As there is an enigmatic sex difference in human depression diagnosis, including the variable of sex in preclinical models of mood disorders is critical. As previously discussed, women are approximately twice as likely as men to be diagnosed with depression across the lifespan²⁹⁴, and these diagnoses often correspond to female-specific changes to the reproductive cycle such as puberty, menstruation, postpartum, and menopause^{295,296}. Meta-analyses demonstrate that adult (18-60yrs) but not aged (>60yrs) males with low testosterone are more likely to experience depression symptoms. These symptoms, including anhedonia, have been shown to be significantly reduced by testosterone treatment²⁹⁷. However, exploring the molecular and physiological etiologies of sex differences in depression has been difficult, in part due to the fact that many

preclinical behavioral models of depression utilize intrasexual aggression, leaving female subjects understudied^{34,38,298}. Recently, new stress models, including SCVS^{41,170}, have attempted to address this inequality of sexes in animal subjects²⁹⁹⁻³⁰². In the current chapter, we employed SCVS in both male and female subjects to explore sex differences in stress outcomes.

Previous work has identified the importance of the NAc in the regulation of SCVS-induced behaviors. The NAc, for example, is the site of extensive transcriptional and epigenetic changes in response to stress, and many studies have implicated steroid hormones and their receptors in regulating these processes^{41,287,303}. Recent work has also demonstrated that stress-induced changes in female rodents may be presynaptic, either at glutamatergic inputs onto NAc medium spiny neurons or in other reward-related circuits^{170,304}. This complements previous work in male animals that has shown that the strength of vHPC-NAc synapses underlies susceptibility to CSDS². Additionally, circulating steroid hormones are known to affect vCA1 structure and function³⁰⁵⁻³⁰⁷ as well as social and hippocampal-dependent learning^{308,309}. Human studies have also demonstrated a decreased hippocampal volume in patients with MDD³¹⁰. Together, these works implicate vHPC as a key mediator of sex differences in stress outcomes in preclinical models and depression development in humans, particularly through its excitatory projections to the NAc.

In this chapter, we showed that vHPC afferents to NAc, but not BLA, are more excitable in female mice, and that testosterone supplementation is sufficient to decrease the excitability of the vHPC-NAc circuit and confer resilience to SCVS in female mouse subjects. As discussed above, vHPC-NAc projections and the strength of the connectivity

between these regions have been shown to modulate social behaviors^{311,312}. Here, we demonstrated vHPC-NAc projection-specific regulation of the likewise positively-valenced measure of sucrose preference, a well-validated measure of anhedonia^{34,313,314}. We confirmed that reduced sucrose preference following SCVS is female-specific and showed that this susceptibility correlated with higher vHPC-NAc, but not vHPC-BLA, excitability. This sex difference was found to be dependent on gonad hormones, as orchidectomy in male mice increased vHPC-NAc excitability and induced anhedonia after SCVS, and testosterone supplementation in female mice decreased vHPC-NAc excitability and prevented SCVS-induced anhedonia. It is important to note, however, that our hormone manipulations were systemic and may therefore act in a non-cell autonomous manner, perhaps exerting their effects indirectly at the level of adjacent circuitry or possibly via the actions of glial support cells. However, we showed using immunohistochemistry that vHPC-NAc projection cells do indeed express AR, and bath application of the AR antagonist flutamide increases vHPC-NAc excitability. Therefore, we hypothesize that direct activation of androgen receptors mediates these effects, potentially via changes in the vHPC-NAc cells themselves.

The baseline sex differences we demonstrated in vHPC-NAc excitability and behavioral responses to stress support work in males that implicates the synaptic strength of vHPC-NAc connectivity as a key regulator of behavioral outcomes following chronic stress^{2,282}, as elevated excitability in female vHPC-NAc projections could drive changes in synaptic strength leading to the observed disparate female susceptibility to SCVS. To demonstrate a definitive link between vHPC-NAc excitability and susceptibility to SCVS-induced anhedonia, we utilized virus-mediated DREADD expression in male and female

mice to artificially increase or decrease projection excitability, respectively. We found that a prolonged (10 day), but not short (during behavior assessment only) systemic administration of CNO in males with excitatory DREADD expression in vHPC-NAc induced anhedonia following SCVS as indicated by decreased sucrose preference. We hypothesize that these prolonged changes in excitability in vHPC-NAc projections may lead to various neuroadaptations, including changes in gene expression and synaptic strength, to drive differential responses to stress. This is supported by our finding of sex differences in circuit-specific gene expression, as well as literature suggesting that long-term alterations in the strength of vHPC-NAc synapses drive changes in motivated behaviors in various pathologies, including mood disorders and drug addiction^{2,282}.

There are obvious differences in sex chromosome gene expression between males and females, but sex differences also occur in somatic chromosome genes in the human brain³¹⁵. Studies utilizing preclinical models suggest that sex differences in somatic gene expression in the HPC may be influenced through the collective actions of cell-autonomous feedback mechanisms³¹⁶, epigenetics³¹⁷, and gonadal hormone effects³¹⁸. Our unbiased approach to interrogate the vHPC-NAc transcriptome revealed myriad genes and pathways of interest. Our IPA analyses demonstrated sex differences in genes of the cAMP signaling pathway, and indeed PKA signaling has recently been shown to be required in females, but not males, for synaptic potentiation³¹⁶. Our TRAP data also showed that female mice have reduced *ADCY1* and *ADCY8* transcription compared to male mice in vHPC-NAc neurons, perhaps indicating reduced phosphorylation of PKA and a failure to potentiate synaptic responses with repeated stress. As previously mentioned, the strength of vHPC-NAc MSN synapses has recently

been shown to regulate reward behaviors²⁸², and the necessity of long-term adaptation following stress to change behavior may explain the differences in anhedonia with different time courses of hormone or vHPC-NAc activity manipulation that we observed. The cAMP signaling pathway and many others that we identified represent exciting subjects for future studies of vHPC-NAc transcriptome with respect to sex differences in stress responses and depression.

The evidence presented in this chapter suggests a baseline sex difference in excitability of a specific brain circuit driven by adult androgens that is causative of stress-induced anhedonia. This discovery may work to explain the observation that women are more than twice as likely as men to experience depression, and elucidates critical knowledge important for our understanding of these sex differences. Our circuit-specific transcriptome studies also provide novel gene expression data that will potentially drive future research necessary to validate molecular targets for sex-specific depression treatments.

IV. VENTRAL HIPPOCAMPUS TO NUCLEUS ACCUMBENS Δ FOSB UNDERLIES RESILIENCE TO SOCIAL STRESS AND REGULATES CIRCUIT-SPECIFIC EXCITABILITY

The experiments in the following chapter are the subject of a manuscript currently in revision at Nature Communications. Dr. Andrew L. Eagle and Claire E. Manning performed the stress, behavior, and microscopy. Elizabeth S. Williams performed the electrophysiology experiments individually and stress protocols with the coauthors.

Introduction

The ventral hippocampus (vHPC), due to its extensive efferent connections with major forebrain structures such as the hypothalamus, amygdala, and nucleus accumbens (NAc)^{74,85}, is a key component of the regulation of an animal's emotional response to stress. As introduced above, perturbations in these responses to stress can cause psychiatric conditions such as depression^{319,320}. The connectivity of vHPC and NAc mediates reward behavior³²¹ and susceptibility to social withdrawal following chronic social defeat stress³²², but the field yet lacks a full understanding of the role of the vHPC in the regulation of regions such as the NAc in the pathogenesis of depressive and anxiety disorders. It is known that stress affects gene expression in vHPC neurons³²³⁻³²⁵, but the mechanisms of circuit-specific changes in gene expression and activity of vHPC outputs in response to stress require further investigation.

The transcription factor Δ FosB is uniquely stable^{326,327}, and induced by chronic neuronal activity throughout the brain³²⁸. In the NAc, Δ FosB mediates stress resilience^{150,158,329} and influences synapses and dendritic morphology of NAc medium spiny neurons³³⁰. Dorsal hippocampus (dHPC) Δ FosB also is also necessary for

learning³³¹, and decreases excitability of CA1 pyramidal neurons in this region³³². Δ FosB is also induced throughout the HPC by stress and antidepressants^{272,329,333,334}, and vHPC CA3 Δ FosB mediates the protective antidepressant effects of ketamine³³⁴. These studies suggest that Δ FosB plays a key role in regulating vHPC function, likely through long-term changes in gene-expression. These changes in gene expression that result in altered vHPC physiology may in turn mediate the development of psychopathologies such as MDD. In the following chapter, circuit-specific CRISPR gene editing is used to investigate the role of Δ FosB in vHPC-NAc projections in resilience to social withdrawal following CSDS. We show that Δ FosB uniquely regulates the excitability of these projections, identifying this molecule as a prime candidate in the mediation of resilience to stress through its effects on vHPC-NAc physiology.

Results

Chronic social defeat stress and fluoxetine induce Δ FosB in ventral hippocampus

To investigate the induction of Δ FosB in vHPC by stress, male C57Bl6/J mice were exposed to CSDS (Figure 1), a well-validated chronic stress model that causes a variety of depressive-like behaviors in susceptible mice, including anhedonia and social withdrawal^{38,270,271}. CSDS increased the number of Δ FosB+ DG neurons in vHPC (Figure 54a, b). Additionally, in accordance with our previous investigation of dHPC^{272,333}, we found that Δ FosB was also induced in all subregions of the vHPC following chronic exposure to the

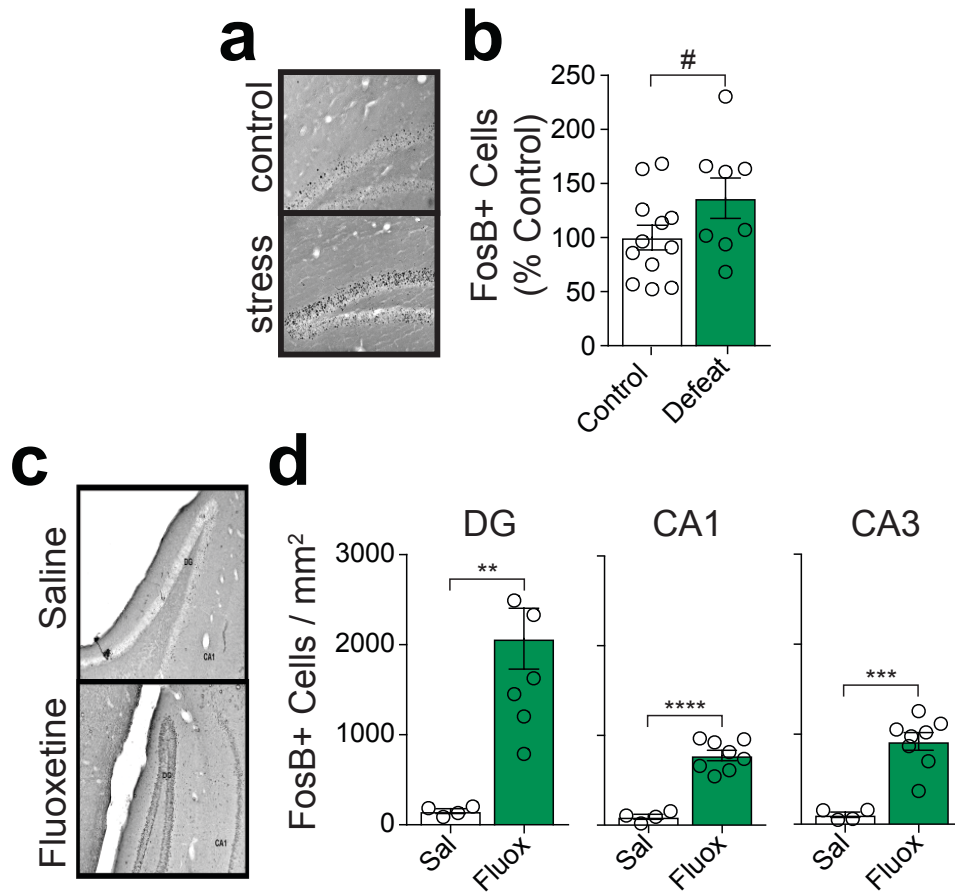


Figure 54 | Chronic social defeat stress and fluoxetine induce Δ FosB in ventral hippocampus.

(a) Representative microscopy of coronal slices stained for Δ FosB in vHPC from control and stressed mice, quantified in (b). Two-tailed t-test: $t(18) = 1.77$, $\#p = 0.0936$ ($n = 12$ control, $n = 8$ stress). (c) Representative microscopy of coronal slices stained for Δ FosB in vHPC dentate gyrus (DG), CA1, and CA3 from mice treated with chronic saline or fluoxetine, quantified in (d). Two-tailed t-test: DG $t(10) = 3.908$, $**p = 0.0029$; CA1 $t(10) = 7.951$, $****p < 0.0001$; CA3 $t(10) = 5.674$, $p = 0.0002$; ($n = 4$ saline, $n = 8$ fluoxetine). All images at 4X magnification.

antidepressant fluoxetine (Figure 54c, d). Considering this finding of its induction in vHPC by chronic stress and antidepressant treatment, vHPC Δ FosB may play a role in mediating resilience to stress, as it is known to do in the NAc¹⁵⁸.

As previously mentioned, the activity of vHPC-NAc projections mediates resilience to CSDS³²² and Δ FosB decreases excitability of dHPC CA1 neurons³³². Therefore, we investigated the role of vHPC-NAc Δ FosB in stress outcomes following CSDS. To label vHPC-NAc projections, we used a transgenic mouse line expressing Cre-dependent GFP (*Rosa26^{eGFP-L10a}*), and injected a persistent, retrograde expressing viral vector carrying Cre recombinase (HSV-hEf1 α -Cre) into the NAc (Figure 55a, left). Three weeks following injection, GFP expression was observed in the CA1 subregion of the vHPC (vCA1) and in other areas from which NAc projections originate (e.g. ventral subiculum and VTA; Figure 55a, right). Labeled mice were then exposed to CSDS and vHPC sections were prepared for immunohistochemistry (IHC) and stained for GFP and Δ FosB. We found that CSDS induced Δ FosB in vHPC-NAc projections (Figure 55b,c), validating its consideration as a regulatory molecule in this circuit in the context of stress.

vHPC-NAc Δ FosB is necessary for resilience to social stress

The above induction studies demonstrate that Δ FosB is induced in vHPC in response to stress and antidepressants, and this includes that in the vHPC-NAc circuit in response to CSDS. To investigate Δ FosB's role in resilience to stress in the hippocampus, we utilized Δ JunD, an inhibitor of Δ FosB's transcriptional capacity¹⁵⁸. Δ JunD, a dominant negative form of Δ FosB's AP-1 complex binding partner, was virally overexpressed in either vHPC or dHPC (Fig. 7a). Mice were then exposed to a subthreshold microdefeat,

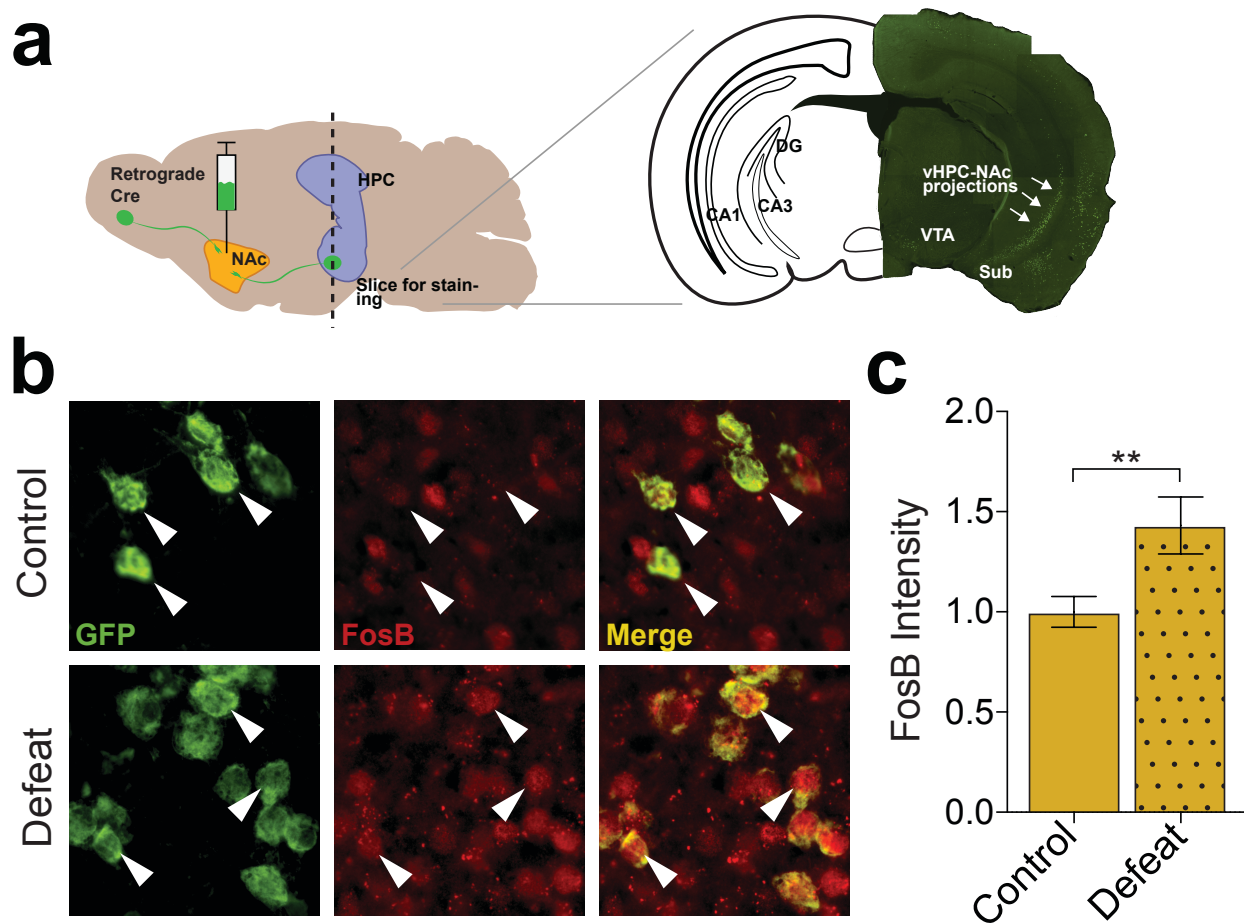


Figure 55 | Δ FosB is induced in vHPC-NAc projections by CSDS.

(a) Schematic depicting viral injection strategy for labeling vHPC-NAc projections (left) and representative coronal section containing labeled NAc projections (right). **(b)** Representative microscopy of vHPC CA1 coronal sections (40X) showing immunofluorescent labeling of NAc-projecting neurons expressing L10-GFP (green, left), Δ FosB (red, middle) and merged images demonstrating projection-specific Δ FosB expression (right). Defeat-stressed mice (bottom; $n=109$ cells) showed an increase Δ FosB signal in GFP-positive cells compared to control-handled mice (top; $n=147$ cells), as indicated by white arrows and quantified in **(c)**. Two-tailed t-test: $t(254) = 2.847$, $**p = 0.0048$. All images at 40X magnification; single data points omitted in **(c)** for clarity.

which causes a social withdrawal only in mice sensitized to stress^{270,271}. The microdefeat paradigm, similar to CSDS, utilized CD-1 aggressors and placed the experimental mouse in the aggressor's home cage for 5 minutes. During this time, the experimental mouse is subjected to attack from the aggressor, and then placed into its own cage to rest for 15 minutes. The stress then repeats twice more with novel aggressors, with a rest period between bouts. After a 24-hour incubation period, the experimental mice were evaluated with the standard social interaction (SI) test. Mice overexpressing Δ JunD in vHPC, but not dHPC, spent less time interacting with a social target and as such had a reduced SI ratio (Figure 56b). These results suggest that Δ FosB in vHPC, but not dHPC, is necessary for resilience to social stress.

This experiment investigated general HPC Δ FosB in the context of stress, but the importance of Δ FosB function in vHPC-NAc still remained unclear. To target Δ FosB in only vHPC-NAc neurons, we utilized a dual viral CRISPR system with two constructs (Cas9 and gRNA) packaged in two separate viral vectors (Figure 57a). With this strategy, a viral vector encoding retrogradely expressing Cas9 endonuclease (HSV-hEfl α -LS1L-Cas9) was injected into the NAc. Following three weeks for retrograde expression and recovery, a viral vector encoding guide RNA (gRNA) specific for exon 1 of *FosB* (HSV-IE4/5-TB-gRNA-eYFP-CMV-IRES-Cre) or a control virus (Scr gRNA; HSV-IE4/5-TB-eYFP-CMV-IRES-Cre) was injected into the vHPC. Only neurons expressing both viruses (i.e. vHPC-NAc projections) had the Cas9 and *FosB* gRNA necessary to edit the *FosB* gene and cause reduction of Δ FosB expression. This dual viral CRISPR approach

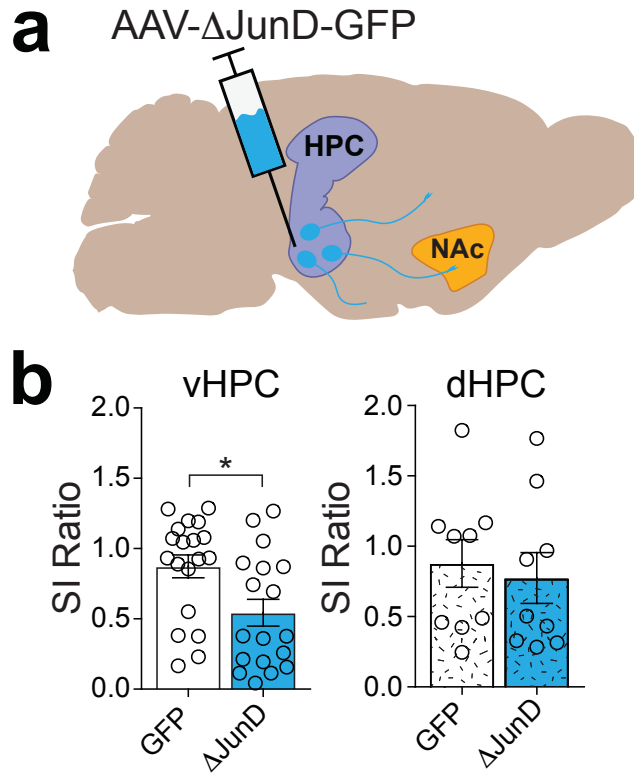


Figure 56 | vHPC Δ FosB is necessary for resilience to social stress.

(a) Schematic depicting viral injection strategy for AAV- Δ JunD-GFP (pictured) or AAV-GFP in vHPC. (b) Inhibition of Δ FosB function in vHPC with Δ JunD reduced SI ratio following social defeat stress when injected in vHPC (left; two-tailed t-test: $t(35) = 2.632$, $*p = 0.0125$; $n=19$ GFP, $n=18$ Δ JunD), but not dHPC (right; two-tailed t-test: $t(16) = 0.4163$, $p = 0.6827$; $n=9$ /group).

was found to decrease the expression of Δ FosB in co-labeled GFP and Cas9 vHPC cells (i.e. vHPC-NAc projections; Figure 57b).

This novel circuit-specific gene editing tool produced silencing of the *FosB* gene (*FosB* KO) leading to reliable reduction of Δ FosB protein expression in vHPC-NAc projections. This allowed us to interrogate the circuit-specific role of Δ FosB in the regulation of stress responses. Adult mice with *FosB* KO in the vHPC-NAc circuit (Figure 57a) were exposed to CSDS and assessed for social withdrawal behavior using the SI test. *FosB* KO in vHPC-NAc increased social withdrawal following CSDS (Figure 57c), and caused a small decrease in locomotor activity (data not shown). These findings suggest that Δ FosB regulates locomotor activity and stress resilience through its activity in vHPC-NAc neurons, consistent with previous findings^{335,336}. *FosB* KO in vHPC-NAc neurons did not, however, affect baseline anxiety measures in the EPM (Figure 57d,e), behavior not typically associated vHPC-NAc function. These findings suggest that Δ FosB expression in vHPC-NAc projections is necessary for resilience to stress, and in the absence of normal levels of Δ FosB expression in this circuit, mice are sensitized specifically to stress-induced social withdrawal behavior.

As vHPC sends projections to other stress-related brain regions (e.g. the BLA³³⁷⁻³³⁹), it was also critical to investigate Δ FosB's role in other circuits in the context of stress. To highlight the circuit-specificity of Δ FosB in mediating stress outcomes, we also investigated *FosB* KO in the vHPC-BLA circuit using the same dual viral CRISPR strategy described above (Figure 58a). *FosB* KO in vHPC-BLA did induce social withdrawal as measured with the SI test, (Figure 58b), however, it reduced anxiety behaviors in the EPM (Figure 58c,d), with no change in locomotor activity (data not shown). Decreased anxiety

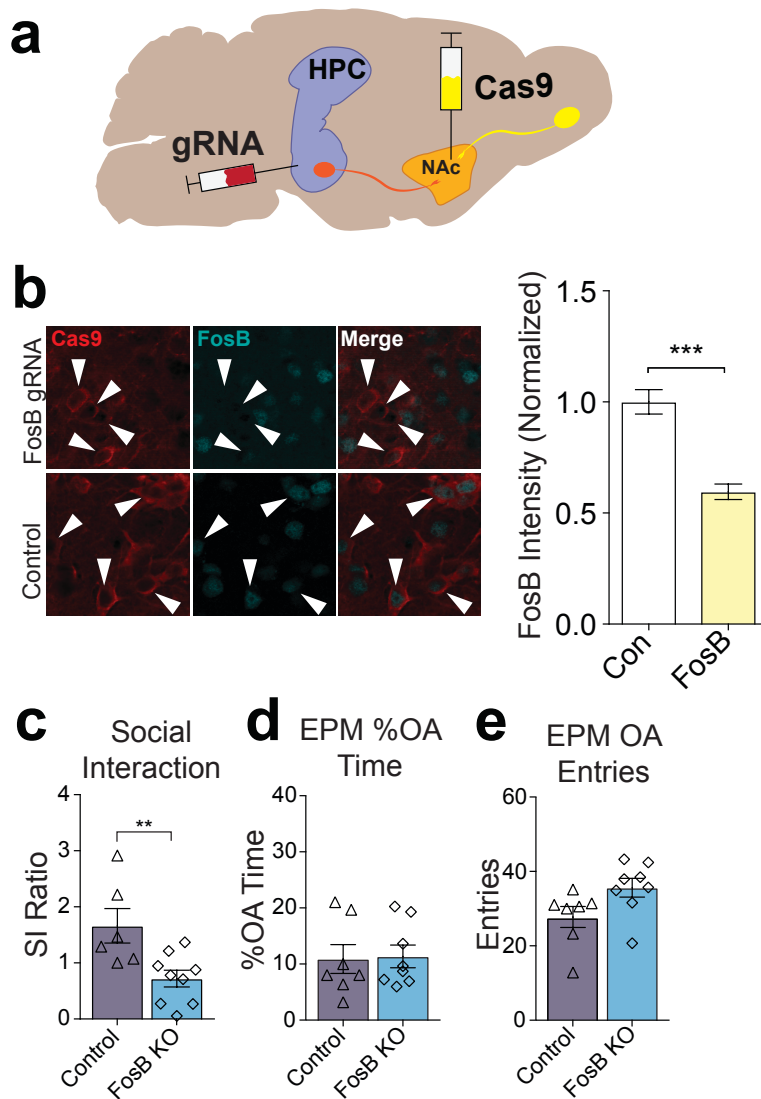


Figure 57 | vHPC-NAc Δ FosB is necessary for resilience to social stress.

(a) Schematic of dual-vector CRISPR strategy to silence *FosB* in vHPC-NAc neurons: retrograde Cre-dependent Cas9 viral vector (Cas9; yellow) is injected into NAc while local vector expressing Cre and *FosB* guide RNA (gRNA; red) is injected into vHPC. *FosB* silencing (*FosB* KO) occurs only in co-transduced vHPC-NAc neurons (orange). **(b, left)** Representative images of Cas9 (red, left), FosB (cyan, middle), and merged (right) from vHPC of mice with control (no gRNA) or *FosB* KO vectors (FosB gRNA). Intensity of FosB staining quantified in **(b, right)**. Two-tailed Mann-Whitney U-test: $U = 5423$, sum of ranks Control = 23483, FosB = 12563, $***p < 0.001$ ($n = 149$ control cells, $n = 119$ FosB gRNA cells). **(c)** *FosB* silencing in vHPC-NAc neurons reduces SI ratio following CSDS. Two-tailed t-test: $t(13) = 3.055$, $**p = 0.0092$ ($n=7$ control, $n=9$ FosB KO). *FosB* silencing in vHPC-NAc does not affect anxiety-like behavior in the elevated plus maze (EPM) % open arm time [two-tailed t-test: $t(13) = 0.1441$, $p = 0.8877$] **(d)** or open arm entries [two-tailed t-test: $t(13) = 2.082$, $p = 0.0576$] **(e)**.

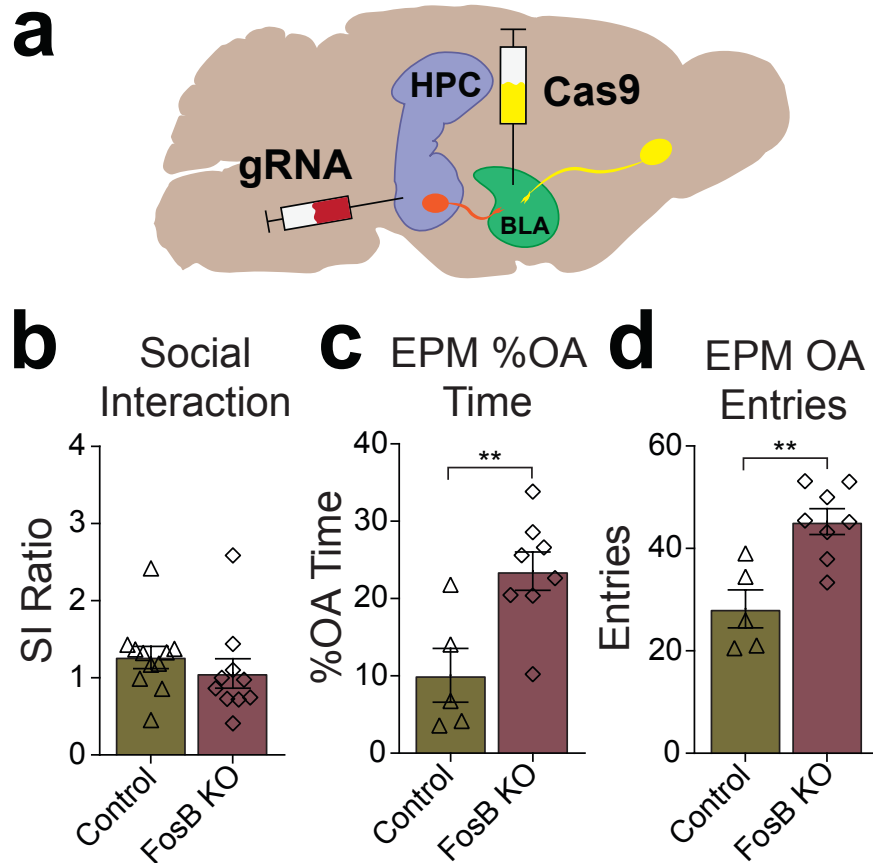


Figure 58 | vHPC-BLA FosB KO is anxiolytic.

(a) Schematic of dual-vector CRISPR strategy to silence *FosB* in vHPC-BLA neurons (same as vHPC-NAc KO strategy in Figure 57). **(b)** *FosB* silencing in vHPC-BLA does not affect SI ratio following CSDS. Two-tailed t-test: $t(19) = 0.8723$, $p = 0.3939$ ($n=11$ control, $n=10$ FosB KO). **(c)** *FosB* silencing in vHPC-BLA decreases anxiety-like behavior in the EPM, increasing open arm time [two-tailed t-test: $t(11) = 3.241$, $**p = 0.0079$] **(c)** and entries [two-tailed t-test: $t(11) = 3.956$, $**p = 0.0022$].

has been demonstrated after vHPC lesions^{320,339,340}, which suggests that Δ FosB in vHPC-BLA projections is necessary for the expression of anxiety behavior. These data, along with the above vHPC-NAc Δ FosB findings, suggest that vHPC *FosB* regulates stress responses in a circuit-specific fashion. Furthermore, these circuit-specific studies work to clarify the role of different vHPC circuits in stress-related disorders, namely depression and anxiety.

Δ FosB regulates vHPC-NAc projection excitability

As previous studies have demonstrated a link between vHPC-NAc activity and CSDS susceptibility³²², we next examined how Δ FosB affected the physiological properties of the vHPC and its projections. To determine Δ FosB's effect on the excitability of vHPC neurons in general, viral-mediated overexpression of Δ FosB was utilized in this region (Figure 59a). Overexpression of Δ FosB reduced the excitability of vCA1 neurons, indicated by a decrease in the number of spikes elicited with increasing current injection (Figure 59b) and an increase in rheobase (Figure 59c). These findings suggest that Δ FosB expression reduces the excitability of vHPC neurons, leading us to question whether this was true of vHPC projections to the NAc, as stress-induced increases in Δ FosB could influence the decreased activity in this circuit known to drive resilience to CSDS³²².

To investigate whether Δ FosB regulates excitability in vHPC-NAc projection neurons specifically, we crossed *floxed FosB* mice (*FosB^{fl/fl}*)²⁶⁷ with the Cre-dependent GFP-L10a (*Rosa26^{eGFP-L10a}*) mice described above to generate floxed FosB/GFP-L10a mice (*FosB* KO) and utilized non-floxed GFP-L10a mice (WT) as controls (Figure 60a).

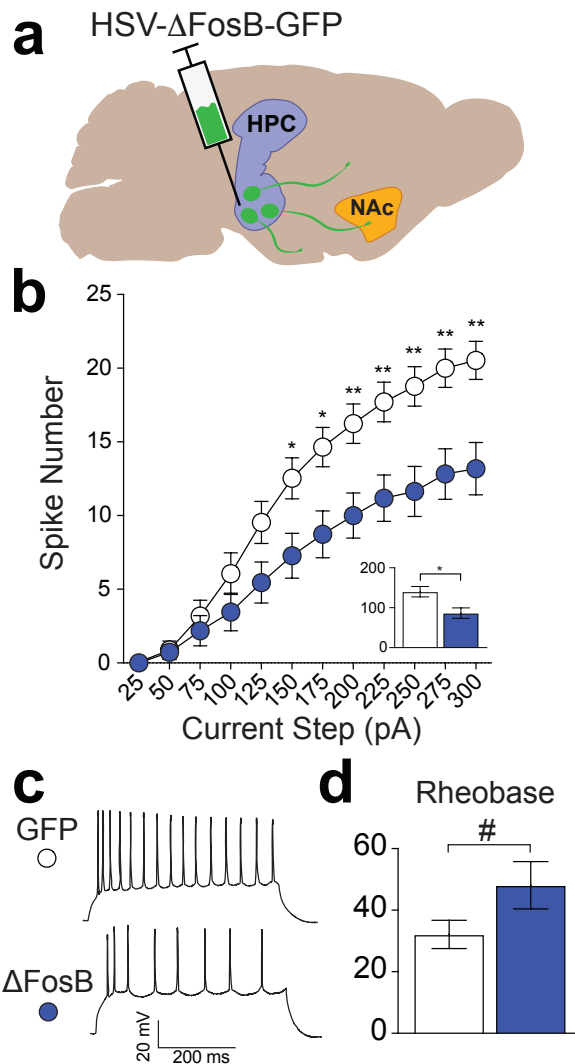


Figure 59 | Δ FosB regulates vHPC neuronal excitability.

(a) Schematic depicting viral injection of HSV vector carrying Δ FosB and GFP (pictured) or GFP. **(b)** Viral overexpression of Δ FosB reduces the number of spikes in vCA1 pyramidal neurons with increasing current injection. Two-way ANOVA, Holm-Sidak multiple comparisons: [25 pA $t(312) = 0.03107$, $p = 0.9957$], [50 pA $t(312) = 0.08191$, $p = 0.9957$], [75 pA $t(312) = 0.5253$, $p = 0.9359$], [100 pA $t(312) = 1.376$, $p = 0.5253$], [125 pA $t(312) = 2.152$, $p = 0.1507$], [150 pA $t(312) = 2.776$, $*p = 0.0345$], [175 pA $t(312) = 3.127$, $*p = 0.0135$], [200 pA $t(312) = 3.293$, $**p = 0.0088$], [225 pA $t(312) = 3.446$, $**p = 0.0058$], [250 pA $t(312) = 3.765$, $**p = 0.0020$], [275 pA $t(312) = 3.793$, $**p = 0.0020$], [300 pA $t(312) = 3.881$, $**p = 0.0015$]. Inset: total spikes for all steps (two-tailed t -test: $t(26) = 2.746$, $*p = 0.0108$; $n = 17$ GFP cells, $n = 11$ Δ FosB cells) **(c)** Representative traces from 200 pA depolarizing current injection in ventral vHPC CA1 neurons expressing GFP or Δ FosB-GFP. **(d)** Δ FosB overexpression in vHPC caused a trend toward an increase in rheobase in pyramidal neurons. Two-tailed t -test, $t(26) = 1.905$, $\#p = 0.0680$.

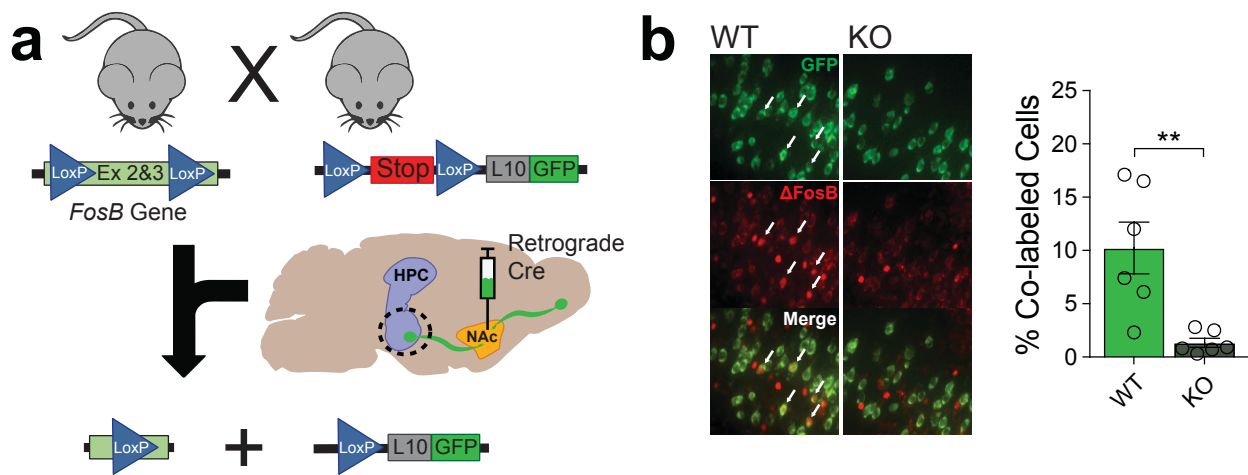


Figure 60 | Δ FosB expression in vHPC-NAc neurons is reduced in FosB circuit-specific KO mice.

(a) Schematic depicting strategy for *FosB* knockout in neurons projecting to NAc. *Floxed FosB* mice (*FosB^{fl/fl}*) were crossed with mice expressing Cre-dependent GFP-L10 ribosomal fusion protein (*Rosa26^{eGFP-L10a}*) to generate floxed *FosB*/GFP-L10 mice (KO) and non-floxed GFP-L10 controls (WT). Retrograde Cre vector was injected in NAc to drive GFP-L10 expression and splice out exons 2 and 3 in *FosB* in NAc-projecting neurons. (b) Representative coronal vHPC microscopy (20X) showing NAc-projecting neurons expressing GFP (green, top), Δ FosB (red, middle), and merge (bottom). White arrows indicate co-labeled L10-GFP and Δ FosB-expressing cells. KO significantly reduces the % of co-labeling of GFP and Δ FosB in vHPC-NAc neurons. Two-tailed Mann-Whitney U-test: U = 2, sum of ranks WT = 55 and KO = 23, **p = 0.0087 (n = 6 mice/group).

Retrograde Cre HSV was injected into the NAc to allow GFP-L10a expression in NAc-projecting neurons of all mice, and knock out of *FosB* expression in NAc-projecting neurons of KO mice (Figure 60b). Whole-cell *ex vivo* slice electrophysiology from L10-GFP+ vCA1-NAc neurons revealed that *FosB* KO causes elevated excitability in NAc-projecting vHPC neurons in male mice as indicated by an increase in the sum of the total number of spikes elicited at all current steps (Figure 61). *FosB* KO did not affect any membrane properties (Figure 62a-f), except for an increase in membrane capacitance (Figure 62d). *FosB* KO in male vHPC-NAc projections did cause an increase in sag ratio, indicating a decrease in I_h current (Figure 62g). Interestingly, *FosB* KO in male vHPC-NAc neurons also caused a decrease in spike frequency adaptation as indicated by lessened increase in the time between spikes over the span of a depolarizing current step (Figure 63a), but did not change the latency to first spike at the same current (Figure 63b). The same experiments performed with female WT and KO mice revealed a similar, but exaggerated, increase in vHPC-NAc excitability, as indicated by a significantly elevated number of spikes at nearly all current steps as well as an increase in the total number of spikes at all steps (Figure 64). *FosB* KO in female vHPC-NAc neurons did cause an increase in input resistance (Figure 65c), but did not affect any other membrane properties (Figure 65a-f) nor sag ratio (Figure 65g). Like male mice, female *FosB* KO mice also showed a decrease in spike frequency adaptation in vHPC-NAc projections (Figure 66a) but no change in latency to first spike (Figure 66b). As reduced activity in excitatory vHPC projections to NAc MSNs has been shown to induce resilience to CSDS and increased activity conversely induces susceptibility³²², and our circuit-specific studies above demonstrate that vHPC-NAc Δ FosB is necessary for CSDS resilience, these

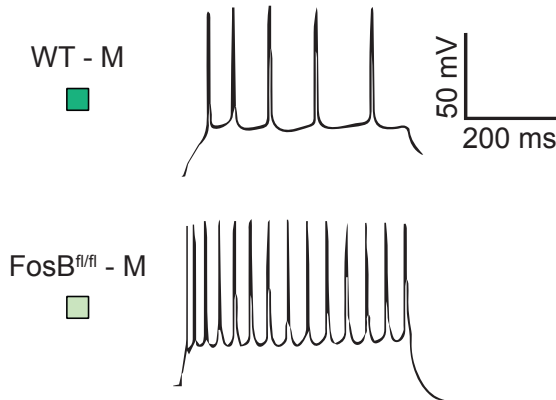
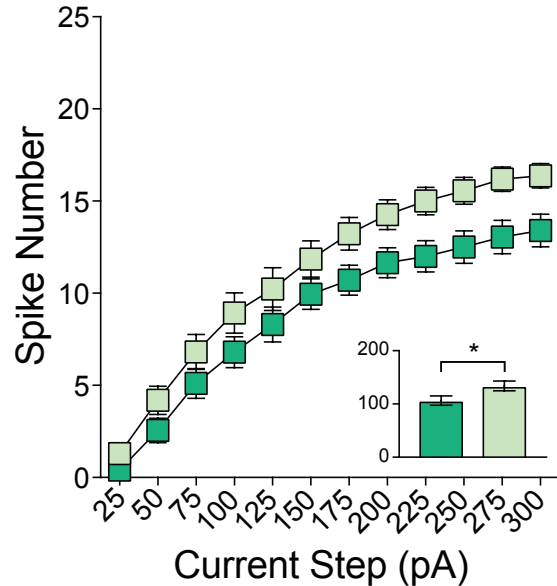


Figure 61 | Δ FosB regulates the cellular excitability of vHPC-NAc neurons in male mice.

(Top) KO of *FosB* increases the number of spikes in vHPC-NAc neurons across increasing depolarizing current injections. Two-way ANOVA, Holm-Sidak multiple comparisons: [25 pA $t(540) = 0.7411$, $p = 0.4589$], [50 pA $t(540) = 1.352$, $p = 0.4495$], [75 pA $t(540) = 1.418$, $p = 0.4495$], [100 pA $t(540) = 1.758$, $p = 0.3910$], [125 pA $t(540) = 1.589$, $p = 0.4495$], [150 pA $t(540) = 0.4495$, $p = 1.573$], [175 pA $t(540) = 2.086$, $p = 0.2347$], [200 pA $t(540) = 2.158$, $p = 0.2253$], [225 pA $t(540) = 2.481$, $p = 0.1264$], [250 pA $t(540) = 2.527$, $p = 0.1224$], [275 pA $t(540) = 2.592$, $p = 0.1113$], [300 pA $t(540) = 2.456$, $p = 0.1264$]. Inset: total spikes for all steps increased with *FosB* KO. Two-tailed t-test: $t(45) = 2.095$, $*p = 0.0418$ ($n = 20$ WT cells from $n = 5$ animals, $n = 27$ KO cells from $n = 8$ animals). (Bottom) Representative voltage traces from 200 pA depolarizing current step vHPC-NAc projections in WT and KO male mice.

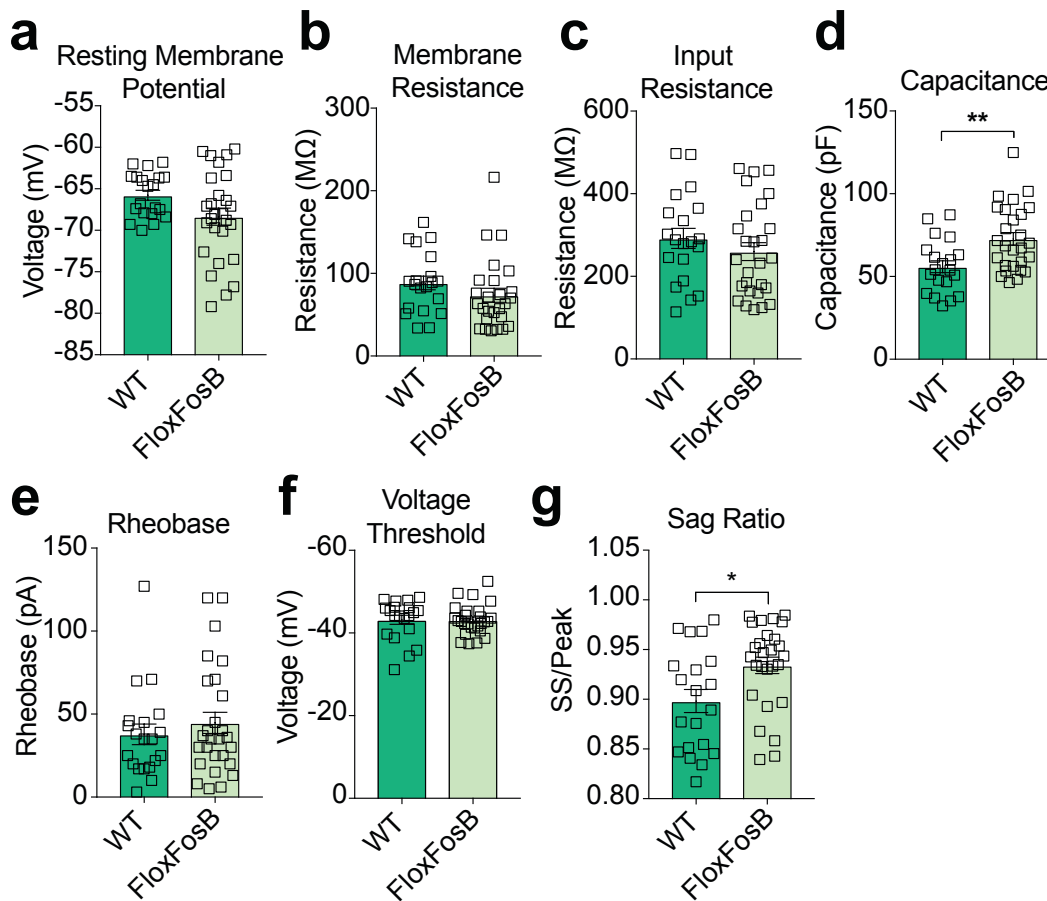


Figure 62 | Membrane properties of male WT vs FosB KO vHPC-NAc projections.

WT and *FosB* KO (FloxFosB) vHPC-NAc projections did not differ in the following membrane properties: **(a)** Resting membrane potential (mV) [two-tailed Mann-Whitney U-test: $U = 198$, sum of ranks WT = 552, KO = 576, $p = 0.1233$]; **(b)** membrane resistance ($M\Omega$) [two-tailed t-test: $t(45) = 1.228$, $p = 0.2262$]; and **(c)** input resistance ($M\Omega$) [two-tailed t-test: $t(45) = 0.9708$, $p = 0.3369$]. *FosB* KO vHPC-NAc projections had a higher membrane capacitance than WT projections [two-tailed t-test: $t(45) = 3.112$, $**p = 0.0032$]. WT and *FosB* KO vHPC-NAc projections did not differ in the measures of **(e)** rheobase (pA) [two-tailed t-test: $t(45) = 0.7551$, $p = 0.4541$] and **(f)** voltage threshold (mV) [two-tailed t-test: $t(45) = 0.0004458$, $p = 0.9996$]. **(g)** *FosB* KO vHPC-NAc projections had a higher sag ratio than WT projections [two-tailed t-test: $t(45) = 2.592$, $*p = 0.0128$], indicating less I_h current.

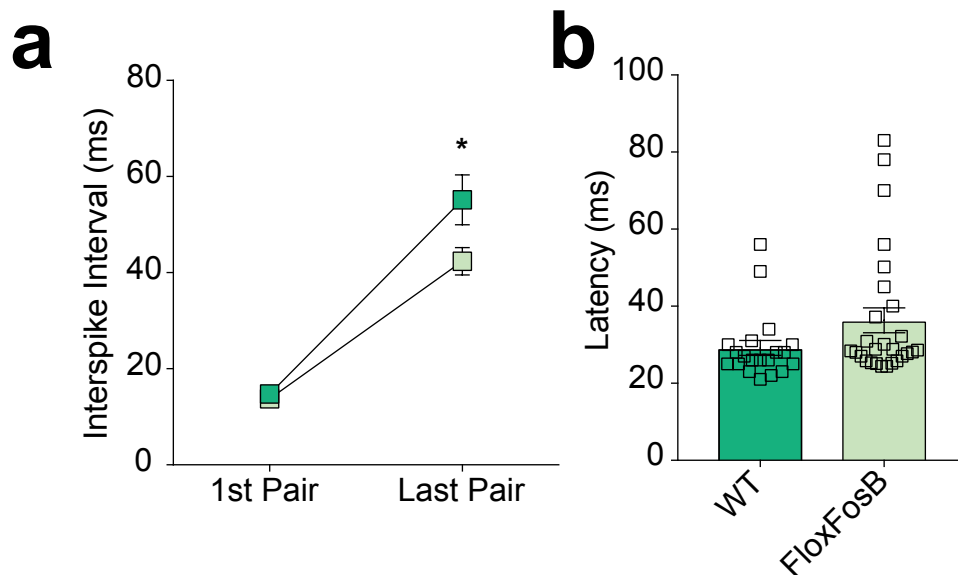


Figure 63 | Spike frequency adaptation is decreased in male FosB KO vHPC-NAc projections.

Interspike interval increases over the course of 500 ms current injection as measured by the time (ms) between the 1st pair of spikes and last pair of spikes. **(a)** Male *FosB* KO (FloxFosB) had less spike frequency adaptation as measured by the interspike interval increase; interspike interval of the last pair of spikes was significantly longer in male WT vHPC-NAc projections than in KO projections. One-way ANOVA: $F(3, 90) = 46.32$; mean difference WT last pair vs. FloxFosB last pair = 12.78, 95% CI = 2.047 to 23.51, * $p = 0.0128$. **(b)** Latency to 1st spike (ms) from beginning of current injection did not differ between male WT and KO vHPC-NAc projection neurons. Two-tailed Mann-Whitney U-test: $U = 181$, sum of ranks WT = 391 and KO = 737, $p = 0.0554$. Interspike intervals and latency to 1st spike were evaluated at the rheobase current for each cell.

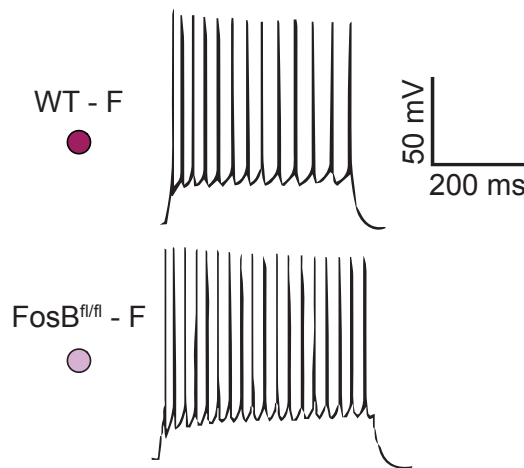
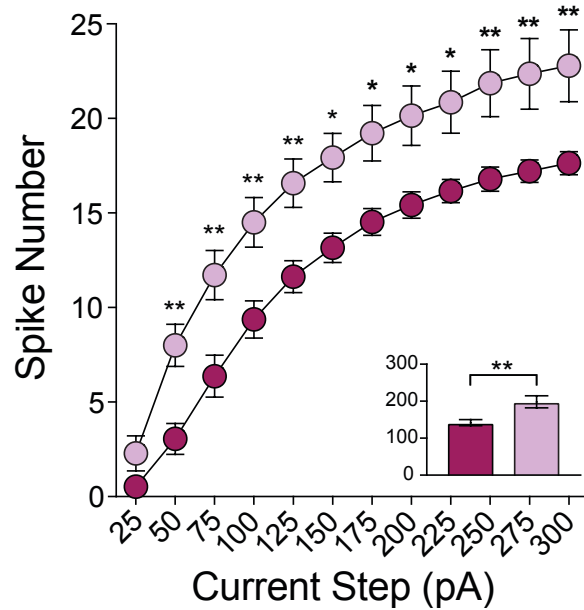


Figure 64 | Δ FosB regulates the cellular excitability of vHPC-NAc neurons in female mice.

(Top) KO of *FosB* increases the number of spikes in vHPC-NAc neurons across increasing depolarizing current injections. Two-way ANOVA, Holm-Sidak multiple comparisons: [25 pA $t(372) = 1.143$, $p = 0.2538$], [50 pA $t(372) = 3.214$, $**p = 0.0099$], [75 pA $t(372) = 3.472$, $**p = 0.0069$], [100 pA $t(372) = 3.333$, $**p = 0.0098$], [125 pA $t(372) = 3.209$, $**p = 0.0099$], [150 pA $t(372) = 3.099$, $*p = 0.0104$], [175 pA $t(372) = 3.045$, $*p = 0.0104$], [200 pA $t(372) = 3.067$, $*p = 0.0104$], [225 pA $t(372) = 3.052$, $*p = 0.0104$], [250 pA $t(372) = 3.292$, $**p = 0.0098$], [275 pA $t(372) = 3.343$, $**p = 0.0098$], [300 pA $t(372) = 3.348$, $**p = 0.0098$]. Inset: total spikes for all steps increased with *FosB* KO. Two-tailed t-test: $t(31) = 3.338$, $**p = 0.0022$ ($n = 19$ WT cells from $n = 4$ animals, $n = 14$ KO cells from $n = 4$ animals). (Bottom) Representative voltage traces from 200 pA depolarizing current step vHPC-NAc projections in WT and KO female mice.

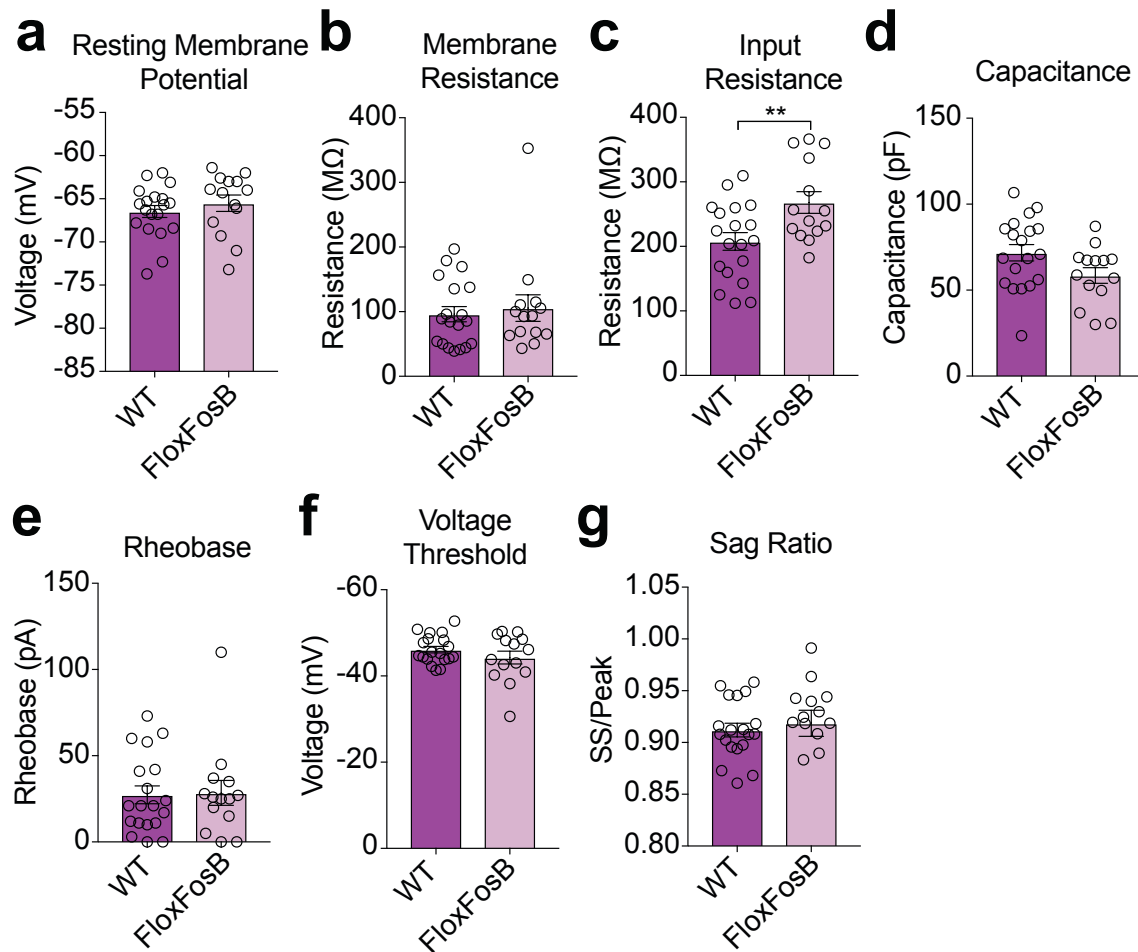


Figure 65 | Membrane properties of female WT vs FosB KO vHPC-NAc projections.

WT and *FosB* KO (FloxFosB) vHPC-NAc projections did not differ in the following membrane properties: **(a)** Resting membrane potential (mV) [two-tailed t-test: $t(31) = 0.8337$, $p = 0.4108$] and **(b)** membrane resistance (MΩ) [two-tailed t-test: $t(31) = 0.4226$, $p = 0.6755$]. **(c)** Input resistance (MΩ) was increased in KO vHPC-NAc projections [two-tailed t-test: $t(31) = 2.816$, $**p = 0.0084$]. WT and *FosB* KO vHPC-NAc projections did not differ in the measures of **(d)** membrane capacitance (pF) [two-tailed t-test: $t(31) = 1.953$, $p = 0.0599$]; **(e)** rheobase (pA) [two-tailed t-test: $t(31) = 0.1287$, $p = 0.8984$]; **(f)** voltage threshold (mV) [two-tailed t-test: $t(31) = 1.187$, $p = 0.2442$]; and **(g)** sag ratio [two-tailed t-test: $t(31) = 0.4986$, $p = 0.6216$].

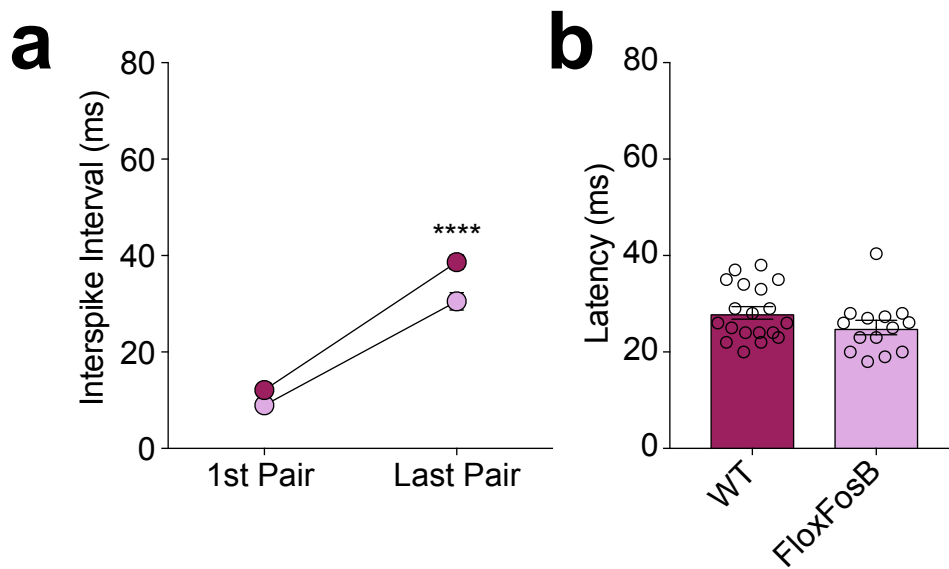


Figure 66 | Spike frequency adaptation is decreased in female FosB KO vHPC-NAc projections.

Interspike interval increases over the course of 500 ms current injection as measured by the time (ms) between the 1st pair of spikes and last pair of spikes. **(a)** Female *FosB* KO (FloxFosB) had less spike frequency adaptation as measured by the interspike interval increase; interspike interval of the last pair of spikes was significantly longer in female WT vHPC-NAc projections than in KO projections. One-way ANOVA: $F(3, 62) = 140.3$; mean difference WT last pair vs. FloxFosB last pair = 8.132, 95% CI = 3.63 to 12.63, **** $p < 0.0001$. **(b)** Latency to 1st spike (ms) from beginning of current injection did not differ between female WT and KO vHPC-NAc projection neurons. Two-tailed t-test: $t(31) = 1.541$, $p = 0.1334$. Interspike intervals and latency to 1st spike were evaluated at the rheobase current for each cell.

electrophysiology studies support stress-induced Δ FosB as a regulator of excitability in this circuit to drive resilience to social withdrawal following CSDS.

To demonstrate the uniqueness of Δ FosB in the vHPC-NAc in the regulation of cellular physiology, we also utilized the same *FosB* KO strategy in the vHPC-BLA circuit by instead injecting retrograde Cre HSV in BLA in *floxed FosB*/L10-GFP (KO) or L10-GFP (WT) mice. Whole-cell patch clamp recordings in *ex vivo* slices of vHPC-BLA projections of male mice showed that *FosB* KO did not cause the same elevated excitability in this circuit as it did in vHPC-NAc projections (Figure 67). *FosB* KO did cause an increase in membrane resistance (Figure 68b), but did not affect any other membrane properties (Figure 68a-e). In female vHPC-BLA neurons, *FosB* KO also did not cause a change in excitability (Figure 69) nor did it affect any membrane properties (Figure 70a-e). Although we did demonstrate the role of Δ FosB in vHPC-BLA projections in the expression of anxiety behaviors, these studies highlight the unique role of Δ FosB in the regulation of cellular excitability in the vHPC-NAc neurons, which may relate its induction in vHPC and NAc to its role in mediating stress responses.

Discussion

The above studies demonstrate that Δ FosB is induced by stress in glutamatergic vHPC-NAc neurons, and that Δ FosB in this circuit is uniquely necessary for resilience to stress. *FosB* and its gene products, including Δ FosB, also appear to have dramatic effects on the excitability of vHPC-NAc projections, with knockout of the *FosB* gene causing an increase in this circuit's responsiveness to current. The mechanism of Δ FosB's effects on cellular excitability still remains to be studied, but with the circuit-specific KO's robust

effect on the interspike interval duration, it is possible that the increase in excitability is achieved through the alteration of ion channels at the cell's membrane. A change in the membrane's passage of current would explain this phenomenon, but would be expected to be accompanied by changes in one or more membrane properties. The only membrane property changed in male vHPC-NAc neurons with *FosB* KO was capacitance, which may relate to a change in the size of cells following KO. *FosB* KO in female vHPC-NAc projections, however, caused an exaggerated increase in cellular excitability when juxtaposed with male projections. This increase in cellular responsiveness to current was indeed accompanied by an increase in membrane input resistance, which may directly explain the differences observed in excitability and spike frequency adaptation. The differences in the magnitude of male and female vHPC-NAc neuron response to *FosB* KO point to possible sex-specific *FosB* regulatory capacities, particularly with regard to the influence of the cell membrane's expression of ion channels. Further investigation regarding Δ FosB's mechanism of modulating cellular excitability in the context of stress will be required, but the current study highlights its importance in the vHPC-NAc circuit in mediating stress resilience, possibly through its effects on cellular excitability.

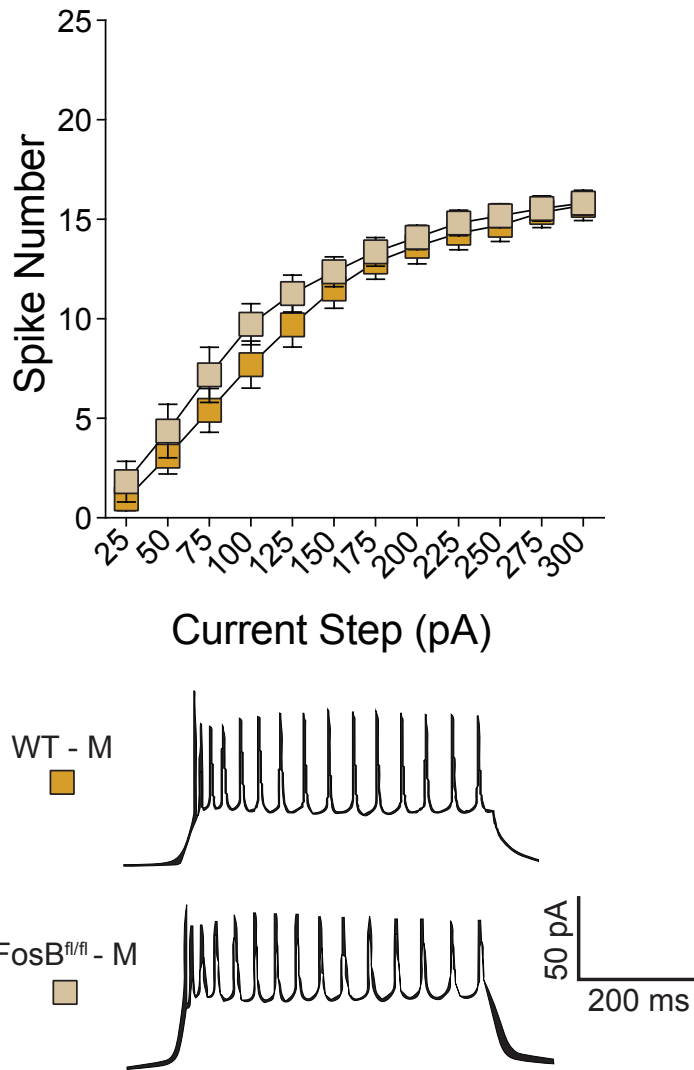


Figure 67 | FosB KO does not affect the cellular excitability of vHPC-BLA neurons in male mice.

(Top) KO of *FosB* does not change the number of spikes in vHPC-BLA neurons across increasing depolarizing current injections. Two-way ANOVA, Holm-Sidak multiple comparisons: [25 pA $t(348) = 0.6193$, $p > 0.9999$], [50 pA $t(348) = 0.9014$, $p = 0.9959$], [75 pA $t(348) = 1.271$, $p = 0.9358$], [100 pA $t(348) = 1.446$, $p = 0.8558$], [125 pA $t(348) = 1.122$, $p = 0.9742$], [150 pA $t(348) = 0.6161$, $p > 0.9999$], [175 pA $t(348) = 0.3664$, $p > 0.9999$], [200 pA $t(348) = 0.3145$, $p > 0.9999$], [225 pA $t(348) = 0.3697$, $p > 0.9999$], [250 pA $t(348) = 0.3437$, $p > 0.9999$], [275 pA $t(348) = 0.1394$, $p > 0.9999$], [300 pA $t(348) = 0.0843$, $p > 0.9999$] ($n = 22$ WT cells from $n = 5$ animals, $n = 12$ KO cells from $n = 4$ animals). (Bottom) Representative voltage traces from 200 pA depolarizing current step vHPC-BLA projections in WT and KO male mice.

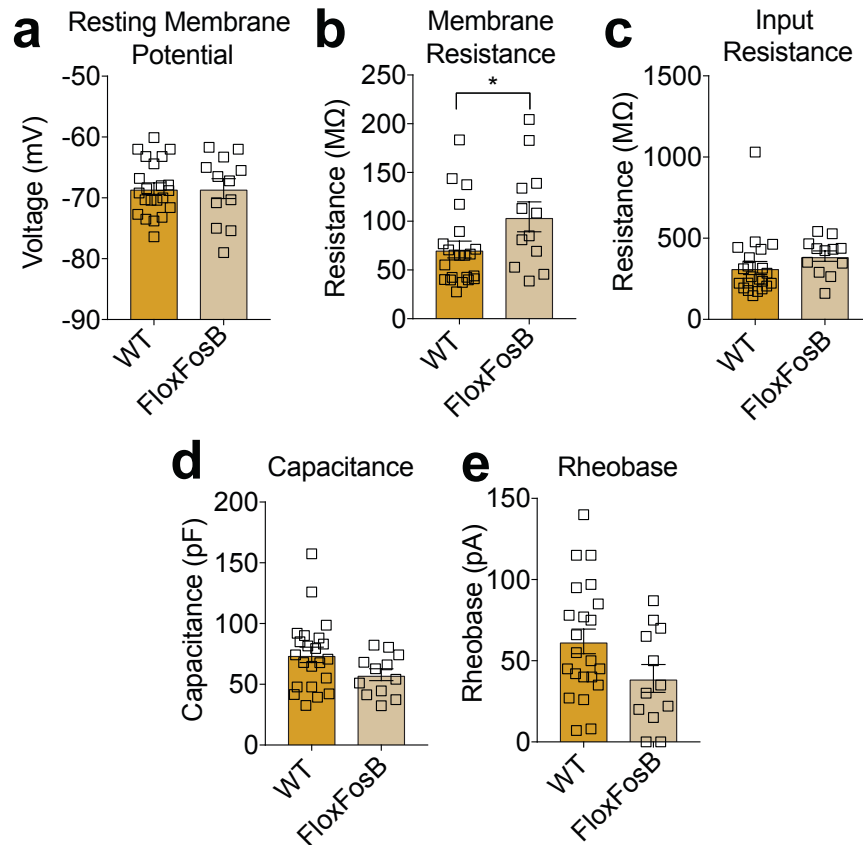


Figure 68 | Membrane properties of male WT vs FosB KO vHPC-BLA projections.

WT and *FosB* KO (FloxFosB) vHPC-BLA projections did not differ in **(a)** Resting membrane potential (mV) [two-tailed t-test: $t(32) = 0.001299$, $p = 0.9990$]. **(b)** KO vHPC-BLA projections had increased membrane resistance (MΩ) [two-tailed t-test: $t(32) = 2.066$, $*p = 0.0470$]. WT and KO vHPC-BLA projections did not differ in any of the following measures: **(c)** input resistance (MΩ) [two-tailed t-test: $t(32) = 1.229$, $p = 0.2282$]; **(d)** membrane capacitance (pF) [two-tailed t-test: $t(32) = 1.763$, $p = 0.0874$]; and **(e)** rheobase (pA) [two-tailed t-test: $t(32) = 1.893$, $p = 0.0674$].

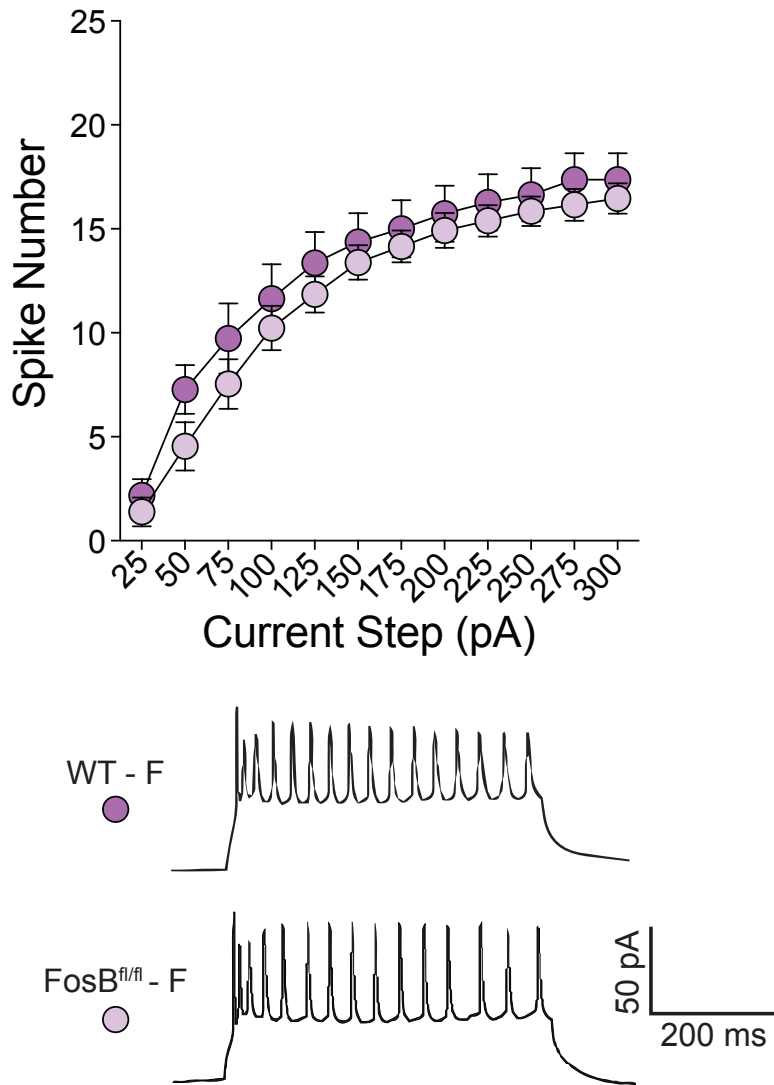


Figure 69 | FosB KO does not affect the cellular excitability of vHPC-BLA neurons in female mice.

(Top) KO of *FosB* does not change the number of spikes in vHPC-BLA neurons across increasing depolarizing current injections. Two-way ANOVA, Holm-Sidak multiple comparisons: [25 pA $t(264) = 0.5072$, $p > 0.9999$], [50 pA $t(264) = 1.739$, $p = 0.6470$], [75 pA $t(264) = 1.392$, $p = 0.8850$], [100 pA $t(348) = 1.446$, $p = 0.8558$], [125 pA $t(348) = 1.122$, $p = 0.9742$], [150 pA $t(348) = 0.6161$, $p > 0.9999$], [175 pA $t(348) = 0.3664$, $p > 0.9999$], [200 pA $t(348) = 0.3145$, $p > 0.9999$], [225 pA $t(348) = 0.3697$, $p > 0.9999$], [250 pA $t(348) = 0.3437$, $p > 0.9999$], [275 pA $t(348) = 0.1394$, $p > 0.9999$], [300 pA $t(348) = 0.0843$, $p > 0.9999$] ($n = 22$ WT cells from $n = 5$ animals, $n = 12$ KO cells from $n = 4$ animals). (Bottom) Representative voltage traces from 200 pA depolarizing current step vHPC-BLA projections in WT and KO male mice.

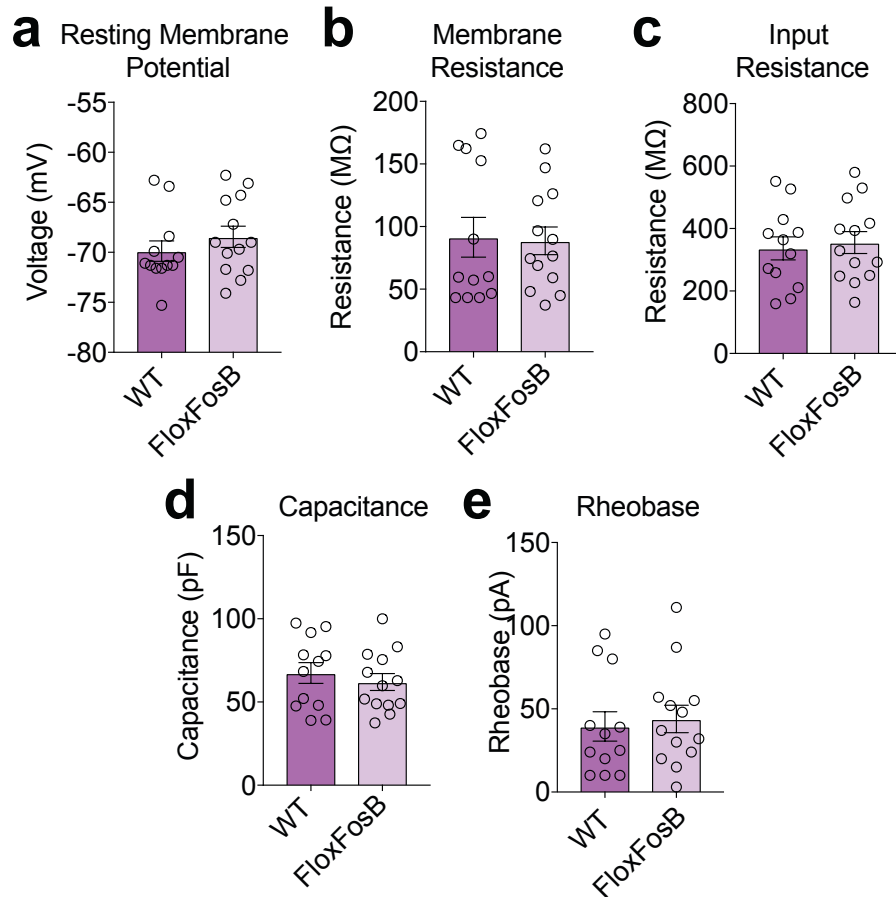


Figure 70 | Membrane properties of female WT vs FosB KO vHPC-BLA projections.

WT and *FosB* KO (FloxFosB) vHPC-BLA projections did not differ in any of the following measures: **(a)** resting membrane potential (mV) [two-tailed t-test: $t(23) = 0.9614$, $p = 0.3463$]; **(b)** membrane resistance (MΩ) [two-tailed t-test: $t(23) = 0.1493$, $p = 0.8826$]; **(c)** input resistance (MΩ) [two-tailed t-test: $t(23) = 0.3648$, $p = 0.7186$]; **(d)** membrane capacitance (pF) [two-tailed t-test: $t(23) = 0.6822$, $p = 0.5019$]; and **(e)** rheobase (pA) [two-tailed t-test: $t(23) = 0.3739$, $p = 0.7119$].

V. SUMMARY, DISCUSSION AND FUTURE DIRECTIONS

Summary

This dissertation investigated the circuit-specific underpinnings of sex differences in stress susceptibility in preclinical models of depression, with focus on the excitatory vHPC-NAc circuit due to its recent discovery as a key mediator of stress outcomes. First, we verified that only female mice were susceptible to SCVS-induced anhedonia as measured by sucrose preference. We next found that vHPC-NAc projections in female mice are more excitable at baseline than those derived from male mice, and that this difference in excitability is possibly due to differential adaptation of male and female cells in response to fluctuating inputs. We discovered that male resilience to SCVS-induced anhedonia as well as the lower excitability in male vHPC-NAc neurons was dependent on the presence of testes-derived hormones, as orchidectomy caused male mice to be susceptible to anhedonia following stress and caused an increase in the excitability of vHPC-NAc projections. This change in physiology was time-dependent, as an extended incubation was necessary to cause the observed change in sucrose preference. In contrast, we found that ovariectomy did not affect the excitability of female vHPC-NAc neurons. The dramatic changes observed in male mice in SCVS-induced anhedonia and vHPC-NAc excitability paired with the absence of these changes in female mice following ovariectomy suggest that androgens in males may confer an active resilience by regulating the physiology of this circuit.

In contrast to the vHPC-NAc circuit, vHPC-BLA neurons were not found to differ in excitability in male and female mice. These projections in male mice did show a slight increase in excitability following orchidectomy, but this change was not as robust as in

the vHPC-NAc circuit. Ovariectomy, like in the vHPC-NAc experiments, did not affect vHPC-BLA physiology. These findings suggest a potential role for androgens in male mice in affecting the global physiology of glutamatergic neurons in the vHPC, but the lack of differences in excitability between male and female vHPC-BLA projections highlights the unique nature of the difference in baseline excitability between male and female vHPC-NAc projections.

We also demonstrated the effectiveness of chronic subcutaneous testosterone administration in ovariectomized female mice in the amelioration of SCVS-induced anhedonia and in the mitigation of vHPC-NAc hyperexcitability. Exogenous testosterone pellets implanted four weeks prior to stress were sufficient to increase sucrose preference in female ovariectomy mice following SCVS. Testosterone pellets also caused a robust decrease in the excitability of vHPC-NAc projections in ovariectomy female mice. These findings support the critical role of androgens in the regulation of vHPC-NAc excitability and consequent resilience to stress-induced anhedonia. To further support this role, we also investigated the effects of the AR antagonist flutamide on the physiology of vHPC-NAc neurons in male mice. Acute flutamide administration caused a small but significant increase in excitability of these projections, as indicated by an increase in the total number of spikes across all current steps, but not an increase in spike number at any individual step. These data, taken together with the above findings, make a strong case for androgens in the regulation of vHPC-NAc physiology to cause the relatively lower excitability in male projections at baseline and confer resilience to stress-induced anhedonia in male mice.

These behavior and electrophysiology experiments paralleled one another to suggest that vHPC-NAc excitability may be responsible for male resilience to anhedonia following SCVS, but they did not establish a causal link. To accomplish this, we employed circuit-specific DREADD expression to artificially change the excitability of vHPC-NAc neurons with the application of the designer drug CNO. When a stimulatory G_q-coupled DREADD was expressed in male vHPC-NAc neurons, we found that long-term, but not short-term, CNO administration induced a substantial decrease in sucrose preference. This decrease was observed in control-handled male mice, with a further decrease in sucrose preference observed in CNO-treated male mice exposed to SCVS. This drastic effect on male susceptibility to anhedonia, even before animals were exposed to stress, demonstrates the key role of vHPC-NAc projections in regulating reward behaviors as well as stress-induced anhedonia. In parallel to the male studies, a G_i-coupled DREADD was expressed in female vHPC-NAc neurons, and the administration of CNO during SCVS and behavioral assessment was found to induce resilience to anhedonia following stress, a departure from previously observed female-only susceptibility to anhedonia in this paradigm. We also demonstrated that CNO administration in the absence of DREADD expression in male mice did not affect SCVS outcomes, which is an important consideration as the use of CNO has come under recent scrutiny³⁴¹ as it is peripherally metabolized to clozapine, which could have unpredictable effects on the circuit or brain as a whole. Overall, our DREADD studies demonstrate a causal link between the excitability of vHPC-NAc neurons in male and female mice and stress-induced changes in behavior, with emphasis on the circuit's control of stress-induced anhedonia.

With the causal link between vHPC-NAc excitability and stress outcomes now established in male and female mice, we then sought to interrogate the circuit-specific mechanisms that may be responsible for regulating projection physiology. To accomplish this, we employed circuit-specific TRAP followed by RNA sequencing to investigate the vHPC-NAc transcriptome in male and female mice. Using the convention of comparing male transcript levels to that of females, we found more downregulated than upregulated genes in the vHPC-NAc circuit in females. This suggests that male mice have more significantly upregulated genes in this circuit; this may represent an additional protective property or properties conferred by active gene expression present in male vHPC-NAc neurons and primes the animal for stress resilience. Hundreds of genes were found to have differential expression in male and female vHPC-NAc neurons, and using pathway analysis, we identified many avenues for future research into the molecular mechanisms of active resilience in male mice that may work to explain the known sex differences in SCVS-induced anhedonia, as well as potential sex differences in other preclinical models of depression and human MDD. The concept of active resilience in males and selected pathways of interest are discussed further below.

Although the sex-specific TRAP sequencing data did not reveal a difference in *FosB* expression between male and female vHPC-NAc neurons, stress and antidepressant induction of Δ FosB in hippocampus²⁷² and its role as a resilience factor in other brain regions^{158,342} drove us to investigate *FosB* gene products in this circuit. Specifically, we evaluated Δ FosB as a potential regulator of vHPC-NAc physiology such that it could contribute to active resilience by attenuating the excitability of these projections. First, we showed that CSDS as well as the antidepressant fluoxetine induce

Δ FosB globally in the ventral hippocampus, verifying its potential as a regulator of cell physiology in this region. We further investigated Δ FosB induction in a circuit-specific fashion, and showed that it is indeed induced by CSDS in vHPC-NAc projections as indicated by co-labeling of L10-GFP and FosB in immunohistochemistry experiments. This discovery, along with the aforementioned reduction in dHPC cellular excitability with overexpression of Δ FosB, made this molecule an excellent candidate for the regulation of projection physiology and the consequential change in stress outcomes.

To evaluate Δ FosB's role in stress resilience, we began by globally overexpressing Δ JunD, an inhibitor of Δ FosB function, in the vHPC or dHPC of male mice. We then assessed behavioral phenotype following subchronic social stress and found that silencing Δ FosB's activity in ventral, but not dorsal, HPC was sufficient to induce susceptibility as indicated by a decreased SI ratio. Next, we investigated Δ FosB's circuit-specific role in stress, and found that knocking out *FosB* expression in vHPC-NAc neurons in male mice using our novel dual-viral CRISPR strategy also caused a reduction in SI ratio following CSDS. We also demonstrated that *FosB* KO in vHPC-BLA neurons was anxiolytic, suggesting that expression of *FosB* gene products may play a role in anxiogenesis, though it had no effect on social interaction score after stress. These experiments identified circuit-specific roles for Δ FosB in regulating stress outcomes, emphasizing that vHPC-NAc Δ FosB function is necessary for resilience to social stress.

Next, we investigated Δ FosB's capacity for regulation of vHPC pyramidal cell excitability. We virally overexpressed Δ FosB in vHPC and found a dramatic decrease in the number of spikes elicited at each increasing current step, and a trend towards an increase in rheobase, indicating that Δ FosB can mediate an overall reduction in cellular

excitability. We then studied the circuit-specific role of *FosB* expression in regulating cellular excitability using a circuit-specific KO strategy in male and female mice. We found that *FosB* KO in both male and female vHPC-NAc neurons did indeed increase cellular excitability compared to control projections. *FosB* KO in both male and female vHPC-NAc projections also caused a decrease in spike frequency adaptation, suggesting that *FosB* gene products, including Δ FosB, may regulate cellular excitability via homeostatic regulation of intrinsic excitability in response to sustained activity of inputs. We also demonstrated that *FosB* KO does not significantly alter cellular physiology in vHPC-BLA projections in male or female mice, emphasizing the specificity of Δ FosB's attenuation of cellular excitability in the vHPC-NAc projections.

Discussion and Future Directions

Resilience as an active process

As mentioned above, the idea of resilience as an active process, particularly in male mice, has gained recent attention due to a variety of studies that show converging evidence to that effect. From a broad perspective, active approaches in humans have been utilized in psychology and psychiatry to promote resilience to stress. These include active coping mechanisms such as cognitive reappraisal (i.e. reframing of adverse events in a positive light) and coping self-efficacy (e.g. mastering the skills necessary to manage a given stressor in increasingly challenging scenarios), as well as basic active approaches such as improving diet, exercise, and sleep³⁴³. Active coping mechanism equivalents have also been observed in rodent stress models of depression; for example, during social defeat stress, mice that display less submissive posturing during aggressive

attacks exhibit less social avoidance later in the social interaction test³⁴⁴. On a deeper level, neurobiological mechanisms of active resilience have also been described. Resilience to social stress has been associated with active genetic and epigenetic changes in distinct brain regions that are not observed in susceptible animals^{34,154}. These changes are discussed below, with implications for the findings presented in this dissertation.

As mentioned previously, c-Fos and *FosB* gene products, including Δ FosB, are induced by chronic stress in various brain regions. One of these regions is the mPFC, where resilient mice show an increase in the expression of these immediate early genes^{345,346}, suggesting that the increase in neuronal activity in this region is an active adaptation that promotes resilience. This was confirmed by optogenetic work demonstrating that non-cell type-specific stimulation of mPFC neurons promotes resilience³⁴⁷. Later studies determined that glutamatergic projections of the mPFC are responsible: specific optogenetic stimulation of glutamatergic neurons is pro-resilient¹⁷¹. Δ FosB is also preferentially induced in the NAc of resilient animals, where it is thought to promote resilience through induction of GluA2 and causing subsequent decrease in AMPAR Ca^{2+} conductivity¹⁵⁸. Our studies demonstrated that Δ FosB is also induced in vHPC-NAc projections, and that *FosB* expression in this circuit is necessary for resilience to social stress. Therefore, the induction of vHPC-NAc Δ FosB, like its induction in the mPFC and NAc, may represent an active mechanism of resilience. In future studies, the experiments conducted in this dissertation regarding *FosB* and its gene products in vHPC-NAc circuit will need to be repeated in female mice. Indeed, the increase in excitability that we observed in vHPC-NAc projections of male mice was also observed in

vHPC-NAc neurons of female mice when *FosB* was knocked out. More experiments will need to be performed to determine the effects of this change in projection physiology on stress outcomes in female mice, possibly using social stress models that facilitate the incorporation of female subjects.

One preclinical stress model that could be utilized to assess social stress outcomes in female mice in the presence of vHPC-NAc *FosB* KO is the vicarious social defeat model³⁴⁸. This model could also be used to directly compare the effects of social stress, rather than SCVS, on the vHPC-NAc circuit and to determine whether gonadal hormone manipulation modulates social stress outcomes in the same manner as we observed in SCVS. The vicarious social defeat stress model utilizes adult male or female C57/Bl6 mice that vicariously experience the social defeat of a male conspecific by a CD1 aggressor. This “emotional” or “psychological” stress is achieved by keeping the experimental mouse on the opposite side of a perforated divider during the attack sessions. The witnessing of aggression is repeated for 10 consecutive days with the experimental mouse housed on the other side of a perforated divider from a different aggressor overnight following each stress session. The witness or vicarious nature of this paradigm avoids the difficulty of achieving aggressive behavior towards experimental female mice, and allows for the use of both sexes in experimental design. Females that experience vicarious social defeat experience many of the depression-like measures of face validity seen with traditional CSDS in male mice: decreased social interaction in the SI test, anhedonia as measured by sucrose preference, increased immobility in TST, and increased serum corticosterone levels. This model also exhibits predictive validity: the susceptible phenotype in females exposed to vicarious defeat stress is mitigated by the

newly-minted antidepressant ketamine. Unlike CSDS, however, susceptibility in the vicarious defeat model is ameliorated by the benzodiazepine chlordiazepoxide, suggesting that an anxiety component may be involved.

As social interaction engages reward circuitry and is a positively-valenced rewarding stimulus³⁴⁹, much like consumption of the sucrose solution in the assessment of hedonic behavior, the use of vicarious defeat stress may indeed induce Δ FosB in vHPC-NAc neurons. Indeed, studies of emotional stress in male mice have shown Δ FosB induction in the HPC³⁵⁰, indicating that this type of stress may have similar effects to CSDS on this region. Future studies could investigate whether this is the case for female mice, and could dissect specific HPC projections, such as vHPC-NAc, in the context of the active resilience mechanism of Δ FosB induction. I predict that *FosB* KO in this circuit would induce susceptibility in both male and female mice in the vicarious defeat paradigm, and that this susceptibility would be dependent upon an increase in vHPC-NAc excitability due to attenuated Δ FosB expression. The vicarious defeat model could also prove valuable in the assessment of social stress in the presence of hormone manipulation. In this scenario, I would predict that testosterone manipulations (removal or replacement) would change stress outcomes. Testosterone may provide an active protection against the effects of emotional stress in the vicarious defeat model, much like it did in our SCVS experiments presented in Chapter III, through attenuation of vHPC-NAc hyperexcitability.

Gene expression changes in stress

Adaptation of the activity and connectivity of brain regions like HPC and NAc in response to stress require corresponding changes in gene expression and epigenetics²⁷⁹.

Seminal experiments investigating gene transcription differences in resilient and susceptible male mouse populations following CSDS have demonstrated that gene regulation may be a mechanism of active resilience. For example, in the NAc, Krishnan et al found that although many of the same genes were upregulated in resilient and susceptible populations, the resilient group had a significantly higher number of genes upregulated that did not overlap with those upregulated in the susceptible group³⁴. The same was true of differentially regulated genes in the VTA: the resilient group had a higher number of upregulated genes than the susceptible group. In both regions, there was also a higher number of downregulated genes in the resilient group than in the susceptible group, indicating that downregulation of certain genes may also represent an active mechanism of resilience. Interestingly, this group found several upregulated K⁺ channels in the VTA of resilient mice, and demonstrated that overexpression of these channels in the VTA of susceptible mice reduced neuronal excitability and reversed the susceptible phenotype in these animals.

In RNAseq studies, Hodes et al also described different transcriptional profiles in the NAc of male and female mice following SCVS. This group found that 17% more genes were differentially regulated by stress in male mice than in female mice, with 40% of these being upregulated and 60% downregulated. In contrast, in female mice, 60% of the differentially regulated genes in the NAc were upregulated and 40% downregulated, with only 3% overlap of differentially regulated genes between the sexes, only 0.5% oppositely regulated between the sexes, and only a single gene upregulated in both sexes. These findings demonstrate that different molecular mechanisms mediate the behavioral phenotypes of male and female mice following SCVS, and, since males are not

susceptible to this stress modality, may point to genetic mechanisms of active resilience in males. This group also described an epigenetic change that is altered in NAc by SCVS in mice as well as in MDD in humans – the upregulation of DNA methyltransferase 3a (Dnmt3a) in both male and female mice. Female mice had higher levels of Dnmt3a, which can lead to transcriptional silencing of genes by adding a sterically hindering methyl group to transcription factor binding sites on DNA, and has been linked to social stress susceptibility³⁵¹. The group also showed that KO of Dnmt3a in NAc in females shifted their gene regulation patterns to closer resemble that of males, indicating that differential epigenetic control of gene expression may also explain sex differences in stress susceptibility. In our interrogation of actively translated genes in vHPC-NAc projections of male and female mice, we found that Dnmt3a was significantly downregulated in these cells in females compared to males. While this may not correspond to the increase that Hodes et al showed within the NAc in female mice, epigenetic influences may cause the differential excitability that we observed between male and female vHPC-NAc projections. For instance, we found other epigenetic regulators, such as histone deacetylases 2 and 5 (Hdac2 and Hdac5), were upregulated in female vHPC-NAc projections compared to males. Histone deacetylases remove positively charged acetyl groups from histones, decreasing their DNA binding and opening up chromatin for facilitation of gene transcription. Indeed, Covington et al demonstrated increased NAc histone acetylation following CSDS, suggesting that epigenetic-mediated silencing of gene transcription may offer beneficial neuronal adaptations following stress¹⁵⁵. This was confirmed by their demonstration of the antidepressant effects of histone deacetylase inhibition. Future studies could focus on epigenetic changes in vHPC-NAc neurons of male and female

mice, as there are clearly differences in the transcription of epigenetic regulators in these projections between the sexes as shown in our RNAseq findings following TRAP. An additional experiment that will be crucial to answering questions about sex differences in gene regulation in the context of stress outcomes will be to perform vHPC-NAc TRAP on stressed male and female mice. This experiment may help to reveal those genes up- or downregulated in male vHPC-NAc neurons that confer resilience to this stress paradigm. Circuit-specific TRAP experiments could also be performed in the presence of gonadectomy to investigate whether gonadal steroid hormones affect the transcriptional profiles of vHPC-NAc neurons in male and female mice.

Intrinsic excitability and plasticity

Intrinsic plasticity encompasses the ability of a neuron's electrical properties and excitability to change with persistent autonomous or synaptic activity. It is defined by the malleability of ion channels, in terms of their expression levels or changes in their physical properties. Intrinsic plasticity is thought to affect many processes, including integration of synaptic inputs and action potential generation. The function of intrinsic plasticity, unlike its more widely studied counterpart, synaptic plasticity, is ill-defined; however, it is thought to be involved in many processes linked to the hippocampus, including learning^{352,353}, memory³⁵⁴, and homeostatic regulation of neuronal excitability^{355,356}.

The integration of synaptic input within a neuron to generate an action potential is dependent upon the number and makeup of the neuron's ion channels. Voltage- and calcium-gated channels in dendrites accomplish this synaptic integration, while channels of the cell body participate in action potential generation. *In vitro* studies have

demonstrated that the electrical features conferred upon a neuron by ion channels, i.e. a neuron's *intrinsic excitability*, are plastic and are subject to modification by various internal and external factors³⁵⁷. Three major mechanisms of intrinsic plasticity have been described: long term plasticity of intrinsic excitability (LTP-IE)³⁵⁸, homeostatic plasticity of intrinsic excitability³⁵⁹, and plasticity of dendritic synaptic input integration³⁶⁰.

Bliss and Lomo, in their seminal work describing the phenomenon of synaptic long-term potentiation (LTP), also recognized that the postsynaptic neuron itself was more likely to fire, or more *excitable*, following the exposure to excitatory postsynaptic potentials (EPSPs) generated by the LTP protocol⁹⁵. This occurrence, known as E-S potentiation, was further described in pyramidal cells following the induction of LTP³⁵⁶. Specifically, pyramidal cells of the CA1 region of the hippocampus have an increased number of action potentials in response to injected current, as well as a decreased AP threshold, following LTP induction. Chavez-Noriega et al postulated that in the CA1, this phenomenon could be the result of an increase in the excitation to inhibition ratio at a given neuron, possibly through a reduction in inhibition via GABA_A signaling. The induction of LTP, however, is not strictly necessary to achieve LTP-IE, as the phenomenon has been observed following injection of repeated depolarizing current without the presence of synaptic stimulation in neurons of the visual cortex³⁶¹ and cerebellum³⁶². Other mechanisms are also possible to achieve LTP-IE, for example, the activation of metabotropic glutamate receptors (mGluRs) in the hippocampus causes a long-term increase in the excitability of CA1 pyramidal neurons by way of the suppression of afterhyperpolarization potentials (AHPs)³⁶³.

Homeostatic plasticity of intrinsic excitability, in contrast to LTP-IE, represents a reactivity of neurons to a change in the activity of inputs that tends to stabilize excitability to a given baseline level. This concept is critical, as neurons usually must function for a long period of an animal's life and must be able to adapt to changes in input as a result of processes critical to the animal's survival and propagation (e.g. learning and development). The homeostasis achieved allows the neuron to maintain functionality, either decreasing excitability in the face of increased input or vice versa. O'Leary et al. demonstrated a shift in cultured hippocampal pyramidal neurons towards decreased excitability after being exposed for days to elevated KCl concentrations, as evidenced by heightened rheobase and a rightward shift in the frequency-current input relationship without a change in AP threshold voltage³⁶⁴. Complementarily, Desai et al showed that cultured cortical pyramidal neurons, when deprived of activity for days, were more sensitive to current injection with a leftward shift in the frequency-current relationship³⁶⁵. In both cases, the homeostatic plasticity of intrinsic excitability was dependent upon functionality of ion channels; regulating voltage-gated ion channel conductances allowed the neurons to maintain a homeostatic, baseline excitability. Although neither the membrane nor input resistance of vHPC-NAc neurons differed between male and female mice in a direction that would explain the change in passage of current such that excitability would change, the voltage threshold of female vHPC-NAc projections was more negative than that of male projections. It is possible that channels responsible for resting membrane properties are unaltered in female vHPC-NAc neurons, but those that are opened in response to activity, such as voltage-gated Na⁺ channels, may explain the hyperexcitability of female projections. Indeed, many voltage-gated channels were

differentially regulated between male and female vHPC-NAc projections, but the directionality of regulation is variable across these channels. Validation of differentially regulated genes will need to be conducted in order to tease out mechanisms by which the voltage threshold of female projections differs. Quantitative PCR (qPCR) is one method of validation that could be used to investigate these channels, and indeed additional TRAP samples for male and female vHPC-NAc neurons have been generated for this purpose. It is possible that differentially regulated ion channels act in concert to cause a less negative voltage threshold in male vHPC-NAc projections, conferring an active mechanism of resilience in males through regulation of excitability.

Dendritic integration of synaptic inputs also exhibits plasticity. This concept represents focused changes in synaptic integration, as opposed to widespread changes in intrinsic excitability of the neuron that leads to differential AP generation. Plasticity of dendritic integration has been observed in hippocampal CA1 pyramidal neurons, where the linearity of summation of EPSPs following LTP induction at a given dendrite was increased based on proximity to the cell body³⁶⁶. In other words, the closer the dendrite was to the cell body, the longer it exhibited increased excitability when detecting the coincidence of inputs, resulting in a summed EPSP with an amplitude closer to what it would be if the expected individual EPSPs were added. This is thought to be due to changes in A-type potassium conductance^{367,368}. This phenomenon may be due to the effect of AP backpropagation from the cell body and axon hillock, where APs are initiated, to dendrites. Backpropagation causes an increase in calcium influx locally in dendrites, which was shown to facilitate spikes in the apical dendrites of CA1 pyramidal neurons in a CaMKII-dependent fashion³⁶⁹. As previously discussed, CA1 pyramidal cell dendritic

spine density varies over the estrous cycle in female rodents¹³⁹, a process that is estradiol- and NMDAR-dependent¹⁴⁰. Future experiments will need to assess female vHPC-NAc excitability over the estrous cycle. If there are differences in the physiology of these projections in proestrus and diestrus phases, it may indicate that dendritic spine density is fluctuating, affecting the intrinsic excitability of these cells. Overall, the above mechanisms of intrinsic excitability and the plasticity thereof may prove to be critical in mediating the observed differences between male and female stress outcomes, as the activity of circuits such as vHPC-NAc in these mice may be key in mediating stress susceptibility.

Final Summary

As described throughout this dissertation, ventral hippocampal circuits are key regulators of the integration of emotion and behavior. Particularly important is the promise that these circuits hold for future treatments of emotion-related pathologies such as depression and anxiety. To achieve this, we must elucidate regulatory mechanisms of these circuits, especially those mechanisms that differ between men and women. However, the mechanisms for differences in circuit physiology cannot yet be fully investigated in humans due to the invasiveness of existing methods; this underscores the need for studies utilizing preclinical models and circuit-specific strategies for uncovering molecular and physiological mechanisms that could lead to potential treatments. The experiments and findings described in this dissertation begin to address the nature of circuit physiology in the context of stress and depression in male and female mice, and may open the doors for the investigation of many new avenues for treatment.

REFERENCES

REFERENCES

- 1 Ramon y Cajal, S. Textura del sistema nervioso del hombre y de los vertebrados: estudios sobre el plan estructural y composición histológica de los centros nerviosos adicionados de consideraciones fisiológicas fundadas en los nuevos descubrimientos. *Moya* (1899).
- 2 Bagot, R. C. *et al.* Ventral hippocampal afferents to the nucleus accumbens regulate susceptibility to depression. *Nat Commun* **6**, 7062, doi:10.1038/ncomms8062 (2015).
- 3 Vakili, K. *et al.* Hippocampal volume in primary unipolar major depression: a magnetic resonance imaging study. *Biol Psychiatry* **47**, 1087-1090 (2000).
- 4 Milne, A. M., MacQueen, G. M. & Hall, G. B. Abnormal hippocampal activation in patients with extensive history of major depression: an fMRI study. *J Psychiatry Neurosci* **37**, 28-36, doi:10.1503/jpn.110004 (2012).
- 5 *World Health Organisation (WHO). Depression and Other Common Mental Disorders: Global Health Estimates.*, <<https://apps.who.int/iris/bitstream/handle/10665/254610/WHO-MSD-MER-2017.2eng.pdf;jsessionid=B1C1FAF375042E9F2A72C24735E6333A?sequence=1>> (2017).
- 6 Kessler, R. C. Epidemiology of women and depression. *J Affect Disord* **74**, 5-13 (2003).
- 7 *Diagnostic and Statistical Manual of Mental Disorders, 5th Edition: DSM-V.* (American Psychiatric Association, 2013).
- 8 Bromet, E. *et al.* Cross-national epidemiology of DSM-IV major depressive episode. *Bmc Med* **9**, 90, doi:10.1186/1741-7015-9-90 (2011).
- 9 Wang, P. S. *et al.* Use of mental health services for anxiety, mood, and substance disorders in 17 countries in the WHO world mental health surveys. *Lancet* **370**, 841-850, doi:Doi 10.1016/S0140-6736(07)61414-7 (2007).
- 10 Global Burden of Disease Study, C. Global, regional, and national incidence, prevalence, and years lived with disability for 301 acute and chronic diseases and injuries in 188 countries, 1990-2013: a systematic analysis for the Global Burden of Disease Study 2013. *Lancet* **386**, 743-800, doi:10.1016/S0140-6736(15)60692-4 (2015).
- 11 Greenberg, P. E., Fournier, A. A., Sisitsky, T., Pike, C. T. & Kessler, R. C. The economic burden of adults with major depressive disorder in the United States (2005 and 2010). *J Clin Psychiatry* **76**, 155-162, doi:10.4088/JCP.14m09298 (2015).

- 12 Penninx, B. W., Milaneschi, Y., Lamers, F. & Vogelzangs, N. Understanding the somatic consequences of depression: biological mechanisms and the role of depression symptom profile. *Bmc Med* **11**, 129, doi:10.1186/1741-7015-11-129 (2013).
- 13 Otte, C. *et al.* Major depressive disorder. *Nat Rev Dis Primers* **2**, 16065, doi:10.1038/nrdp.2016.65 (2016).
- 14 Seedat, S. *et al.* Cross-National Associations Between Gender and Mental Disorders in the World Health Organization World Mental Health Surveys. *Arch Gen Psychiat* **66**, 785-795, doi:DOI 10.1001/archgenpsychiatry.2009.36 (2009).
- 15 Eaton, W. W. *et al.* Natural history of diagnostic interview schedule DSM-IV major depression - The Baltimore Epidemiologic Catchment Area Follow-up. *Arch Gen Psychiat* **54**, 993-999 (1997).
- 16 Douglas, J. & Scott, J. A systematic review of gender-specific rates of unipolar and bipolar disorders in community studies of pre-pubertal children. *Bipolar Disord* **16**, 5-15, doi:10.1111/bdi.12155 (2014).
- 17 Avenevoli, S., Swendsen, J., He, J. P., Burstein, M. & Merikangas, K. R. Major depression in the national comorbidity survey-adolescent supplement: prevalence, correlates, and treatment. *J Am Acad Child Adolesc Psychiatry* **54**, 37-44 e32, doi:10.1016/j.jaac.2014.10.010 (2015).
- 18 Marcus, S. M. *et al.* Sex differences in depression symptoms in treatment-seeking adults: confirmatory analyses from the Sequenced Treatment Alternatives to Relieve Depression study. *Compr Psychiatry* **49**, 238-246, doi:10.1016/j.comppsy.2007.06.012 (2008).
- 19 Takayanagi, Y. *et al.* Accuracy of reports of lifetime mental and physical disorders: results from the Baltimore Epidemiological Catchment Area study. *JAMA Psychiatry* **71**, 273-280, doi:10.1001/jamapsychiatry.2013.3579 (2014).
- 20 Kendler, K. S. & Myers, J. The boundaries of the internalizing and externalizing genetic spectra in men and women. *Psychol Med* **44**, 647-655, doi:10.1017/S0033291713000585 (2014).
- 21 Kuehner, K. Why is depression more common among women than among men? *Lancet Psychiatry* **4**, 146-158 (2017).
- 22 Sullivan, P. F., Neale, M. C. & Kendler, K. S. Genetic epidemiology of major depression: review and meta-analysis. *Am J Psychiatry* **157**, 1552-1562, doi:10.1176/appi.ajp.157.10.1552 (2000).
- 23 Flint, J. & Kendler, K. S. The genetics of major depression. *Neuron* **81**, 484-503 (2014).

- 24 Martel, M. M. Sexual selection and sex differences in the prevalence of childhood externalizing and adolescent internalizing disorders. *Psychol Bull* **139**, 1221-1259, doi:10.1037/a0032247 (2013).
- 25 Kajantie, E. & Phillips, D. I. The effects of sex and hormonal status on the physiological response to acute psychosocial stress. *Psychoneuroendocrinology* **31**, 151-178, doi:10.1016/j.psyneuen.2005.07.002 (2006).
- 26 Het, S., Schoofs, D., Rohleder, N. & Wolf, O. T. Stress-induced cortisol level elevations are associated with reduced negative affect after stress: indications for a mood-buffering cortisol effect. *Psychosom Med* **74**, 23-32, doi:10.1097/PSY.0b013e31823a4a25 (2012).
- 27 Garcia-Moreno, C. *et al.* Addressing violence against women: a call to action. *Lancet* **385**, 1685-1695, doi:10.1016/S0140-6736(14)61830-4 (2015).
- 28 Stoltenborgh, M., Bakersmans-Kranenburg, M. J., Alink, L. R. & Ijzendoorn, M. H. The prevalence of child maltreatment across the globe: review of a series of meta-analyses. *Child Abuse Rev* **24**, 37-50 (2015).
- 29 Platt, J., Prins, S., Bates, L. & Keyes, K. Unequal depression for equal work? How the wage gap explains gendered disparities in mood disorders. *Soc Sci Med* **149**, 1-8 (2016).
- 30 Willner, P. The validity of animal models of depression. *Psychopharmacology (Berl)* **83**, 1-16 (1984).
- 31 Muller, M. B. *et al.* Limbic corticotropin-releasing hormone receptor 1 mediates anxiety-related behavior and hormonal adaptation to stress. *Nat Neurosci* **6**, 1100-1107, doi:10.1038/nn1123 (2003).
- 32 Tye, K. M. & Deisseroth, K. Optogenetic investigation of neural circuits underlying brain disease in animal models. *Nat Rev Neurosci* **13**, 251-266, doi:10.1038/nrn3171 (2012).
- 33 McEwen, B. S. Central effects of stress hormones in health and disease: Understanding the protective and damaging effects of stress and stress mediators. *Eur J Pharmacol* **583**, 174-185, doi:10.1016/j.ejphar.2007.11.071 (2008).
- 34 Krishnan, V. *et al.* Molecular Adaptations Underlying Susceptibility and Resistance to Social Defeat in Brain Reward Regions. *Cell* **131**, 391-404, doi:10.1016/j.cell.2007.09.018 (2007).
- 35 Brown, G. W. in *Life events and illness*. (eds S. Stanford & D.C. Blanchard) 20-40 (Academic Press, 1993).

- 36 Martinez, M., Calvo-Torrent, A. & Pico-Alfonso, M. A. Social defeat and subordination as models of social stress in laboratory rodents: A review. *Aggressive Behavior* **24**, 241-256 (1998).
- 37 Willner, P., Muscat, R. & Papp, M. Chronic mild stress-induced anhedonia: a realistic animal model of depression. *Neurosci Biobehav Rev* **16**, 525-534 (1992).
- 38 Berton, O. *et al.* Essential role of BDNF in the mesolimbic dopamine pathway in social defeat stress. *Science* **311**, 864-868, doi:10.1126/science.1120972 (2006).
- 39 Tsankova, N. M. *et al.* Sustained hippocampal chromatin regulation in a mouse model of depression and antidepressant action. *Nat Neurosci* **9**, 519-525, doi:10.1038/nn1659 (2006).
- 40 Beery, A. K. & Zucker, I. Sex bias in neuroscience and biomedical research. *Neurosci Biobehav Rev* **35**, 565-572, doi:10.1016/j.neubiorev.2010.07.002 (2011).
- 41 Hodes, G. E. *et al.* Sex Differences in Nucleus Accumbens Transcriptome Profiles Associated with Susceptibility versus Resilience to Subchronic Variable Stress. *J Neurosci* **35**, 16362-16376, doi:10.1523/JNEUROSCI.1392-15.2015 (2015).
- 42 Herman, J. P., Ostrander, M. M., Mueller, N. K. & Figueiredo, H. Limbic system mechanisms of stress regulation: hypothalamo-pituitary-adrenocortical axis. *Prog Neuropsychopharmacol Biol Psychiatry* **29**, 1201-1213, doi:10.1016/j.pnpbp.2005.08.006 (2005).
- 43 Owens, M. J. & Nemeroff, C. B. Physiology and pharmacology of corticotropin-releasing factor. *Pharmacol Rev* **43**, 425-473 (1991).
- 44 Walker, D. L., Toufexis, D. J. & Davis, M. Role of the bed nucleus of the stria terminalis versus the amygdala in fear, stress, and anxiety. *Eur J Pharmacol* **463**, 199-216 (2003).
- 45 Nemeroff, C. B. *et al.* Elevated concentrations of CSF corticotropin-releasing factor-like immunoreactivity in depressed patients. *Science* **226**, 1342-1344 (1984).
- 46 De Bellis, M. D., Gold, P. W., Geraciotti, T. D., Jr., Listwak, S. J. & Kling, M. A. Association of fluoxetine treatment with reductions in CSF concentrations of corticotropin-releasing hormone and arginine vasopressin in patients with major depression. *Am J Psychiatry* **150**, 656-657, doi:10.1176/ajp.150.4.656 (1993).
- 47 Heuser, I. *et al.* Cerebrospinal fluid concentrations of corticotropin-releasing hormone, vasopressin, and somatostatin in depressed patients and healthy controls: response to amitriptyline treatment. *Depress Anxiety* **8**, 71-79 (1998).

- 48 Wang, S. S., Kamphuis, W., Huitinga, I., Zhou, J. N. & Swaab, D. F. Gene expression analysis in the human hypothalamus in depression by laser microdissection and real-time PCR: the presence of multiple receptor imbalances. *Mol Psychiatry* **13**, 786-799, 741, doi:10.1038/mp.2008.38 (2008).
- 49 Merali, Z. *et al.* Dysregulation in the suicide brain: mRNA expression of corticotropin-releasing hormone receptors and GABA(A) receptor subunits in frontal cortical brain region. *J Neurosci* **24**, 1478-1485, doi:10.1523/JNEUROSCI.4734-03.2004 (2004).
- 50 Kitay, J. I. Sex differences in adrenal cortical secretion in the rat. *Endocrinology* **68**, 818-824, doi:10.1210/endo-68-5-818 (1961).
- 51 Heinsbroek, R. P., Van Haaren, F., Feenstra, M. G., Endert, E. & Van de Poll, N. E. Sex- and time-dependent changes in neurochemical and hormonal variables induced by predictable and unpredictable footshock. *Physiol Behav* **49**, 1251-1256 (1991).
- 52 Seale, J. V., Wood, S. A., Atkinson, H. C., Harbuz, M. S. & Lightman, S. L. Gonadal steroid replacement reverses gonadectomy-induced changes in the corticosterone pulse profile and stress-induced hypothalamic-pituitary-adrenal axis activity of male and female rats. *J Neuroendocrinol* **16**, 989-998, doi:10.1111/j.1365-2826.2004.01258.x (2004).
- 53 Desbonnet, L., Garrett, L., Daly, E., McDermott, K. W. & Dinan, T. G. Sexually dimorphic effects of maternal separation stress on corticotrophin-releasing factor and vasopressin systems in the adult rat brain. *Int J Dev Neurosci* **26**, 259-268, doi:10.1016/j.ijdevneu.2008.02.004 (2008).
- 54 Iwasaki-Sekino, A., Mano-Otagiri, A., Ohata, H., Yamauchi, N. & Shibasaki, T. Gender differences in corticotropin and corticosterone secretion and corticotropin-releasing factor mRNA expression in the paraventricular nucleus of the hypothalamus and the central nucleus of the amygdala in response to footshock stress or psychological stress in rats. *Psychoneuroendocrinology* **34**, 226-237, doi:10.1016/j.psyneuen.2008.09.003 (2009).
- 55 Sterrenburg, L. *et al.* Chronic stress induces sex-specific alterations in methylation and expression of corticotropin-releasing factor gene in the rat. *PLoS One* **6**, e28128, doi:10.1371/journal.pone.0028128 (2011).
- 56 McAlinn, H. R. *et al.* Sex Differences in the Subcellular Distribution of Corticotropin-Releasing Factor Receptor 1 in the Rat Hippocampus following Chronic Immobilization Stress. *Neuroscience* **383**, 98-113, doi:10.1016/j.neuroscience.2018.05.007 (2018).
- 57 Bangasser, D. A. & Valentino, R. J. Sex differences in molecular and cellular substrates of stress. *Cell Mol Neurobiol* **32**, 709-723, doi:10.1007/s10571-012-9824-4 (2012).

- 58 Hendler, T. *et al.* Sensing the invisible: differential sensitivity of visual cortex and amygdala to traumatic context. *Neuroimage* **19**, 587-600 (2003).
- 59 Lieberman, M. D., Straccia, M. A., Meyer, M. L., Du, M. & Tan, K. M. Social, self, (situational), and affective processes in medial prefrontal cortex (MPFC): Causal, multivariate, and reverse inference evidence. *Neurosci Biobehav Rev* **99**, 311-328, doi:10.1016/j.neubiorev.2018.12.021 (2019).
- 60 Maren, S. & Quirk, G. J. Neuronal signalling of fear memory. *Nat Rev Neurosci* **5**, 844-852, doi:10.1038/nrn1535 (2004).
- 61 Drevets, W. C. Neuroimaging abnormalities in the amygdala in mood disorders. *Ann N Y Acad Sci* **985**, 420-444 (2003).
- 62 Pizzagalli, D. A. *et al.* Functional but not structural subgenual prefrontal cortex abnormalities in melancholia. *Molecular Psychiatry* **9**, 393-405 (2004).
- 63 Radley, J. J. *et al.* Chronic behavioral stress induces apical dendritic reorganization in pyramidal neurons of the medial prefrontal cortex. *Neuroscience* **125**, 1-6, doi:10.1016/j.neuroscience.2004.01.006 (2004).
- 64 Rosenkranz, J. A., Venheim, E. R. & Padival, M. Chronic stress causes amygdala hyperexcitability in rodents. *Biol Psychiatry* **67**, 1128-1136, doi:10.1016/j.biopsych.2010.02.008 (2010).
- 65 Vyas, A., Mitra, R., Shankaranarayana Rao, B. S. & Chattarji, S. Chronic stress induces contrasting patterns of dendritic remodeling in hippocampal and amygdaloid neurons. *J Neurosci* **22**, 6810-6818, doi:20026655 (2002).
- 66 Shansky, R. M. *et al.* Estrogen promotes stress sensitivity in a prefrontal cortex-amygdala pathway. *Cereb Cortex* **20**, 2560-2567, doi:10.1093/cercor/bhq003 (2010).
- 67 Bangasser, D. A. & Valentino, R. J. Sex differences in stress-related psychiatric disorders: neurobiological perspectives. *Front Neuroendocrinol* **35**, 303-319, doi:10.1016/j.yfrne.2014.03.008 (2014).
- 68 Bangasser, D. A., Zhang, X., Garachh, V., Hanhauser, E. & Valentino, R. J. Sexual dimorphism in locus coeruleus dendritic morphology: a structural basis for sex differences in emotional arousal. *Physiol Behav* **103**, 342-351, doi:10.1016/j.physbeh.2011.02.037 (2011).
- 69 Curtis, A. L., Bethea, T. & Valentino, R. J. Sexually dimorphic responses of the brain norepinephrine system to stress and corticotropin-releasing factor. *Neuropsychopharmacology* **31**, 544-554, doi:10.1038/sj.npp.1300875 (2006).
- 70 Scoville, W. B. & Milner, B. Loss of recent memory after bilateral hippocampal lesions. *J Neurol Neurosurg Psychiatry* **20**, 11-21 (1957).

- 71 Squire, L. R. Memory and the Hippocampus: a synthesis from findings with rats, monkeys, and humans. *Psychol Rev* **99**, 194-231 (1992).
- 72 Morris, R. G., Garrud, P., Rawlins, J. N. & O'Keefe, J. Place navigation impaired in rats with hippocampal lesions. *Nature* **297**, 681-683 (1982).
- 73 Ralsman, G., Cowan, W. M. & Powell, T. P. S. The extrinsic afferent, commissural, and association fibres of the hippocampus. *Brain Res* **88** (1965).
- 74 Amaral, D. G. & Witter, M. P. The three-dimensional organization of the hippocampal formation: a review of anatomical data. *Neuroscience* **31**, 571-591 (1989).
- 75 Andersen, P. in *The Hippocampus* (eds R.L. Isaacson & K.H. Pribram) (Springer, 1975).
- 76 O'Keefe, J. & Dostrovsky, J. The hippocampus as a spatial map: preliminary evidence from unit activity in the freely-moving rat. *Brain Res* (1971).
- 77 Fernández, G. *et al.* Successful verbal encoding into episodic memory engages the posterior hippocampus: a parametrically analyzed functional magnetic resonance imaging study. *J Neurosci* **18**, 1841-1847 (1998).
- 78 Rombouts, S. A. *et al.* Visual association encoding activates the medial temporal lobe: a functional magnetic resonance imaging study. *Hippocampus* **7**, 594-601, doi:10.1002/(SICI)1098-1063(1997)7:6<594::AID-HIPO2>3.0.CO;2-F (1997).
- 79 Andersen, P., Bliss, T. V. P. & Skrede, K. K. Lamellar organization of hippocampal excitatory pathways. *Exp Brain Res* **13** (1971).
- 80 Dougherty, K. A., Islam, T. & Johnston, D. Intrinsic excitability of CA1 pyramidal neurones from the rat dorsal and ventral hippocampus. *J Physiol* **590**, 5707-5722, doi:10.1113/jphysiol.2012.242693 (2012).
- 81 Paptheodoropoulos, C., Asprodini, E., Nikita, I., Koutsona, C. & Kostopoulos, G. Weaker synaptic inhibition in CA1 region of ventral compared to dorsal rat hippocampal slices. *Brain Res* **948**, 117-121 (2002).
- 82 Hughes, K. R. Dorsal and ventral hippocampus lesions and maze learning: influence of preoperative environment. *Can J Psychol* **19**, 325-332 (1965).
- 83 Moser, M. B., Moser, E. I., Forrest, E., Andersen, P. & Morris, R. G. Spatial learning with a minislab in the dorsal hippocampus. *Proc Natl Acad Sci U S A* **92**, 9697-9701 (1995).
- 84 Jung, M. W., Wiener, S. I. & McNaughton, B. L. Comparison of spatial firing characteristics of units in dorsal and ventral hippocampus of the rat. *J Neurosci* **14**, 7347-7356 (1994).

- 85 Witter, M. P., Groenewegen, H. J., Lopes da Silva, F. H. & Lohman, A. H. M. Functional organization of the extrinsic and intrinsic circuitry of the parahippocampal region. *Progress in neurobiology* **33**, 161-253 (1989).
- 86 Rudy, J. W. & Matus-Amat, P. The ventral hippocampus supports a memory representation of context and contextual fear conditioning: implications for a unitary function of the hippocampus. *Behav Neurosci* **119**, 154-163, doi:10.1037/0735-7044.119.1.154 (2005).
- 87 Kjelstrup, K. G. *et al.* Reduced fear expression after lesions of the ventral hippocampus. *Proc Natl Acad Sci U S A* **99**, 10825-10830, doi:10.1073/pnas.152112399 (2002).
- 88 Maren, S. & Holt, W. G. Hippocampus and Pavlovian fear conditioning in rats: muscimol infusions into the ventral, but not dorsal, hippocampus impair the acquisition of conditional freezing to an auditory conditional stimulus. *Behavioral Neuroscience* **118**, 97-110 (2004).
- 89 van Groen, T. & Wyss, J. M. Extrinsic projections from area CA1 of the rat hippocampus: olfactory, cortical, subcortical, and bilateral hippocampal formation projections. *J Comp Neurol* **302**, 515-528, doi:10.1002/cne.903020308 (1990).
- 90 Langer, S. Z. 25 Years since the discovery of presynaptic receptors: present knowledge and future perspectives. *Trends in Pharmacological Sciences* **18**, 95-99 (1997).
- 91 Sanacora, G., Treccani, G. & Popoli, M. Towards a glutamate hypothesis of depression An emerging frontier of neuropsychopharmacology for mood disorders. *Neuropharmacology* **62**, 63-77, doi:10.1016/j.neuropharm.2011.07.036 (2012).
- 92 Douglas, R. J. & Martin, K. A. Mapping the matrix: the ways of neocortex. *Neuron* **56**, 226-238, doi:10.1016/j.neuron.2007.10.017 (2007).
- 93 Kandel, E. R., Jessel, T. & Schwartz, J. H. *Principles of neural science*. 5th edn, (McGraw-Hill Education/Medical, 2013).
- 94 Malenka, R. C. & Nicoll, R. A. Long-term potentiation--a decade of progress? *Science* **285**, 1870-1874 (1999).
- 95 Bliss, T. V. & Lomo, T. Long-lasting potentiation of synaptic transmission in the dentate area of the anaesthetized rabbit following stimulation of the perforant path. *J Physiol* **232**, 331-356 (1973).
- 96 Davies, S. N., Lester, R. A., Reymann, K. G. & Collingridge, G. L. Temporally distinct pre- and post-synaptic mechanisms maintain long-term potentiation. *Nature* **338**, 500-503, doi:10.1038/338500a0 (1989).

- 97 Lisman, J., Schulman, H. & Cline, H. The molecular basis of CaMKII function in synaptic and behavioural memory. *Nat Rev Neurosci* **3**, 175-190, doi:10.1038/nrn753 (2002).
- 98 Benke, T. A., Luthi, A., Isaac, J. T. & Collingridge, G. L. Modulation of AMPA receptor unitary conductance by synaptic activity. *Nature* **393**, 793-797, doi:10.1038/31709 (1998).
- 99 Bear, M. F. & Malenka, R. C. Synaptic plasticity: LTP and LTD. *Curr Opin Neurobiol* **4**, 389-399 (1994).
- 100 Magarinos, A. M. & McEwen, B. S. Stress-induced atrophy of apical dendrites of hippocampal CA3c neurons: comparison of stressors. *Neuroscience* **69**, 83-88 (1995).
- 101 Pawlak, R. *et al.* Tissue plasminogen activator and plasminogen mediate stress-induced decline of neuronal and cognitive functions in the mouse hippocampus. *Proc Natl Acad Sci U S A* **102**, 18201-18206, doi:10.1073/pnas.0509232102 (2005).
- 102 Alfarez, D. N., Joels, M. & Krugers, H. J. Chronic unpredictable stress impairs long-term potentiation in rat hippocampal CA1 area and dentate gyrus in vitro. *Eur J Neurosci* **17**, 1928-1934 (2003).
- 103 Schmidt, M. V. *et al.* Individual stress vulnerability is predicted by short-term memory and AMPA receptor subunit ratio in the hippocampus. *J Neurosci* **30**, 16949-16958 (2010).
- 104 Kallarackal, A. J. *et al.* Chronic stress induces a selective decrease in AMPA receptor-mediated synaptic excitation at hippocampal temporoammonic-CA1 synapses. *J Neurosci* **33**, 15669-15674 (2013).
- 105 Chourbaji, S. *et al.* AMPA receptor subunit 1 (GluR-A) knockout mice model the glutamate hypothesis of depression. *FASEB J* **22**, 3129-3134, doi:10.1096/fj.08-106450 (2008).
- 106 Shigemoto, R. *et al.* Differential presynaptic localization of metabotropic glutamate receptor subtypes in the rat hippocampus. *J Neurosci* **17**, 7503-7522 (1997).
- 107 Charpak, S., Gahwiler, B. H., Do, K. Q. & Knopfel, T. Potassium conductances in hippocampal neurons blocked by excitatory amino-acid transmitters. *Nature* **347**, 765-767, doi:10.1038/347765a0 (1990).
- 108 Nakamura, T., Barbara, J. G., Nakamura, K. & Ross, W. N. Synergistic release of Ca²⁺ from IP₃-sensitive stores evoked by synaptic activation of mGluRs paired with backpropagating action potentials. *Neuron* **24**, 727-737 (1999).

- 109 Wieronska, J. M. *et al.* Changes in the expression of metabotropic glutamate receptor 5 (mGluR5) in the rat hippocampus in an animal model of depression. *Pol J Pharmacol* **53**, 659-662 (2001).
- 110 Chaki, S. *et al.* MGS0039: a potent and selective group II metabotropic glutamate receptor antagonist with antidepressant-like activity. *Neuropharmacology* **46**, 457-467, doi:10.1016/j.neuropharm.2003.10.009 (2004).
- 111 Kuffler, S. W. & Edwards, C. Mechanism of gamma aminobutyric acid (GABA) action and its relation to synaptic inhibition. *J Neurophysiol* **21**, 589-610, doi:10.1152/jn.1958.21.6.589 (1958).
- 112 Luscher, B., Shen, Q. & Sahir, N. The GABAergic deficit hypothesis of major depressive disorder. *Mol Psychiatry* **16**, 383-406, doi:10.1038/mp.2010.120 (2011).
- 113 Prut, L. *et al.* A reduction in hippocampal GABA(A) receptor alpha5 subunits disrupts the memory for location of objects in mice. *Genes Brain Behav* **9**, 478-488 (2010).
- 114 Crestani, F. *et al.* Trace fear conditioning involves hippocampal α 5 GABAA receptors. *PNAS* **99**, 8980-8985 (2002).
- 115 Holm, M. M. *et al.* Hippocampal GABAergic dysfunction in a rat chronic mild stress model of depression. *Hippocampus* **21**, 422-433, doi:10.1002/hipo.20758 (2011).
- 116 Martisova, E. *et al.* Long lasting effects of early-life stress on glutamatergic/GABAergic circuitry in the rat hippocampus. *Neuropharmacology* **62**, 1944-1953, doi:10.1016/j.neuropharm.2011.12.019 (2012).
- 117 Sudweeks, S. N. & Yakel, J. L. Functional and molecular characterization of neuronal nicotinic ACh receptors in rat CA1 hippocampal neurons. *J Physiol* **527 Pt 3**, 515-528 (2000).
- 118 Marchi, M. & Raiteri, M. Interaction acetylcholine-glutamate in rat hippocampus: involvement of two subtypes of M-2 muscarinic receptors. *J Pharmacol Exp Ther* **248**, 1255-1260 (1989).
- 119 Gray, R., Rajan, A. S., Radcliffe, K. A., Yakehiro, M. & Dani, J. A. Hippocampal synaptic transmission enhanced by low concentrations of nicotine. *Nature* **383**, 713-716, doi:10.1038/383713a0 (1996).
- 120 Lopes da Silva, F. H., Witter, M. P., Boeijinga, P. H. & Lohman, A. H. Anatomic organization and physiology of the limbic cortex. *Physiol Rev* **70**, 453-511, doi:10.1152/physrev.1990.70.2.453 (1990).

- 121 Gasbarri, A., Campana, E., Pacitti, C., Hajdu, F. & Tombol, T. Organization of the projections from the ventral tegmental area of Tsai to the hippocampal formation in the rat. *J Hirnforsch* **32**, 429-437 (1991).
- 122 Andrade, R. Regulation of membrane excitability in the central nervous system by serotonin receptor subtypes. *Ann N Y Acad Sci* **861** (1998).
- 123 Madison, D. V. & Nicoll, R. A. Actions of noradrenaline recorded intracellularly in rat hippocampal CA1 pyramidal neurones, in vitro. *J Physiol* **372**, 221-244 (1986).
- 124 Malenka, R. C. & Nicoll, R. A. Dopamine decreases the calcium-activated afterhyperpolarization in hippocampal CA1 pyramidal cells. *Brain Res* **379**, 210-215 (1986).
- 125 Bergles, D. E., Doze, V. A., Madison, D. V. & Smith, S. J. Excitatory actions of norepinephrine on multiple classes of hippocampal CA1 interneurons. *J Neurosci* **16**, 572-585 (1996).
- 126 McMahan, L. L. & Kauer, J. A. Hippocampal interneurons are excited via serotonin-gated ion channels. *J Neurophysiol* **78**, 2493-2502, doi:10.1152/jn.1997.78.5.2493 (1997).
- 127 Katsuki, H., Izumi, Y. & Zorumski, C. F. Noradrenergic regulation of synaptic plasticity in the hippocampal CA1 region. *J Neurophysiol* **77**, 3013-3020, doi:10.1152/jn.1997.77.6.3013 (1997).
- 128 Huang, Y. Y. & Kandel, E. R. D1/D5 receptor agonists induce a protein synthesis-dependent late potentiation in the CA1 region of the hippocampus. *Proc Natl Acad Sci U S A* **92**, 2446-2450 (1995).
- 129 MacQueen, G. M. *et al.* Course of illness, hippocampal function, and hippocampal volume in major depression. *Proc Natl Acad Sci U S A* **100**, 1387-1392, doi:10.1073/pnas.0337481100 (2003).
- 130 Frodl, T. *et al.* Hippocampal changes in patients with a first episode of major depression. *Am J Psychiatry* **159**, 1112-1118, doi:10.1176/appi.ajp.159.7.1112 (2002).
- 131 Mervaala, E. *et al.* Quantitative MRI of the hippocampus and amygdala in severe depression. *Psychol Med* **30**, 117-125 (2000).
- 132 Beyer, J. L. & Krishnan, K. R. Volumetric brain imaging findings in mood disorders. *Bipolar Disord* **4**, 89-104 (2002).
- 133 Bremner, J. D. *et al.* MRI-based measurement of hippocampal volume in patients with combat-related posttraumatic stress disorder. *Am J Psychiatry* **152**, 973-981, doi:10.1176/ajp.152.7.973 (1995).

- 134 Sheline, Y. I., Wang, P. W., Gado, M. H., Csernansky, J. G. & Vannier, M. W. Hippocampal atrophy in recurrent major depression. *Proc Natl Acad Sci U S A* **93**, 3908-3913 (1996).
- 135 Sheline, Y. I., Sanghavi, M., Mintun, M. A. & Gado, M. H. Depression duration but not age predicts hippocampal volume loss in medically healthy women with recurrent major depression. *J Neurosci* **19**, 5034-5043 (1999).
- 136 Malberg, J. E., Eisch, A. J., Nestler, E. J. & Duman, R. S. Chronic antidepressant treatment increases neurogenesis in adult rat hippocampus. *J Neurosci* **20**, 9104-9110 (2000).
- 137 Rajkowska, G. Postmortem studies in mood disorders indicate altered numbers of neurons and glial cells. *Biol Psychiatry* **48**, 766-777 (2000).
- 138 Czeh, B. *et al.* Stress-induced changes in cerebral metabolites, hippocampal volume, and cell proliferation are prevented by antidepressant treatment with tianeptine. *Proc Natl Acad Sci U S A* **98**, 12796-12801, doi:10.1073/pnas.211427898 (2001).
- 139 Woolley, C. S., Gould, E., Frankfurt, M. & McEwen, B. S. Naturally occurring fluctuation in dendritic spine density on adult hippocampal pyramidal neurons. *J Neurosci* **10**, 4035-4039 (1990).
- 140 Woolley, C. S. & McEwen, B. S. Estradiol regulates hippocampal dendritic spine density via an N-methyl-D-aspartate receptor-dependent mechanism. *J Neurosci* **14**, 7680-7687 (1994).
- 141 Shors, T. J., Chua, C. & Falduto, J. Sex differences and opposite effects of stress on dendritic spine density in the male versus female hippocampus. *J Neurosci* **21**, 6292-6297 (2001).
- 142 Shors, T. J., Falduto, J. & Leuner, B. The opposite effects of stress on dendritic spines in male vs. female rats are NMDA receptor-dependent. *Eur J Neurosci* **19**, 145-150 (2004).
- 143 Berridge, K. C. & Kringelbach, M. L. Pleasure systems in the brain. *Neuron* **86**, 646-664, doi:10.1016/j.neuron.2015.02.018 (2015).
- 144 Malenka, R. C., Nestler, E. J. & Hyman, S. E. *Molecular Neuropharmacology: A Foundation for Clinical Neuroscience*. 2nd edn, 147-148 (McGraw-Hill Medical, 2009).
- 145 Zahm, D. S. Functional-anatomical implications of the nucleus accumbens core and shell subterritories. *Ann N Y Acad Sci* **877**, 113-128 (1999).

- 146 Newton, S. S. *et al.* Inhibition of cAMP response element-binding protein or dynorphin in the nucleus accumbens produces an antidepressant-like effect. *J Neurosci* **22**, 10883-10890 (2002).
- 147 Rada, P. Glutamate release in the nucleus accumbens is involved in behavioral depression during the Porsolt swim test. *Neuroscience* **119** (2003).
- 148 Christoffel, D. J., Golden, S. A. & Russo, S. J. Structural and synaptic plasticity in stress-related disorders. *Rev Neurosci* **22**, 535-549, doi:10.1515/RNS.2011.044 (2011).
- 149 Yager, L. M., Garcia, A. F., Wunsch, A. M. & Ferguson, S. M. The ins and outs of the striatum: role in drug addiction. *Neuroscience* **301**, 529-541, doi:10.1016/j.neuroscience.2015.06.033 (2015).
- 150 Robison, A. J. & Nestler, E. J. Transcriptional and epigenetic mechanisms of addiction. *Nat Rev Neurosci* **12**, 623-637, doi:10.1038/nrn3111 (2011).
- 151 Self, D. W., Barnhart, W. J., Lehman, D. A. & Nestler, E. J. Opposite modulation of cocaine-seeking behavior by D1- and D2-like dopamine receptor agonists. *Science* **271**, 1586-1589 (1996).
- 152 Kupchik, Y. M. *et al.* Coding the direct/indirect pathways by D1 and D2 receptors is not valid for accumbens projections. *Nat Neurosci* **18** (2015).
- 153 Goggi, J., Pullar, I. A., Carney, S. L. & Bradford, H. F. Signalling pathways involved in the short-term potentiation of dopamine release by BDNF. *Brain Res* **968**, 156-161 (2003).
- 154 Wilkinson, M. B. *et al.* Imipramine treatment and resiliency exhibit similar chromatin regulation in the mouse nucleus accumbens in depression models. *J Neurosci* **29**, 7820-7832, doi:10.1523/JNEUROSCI.0932-09.2009 (2009).
- 155 Covington, H. E., 3rd *et al.* Antidepressant actions of histone deacetylase inhibitors. *J Neurosci* **29**, 11451-11460, doi:10.1523/JNEUROSCI.1758-09.2009 (2009).
- 156 Nestler, E. J. FosB: a transcriptional regulator of stress and antidepressant responses. *Eur J Pharmacol* **753**, 66-72, doi:10.1016/j.ejphar.2014.10.034 (2015).
- 157 Perrotti, L. I. *et al.* Induction of deltaFosB in reward-related brain structures after chronic stress. *J Neurosci* **24**, 10594-10602, doi:10.1523/JNEUROSCI.2542-04.2004 (2004).
- 158 Vialou, V. *et al.* DeltaFosB in brain reward circuits mediates resilience to stress and antidepressant responses. *Nat Neurosci* **13**, 745-752, doi:10.1038/nn.2551 (2010).

- 159 Ulery-Reynolds, P. G., Castillo, M. A., Vialou, V., Russo, S. J. & Nestler, E. J. Phosphorylation of DeltaFosB mediates its stability in vivo. *Neuroscience* **158**, 369-372, doi:10.1016/j.neuroscience.2008.10.059 (2009).
- 160 Nestler, E. J. Review. Transcriptional mechanisms of addiction: role of DeltaFosB. *Philos Trans R Soc Lond B Biol Sci* **363**, 3245-3255, doi:10.1098/rstb.2008.0067 (2008).
- 161 Lobo, M. K. *et al.* DeltaFosB induction in striatal medium spiny neuron subtypes in response to chronic pharmacological, emotional, and optogenetic stimuli. *J Neurosci* **33**, 18381-18395, doi:10.1523/JNEUROSCI.1875-13.2013 (2013).
- 162 Ohnishi, Y. N. *et al.* FosB Is Essential for the Enhancement of Stress Tolerance and Antagonizes Locomotor Sensitization by Δ FosB. *Biol Psychiatry* **70**, 487-495 (2011).
- 163 Kelz, M. B. *et al.* Expression of the transcription factor deltaFosB in the brain controls sensitivity to cocaine. *Nature* **401**, 272-276, doi:10.1038/45790 (1999).
- 164 Anker, J. J. & Carroll, M. E. in *Biological basis of sex differences in psychopharmacology* 73-96 (Springer, 2010).
- 165 Russo, S. J. *et al.* Sex differences in the conditioned rewarding effects of cocaine. *Brain Res* **970**, 214-220 (2003).
- 166 Becker, J. B. & Hu, M. Sex differences in drug abuse. *Front Neuroendocrinol* **29**, 36-47, doi:10.1016/j.yfrne.2007.07.003 (2008).
- 167 Kritzer, M. F. Selective colocalization of immunoreactivity for intracellular gonadal hormone receptors and tyrosine hydroxylase in the ventral tegmental area, substantia nigra, and retrorubral fields in the rat. *J Comp Neurol* **379**, 247-260 (1997).
- 168 Forlano, P. M. & Woolley, C. S. Quantitative analysis of pre- and postsynaptic sex differences in the nucleus accumbens. *J Comp Neurol* **518**, 1330-1348, doi:10.1002/cne.22279 (2010).
- 169 Wissman, A. M., May, R. M. & Woolley, C. S. Ultrastructural analysis of sex differences in nucleus accumbens synaptic connectivity. *Brain Struct Funct* **217**, 181-190, doi:10.1007/s00429-011-0353-6 (2012).
- 170 Brancato, A. *et al.* Sub-chronic variable stress induces sex-specific effects on glutamatergic synapses in the nucleus accumbens. *Neuroscience* **350**, 180-189, doi:10.1016/j.neuroscience.2017.03.014 (2017).
- 171 Russo, S. J. & Nestler, E. J. The brain reward circuitry in mood disorders. *Nat Rev Neurosci* **14**, 609-625, doi:10.1038/nrn3381 (2013).

- 172 Thompson, S. M. *et al.* An excitatory synapse hypothesis of depression. *Trends Neurosci* **38**, 279-294, doi:10.1016/j.tins.2015.03.003 (2015).
- 173 Day, J. J., Roitman, M. F., Wightman, R. M. & Carelli, R. M. Associative learning mediates dynamic shifts in dopamine signaling in the nucleus accumbens. *Nat Neurosci* **10**, 1020-1028, doi:10.1038/nn1923 (2007).
- 174 Berridge, K. C. The debate over dopamine's role in reward: the case for incentive salience. *Psychopharmacology (Berl)* **191**, 391-431, doi:10.1007/s00213-006-0578-x (2007).
- 175 Stuber, G. D. *et al.* Reward-predictive cues enhance excitatory synaptic strength onto midbrain dopamine neurons. *Science* **321**, 1690-1692, doi:10.1126/science.1160873 (2008).
- 176 Pennartz, C. M., Ito, R., Verschure, P. F., Battaglia, F. P. & Robbins, T. W. The hippocampal-striatal axis in learning, prediction and goal-directed behavior. *Trends Neurosci* **34**, 548-559, doi:10.1016/j.tins.2011.08.001 (2011).
- 177 Wolf, M. E. & Ferrario, C. R. AMPA receptor plasticity in the nucleus accumbens after repeated exposure to cocaine. *Neurosci Biobehav Rev* **35**, 185-211, doi:10.1016/j.neubiorev.2010.01.013 (2010).
- 178 Sun, X., Milovanovic, M., Zhao, Y. & Wolf, M. E. Acute and chronic dopamine receptor stimulation modulates AMPA receptor trafficking in nucleus accumbens neurons cocultured with prefrontal cortex neurons. *J Neurosci* **28**, 4216-4230, doi:10.1523/JNEUROSCI.0258-08.2008 (2008).
- 179 Kahn, I. & Shohamy, D. Intrinsic connectivity between the hippocampus, nucleus accumbens, and ventral tegmental area in humans. *Hippocampus* **23**, 187-192 (2013).
- 180 Britt, J. P. *et al.* Synaptic and behavioral profile of multiple glutamatergic inputs to the nucleus accumbens. *Neuron* **76**, 790-803, doi:10.1016/j.neuron.2012.09.040 (2012).
- 181 Hull, C., Isaacson, J. S. & Scanziani, M. Postsynaptic mechanisms govern the differential excitation of cortical neurons by thalamic inputs. *J Neurosci* **29**, 9127-9136, doi:10.1523/JNEUROSCI.5971-08.2009 (2009).
- 182 O'Donnell, P. & Grace, A. A. Synaptic interactions among excitatory afferents to nucleus accumbens neurons: hippocampal gating of prefrontal cortical input. *J Neurosci* **15**, 3622-3639 (1995).
- 183 LeGates, T. A. *et al.* Reward behaviour is regulated by the strength of hippocampus–nucleus accumbens synapses. *Nature* **564**, 258-262 (2018).

- 184 Nicoll, R. A. & Malenka, R. C. Contrasting properties of two forms of long-term potentiation in the hippocampus. *Nature* **377**, 115-118, doi:10.1038/377115a0 (1995).
- 185 Hodgkin, A. L. The Ionic Basis of Electrical Activity in Nerve and Muscle. *Biol Rev* **26**, 339-409, doi:DOI 10.1111/j.1469-185X.1951.tb01204.x (1951).
- 186 Lesage, F. & Lazdunski, M. Molecular and functional properties of two-pore-domain potassium channels. *Am J Physiol Renal Physiol* **279**, F793-801, doi:10.1152/ajprenal.2000.279.5.F793 (2000).
- 187 Taverna, S., Tkatch, T., Metz, A. E. & Martina, M. Differential expression of TASK channels between horizontal interneurons and pyramidal cells of rat hippocampus. *Journal of Neuroscience* **25**, 9162-9170, doi:10.1523/Jneurosci.2454-05.2005 (2005).
- 188 Vergara, C., Latorre, R., Marrion, N. V. & Adelman, J. P. Calcium-activated potassium channels. *Curr Opin Neurobiol* **8**, 321-329 (1998).
- 189 Storm, J. F. Action potential repolarization and a fast after-hyperpolarization in rat hippocampal pyramidal cells. *J Physiol* **385**, 733-759 (1987).
- 190 Lancaster, B. & Adams, P. R. Calcium-dependent current generating the afterhyperpolarization of hippocampal neurons. *J Neurophysiol* **55**, 1268-1282, doi:10.1152/jn.1986.55.6.1268 (1986).
- 191 Pongs, O. Voltage-gated potassium channels: from hyperexcitability to excitement. *FEBS Lett* **452**, 31-35 (1999).
- 192 Hoffman, D. A., Magee, J. C., Colbert, C. M. & Johnston, D. K⁺ channel regulation of signal propagation in dendrites of hippocampal pyramidal neurons. *Nature* **387**, 869-875, doi:10.1038/43119 (1997).
- 193 Roeper, J., Lorra, C. & Pongs, O. Frequency-dependent inactivation of mammalian A-type K⁺ channel KV1.4 regulated by Ca²⁺/calmodulin-dependent protein kinase. *J Neurosci* **17**, 3379-3391 (1997).
- 194 Kratzer, S. *et al.* Activation of CRH receptor type 1 expressed on glutamatergic neurons increases excitability of CA1 pyramidal neurons by the modulation of voltage-gated ion channels. *Front Cell Neurosci* **7**, 91, doi:10.3389/fncel.2013.00091 (2013).
- 195 Yu, F. H. & Catterall, W. A. Overview of the voltage-gated sodium channel family. *Genome Biol* **4**, 207 (2003).
- 196 Rogawski, M. A. & Löscher, W. The neurobiology of antiepileptic drugs. *Nat Rev Neurosci* **5**, 553-564 (2004).

- 197 Xie, X. & Hagan, R. M. Cellular and molecular actions of lamotrigine: Possible mechanisms of efficacy in bipolar disorder. *Neuropsychobiology* **38**, 119-130, doi:10.1159/000026527 (1998).
- 198 Calabrese, J. R., Rapport, D. J., Shelton, M. D. & Kimmel, S. E. Clinical studies on the use of lamotrigine in bipolar disorder. *Neuropsychobiology* **38**, 185-191, doi:Doi 10.1159/000026535 (1998).
- 199 Ghaemi, S. N., Shirizadi, A. A. & Filkowski, M. Publication Bias and the Pharmaceutical Industry: The Case of Lamotrigine in Bipolar Disorder. *Medscape J Med* **10** (2008).
- 200 Dolphin, A. C. A short history of voltage-gated calcium channels. *Br J Pharmacol* **147 Suppl 1**, S56-62, doi:10.1038/sj.bjp.0706442 (2006).
- 201 Sudhof, T. C. Calcium control of neurotransmitter release. *Cold Spring Harb Perspect Biol* **4**, a011353, doi:10.1101/cshperspect.a011353 (2012).
- 202 Ertel, E. A. *et al.* Nomenclature of voltage-gated calcium channels. *Neuron* **25**, 533-535 (2000).
- 203 Green, E. K. *et al.* The bipolar disorder risk allele at CACNA1C also confers risk of recurrent major depression and of schizophrenia. *Mol Psychiatry* **15**, 1016-1022 (2010).
- 204 Berger, S. M. & Bartsch, D. The role of L-type voltage-gated calcium channels Cav1.2 and Cav1.3 in normal and pathological brain function. *Cell Tissue Res* **357**, 463-476, doi:10.1007/s00441-014-1936-3 (2014).
- 205 Moghaddam, B., Adams, B., Verma, A. & Daly, D. Activation of glutamatergic neurotransmission by ketamine: a novel step in the pathway from NMDA receptor blockade to dopaminergic and cognitive disruptions associated with the prefrontal cortex. *J Neurosci* **17**, 2921-2927 (1997).
- 206 Garcia, L. S. *et al.* Acute administration of ketamine induces antidepressant-like effects in the forced swimming test and increases BDNF levels in the rat hippocampus. *Prog Neuropsychopharmacol Biol Psychiatry* **32**, 140-144, doi:10.1016/j.pnpbp.2007.07.027 (2008).
- 207 Mastrodonato, A. *et al.* Ventral CA3 Activation Mediates Prophylactic Ketamine Efficacy Against Stress-Induced Depressive-like Behavior. *Biol Psychiatry* **84**, 846-856, doi:10.1016/j.biopsych.2018.02.011 (2018).
- 208 Cohen, C., Perrault, G. & Sanger, D. J. Assessment of the antidepressant-like effects of L-type voltage-dependent channel modulators. *Behav Pharmacol* **8**, 629-638 (1997).

- 209 Srivastava, S. K. & Nath, C. The differential effects of calcium channel blockers in the behavioural despair test in mice. *Pharmacol Res* **42**, 293-297, doi:10.1006/phrs.2000.0696 (2000).
- 210 Noam, Y. *et al.* Trafficking and surface expression of hyperpolarization-activated cyclic nucleotide-gated channels in hippocampal neurons. *J Biol Chem* **285**, 14724-14736, doi:10.1074/jbc.M109.070391 (2010).
- 211 Monteggia, L. M., Eisch, A. J., Tang, M. D., Kaczmarek, L. K. & Nestler, E. J. Cloning and localization of the hyperpolarization-activated cyclic nucleotide-gated channel family in rat brain. *Brain Res Mol Brain Res* **81**, 129-139 (2000).
- 212 Robinson, R. B. & Siegelbaum, S. A. Hyperpolarization-activated cation currents: from molecules to physiological function. *Annu Rev Physiol* **65**, 453-480, doi:10.1146/annurev.physiol.65.092101.142734 (2003).
- 213 Ku, S. M. & Han, M. H. HCN Channel Targets for Novel Antidepressant Treatment. *Neurotherapeutics* **14**, 698-715, doi:10.1007/s13311-017-0538-7 (2017).
- 214 Lewis, A. S. *et al.* Deletion of the hyperpolarization-activated cyclic nucleotide-gated channel auxiliary subunit TRIP8b impairs hippocampal Ih localization and function and promotes antidepressant behavior in mice. *J Neurosci* **31**, 7424-7440, doi:10.1523/JNEUROSCI.0936-11.2011 (2011).
- 215 Magee, J. C. Dendritic hyperpolarization-activated currents modify the integrative properties of hippocampal CA1 pyramidal neurons. *J Neurosci* **18**, 7613-7624 (1998).
- 216 Tsay, D., Dudman, J. T. & Siegelbaum, S. A. HCN1 channels constrain synaptically evoked Ca²⁺ spikes in distal dendrites of CA1 pyramidal neurons. *Neuron* **56**, 1076-1089, doi:10.1016/j.neuron.2007.11.015 (2007).
- 217 Fan, Y. *et al.* Activity-dependent decrease of excitability in rat hippocampal neurons through increases in I(h). *Nat Neurosci* **8**, 1542-1551 (2005).
- 218 Jones, R. E. & Lopez, K. H. *Human Reproductive Biology*. 4th Edition edn, (Academic Press, 2014).
- 219 Woolley, C. S. & Schwartzkroin, P. A. Hormonal effects on the brain. *Epilepsia* **39 Suppl 8**, S2-8 (1998).
- 220 Pfaff, D. & Keiner, M. Atlas of estradiol-concentrating cells in the central nervous system of the female rat. *J Comp Neurol* **151**, 121-158, doi:10.1002/cne.901510204 (1973).

- 221 Loy, R., Gerlach, J. L. & McEwen, B. S. Autoradiographic localization of estradiol-binding neurons in the rat hippocampal formation and entorhinal cortex. *Brain Res* **467**, 245-251 (1988).
- 222 Kato, J. in *Actions of Progesterone on the Brain. Current Topics in Neuroendocrinology* Vol. 5 (eds D. Ganten & D. Pfaff) (Springer, 1985).
- 223 Pelletier, G., Liao, N., Follea, N. & Govindan, M. V. Mapping of estrogen receptor-producing cells in the rat brain by in situ hybridization. *Neurosci Lett* **94**, 23-28 (1988).
- 224 DonCarlos, L. L., Monroy, E. & Morrell, J. I. Distribution of estrogen receptor-immunoreactive cells in the forebrain of the female guinea pig. *J Comp Neurol* **305**, 591-612 (1991).
- 225 Schumacher, M. Rapid membrane effects of steroid hormones: an emerging concept in neuroendocrinology. *Trends Neurosci* **13**, 359-362, doi:10.1016/0166-2236(90)90016-4 (1990).
- 226 Majewska, M. D. Neurosteroids: endogenous bimodal modulators of the GABAA receptor. Mechanism of action and physiological significance. *Prog Neurobiol* **38**, 379-395 (1992).
- 227 Wong, M. & Moss, R. L. Long-term and short-term electrophysiological effects of estrogen on the synaptic properties of hippocampal CA1 neurons. *J Neurosci* **12**, 3217-3225 (1992).
- 228 Gu, Q. & Moss, R. L. 17β -Estradiol Potentiates Kainate-Induced Currents via Activation of the cAMP Cascade. *J Neurosci* **16**, 3620-3629 (1996).
- 229 Moss, R. L., Gu, Q. & Wong, M. Estrogen: nontranscriptional signaling pathway. *Recent Prog Horm Res* **52**, 33-68; discussion 68-39 (1997).
- 230 Warren, S. G., Humphreys, A. G., Juraska, J. M. & Greenough, W. T. LTP varies across the estrous cycle: enhanced synaptic plasticity in proestrus rats. *Brain Res* **703**, 26-30 (1995).
- 231 Cordoba Montoya, D. A. & Carrer, H. F. Estrogen facilitates induction of long term potentiation in the hippocampus of awake rats. *Brain Res* **778**, 430-438 (1997).
- 232 Joels, M. & Karst, H. Effects of estradiol and progesterone on voltage-gated calcium and potassium conductances in rat CA1 hippocampal neurons. *J Neurosci* **15**, 4289-4297 (1995).
- 233 Gould, E., Woolley, C. S., Frankfurt, M. & McEwen, B. S. Gonadal steroids regulate dendritic spine density in hippocampal pyramidal cells in adulthood. *J Neurosci* **10**, 1286-1291 (1990).

- 234 McEwen, B. S. Plasticity of the hippocampus: adaptation to chronic stress and allostatic load. *Ann N Y Acad Sci* **933**, 265-277 (2001).
- 235 Shors, T. J. & Leuner, B. Estrogen-mediated effects on depression and memory formation in females. *J Affect Disord* **74** (2003).
- 236 Bowman, R. E., Ferguson, D. & Luine, V. N. Effects of chronic restraint stress and estradiol on open field activity, spatial memory, and monoaminergic neurotransmitters in ovariectomized rats. *Neuroscience* **113**, 401-410 (2002).
- 237 Toufexis, D. J., Myers, K. M., Bowser, M. E. & Davis, M. Estrogen disrupts the inhibition of fear in female rats, possibly through the antagonistic effects of estrogen receptor alpha (ER α) and ER beta. *J Neurosci* **27**, 9729-9735 (2007).
- 238 Shansky, R. M. *et al.* Estrogen mediates sex differences in stress-induced prefrontal cortex dysfunction. *Mol Psychiatry* **9**, 531-538, doi:10.1038/sj.mp.4001435 (2004).
- 239 Shores, M. M. *et al.* Increased incidence of diagnosed depressive illness in hypogonadal older men. *Arch Gen Psychiatry* **61**, 162-167, doi:10.1001/archpsyc.61.2.162 (2004).
- 240 Zarrouf, F. A., Artz, S., Griffith, J., Sirbu, C. & Kommor, M. Testosterone and depression: systematic review and meta-analysis. *J Psychiatr Pract* **15**, 289-305, doi:10.1097/01.pra.0000358315.88931.fc (2009).
- 241 Kanayama, G., Amiaz, R., Seidman, S. & Pope, H. G., Jr. Testosterone supplementation for depressed men: current research and suggested treatment guidelines. *Exp Clin Psychopharmacol* **15**, 529-538, doi:10.1037/1064-1297.15.6.529 (2007).
- 242 Walther, A., Breidenstein, J. & Miller, R. Association of Testosterone Treatment With Alleviation of Depressive Symptoms in Men: A Systematic Review and Meta-analysis. *JAMA Psychiatry* **76**, 31-40, doi:10.1001/jamapsychiatry.2018.2734 (2019).
- 243 Miller, K. K. *et al.* Low-dose transdermal testosterone augmentation therapy improves depression severity in women. *CNS Spectr* **14**, 688-694 (2009).
- 244 Frye, C. A., Duncan, J. E., Basham, M. & Erskine, M. S. Behavioral effects of 3 α -androstenediol II: Hypothalamic and preoptic area actions via a GABAergic mechanism. *Behavioural Brain Research* **79**, 119-130 (1996).
- 245 Pak, T. R. *et al.* The Androgen Metabolite, 5 α -Androstane-3 β , 17 β -Diol, Is a Potent Modulator of Estrogen Receptor- β 1-Mediated Gene Transcription in Neuronal Cells. *Endocrinology* **146**, 147-155 (2005).

- 246 Nestler, E. J., Hyman, S. E. & Malenka, R. C. *Molecular Neuropharmacology: A Foundation for Clinical Neuroscience*. (McGraw-Hill Medical, 2009).
- 247 Cato, A. C., Nestl, A. & Mink, S. Rapid actions of steroid receptors in cellular signaling pathways. *Sci STKE* **2002**, re9, doi:10.1126/stke.2002.138.re9 (2002).
- 248 Kubli-Garfias, C., Canchola, E., Arauz-Contreras, J. & Feria-Velasco, A. Depressant effect of androgens on the cat brain electrical activity and its antagonism by ruthenium red. *Neuroscience* **7**, 2777-2782 (1982).
- 249 Smith, M. D., Jones, L. S. & Wilson, M. A. Sex differences in hippocampal slice excitability: role of testosterone. *Neuroscience* **109**, 517-530 (2002).
- 250 Slob, A. K., Bogers, H. & van Stolk, M. A. Effects of gonadectomy and exogenous gonadal steroids on sex differences in open field behaviour of adult rats. *Behav Brain Res* **2**, 347-362 (1981).
- 251 Fernandez-Guasti, A. & Martinez-Mota, L. Anxiolytic-like actions of testosterone in the burying behavior test: role of androgen and GABA-benzodiazepine receptors. *Psychoneuroendocrinology* **30**, 762-770, doi:10.1016/j.psyneuen.2005.03.006 (2005).
- 252 Frye, C. A. & Seliga, A. M. Testosterone increases analgesia, anxiolysis, and cognitive performance of male rats. *Cogn Affect Behav Neurosci* **1**, 371-381 (2001).
- 253 Wainwright, S. R., Lieblich, S. E. & Galea, L. A. Hypogonadism predisposes males to the development of behavioural and neuroplastic depressive phenotypes. *Psychoneuroendocrinology* **36**, 1327-1341, doi:10.1016/j.psyneuen.2011.03.004 (2011).
- 254 Bitran, D., Kellogg, C. K. & Hilvers, R. J. Treatment with an anabolic-androgenic steroid affects anxiety-related behavior and alters the sensitivity of cortical GABAA receptors in the rat. *Horm Behav* **27**, 568-583, doi:10.1006/hbeh.1993.1041 (1993).
- 255 Carrier, N. & Kabbaj, M. Testosterone and imipramine have antidepressant effects in socially isolated male but not female rats. *Hormones and Behavior* **61**, 678-685 (2012).
- 256 Herrera-Perez, J. J., Martinez-Mota, L., Chavira, R. & Fernandez-Guasti, A. Testosterone prevents but not reverses anhedonia in middle-aged males and lacks an effect on stress vulnerability in young adults. *Hormones and Behavior* **61**, 623-630 (2012).
- 257 Carrier, N. & Kabbaj, M. Extracellular signal-regulated kinase 2 signaling in the hippocampal dentate gyrus mediates the antidepressant effects of testosterone. *Biol Psychiatry* **71**, 642-651, doi:10.1016/j.biopsych.2011.11.028 (2012).

- 258 Frye, C. A. & Walf, A. A. Depression-like behavior of aged male and female mice is ameliorated with administration of testosterone or its metabolites. *Physiol Behav* **97** (2009).
- 259 Frye, C. A. & Lacey, E. H. Posttraining androgens' enhancement of cognitive performance is temporally distinct from androgens' increases in affective behavior. *Cognitive, Affective, and Behavioral Neuroscience* **1**, 172-182 (2001).
- 260 Isgor, C. & Sengelaub, D. R. Prenatal gonadal steroids affect adult spatial behavior, CA1 and CA3 pyramidal cell morphology in rats. *Horm Behav* **34**, 183-198, doi:10.1006/hbeh.1998.1477 (1998).
- 261 Isgor, C. & Sengelaub, D. R. Effects of neonatal gonadal steroids on adult CA3 pyramidal neuron dendritic morphology and spatial memory in rats. *J Neurobiol* **55**, 179-190, doi:10.1002/neu.10200 (2003).
- 262 Zhang, J. M., Tonelli, L., Regenold, W. T. & McCarthy, M. M. Effects of neonatal flutamide treatment on hippocampal neurogenesis and synaptogenesis correlate with depression-like behaviors in preadolescent male rats. *Neuroscience* **169**, 544-554, doi:10.1016/j.neuroscience.2010.03.029 (2010).
- 263 Meydan, S. *et al.* Effects of testosterone on orchietomy-induced oxidative damage in the rat hippocampus. *J Chem Neuroanat* **40**, 281-285, doi:10.1016/j.jchemneu.2010.07.006 (2010).
- 264 Frye, C. A. & McCormick, C. M. The neurosteroid, 3alpha-androstanediol, prevents inhibitory avoidance deficits and pyknotic cells in the granule layer of the dentate gyrus induced by adrenalectomy in rats. *Brain Res* **855**, 166-170 (2000).
- 265 MacLusky, N. J., Hajszan, T., Prange-Kiel, J. & Leranth, C. Androgen modulation of hippocampal synaptic plasticity. *Neuroscience* **138**, 957-965, doi:10.1016/j.neuroscience.2005.12.054 (2006).
- 266 Teyler, T. J., Vardaris, R. M., Lewis, D. & Rawitch, A. B. Gonadal steroids: effects on excitability of hippocampal pyramidal cells. *Science* **209**, 1017-1018 (1980).
- 267 Ohnishi, Y. N. *et al.* Generation and validation of a floxed FosB mouse line. *bioRxiv*, doi:10.1101/179309 (2017).
- 268 Brown, J. A. *et al.* Loss of Action via Neurotensin-Leptin Receptor Neurons Disrupts Leptin and Ghrelin-Mediated Control of Energy Balance. *Endocrinology*, doi:10.1210/en.2017-00122 (2017).
- 269 Overk, C. R. *et al.* Effects of aromatase inhibition versus gonadectomy on hippocampal complex amyloid pathology in triple transgenic mice. *Neurobiol Dis* **45**, 479-487, doi:10.1016/j.nbd.2011.08.035 (2012).

- 270 Krishnan, V. *et al.* Molecular adaptations underlying susceptibility and resistance to social defeat in brain reward regions. *Cell* **131**, 391-404, doi:<http://dx.doi.org/10.1016/j.cell.2007.09.018> (2007).
- 271 Golden, S. A., Covington, H. E., Berton, O. & Russo, S. J. A standardized protocol for repeated social defeat stress in mice. *Nat. Protoc.* **6**, 1183-1191, doi:10.1038/nprot.2011.361 (2011).
- 272 Vialou, V. *et al.* Differential induction of FosB isoforms throughout the brain by fluoxetine and chronic stress. *Neuropharmacology* **99**, 28-37, doi:10.1016/j.neuropharm.2015.07.005 (2015).
- 273 Eagle, A. L. *et al.* Experience-Dependent Induction of Hippocampal DeltaFosB Controls Learning. *J Neurosci* **35**, 13773-13783, doi:10.1523/JNEUROSCI.2083-15.2015 (2015).
- 274 Ahmadiani, A., Mandgary, A. & Sayyah, M. Anitconvulsant effect of flutamide on seizures induced by pentylenetetrazole: involvement of benzodiazepine receptors. *Epilepsia* **44**, 629-635 (2003).
- 275 Heiman, M., Kulicke, R., Fenster, R. J., Greengard, P. & Heintz, N. Cell type-specific mRNA purification by translating ribosome affinity purification (TRAP). *Nat Protoc* **9**, 1282-1291, doi:10.1038/nprot.2014.085 (2014).
- 276 Marcus, S. M. *et al.* Gender differences in depression: findings from the STAR*D study. *J Affect Disord* **87**, 141-150, doi:10.1016/j.jad.2004.09.008 (2005).
- 277 Dalla, C. *et al.* Chronic mild stress impact: are females more vulnerable? *Neuroscience* **135**, 703-714, doi:10.1016/j.neuroscience.2005.06.068 (2005).
- 278 Trainor, B. C. *et al.* Sex differences in social interaction behavior following social defeat stress in the monogamous California mouse (*Peromyscus californicus*). *PLoS One* **6**, e17405, doi:10.1371/journal.pone.0017405 (2011).
- 279 LaPlant, Q. *et al.* Dnmt3a regulates emotional behavior and spine plasticity in the nucleus accumbens. *Nat Neurosci* **13**, 1137-1143, doi:10.1038/nn.2619 (2010).
- 280 Muir, J. *et al.* In Vivo Fiber Photometry Reveals Signature of Future Stress Susceptibility in Nucleus Accumbens. *Neuropsychopharmacology* **43**, 255-263, doi:10.1038/npp.2017.122 (2018).
- 281 Vialou, V. *et al.* Prefrontal Cortical Circuit for Depression- and Anxiety-Related Behaviors Mediated by Cholecystokinin: Role of Δ FosB. *J Neurosci* **34**, 3878-3887 (2011).
- 282 LeGates, T. A. *et al.* Reward behaviour is regulated by the strength of hippocampus–nucleus accumbens synapses. *Nature* **564**, 258-262 (2018).

- 283 Faneselow, M. S. & Dong, H. Are the Dorsal and Ventral Hippocampus Functionally Distinct Structures? *Neuron* **65**, 7-19 (2010).
- 284 Okuyama, T., Kitamura, T., Roy, D. S., Itohara, S. & Tonegawa, S. Ventral CA1 neurons store social memory. *Science* **353**, 1536-1541, doi:10.1126/science.aaf7003 (2016).
- 285 Ramirez, S. *et al.* Activating positive memory engrams suppresses depression-like behaviour. *Nature* **522**, 335-339, doi:10.1038/nature14514 (2015).
- 286 Maren, S., De Oca, B. & Fanselow, M. S. Sex differences in hippocampal long-term potentiation (LTP) and Pavlovian fear conditioning in rats: positive correlation between LTP and contextual learning. *Brain Research* **661**, 25-34 (1994).
- 287 Lorsch, Z. S. *et al.* Estrogen receptor alpha drives pro-resilient transcription in mouse models of depression. *Nat Commun* **9**, 1116, doi:10.1038/s41467-018-03567-4 (2018).
- 288 Zhang, S. *et al.* Sex Differences in the Neuroadaptations of Reward-related Circuits in Response to Subchronic Variable Stress. *Neuroscience* **376**, 106-116 (2018).
- 289 Eagle, A., Mazei-Robison, M. & Robison, A. J. Sucrose Preference Test to Measure Stress-Induced Anhedonia. *Bio-Protocol* **6** (2016).
- 290 Willner, P., Towell, A., Sampson, D., Sophokleous, S. & Muscat, R. Reduction of sucrose preference by chronic unpredictable mild stress, and its restoration by a tricyclic antidepressant. *Psychopharmacology (Berl)* **93**, 358-364 (1987).
- 291 Sarno, E. & Robison, A. J. Emerging role of viral vectors for circuit-specific gene interrogation and manipulation in rodent brain. *Pharmacol Biochem Behav* **174**, 2-8, doi:10.1016/j.pbb.2018.04.008 (2018).
- 292 Archer, B. T., Ozcelik, T., Jahn, R., Francke, U. & Südhof, T. C. Structures and chromosomal localizations of two human genes encoding synaptobrevins 1 and 2. *J Biol Chem* **265**, 17267-17273 (1990).
- 293 Cahoy, J. D. *et al.* A Transcriptome Database for Astrocytes, Neurons, and Oligodendrocytes: A New Resource for Understanding Brain Development and Function. *J Neurosci* **28**, 264-278 (2008).
- 294 Kessler, R. C. *et al.* Lifetime prevalence and age-of-onset distributions of DSM-IV disorders in the National Comorbidity Survey Replication. *Arch Gen Psychiatry* **62**, 593-602, doi:10.1001/archpsyc.62.6.593 (2005).

- 295 Maki, P. M. *et al.* Guidelines for the evaluation and treatment of perimenopausal depression: summary and recommendations. *Menopause (New York, N.Y.)* **25**, 1069-1085, doi:10.1097/gme.0000000000001174 (2018).
- 296 Stickel, S. *et al.* Neural correlates of depression in women across the reproductive lifespan - An fMRI review. *Journal of affective disorders* **246**, 556-570, doi:10.1016/j.jad.2018.12.133 (2018).
- 297 Amanatkar, H. R. & Chibnall, J. T. Impact of exogenous testosterone on mood: A systematic review and meta-analysis of randomized placebo-controlled trials. *Ann Clin Psychiatry* **26**, 19-32 (2014).
- 298 Sial, O. K., Warren, B. L., Alcantara, L. F., Parise, E. M. & Bolanos-Guzman, C. A. Vicarious social defeat stress: Bridging the gap between physical and emotional stress. *Journal of neuroscience methods* **258**, 94-103, doi:10.1016/j.jneumeth.2015.10.012 (2016).
- 299 Riggs LM, A. J., Hernandez M, Flores-Ramirez FJ, Iñiguez SD. . Witness defeat: A novel animal model of vicarious stress-induced depression in female c57bl/6 mice. *Poster. International Behavioral Neuroscience Society (IBNS), Victoria, Canada.* (2015).
- 300 Takahashi, A. *et al.* Establishment of a repeated social defeat stress model in female mice. *Sci Rep* **7**, 12838, doi:10.1038/s41598-017-12811-8 (2017).
- 301 Harris, A. Z. *et al.* A Novel Method for Chronic Social Defeat Stress in Female Mice. *Neuropsychopharmacology : official publication of the American College of Neuropsychopharmacology* **43**, 1276-1283, doi:10.1038/npp.2017.259 (2018).
- 302 Steinman, M. Q. *et al.* Hypothalamic vasopressin systems are more sensitive to the long term effects of social defeat in males versus females. *Psychoneuroendocrinology* **51C**, 122-134, doi:10.1016/j.psyneuen.2014.09.009 (2014).
- 303 LaPlant, Q. *et al.* Role of Nuclear Factor κ B in Ovarian Hormone-Mediated Stress Hypersensitivity in Female Mice. *Biological psychiatry* **65**, 874-880, doi:10.1016/j.biopsych.2009.01.024 (2009).
- 304 Zhang, S. *et al.* Sex Differences in the Neuroadaptations of Reward-related Circuits in Response to Subchronic Variable Stress. *Neuroscience* **376**, 108-116, doi:10.1016/j.neuroscience.2018.02.021 (2018).
- 305 Leranath, C., Petnehazy, O. & MacLusky, N. J. Gonadal Hormones Affect Spine Synaptic Density in the CA1 Hippocampal Subfield of Male Rats. *J Neurosci* **23**, 1588-1592 (2003).
- 306 Woolley, C. S., Weiland, N. G., McEwen, B. S. & Schwartzkroin, P. A. Estradiol increases the sensitivity of hippocampal CA1 pyramidal cells to NMDA receptor-

- mediated synaptic input: correlation with dendritic spine density. *J Neurosci* **17**, 1848-1859 (1997).
- 307 Woolley, C. S. & McEwen, B. S. Estradiol mediates fluctuation in hippocampal synapse density during the estrous cycle in the adult rat. *J Neurosci* **12**, 2549-2554 (1992).
- 308 Frick, K. M. Estrogens and age-related memory decline in rodents: what have we learned and where do we go from here? *Hormones and behavior* **55**, 2-23, doi:10.1016/j.yhbeh.2008.08.015 (2009).
- 309 Choleris, E., Clipperton-Allen, A. E., Phan, A., Valsecchi, P. & Kavaliers, M. Estrogenic involvement in social learning, social recognition and pathogen avoidance. *Front Neuroendocrinol* **33**, 140-159, doi:10.1016/j.yfrne.2012.02.001 (2012).
- 310 Hastings, R., Parsey, R., Oquendo, M., Arango, V. & Mann, J. Volumetric Analysis of the Prefrontal Cortex, Amygdala, and Hippocampus in Major Depression. *Neuropsychopharmacology* **29**, 952-959 (2004).
- 311 Bagot, R. C. *et al.* Circuit-wide Transcriptional Profiling Reveals Brain Region-Specific Gene Networks Regulating Depression Susceptibility. *Neuron* **90**, 969-983, doi:10.1016/j.neuron.2016.04.015 (2016).
- 312 Okuyama, T., Kitamura, T., Roy, D. S., Itohara, S. & Tonegawa, S. Ventral CA1 neurons store social memory. *Science (New York, N.Y.)* **353**, 1536, doi:10.1126/science.aaf7003 (2016).
- 313 Papp, M., Willner, P. & Muscat, R. An animal model of anhedonia: attenuation of sucrose consumption and place preference conditioning by chronic unpredictable mild stress. *Psychopharmacology (Berl)* **104**, 255-259 (1991).
- 314 Pizzagalli, D. A. Depression, Stress, and Anhedonia: Toward a Synthesis and Integrated Model. *Annu Rev Clin Psychol* **10**, 393-423 (2014).
- 315 Labonté, B. *et al.* Sex-specific transcriptional signatures in human depression. *Nature Medicine* **23**, 1102-1111 (2017).
- 316 Jain, A., Huang, G. Z. & Woolley, C. S. Latent sex differences in molecular signaling that underlies excitatory synaptic potentiation in the hippocampus. *J Neurosci* **39**, 1552-1565 (2019).
- 317 Bale, T. L. Sex differences in prenatal epigenetic programming of stress pathways. *The International Journal on the Biology of Stress* **14**, 348-356 (2011).
- 318 Ramzan, F., Azam, A. B., Monks, D. A. & Zovkic, I. B. Androgen receptor is a negative regulator of contextual fear memory in male mice. *Hormones and Behavior* **106**, 10-18, doi:10.1016/j.yhbeh.2018.08.012 (2018).

- 319 Fanselow, M. S. & Dong, H.-W. Are the dorsal and ventral hippocampus functionally distinct structures? *Neuron* **65**, 7-19, doi: 10.1016/j.neuron.2009.11.031 (2010).
- 320 Bannerman, D. M. *et al.* Regional dissociations within the hippocampus—memory and anxiety. *Neurosci. Biobehav. Rev.* **28**, 273-283, doi: 10.1016/j.neubiorev.2004.03.004 (2004).
- 321 LeGates, T. A. *et al.* Reward behaviour is regulated by the strength of hippocampus–nucleus accumbens synapses. *Nature*, doi:10.1038/s41586-018-0740-8 (2018).
- 322 Bagot, R. C. *et al.* Ventral hippocampal afferents to the nucleus accumbens regulate susceptibility to depression. *Nature Communications* **6**, 7062, doi:10.1038/ncomms8062 (2015).
- 323 Floriou-Servou, A. *et al.* Distinct proteomic, transcriptomic, and epigenetic stress responses in dorsal and ventral hippocampus. *Biol. Psychiatry* **84**, 531-541, doi:10.1016/j.biopsych.2018.02.003 (2018).
- 324 Pacheco, A. *et al.* Chronic stress triggers expression of immediate early genes and differentially affects the expression of AMPA and NMDA subunits in dorsal and ventral hippocampus of rats. *Front Mol Neurosci* **10**, 244, doi:10.3389/fnmol.2017.00244 (2017).
- 325 Kenworthy, C. A. *et al.* Social defeat induces changes in histone acetylation and expression of histone modifying enzymes in the ventral hippocampus, prefrontal cortex, and dorsal raphe nucleus. *Neuroscience* **264**, 88-98, doi:https://doi.org/10.1016/j.neuroscience.2013.01.024 (2014).
- 326 Carle, T. L. *et al.* Proteasome-dependent and -independent mechanisms for FosB destabilization: identification of FosB degron domains and implications for Δ FosB stability. *Eur. J. Neurosci.* **25**, 3009-3019, doi:10.1111/j.1460-9568.2007.05575.x (2007).
- 327 Ulery, P. G., Rudenko, G. & Nestler, E. J. Regulation of Δ FosB stability by phosphorylation. *J Neurosci* **26**, 5131-5142, doi:10.1523/jneurosci.4970-05.2006 (2006).
- 328 Nestler, E. J., Kelz, M. B. & Chen, J. Δ FosB: a molecular mediator of long-term neural and behavioral plasticity. *Brain Res.* **835**, 10-17, doi: 10.1016/S0006-8993(98)01191-3 (1999).
- 329 Perrotti, L. I. *et al.* Induction of Δ FosB in reward-related brain structures after chronic stress. *J Neurosci* **24**, 10594-10602, doi:10.1523/jneurosci.2542-04.2004 (2004).

- 330 Grueter, B. A., Robison, A. J., Neve, R. L., Nestler, E. J. & Malenka, R. C. FosB differentially modulates nucleus accumbens direct and indirect pathway function. *Proc. Natl. Acad. Sci. U. S. A.* **110**, 1923-1928, doi:10.1073/pnas.1221742110 (2013).
- 331 Eagle, A. L. *et al.* Experience-dependent induction of hippocampal Δ FosB controls learning. *J Neurosci* **35**, 13773-13783 (2015).
- 332 Eagle, A. L., Williams, E. S., Beatty, J. A., Cox, C. L. & Robison, A. J. Δ FosB decreases excitability of dorsal hippocampal CA1 neurons. *eNeuro* **5**, ENEURO.0104-0118.2018, doi:10.1523/ENEURO.0104-18.2018 (2018).
- 333 Cooper, S. E. *et al.* Comparison of chronic physical and emotional social defeat stress effects on mesocorticolimbic circuit activation and voluntary consumption of morphine. *Scientific Reports* **7**, 8445, doi:10.1038/s41598-017-09106-3 (2017).
- 334 Mastrodonato, A. *et al.* Ventral CA3 activation mediates prophylactic ketamine efficacy against stress-induced depressive-like behavior. *Biol. Psychiatry* **84**, 846-856, doi: 10.1016/j.biopsych.2018.02.011 (2018).
- 335 Blaha, C. D., Yang, C. R., Floresco, S. B., Barr, A. M. & Phillips, A. G. Stimulation of the ventral subiculum of the hippocampus evokes glutamate receptor-mediated changes in dopamine efflux in the rat nucleus accumbens. *Eur. J. Neurosci.* **9**, 902-911, doi:10.1111/j.1460-9568.1997.tb01441.x (1997).
- 336 Floresco, S. B., Todd, C. L. & Grace, A. A. Glutamatergic afferents from the hippocampus to the nucleus accumbens regulate activity of ventral tegmental area dopamine neurons. *J Neurosci* **21**, 4915-4922 (2001).
- 337 Fanselow, M. S. & LeDoux, J. E. Why we think plasticity underlying pavlovian fear conditioning occurs in the basolateral amygdala. *Neuron* **23**, 229-232, doi:10.1016/S0896-6273(00)80775-8 (1999).
- 338 Etkin, A. *et al.* Individual differences in trait anxiety predict the response of the basolateral amygdala to unconsciously processed fearful faces. *Neuron* **44**, 1043-1055, doi: 10.1016/j.neuron.2004.12.006 (2004).
- 339 Sierra-Mercado, D., Padilla-Coreano, N. & Quirk, G. J. Dissociable Roles of Prelimbic and Infralimbic Cortices, Ventral Hippocampus, and Basolateral Amygdala in the Expression and Extinction of Conditioned Fear. *Neuropsychopharmacol* **36**, 529-538, doi:10.1038/npp.2010.184 (2011).
- 340 Kjelstrup, K. G. *et al.* Reduced fear expression after lesions of the ventral hippocampus. *Proceedings of the National Academy of Sciences* **99**, 10825-10830, doi:10.1073/pnas.152112399 (2002).

- 341 Gomez, J. L. *et al.* Chemogenetics revealed: DREADD occupancy and activation via converted clozapine. *Science* **357**, 503-507, doi:10.1126/science.aan2475 (2017).
- 342 Robison, A. J. *et al.* Fluoxetine epigenetically alters the CaMKIIalpha promoter in nucleus accumbens to regulate DeltaFosB binding and antidepressant effects. *Neuropsychopharmacology* **39**, 1178-1186, doi:10.1038/npp.2013.319 (2014).
- 343 Southwick, S. M. & Charney, D. S. The Science of Resilience: Implications for the Prevention and Treatment of Depression. *Science* **338**, 79-82 (2012).
- 344 Wood, S. K., Walker, H. E., Valentino, R. J. & Bhatnagar, S. Individual differences in reactivity to social stress predict susceptibility and resilience to a depressive phenotype: role of corticotropin-releasing factor. *Endocrinology* **151**, 1795-1805, doi:10.1210/en.2009-1026 (2010).
- 345 Adamec, R., Toth, M., Haller, J., Halasz, J. & Blundell, J. A comparison of activation patterns of cells in selected prefrontal cortical and amygdala areas of rats which are more or less anxious in response to predator exposure or submersion stress. *Physiol Behav* **105**, 628-638 (2012).
- 346 Lehmann, M. L. & Herkenham, M. Environmental Enrichment Confers Stress Resiliency to Social Defeat through an Infralimbic Cortex-Dependent Neuroanatomical Pathway. *J Neurosci* **31**, 6159-6173, doi: 10.1523/JNEUROSCI.0577-11.2011 (2011).
- 347 Covington, H. E., 3rd *et al.* Antidepressant effect of optogenetic stimulation of the medial prefrontal cortex. *J Neurosci* **30**, 16082-16090, doi: 10.1523/jneurosci.1731-10.2010 (2010).
- 348 Iniguez, S. D. *et al.* Vicarious Social Defeat Stress Induces Depression-Related Outcomes in Female Mice. *Biol Psychiatry* **83**, 9-17, doi:10.1016/j.biopsych.2017.07.014 (2018).
- 349 Trezza, V., Campolongo, P. & Vanderschuren, L. J. Evaluating the rewarding nature of social interactions in laboratory animals. *Dev Cogn Neurosci* **1**, 444-458, doi: 10.1016/j.dcn.2011.05.007 (2011).
- 350 Cooper, S. E. *et al.* Comparison of chronic physical and emotional social defeat stress effects on mesocorticolimbic circuit activation and voluntary consumption of morphine. *Sci Rep* **7**, 8445, doi: 10.1038/s41598-017-09106-3 (2017).
- 351 Laplant, Q. *et al.* Dnmt3a regulates emotional behavior and spine plasticity in the nucleus accumbens. *Nat Neurosci* **13**, 1137-1143 (2014).
- 352 Alkon, D. L., Lederhendler, I. & Shoukimas, J. J. Primary changes of membrane currents during retention of associative learning. *Science* **215**, 693-695 (1982).

- 353 Oh, M. M., Kuo, A. G., Wu, W. W., Sametsky, E. A. & Disterhoft, J. F. Watermaze learning enhances excitability of CA1 pyramidal neurons. *J Neurophysiol* **90**, 2171-2179, doi:10.1152/jn.01177.2002 (2003).
- 354 Alkon, D. L. Calcium-mediated reduction of ionic currents: a biophysical memory trace. *Science* **226**, 1037-1045 (1984).
- 355 Brickley, S. G., Revilla, V., Cull-Candy, S. G., Wisden, W. & Farrant, M. Adaptive regulation of neuronal excitability by a voltage-independent potassium conductance. *Nature* **409**, 88-92, doi:10.1038/35051086 (2001).
- 356 Chavez-Noriega, L. E., Halliwell, J. V. & Bliss, T. V. A decrease in firing threshold observed after induction of the EPSP-spike (E-S) component of long-term potentiation in rat hippocampal slices. *Exp Brain Res* **79**, 633-641 (1990).
- 357 Turrigiano, G., Abbott, L. F. & Marder, E. Activity-dependent changes in the intrinsic properties of cultured neurons. *Science* **264**, 974-977 (1994).
- 358 Daoudal, G. & Debanne, D. Long-term plasticity of intrinsic excitability: learning rules and mechanisms. *Learn Mem* **10**, 456-465, doi:10.1101/lm.64103 (2003).
- 359 Zhang, W. & Linden, D. J. The other side of the engram: experience-driven changes in neuronal intrinsic excitability. *Nat Rev Neurosci* **4**, 885-900, doi:10.1038/nrn1248 (2003).
- 360 Frick, A. & Johnston, D. Plasticity of dendritic excitability. *J Neurobiol* **64**, 100-115, doi:10.1002/neu.20148 (2005).
- 361 Cudmore, R. H. & Turrigiano, G. G. Long-term potentiation of intrinsic excitability in LV visual cortical neurons. *J Neurophysiol* **92**, 341-348, doi:10.1152/jn.01059.2003 (2004).
- 362 Aizenman, C. D. & Linden, D. J. Rapid, synaptically driven increases in the intrinsic excitability of cerebellar deep nuclear neurons. *Nat Neurosci* **3**, 109-111, doi:10.1038/72049 (2000).
- 363 Ireland, D. R. & Abraham, W. C. Group I mGluRs increase excitability of hippocampal CA1 pyramidal neurons by a PLC-independent mechanism. *J Neurophysiol* **88**, 107-116, doi:10.1152/jn.2002.88.1.107 (2002).
- 364 O'Leary, T., van Rossum, M. C. & Wyllie, D. J. Homeostasis of intrinsic excitability in hippocampal neurones: dynamics and mechanism of the response to chronic depolarization. *J Physiol* **588**, 157-170, doi:10.1113/jphysiol.2009.181024 (2010).
- 365 Desai, N. S., Rutherford, L. C. & Turrigiano, G. G. Plasticity in the intrinsic excitability of cortical pyramidal neurons. *Nat Neurosci* **2**, 515-520, doi:10.1038/9165 (1999).

- 366 Xu, N. L., Ye, C. Q., Poo, M. M. & Zhang, X. H. Coincidence detection of synaptic inputs is facilitated at the distal dendrites after long-term potentiation induction. *Journal of Neuroscience* **26**, 3002-3009, doi:10.1523/Jneurosci.5220-05.2006 (2006).
- 367 Frick, A., Magee, J. & Johnston, D. LTP is accompanied by an enhanced local excitability of pyramidal neuron dendrites. *Nature Neuroscience* **7**, 126-135, doi:10.1038/nn1178 (2004).
- 368 Kim, J., Jung, S. C., Clemens, A. M., Petralia, R. S. & Hoffman, D. A. Regulation of dendritic excitability by activity-dependent trafficking of the A-type K⁺ channel subunit Kv4.2 in hippocampal neurons. *Neuron* **54**, 933-947, doi:10.1016/j.neuron.2007.05.026 (2007).
- 369 Tsubokawa, H., Offermanns, S., Simon, M. & Kano, M. Calcium-dependent persistent facilitation of spike backpropagation in the CA1 pyramidal neurons. *J Neurosci* **20**, 4878-4884 (2000).